School Of Applied Science

Development of the Portable Satellite Laser Ranging System

Mark A. Broomhall

This thesis is presented for the Degree of

Master of Science

of

Curtin University of Technology

July 2003

Abstract

The Portable Satellite Laser Ranger (PSLR) is a light weight, highly portable satellite laser ranging system which employs many of the techniques and equipment types of larger fixed systems. It has a primary telescope aperture of 62 cm and uses a 150 ps pulse of 130 mJ at the second harmonic wavelength of 532 nm. The system is designed to use as little ancillary equipment as possible and only requires one small instrument rack and one PC based control computer. All of the control features of the system are based or installed in the control computer.

The PSLR project at Curtin University was concerned with repairing and upgrading the PSLR to return the system to operational capacity. This involved the replacement of missing control components, repair of some hardware, modifications to the control program, and several calibration and operational tests. These tests showed that the PSLR system was capable of a ranging accuracy to fixed targets of 8.5 mm with an average accuracy of 23 mm. They showed that the PSLR was capable, in selective conditions, to track star ephemerides to less than 54". The mount error (standard deviation) over several orientations was shown to be 0.253° in elevation and 0.337° in azimuth.

This dissertation will discuss; i) the operation of the equipment used with the PSLR and similar systems, the steps taken to repair or replace the necessary equipment, ii) the tests required to calibrate or evaluate various sub-systems of the PSLR and, iii) the results and conclusions drawn as a result.

Acknowledgments

I would like to thank the following people for their assistance in the completion of this thesis:

Associate Professor Mervyn J. Lynch for his support and assistance with the tasks involved in the PSLR project and in the preparation of this thesis.

Don Smith (Electronics), Leon Majewski and Dave Foster (Software development) for their support, helpful criticism and extensive knowledge during the project.

Sir Laurence Brodie-Hall for showing faith and allowing the project to succeed or fail on its own merits.

Kerry Stokes and the staff of Australian Capital Equity (David Aspinall, Marie-Louise Martin, Kirsty Burnett).

The members of the Remote Sensing and Satellite Research Group for many hours of unrequited assistance.

Contents

List of Figures

List of Tables

Chapter 1

PSLR project aims

1.1 Background

This thesis was initially intended to be based on the task of preparing an error calculation method and a final absolute accuracy figure for the Portable satellite laser ranger (PSLR). This work was to be carried out on a functioning instrument with the help and guidance of the Latvian personnel who developed the PSLR. This project began at Curtin University in March of 1999 and by August of that year, after discussions with members of the Latvian development team, it was decided that they would not be participating any further with the project .

The instrument was, at this time, still located in Latvia. Personnel from the Australian company that owns the PSLR equipment journeyed to Riga, Latvia to retrieve the instrument. The instrument was dismantled, packed into several trunks and boxes before being transported to Curtin University. The equipment, such as it was, arrived at Curtin University on the 11^{th} of May, 1999.

After cataloging the components of the PSLR system, the instrument was re-assembled in the workshop basically to determine how this was accomplished as there was no construction manual, notes or indication of any sort as to how this was done. Once the instrument was reassembled it was discovered that key components of the system were missing, most notably two computer expansion cards that

controlled the mount motion and the station timing. The control software was also discovered to be incomplete as it was unable to be compiled.

As the PSLR was non-functional, it was decided to change the aims of this thesis to reflect the new goals of the PSLR project at Curtin University.

1.2 Revised aims of the PSLR project

The aim was to develop the system to a point where it was able to replicate its performance when it was previously a complete system in working order. This level of performance was determined from two sources.

1. The only operational document on the PSLR was an incomplete program users manual. This document was designed as a help menu option with the PSLR control program. It gave some insight into the operation of the PSLR and was the only indication two control cards were missing form the delivered equipment. It also provided information on the timing parameters (performance, mode of operation etc), and some indication of the mount drive method and capabilities. These capabilities would need to be matched or improved to return the PSLR to its previous level of performance.

2. The second source was a set of print outs from a tracking campaign conducted by the PSLR at the Yarragadee laser ranging facility in Western Australia. This campaign was conducted from January to April 1996. The print outs show all of the relevant information for a tracking pass of a satellite.

   Examples of these print outs can be seen in figures 1.1 and 1.2. The top of each figure represents all of the distance readings to the satellites, the circular graph on the left shows the position of the satellite with respect to telescope zenith and the figures on the right show recorded information such as atmospheric readings and calculated information such as the range error. The two figures of most interest are RMS of fit and normal point RMS of fit. The RMS of fit

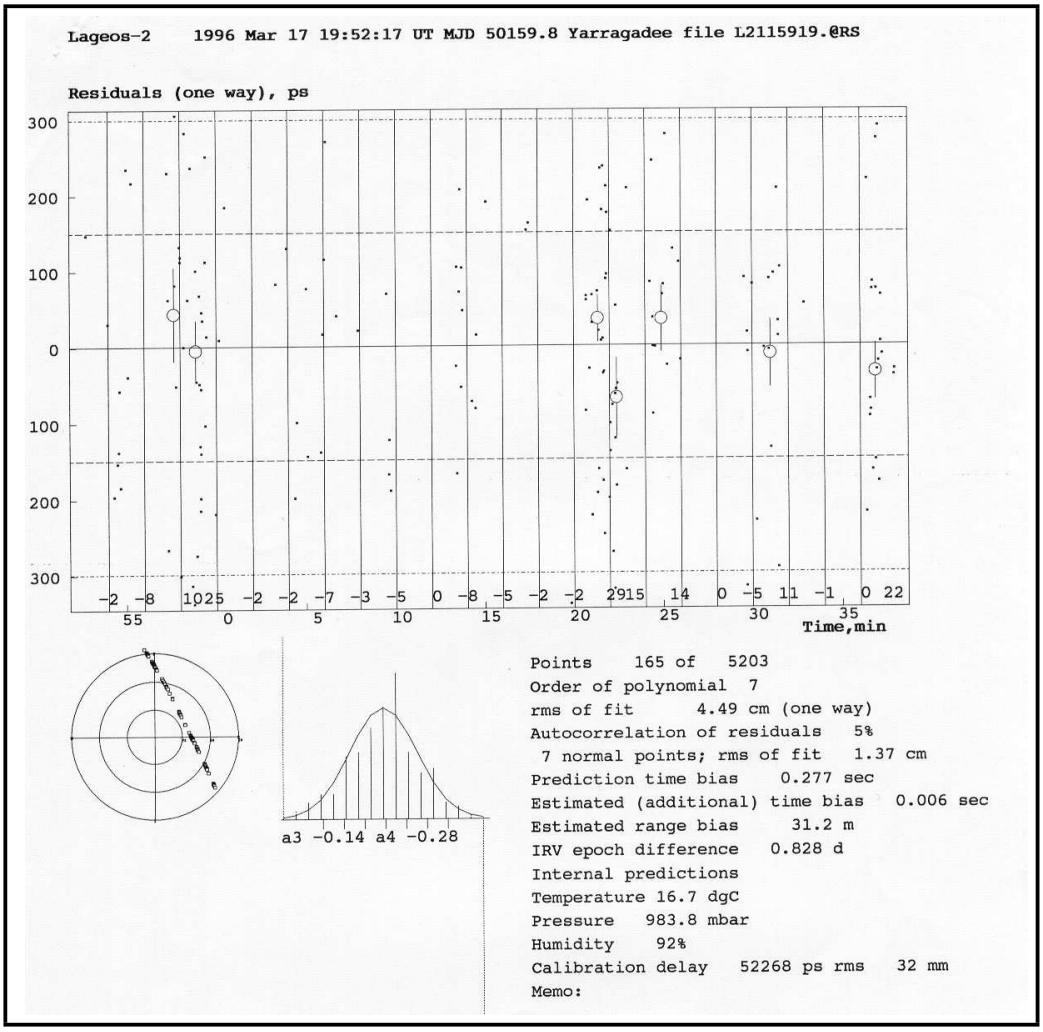

Figure 1.1: Print out of a tracking pass for LAGEOS2.

is what is known as the single shot error or the average that each individual return is from the expected value. The normal point RMS is the average that the normal point reduced data is in error from the expected value (see section 2.4.6, page 49). These are the most telling figures of the performance of a laser ranging system. These print outs are representative of several passes to several satellites. Some of the results are better but many are worse. In general the normal point RMS is 1.5 - 2.0 cm and this is the figure the PSLR project hoped to achieve.

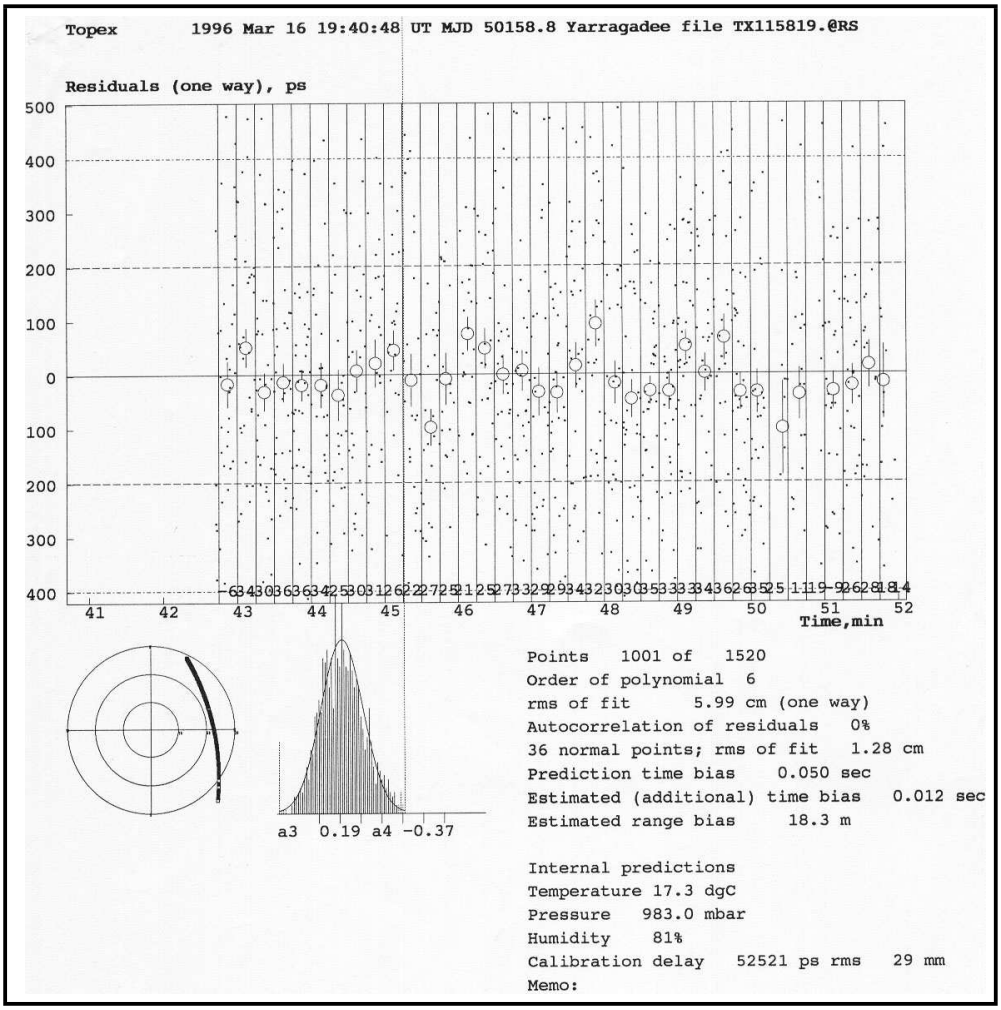

Figure 1.2: Print out for a tracking pass for TOPEX/Poseidon.

The PSLR project at Curtin University expected to achieve similar precision figures with a reconstructed instrument and hoped to improve these figures with newer equipment.

The aims of the project were three-fold:

1. To determine what was missing from the PSLR system, replace these components and correctly assemble the instrument.

2. To integrate new components into the existing system and make the instrument fully operational.

3. To conduct operational tests to determine the accuracy, durability and possible improvements to the system.

The aim of this thesis was to discuss the work involved in the three project tasks outlined above. Initially this would require replacing all of the missing literature for the various components of the PSLR and becoming proficient in their operation. Secondly, new equipment to replace the missing components would need to be investigated, installed and tested. Lastly, the PSLR would need to be tested as a fully operational system and its performance compared to the expected benchmarks from the Latvian supplied test results (see figures 1.1 and 1.2).

These aims are covered by the general title of this thesis which is "The development of the Portable satellite laser ranging system".

Chapter 2

An Introduction to Satellite Laser Ranging

Satellite Laser Ranging (SLR), in essence is a method of satellite tracking. SLR is still the most accurate satellite tracking technique available with single shot positional accuracies under a centimeter and normal point corrected data able to claim precision of just a few millimeters. With many of the scientific applications that regularly use SLR data requiring continual improvements in data precision to advance modelling accuracy, SLR remains as the only currently available approach which satisfy this constant demand.

The SLR tracking method requires a pulsed laser source and a telescope to collect the reflected laser light on its return. The laser provides a detectable link between a fixed station and a distant satellite moving at a large velocity. The telescope and associated equipment determine a very precise location and velocity for both the satellite and station from the data provided by the laser beam.

Information from the interaction between the satellite and the station can be used to determine the real relative position and velocity of each body. This relationship is, however, somewhat cyclic, as in order to determine satellite position, its location and velocity needs to be known with fair precision before ranging is initiated. While it may seem unnecessary to track a satellite when the orbital information is already

well known, it makes more sense when the process of laser ranging reveals that not only are orbits constantly changing but the stations which are used to collect data themselves are also continually moving (although very slowly) with respect to the Earth's centre of gravity. The SLR data are then used to improve the orbital predictions for the tracked satellites which, in turn, makes the satellites easier to track. The better the data from satellite tracking, the better the results from the models that use SLR data (such as the geopotential field model for the Earth).

2.1 A brief history of satellite laser ranging

The Laser (Light amplification by the stimulated emission of radiation), was invented either in the late 1950s by Gordon Gould or in 1960 by Thomas Maiman. Thomas Maiman did invent the first solid state ruby laser at Hughes Aircraft Laboratories in early 1960.

At this time, orbital tracking of satellites was accomplished using microwave radar which was capable of accuracies of around 50 m.

With the advent of the new laser technology it was expected that this figure could be markedly reduced. The laser produced a monochromatic light source that could be directed on a very tight beam and be could be clearly distinguished from background radiation. Using a specially designed optical device called a retroreflector or corner cube reflector (CCR) (see section 2.4.1.3), a method was soon developed to range to a satellite using a laser pulse.

To paraphrase (Degnan, 1996), two and a half years after the development of the first ruby laser, the Explorer 22/Beacon-B satellite was launched into an orbit of approximately 1000 kms. A few weeks later at 10:26 GMT on the 31^{st} of October, 1964, at the Goddard Space Flight Center (GSFC) in Greenbelt, Maryland, the first few weak returns from Beacon-B were recorded by oscilloscope, and thus the field of satellite laser ranging was born. This campaign recorded range accuracies of 2 to 3 m, a factor of 15 - 25 times better than the previous tracking technique, thereby

proving the value of this new technique.

The first international SLR campaign began in early 1967 and involved three French run stations in France, Algeria and Greece, and two U.S.A based stations in Greenbelt and New Mexico. These stations tracked three new Beacon satellites (as well as the original Beacon 22) and two new French satellites, designated Diadem 1 and 2. This campaign lead to the first comprehensive SLR based Earth gravity model, giving accuracies to 5 m.

The year 1969 saw the first daylight ranging tests carried out by NASA/GSFC and the placement of the first lunar laser ranging target by the Apollo 11 crew.

1972 saw the first stations successfully operate in Czechoslovakia by the Czech Technical institute. This group sponsored stations in Poland, Latvia, Bolivia, Cuba and India. U.S.A sponsored systems had been deployed to Peru, Brazil and South Africa so SLR had become truly global.

With many stations producing data at sub-meter levels the Global datum was fixed to a precision of $\pm$ 5 m.

In 1975 the first satellite dedicated specifically for SLR, Starlette, was launched by the French space agency (CNES). This was quickly followed in 1976 by the NASA launch of LAGEOS 1. These type of satellites were used extensively for geodetic studies and the examination of the terrestrial gravity field. These satellites together with LAGEOS 2 and Stella (launched in the 1990s) are still extensively tracked and still play a valuable role in geodetic science.

The latter half of the 1970s and early 1980s saw improvements in laser technology. In 1981, the MOBLAS-4 station at GSFC achieved a single shot precision of 1.5 cm using a mode-locked solid state laser in conjunction with a new type of photodetector. In the latter half of the 1980s sub-centimeter single shot accuracies were regularly being achieved (ILRS, 2003a).

The first highly portable system was introduced in the 1980s by the University of Texas, the TLRS-1. This preceded other portable systems introduced by Germany, Holland and Japan. These early portable systems were principally used to study

plate tectonics in areas of high instability.

The first of the current GPS satellites (Block 2) was launched on the 14^{th} of February, 1989. This was followed by the gradual launch of 23 other satellites to complete the network. The United States Air Force announced that the NAVSTAR GPS system was fully operational on the 17^{th} of July, 1994 (Red Sword Corporation, 1998). As civilian GPS receivers were soon able to produce comparable range figures to portable SLR, most portable SLR program were considerably scaled back.

The later half of the 1990s saw a considerable increase in new technologies, new approaches to laser ranging, and new scientific applications of laser ranging. This included; i) the regular use of high gain semiconductor detectors for single photon laser ranging, ii) the use of dual colour laser transmission to determine "real-time" atmospheric effects, and iii) "time-transfer" by laser between laser ranging stations.

2.2 The current state of SLR

The current SLR systems are far superior to the original SLR systems developed in the early 1960s. The initial ranging tests to the Beacon 1 satellite gave ranges to tens of meters. Current SLR systems are capable of single shot precision (to LAGEOS) of less than 10mm RMS and a normal point (NP) precision of just a few mm RMS (with the best systems).

The current performance comparisons for the global SLR network (see map from figure 2.3, page 12) (at the time of preparation of this document) can be seen in figures 2.1 and 2.2 (International Laser Ranging Service (ILRS), 2003).

Many of the current SLR systems design basics do not vary greatly from the initial SLR systems. They are comprised of large solid state lasers which employ high energy extraction pulsed operation, and are designed to keep the pulse duration small while maintaining good pulse stability. They have large mirrors for collecting the return signal from the laser, and they generally employ a photomultiplier tube detector. They have pulse conditioning electronics and a time interval counter to

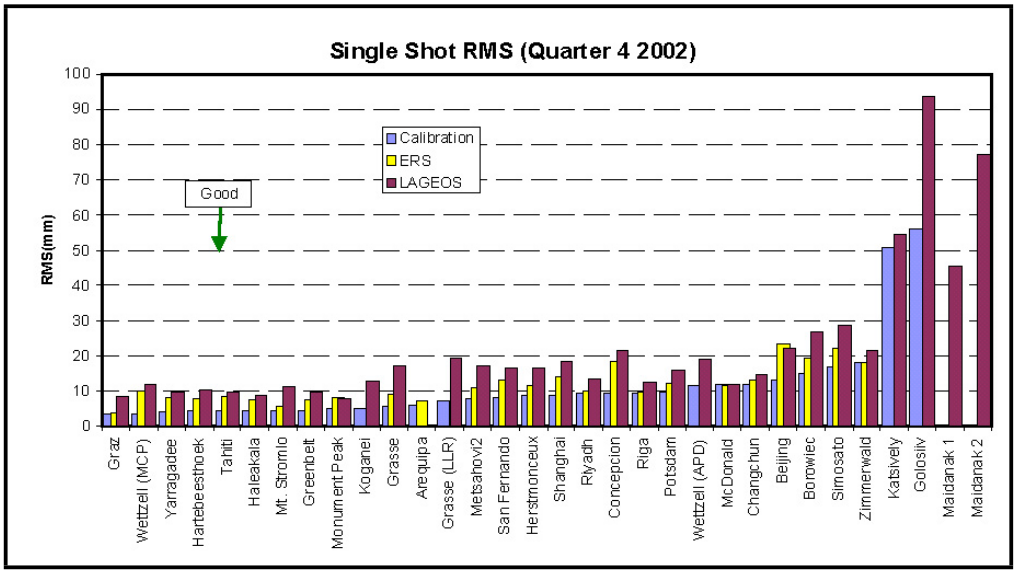

Figure 2.1: Fourth quarter 2002 SLR network performance comparison, single shot accuracy.

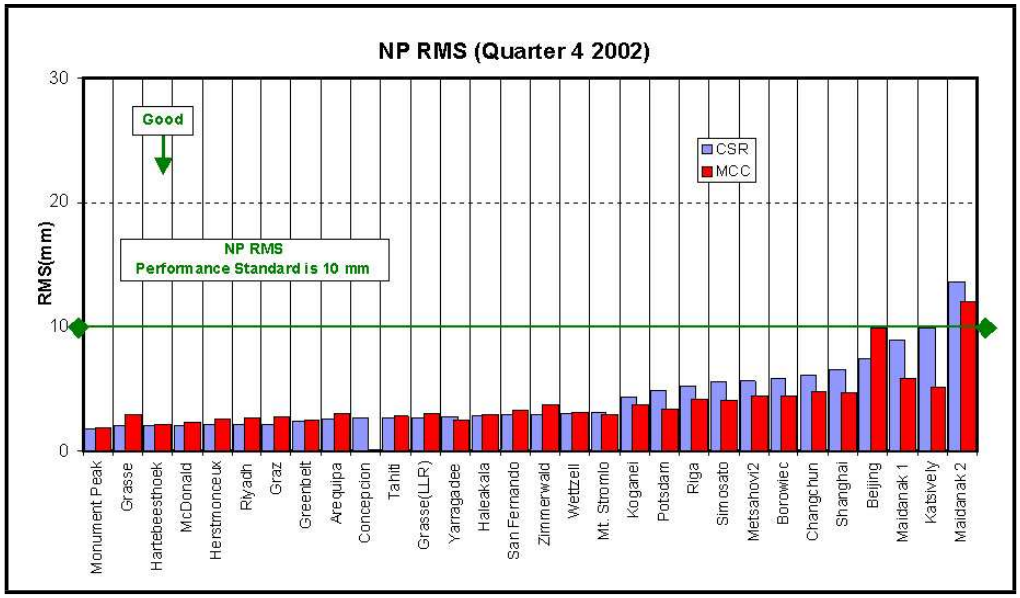

Figure 2.2: Fourth quarter 2002 SLR network performance comparison, NP accuracy.

register ranging epoch or measure time-of-flight.

The obvious question is why have the accuracy of SLR improved by an order of magnitude for each decade since it began? The modern SLR system achieves the superlative accuracy by using equipment that is significantly better than the early

systems, and by applying the knowledge and experience gained by over 40 years of laser ranging. SLR, while only a small field of study, is comprised of a dedicated group of scientists, many of whom have worked in the field since its inception. When this dedication is coupled with the skill and experience of the station operators, many of whom have also spent decades in the field, steady improvement is to be expected. Automation has meant that while early systems required many personnel, scientists and operators, to run the system, modern stations require very few, single operator, or in the case of systems such as Mount Stromlo or the yet to be deployed SLR2000, no operators at all. The increase in computing power and commercially available hardware has significantly reduced the need for scientific and technical support for SLR systems.

Some of the more recent improvements in the field of SLR come through the modelling and understanding of the effect of the environment and the satellite target itself on the ranging result. In fact, with modern SLR equipment capable of sub-millimeter ranging, the single largest source of error is now target and environment related.

It is fair to say that best of these "second generation" systems have just about reached the limit of the accuracy possible even with the improvements in equipment, modelling of the non-station error sources and best operating practices developed since the field of SLR began. MOBLAS-5 is a good example of a second generation system that, while still one of the best performed systems in the ILRS, it is essentially using techniques that are 10 - 20 years old. The MOBLAS-5 system at Yarragadee consistently lead the performance ratings (see figures 2.1 and 2.2) but other stations are starting to move up the list.

Over recent years the global coverage by SLR stations has improved. Figure 2.3 (ILRS, 2003b) shows the current fixed SLR locations, proposed new system locations, and indicates the country of origin of the four operational portable systems. There are obvious large gaps in the network, especially in the Southern hemisphere (due in part to the large expanse of oceans which do not contain suitable land to

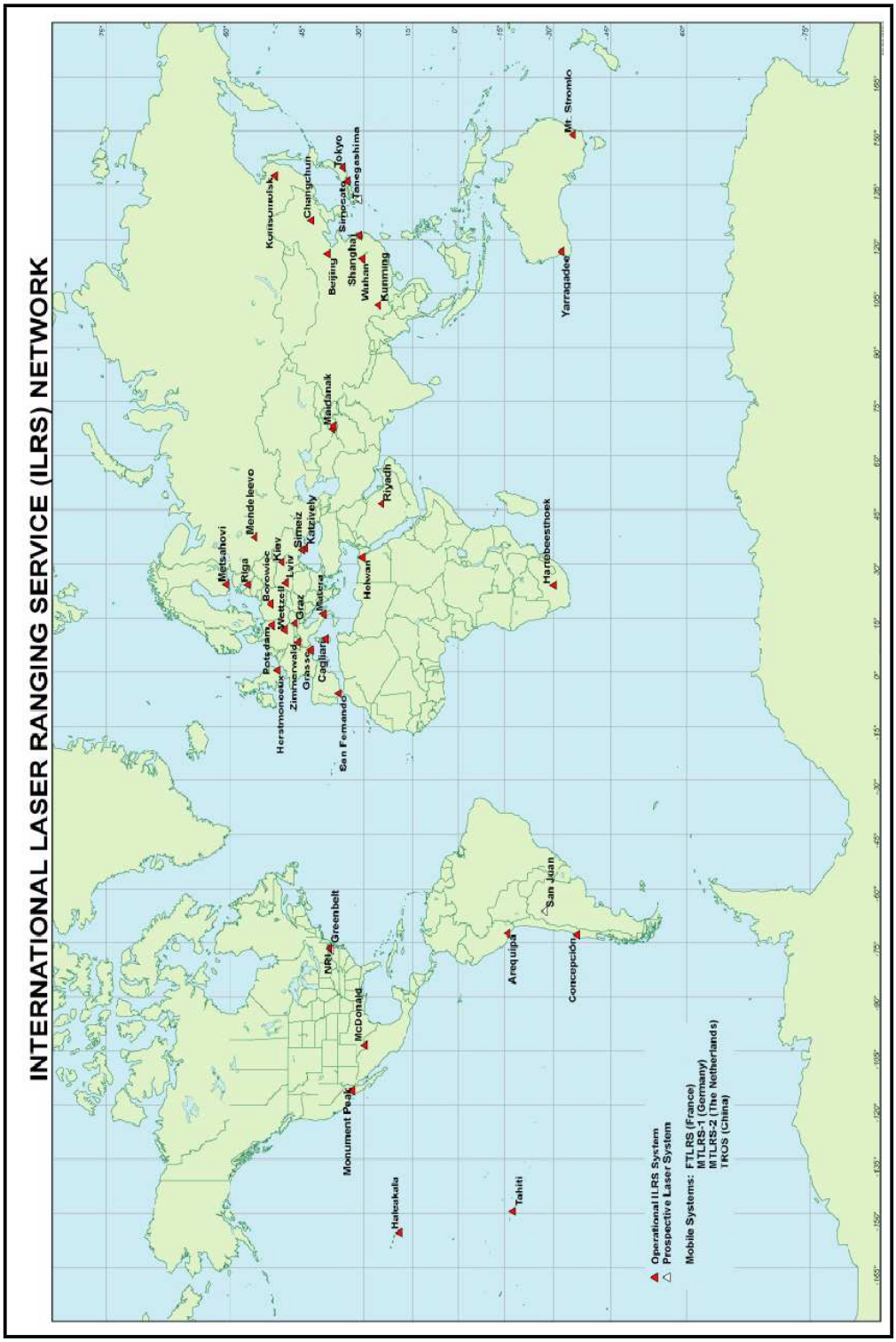

Figure 2.3: ILRS network station location map.

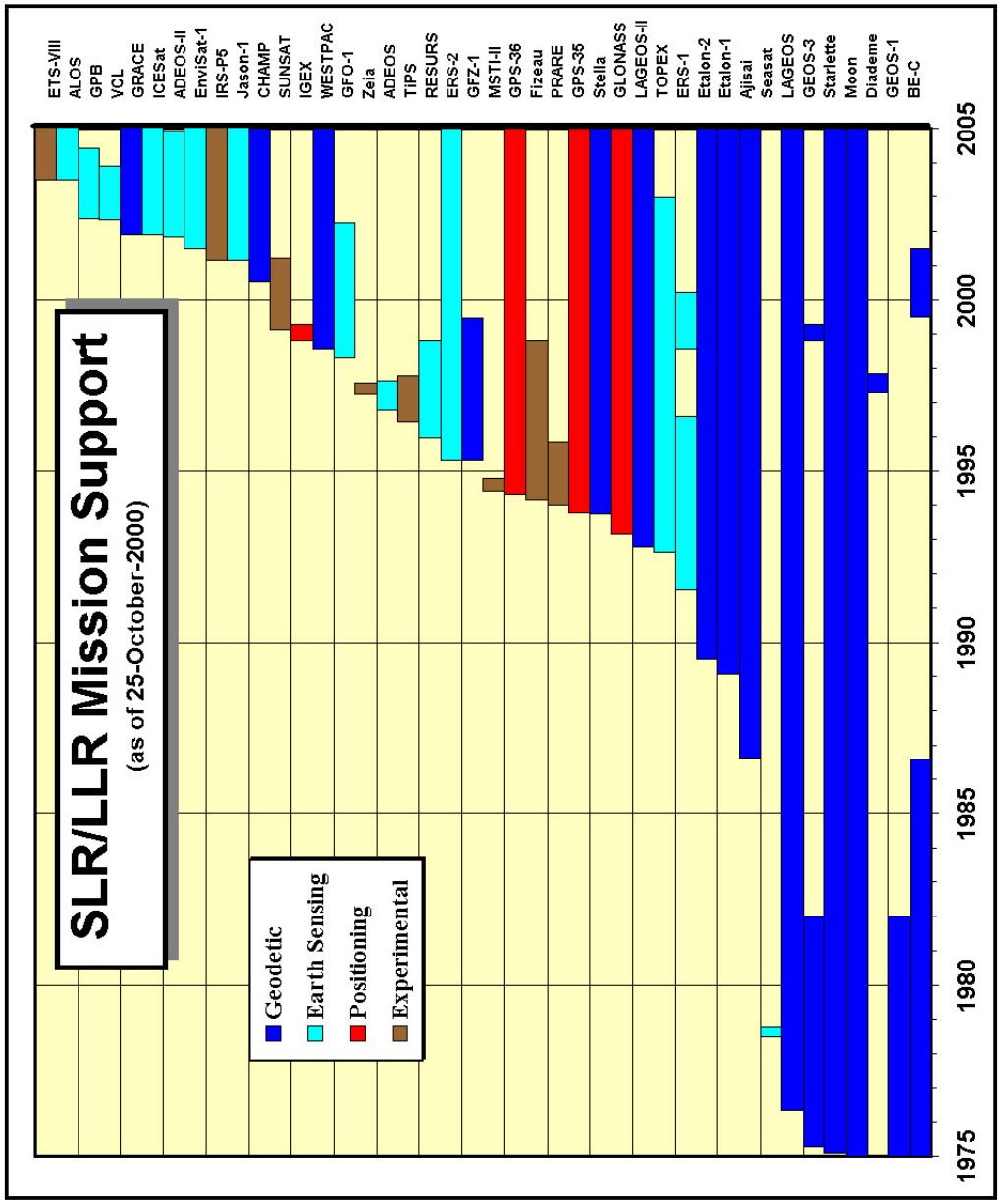

Figure 2.4: Satellites tracked by the ILRS, showing mission duration, type of mission and satellite name.

locate a station), and no coverage at the poles. Ideally, the ILRS network would cover the globe with a standard concentration to achieve the best results.

In the 1970s 5 satellites were regularly tracked by the International Laser Ranging Service (ILRS). This will increase to 28 or more by 2005. Figure 2.4 (ILRS, 2003) shows the support for various satellite missions over a 30 year period. These satellites

include those specifically designed for laser tracking (regular spherical satellites such as LAGEOS and GFZ-1) as well as satellites that use SLR for calibration of on-board tracking instruments (irregular shaped satellite such as TOPEX-POSEIDON or GRACE that have retroreflectors fitted).

The increase in both the number of satellites being tracked (in all manner of orbital heights, orientations and eccentricities), and the number of high precision laser ranging stations has seen the ranging precision increase from 3 m in 1964 to under 2 mm for the very best stations in 2003, a 1500 times increase in 40 years. With new satellite missions and continued improvements in technology, station design and orbital modelling, the ILRS is confident of achieving sub-millimeter accuracy before the end of the decade.

2.3 An introduction to portable satellite laser ranging

This dissertation will explain the principles and design of SLR and the function and operation of much of the equipment used in contemporary SLR systems. This discussion will focus on equipment used with the Portable Satellite Laser Ranger (PSLR) system and the development of this instrument. The PSLR is a light weight (approximately 500 kg total mass), and highly portable system which is designed to emulate most of the functions of a larger fixed system (see figure 2.5).

The present chapter introduces the approach to SLR the process and gives some explanation of the uses of SLR generated data.

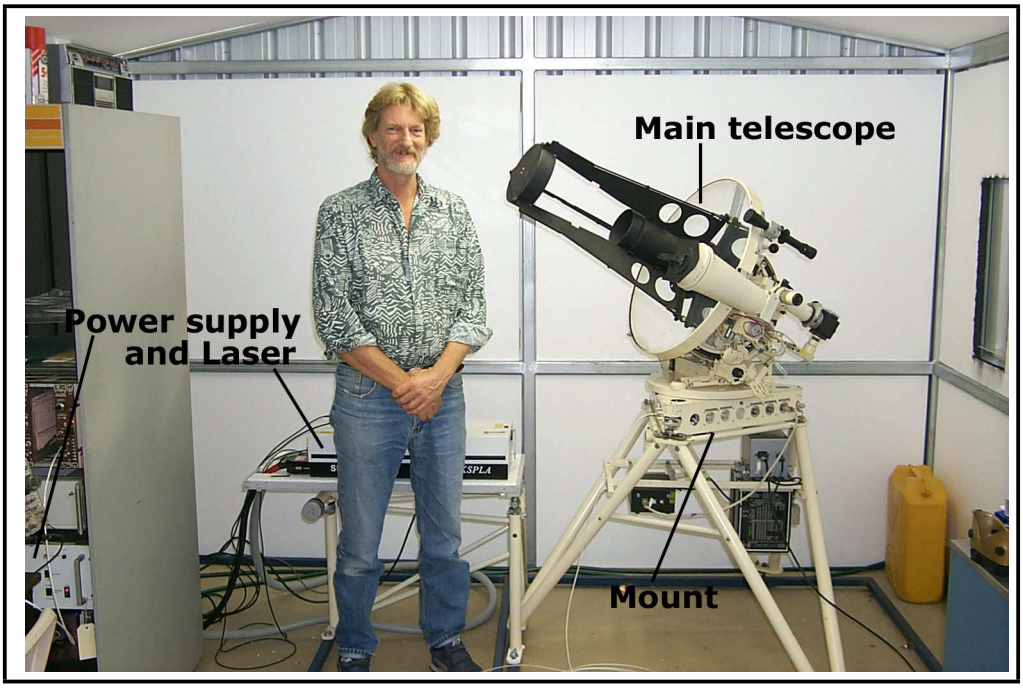

Figure 2.5: The PSLR showing the telescope, mount, laser and most of the ancillary electronic equipment.

2.4 Overview of the Satellite laser ranging Process

Satellite laser ranging forms an important part of several areas of scientific endeavour from geodetic studies to lunar orbital determination and measurement of the Earth's gravitational field.

The SLR process involves firing a laser beam from a ground station at a specially equipped satellite. The laser beam is reflected from the satellite and the return beam is collected and detected by the SLR ground station. The time of flight of the laser beam t is recorded and a range measurement R is calculated as half the time of flight multiplied by the speed of light in the atmosphere $\acute{c}$ (Degnan, 1985),

$$R = \frac{1}{2}\acute{c} \times t. \tag{2.1}$$

As well as measuring the distance to the satellite, the direction of the satellite

relative to the ground station is noted from the pointing direction of the ground station telescope. The position of the satellite can then be determined as the ground station position is known so the position of the satellite can be calculated from its relative direction and distance from the SLR station.

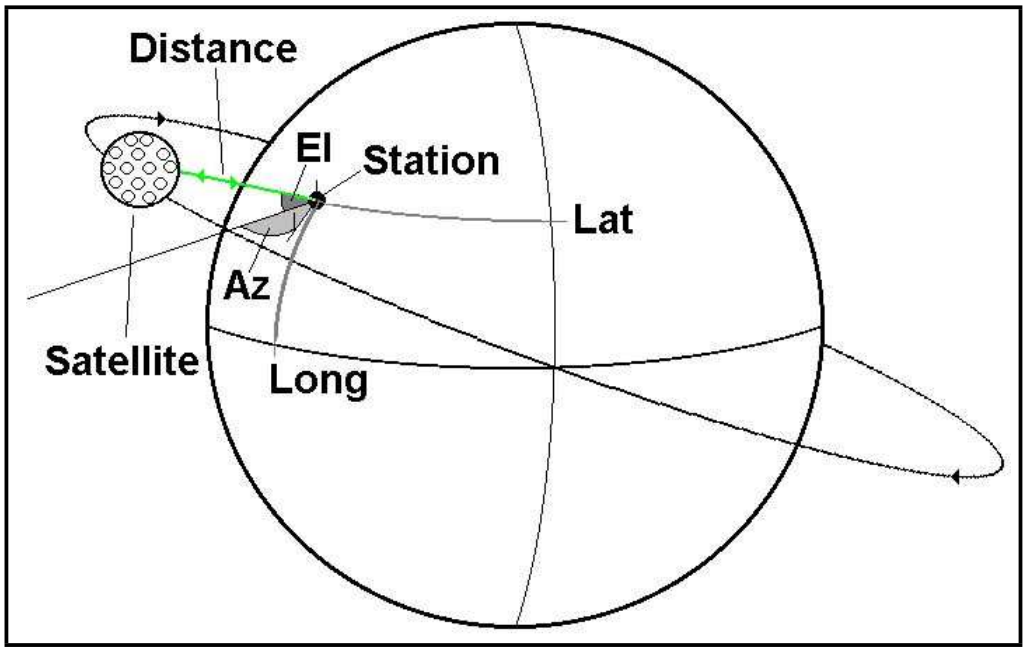

Figure 2.6: Representation of the position determination method used by SLR stations.

This is illustrated in figure 2.6. The angles marked as El and Az indicate the pointing direction of the station telescope. El refers to the elevation of the telescope from local horizontal and Az refers to azimuth or angle measurement from due north. The distance is measured by the time of flight of the laser beam. The position of the satellite with respect to the centre of the Earth is determined using its relative position to the SLR station. This is possible as the SLR stations position with respect to the centre of the earth is known. The position of the satellite can now be determined in the same reference frame as the station. This is commonly called the terrestrial reference frame and the inclusion of the satellite into this reference frame allows for some interesting science. If several laser shots to a satellite are recorded as the satellite travels over the SLR station, an orbital arc is obtained. This allows orbital modelling calculations to infer an entire orbital ephemeris. If

this is combined with orbital arcs from other stations, a highly accurate orbital determination can produce a highly accurate orbital ephemeris. From the simple determination of distance and direction it is possible to predict to within a couple of millimeters the position of a satellite. Depending on the satellite of interest these predictions may allow accurate ephemeris calculations to be performed for several days (LAGEOS). Low Earth Orbit satellites may require several updated predictions every day to calculate accurate ephemerides.

So how is all of this precise orbital determination achieved?

Satellite laser ranging stations are comprised of several sub-systems. These include:

1. Laser source
2. Detection system
3. Event timing instrumentation
4. Station timing/atomic clock/GPS
5. Transmitting and receiving telescope(s) and optics
6. Satellite tracking/mount positioning facilities
7. Data calculation and analysis software
8. Communication

The major processes involved in tracking a satellite and acquiring SLR data are shown in figure 2.7, for systems similar to the PSLR. The first step before any tracking run is retrieval of the appropriate Inter Range Vector (IRV) file from one of the International Laser Ranging Service (ILRS) data centre servers. These IRVs provide information so the SLR station computer can complete step 2, calculation of the satellite ephemeris information before a tracking run. The control computer uses this ephemeris information to position then move the telescope mount so that

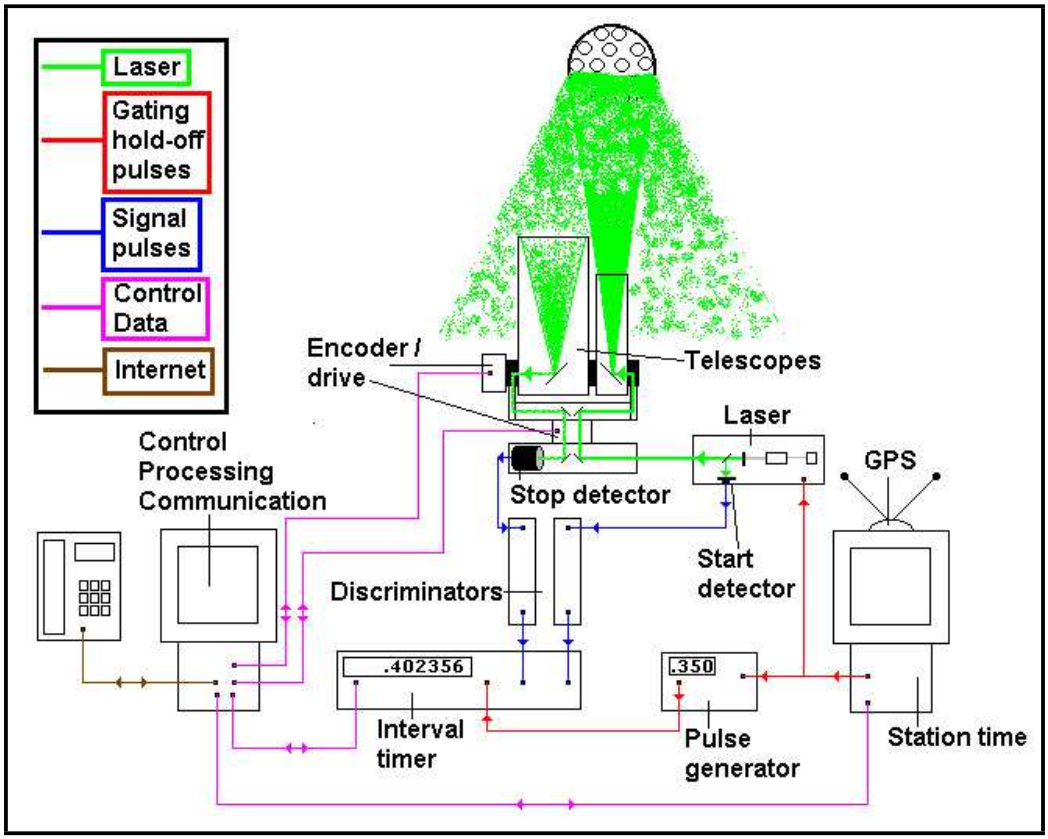

Figure 2.7: Schematic representation of a typical SLR engaged in satellite tracking. This diagram shows the major systems and how they are interconnected.

the telescopes are looking at and following the position of the satellite to be tracked. The position of the telescopes is critical so the ephemeris information is calculated so a position can be fixed at a given time. This time is provided by the station timing system. The timing system consists of at least 1 GPS unit which consistently synchronises the station time to UTC within 100 ns or better. The timing system may also make use of Caesium or Rubidium primary frequency standards or some other type of high precision frequency synthesiser to provide time to the SLR station when the GPS is unavailable.

Once the telescope(s) are following the position of the satellite, the laser is instructed to fire. It is common for the laser to fire on at the beginning of a second (as determined by the station timing system) at a rate determined by the distanced to

the satellite. This rate will ensure that there will be only one laser pulse in transit at any one time so the closer that satellite to the Earth, the faster the possible firing rate. The pulse that causes the laser to fire will also trigger the pulse generator. The purpose of the pulse produced by the generator is covered in section 2.4.3. The laser beam, as it exits the unit, has a small percentage of the beam directed onto a high speed optical sensor (shown as the start detector, figure 2.7). This produces an electrical pulse that is passed to a discriminator. The discriminator is designed to filter the output from the sensor and reject any pulse that is considered to be noise. It also either shapes the input pulse or produces another pulse which will be suitable for use with a time interval counter. When a definite signal is produced, the discriminator produces an output pulse that is used to start the operation of the interval counter. By this stage the laser beam has passed through the directive optics of the mount, exited the output telescope, and begun the journey to the satellite. While figure 2.7 shows the beam being expanded by the telescope, this is not the case. The beam diffraction is kept to a minimum but due to the enormous distances it travels, the beam will expand considerably.

If the previous processes have been sufficiently accurate, the laser beam will intercept the retroreflector equipped satellite. The retroreflectors will reflect the beam from the satellite back along the original path. The divergence of the beam may be affected slightly by the retroreflectors giving rise to a very weak beam by the time it has returned to the tracking telescopes. A portion of the return beam (which may only constitute a single figure number of photons) is collected by the main receive telescope and focused onto the stop detector (see figure 2.7). This will produce an electronic pulse that is directed to a discriminator which eventually stops the interval timer.

The time interval recorded by the interval timer, the position of the telescope mounts as indicated by the axes encoders, the station time, and various other sensor information is recorded by the processing computer at some time during the laser transit process described above. Depending on the satellite being tracked, this could

result in several thousand laser transit samples while the satellite is visible to the tracking telescopes.

The information is combined both at the station and later, via an internet connection, at a data centre (with other SLR station data), to produce a detailed orbital path for the satellite. It is this information that is used for various scientific applications such as: precise orbital determination, geodesy, gravitational analysis and global environmental modelling.

The above SLR process can be described as conventional. It is the type of process utilised by the PSLR and, as a consequence, the equipment and methods used in the conventional process are discussed in greater detail in the dissertation. Other equipment and methods are discussed where there is an expectation that, as the PSLR instrument evolves, some use will be made of these.

Detailed descriptions of the equipment used in the above sub-systems is the focus of chapter 3. The following sections will introduce these sub-systems and indicate how each is involved in the SLR process.

2.4.1 Laser source

While most people are familiar with lasers, somewhat fewer have knowledge or experience with pulsed lasers. Pulsed lasers do not constantly produce light output and, for a variety of reasons, the output is deliberately switched on and off. Pulsed lasers are ideal for SLR systems as they have two distinct advantages over constant wave (CW) lasers.

1. As pulsed lasers blink on and off it is possible to use this feature for ranging/timing. The departure of the laser pulse from the laser can be detected by high speed photodetectors (such as PIN diodes) if a small part of the pulse is directed into a detector.

2. Pulsed lasers have the ability to produce very high power levels per pulse.

As an example the PSLR laser, at its maximum, produces a primary pulse of 250×10^{-3} Joules. This pulse has a duration of approximately 130×10^{-12} seconds. As power equals energy divided by time the pulse power of the PSLR laser is 1.92×10^{9} watts.

This high power will ensure that at least some photons will make the round trip through the atmosphere, via the target, so they can trigger a return detector. The majority of SLR systems around the world still use this type of pulsed laser. Many systems, such as the "SLR2000" (Degnan, 2001), have moved away from such lasers and have opted for much lower power with far higher repetition rates. The laser planned for use with the SLR2000 is a diode pumped microchip laser operated at an output energy of 135 μJ with a 2 kHz repetition rate. While the return signal is very small (typically much less than 1 photon per pulse), the signal can be extracted from background noise using post-detection Poisson filtering techniques. While not as straightforward as time of flight measurement using an interval timer, it makes the SLR2000 eye safe and removes the need for high voltage,and high current power supplies. The SLR2000 laser unit will operate on 1 watt from a DC power supply. The PSLR laser power supply uses close to 2400 watts and requires the use of a large heat exchange unit.

The laser ranging process begins with the firing of the laser source. This process is slightly different when using a high repetition rate laser so all references to the process will assume a low repetition rate system using a time interval counter rather than an event timer.

The laser source fires and is directed into an output telescope. This laser fire event triggers a detector which in turn starts the interval counter. The output telescope will be following the path of a satellite at this time so the laser beam will be directed towards the target/s located on the satellite. The telescopes and optical designs used by various stations can vary significantly.

2.4.1.1 SLR telescope types

While there are many varied designs and schemes in use throughout the SLR community, in general there are two types of optical schemes, paraxial and coaxial. Each type of optical system has its advantages and drawbacks. With a coaxial system the output laser pulse and return pulse use the same telescope system. Paraxial systems separate the output optical system from the return optical system and requires two telescopes.

Paraxial systems use two telescopes so it is possible to use significantly different optics in each telescope system and it removes the need for flip mirrors or spinning apertures to isolate the transmit and receive optical systems.

A coaxial system is easier to align, maintain and calibrate. Coaxial systems use a single telescope so common alignment and differential flexure are not problems. They do require some method of preventing the output pulse from entering the return detector before it has made the journey back from a target satellite. This can be accomplished using a mechanical flip mirror which will flip in and out of the optical path to either let the laser pulse exit or direct the return pulse to the detector. Optical separation can also be achieved using specially designed optical splitters, polarisers and de-couplers. Once the laser pulse has left the SLR output path it must pass through the atmosphere as it travels to the satellite. This presents a set of problems that must be overcome if the laser beam is to successfully hit the target.

2.4.1.2 Atmospheric effect on laser transmission

Light, like all electromagnetic radiation, is affected by the medium through which it travels. When light moves from one medium to another there is a change of speed where generally the higher the electron density, the slower the speed of light in the medium. This change in speed also causes light to bend or refract. The amount and direction of bending is principally a result of the difference in density of the two mediums and the frequency of the light. The Earth's atmosphere is

not a homogenous medium and contains gases, aerosols and other particulate which complicate the determination of the effect of the medium change. The atmosphere is also much denser at sea level. The change in atmospheric density from the surface of the earth to space is also not constant. The result of these factors is that as light is transmitted through the atmosphere there is constant but uneven bending or refraction of the light. As the laser beam from an SLR station must end up at the right point in space and the speed of the beam must be known for accurate range calculations, it is essential that the amount of refraction and the average velocity for the trip is known. The amount of refraction expressed as a deviation in angle from one medium to another is expressed by Snell's law which is shown in equation 2.2 and demonstrated in figure 2.8.

$$\frac{n_1}{n_2} = \frac{sin\theta_2}{sin\theta_1} \tag{2.2}$$

where n_1, n_2 are the refractive indices of the two mediums and θ_1 ,θ_2 are the angles of the beam from the local zenith.

If the Earth atmosphere is composed of concentric spherical shells with well defined refractive indices, the optical path length from a ground station to a satellite could be determined by knowing the initial launch angle of a light beam and determining path lengths through each shell using Snell's law. As the atmospheric refractive index is non-uniform and approaches the value for a vacuum ($n = 1$) with increasing distance from the surface of the Earth, any calculation of path length must contain the integral of refractive index with respect to distance. The optical path length for a pulsed laser source is given by (Abshire and Gardner, 1985),

$$R_0 = \int_{r0}^{r1} \frac{n_g}{\sin\theta} dr, \tag{2.3}$$

where the value n_g is the group index of refraction and the angle θ is determined by Snell's law for a spherically stratified medium.

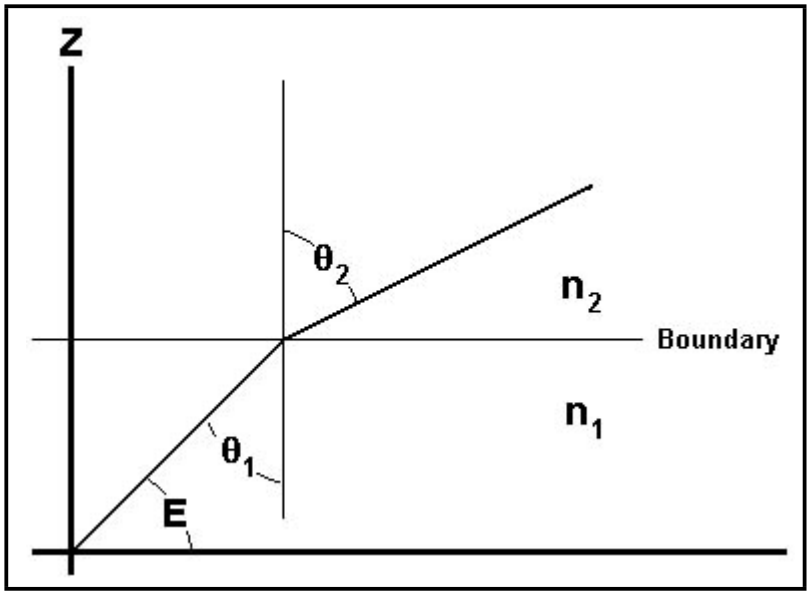

Figure 2.8: Graphical example of Snell's law, where E is the elevation at which the light beam starts through the atmosphere, Z is local zenith and the boundary marks the transition from one atmospheric shell to another.

In the case of a ranging station, θ depends upon the position of the station (latitude, height above the centre of the earth) and the angle of launch of the light beam. This could be determined using (Abshire and Gardner, 1985),

$$nr\cos\theta = n_0 r_0 \cos\theta_0, \tag{2.4}$$

where n_0 is the local refractive index, r_0 is the local distance from the centre of the Earth, θ_0 is the launch or zenith angle of the light pulse, and θ is formed by the line from the centre of the Earth, parallel to the pulse launch angle and the actual optical path as shown in 2.9(Abshire and Gardner, 1985).

If n_g is expressed in terms of the group refractivity N_g for air it becomes (Radarmet, 2002),

$$n_g = 1 + 10^{-6} N_g. \tag{2.5}$$

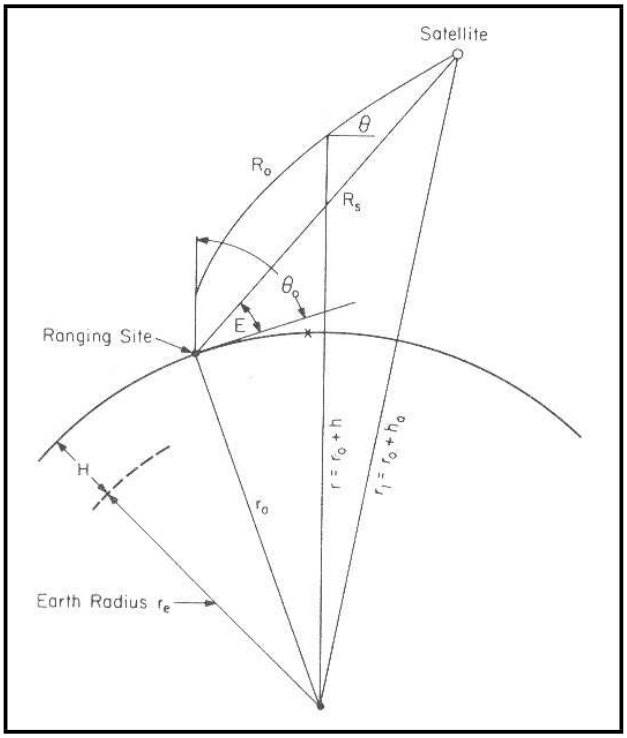

Figure 2.9: Station/target geometry showing the true range R_s, verses the optical length R_o.

If the group (average) refractive index can be determined then the atmospheric or range correction AC can be calculated by (Abshire and Gardner, 1985),

$$\begin{aligned} AC &= R_0 - R_s \\ &= 10^{-6} \int_{r0}^{r1} \frac{n_g}{\sin\theta} dr + [\int_{r0}^{r1} \frac{dr}{\sin\theta} - R_s], \end{aligned} \tag{2.6}$$

where R_o and R_s are the optical path length and the true range respectively (see figure 2.9).

The terms in equation 2.6 can be grouped so that the first term is the residual group velocity error and the second term is the difference in the true range R_s (straight line path) and the optical path R_o. While the path error can produce a range uncertainty of 3 - 4 cm below elevations of 10^0, and given that in practical laser ranging applications observational elevations are above 20^o, and this term

becomes almost negligible above elevations of 30^o, this error is ignored (Abshire and Gardner, 1985). The group velocity error ranges from 2.5 m at zenith to almost 13 m at elevations of 10^o (Degnan, 1985), which certainly can not be ignored This results in a simple estimation of atmospheric correction for pulsed laser systems expressed in terms of θ (already determined) and N_g.

The group refractive index N_g can be estimated at optical wavelengths by taking a number of atmospheric readings which yield the wet and dry air density and the wet and dry air refractivity at defined wavelengths. This was simplified by Marini and Murray in 1973 by taking numerous atmospheric readings and improved over time to yield an empirical formula for N_g (Abshire and Gardner, 1985),

$$N_g = (\frac{273.15}{1013.25}\frac{P}{T}n_g) - 11.27(\frac{e}{T}), \text{ and} \tag{2.7}$$

$$n_g = 287.6155 + \frac{4.8866}{\lambda^2} + \frac{0.068}{\lambda^4}, \tag{2.8}$$

where λ is the wavelength of the ranging laser in μm, (P is the total atmospheric pressure in hPa, T is the temperature in K, e is the partial pressure of water vapour also in hPa, all surface measurements at the station), n_g is the group refractive index of standard air with 0.0375% CO_2, T = 273.15 K, P = 1013.25 hPa, and e = 0.0 hPa. Calculation of e can be achieved by (Mendes and Pavlis, 2002),

$$\begin{aligned} e =& 0.01exp^{\alpha} \\ \alpha =& 1.2378847^{-5}T^2 - 1.9121316 \times 10^{-2}T \\ &+ 33.93711047 - 6.34316453T^{-1} \end{aligned} \tag{2.9}$$

This simple atmospheric correction calculation is ideal for SLR stations as it only requires local atmospheric measurements to be taken at the ranging site. Since most stations do not range below 20^0 (although the stations that can is increasing consistently), as attenuation below this elevation reduces signal intensity significantly,

the Marini-Murray model is still useful. It can reduce a range error of 2.5 m at an elevation of 90^0 to between 0.5 - 1.5 cm (Degnan, 1985). If the determined atmospheric range correction figure is far less than than the precision level of a stations equipment, then there would be no need for a better estimate of atmospheric effect. As equipment and expertise has increased, it is possible to record single shot ranges to the millimeter accuracy level. The atmospheric uncertainty is now, by far the largest contributor to range uncertainty. For this reason a good deal of work has focused on improving models and techniques to remove atmospheric uncertainty. There are two ways to effectively determine the atmospheric uncertainty (Abshire and Gardner, 1985):

1. Take terrestrial measurements of the air column at several widely spaced points around the ranging station to improve the correction model.

2. Directly measure the refractivity of the path travelled by the ranging laser.

The atmospheric correction model mentioned above in equations (2.5 - 2.9) relies on the assumption that the atmosphere is spherically uniform at a given range which means that it assumes a vertical refractivity gradient but no changes in refractivity "horizontally" in the atmosphere. As this is not the case, some estimation of the horizontal refractivity gradient must be added to the correction model. This requires placing atmospheric sensors at some evenly distributed distance around a ranging site. This does not measure atmospheric turbulence. Turbulence can be thought of as micro mixing of the air mass caused by temperature and pressure fluctuations. These fluctuations in pressure and temperature cause fluctuations in the refractivity that cannot be accurately determined by modelling. The RMS path length deviation due to turbulence at elevation angles $\leq 10^0$ can be up to 1 cm but may only contribute a few millimeters at higher elevation angles.

One method of eliminating many of these errors is termed "two-colour" laser ranging which is able to directly measure the refractivity of the atmosphere for every laser shot. The speed of EM radiation propagation through a medium is a

result of the effective properties of the medium and the frequency of the radiation. If it is possible to measure the speed of propagation for two frequencies then it is possible to infer the properties of the medium. It is possible to obtain a value for atmospheric correction AC by obtaining the optical path lengths for two different frequencies, using SLR techniques. Specifically (Abshire and Gardner, 1985),

$$\begin{aligned} AC =& \gamma(L_2 - L_1), \text{ where} \\ \gamma =& \frac{n_{g2} - 1}{n_{g2} - n_{g1}}, \end{aligned} \tag{2.10}$$

given, L_1, L_2 are the optical ranges at λ_1, λ_2, and n_{g1}, n_{g2} are the group refractivities at λ_1, λ_2.

Although this seems an attractive option, in practice the task of differentiating between the optical paths of two frequencies is quite difficult with the difference in actual optical path length being very small. To obtain any useful data, a system capable of measuring the propagation time of the two frequencies to a few picoseconds is required. Currently the only instrument able to do this in real time is a streak camera. The streak camera has a photocathode at the front of the detector, a screen at the far end of the detector, and a set of plates under the influence of a very high speed swept magnetic field. Photons returning from a satellite strike the photocathode and produce photoelectrons. These photoelectrons are accelerated to sweep plates where an ultra fast electric field is increased across the plates. The photoelectrons will deviate dependant on the electric field strength and will be deviated differentially dependant on their energy. This energy will be determined by the frequency of the photon and the work function of the photocathode (see section 3.3.2.1, page 78). They will form an image on the distant screen with the initially produced photoelectrons at one end of the image, and the later photoelectrons at the other. This provides a mechanism for separating the return signal to retrieve

temporal information. The image on the screen will appear as a spacial sequence of dots. The intensity of the dots will be proportional to the energy of the particular photoelectron that produced the dot. By comparing the distance between dissimilar dots, the difference in propagation time can be deduced.

A few SLR stations throughout the world have introduced or have plans to introduce "two-colour" laser ranging. At this time it is not really feasible to equip a portable system with "two-colour" capability. With the advent of "two-colour" laser ranging at other sites, the improvement in the understanding of the effect of the atmosphere on range results should improve modelling and thus benefit all SLR systems.

2.4.1.3 Signal link considerations

Once a laser beam has travelled from the SLR station through the maelstrom of the atmosphere it will, if all has gone according to plan, hit the target satellite being tracked. There are several tens of satellites commonly tracked by the SLR community. Although the designs of the satellites vary greatly, they all share one common feature. All of these satellites are equipped with target retroreflectors. Retro or corner reflectors comprise three flat mirrors that meet at a common corner with all the flat mirrors 90^0 apart. Solid retroreflectors are more common and can be imagined as a slice diagonally through a cube (which was completely silvered on the outside) yielding two identical halves or two retroreflectors.

The effect of retroreflectors on a beam of light is illustrated in figure 2.10. When a ray of light is incident on a retroreflector, the light is reflected in an exact path, parallel to the initial incident light but in precisely the opposite direction. This ensures, in the event that a laser beam from an SLR station hits a target satellite, the remnants of the initial beam will be directed exactly back to the SLR station. The returning laser pulse will then repeat the path of the initial pulse and return to the SLR station. Retroreflectors are essential to ensure that a signal is returned, as the initial signal sent from the SLR station is in part absorbed or scattered by the atmo-

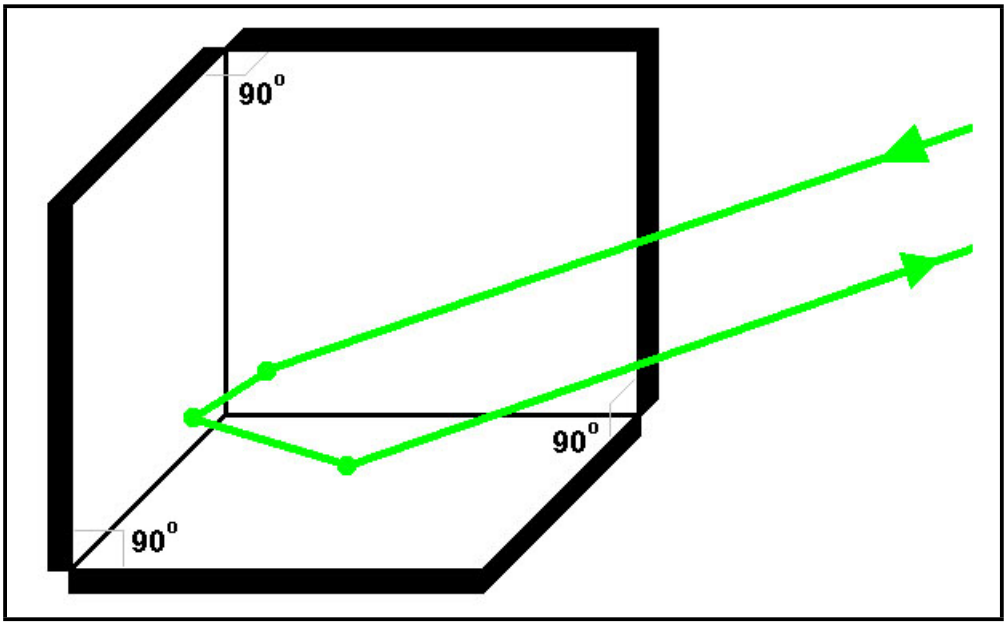

Figure 2.10: Example of the parallel return path of a laser beam when incident on a retroreflector.

sphere and the beam diameter at satellite distances is quite large (due to divergence from a finite aperture source), so only a small portion actually encounters the target satellite. The return beam from the satellite will have a similar divergence so the beam area at the SLR station will also be large. Even with the target retroreflectors mounted on tracked satellites, the signal received at the return telescope is small.

The type, number and orientation of retroreflectors on a satellite will affect the return signal strength at the ground station.

Retroreflector types

The two main types of retroreflectors used for laser ranging targets are hollow and solid quartz. The major difference between these two types is the loss of optical cross section due to the angle of incident. The optical cross section of a retroreflector can be defined by σ_{cc} (Degnan, 1993):

$$\sigma_{cc} = \rho A_{cc}(\frac{4\pi}{\Omega}) = \rho A_{cc}(\frac{4\pi A_{cc}}{\lambda^2}) \tag{2.11}$$

where ρ is retroreflector reflectivity, $A_{cc} = \pi {R_{cc}}^2$ is the light collecting area of the

retro and $\frac{4\pi}{\Omega}$ is the on-axis retroreflector gain where Ω is the effective solid angle occupied by the far field diffraction pattern of the retroreflector.

The target retroreflectors used with the PSLR have a diameter of 62 mm so substituting this value into equation 2.11 and assuming a reflectivity (ρ) of 0.9, the optical cross-section is $3.642 \times 10^8 m^2$

For a circular aperture (once again the most common type) the retroreflector produces a reflected wave with an Airy pattern.

Equation 2.11 is only valid when there is no angle of incident between the direction of the incoming light and the normal of the front face of the retroreflector. If the incoming light is off normal the effective retroreflector area is reduced by the factor (Degnan, 1993):

$$\eta(\theta_{inc}) = \frac{2}{\pi}(\sin^{-1}\mu - \sqrt{2}\mu\tan\theta_{ref})\cos\theta_{inc} \tag{2.12}$$

where θ_{inc} and θ_{ref} are determined by Snell's law (equation 2.2) where θ_{inc} would be represented by θ_1 and θ_{ref} would be represented by θ_2 from figure 2.8.

The quantity μ from equation 2.12 is given by (Degnan, 1993):

$$\mu = \sqrt{1 - 2\tan^2\theta_{ref}}. \tag{2.13}$$

The effective cross-section ends up as (Degnan, 1993):

$$\sigma_{eff}(\theta_{inc}) = \eta^2(\theta_{inc})\sigma_{cc}. \tag{2.14}$$

If η^2 from equations 2.12 and 2.14 is plotted against the angle of incident for a hollow cube, and solid cubes with different refractive indices, it indicates one of the advantages or disadvantages of solid retroreflectors (see figure 2.11).

The hollow retroreflector cross-section in figure 2.11 drops to 50% of the maximum value at an angle of incident of just over 10^o and to almost zero at 35^o. The

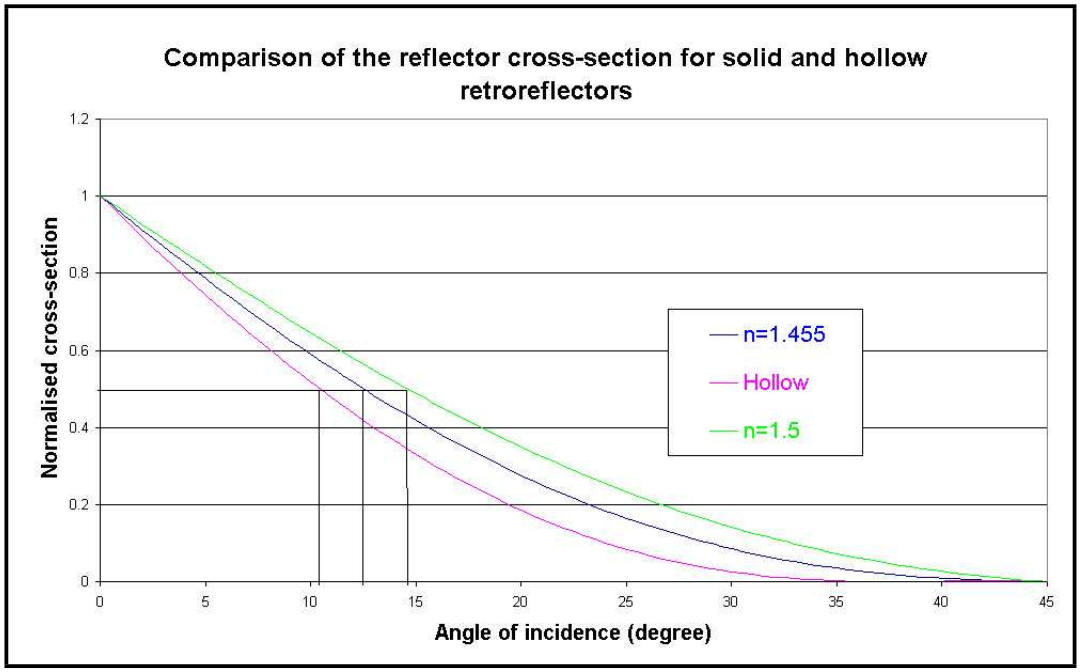

Figure 2.11: Comparison of the reflector cross-section for hollow and solid retroreflectors

.

two solid retroreflectors show that as the refractive index of the construction material increases, it extends the effective angle of incident and increases the maximum angle of incident.

If the maximum reflection cross-section is required then solid retroreflectors are definitely the preferred option. If, for some reason a smaller off-normal effective cross-section and solid retroreflectors are preferred over open retro's, the solid retro can be recessed into a holder thus giving the same on-normal cross-section but restricting the effective angle of incident.

One other consideration when choosing retroreflectors is the velocity aberration induced by the high perpendicular velocity of a satellite with respect to the propagation direction of a laser pulse. This effect is expressed in figure 2.12.

As the velocity increases the aberration also increases. If the FFDP is angularly small then it is possible that the velocity aberration will cause the return signal from the retroreflector to fall outside the field of view of the receive optical system even

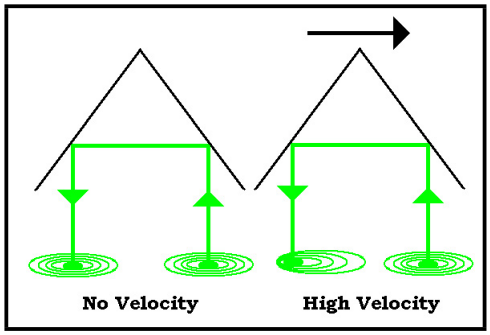

Figure 2.12: Illustration of the effect of a laser returned by a retroreflector at the high orbital speeds of some satellites. The rings represent the far field diffraction pattern (FFDP)of a normal pulsed laser. The right hand side of the figure shows how this FFDP is 'skewed' when reflected by a retroreflector at high perpendicular velocity.

with perfect telescope pointing. Velocity aberration becomes a problem with LEO satellites where the tangential velocity is high due to the low orbit. In such cases it is necessary to increase the FFDP of the retroreflectors on the satellite. This is generally done by increasing the dihedral angles of the retroreflector by less than two arcseconds or even grinding a lens into the face of the retroreflector (Degnan, 1993). This is known as 'spoiling' of the retroreflector.

Satellite optical cross-section

A satellites optical cross-section depends mostly on the number of retroreflectors attached to the satellite but is also largely dependant on their orientation on the satellite. Irregular shaped satellites may have only a single retro or an entire array (such as TOPEX-POSEIDON). These retroreflectors are placed at nadir if possible to allow consistent ranging. In general the size of an array depends on the normal orbital height of the satellite, the higher the orbit, the larger array as the up-link signal will be smaller at greater distance. This holds true for the spherical geodetic satellites with STARLETTE (960 km), LAGEOS (6000 km) and ETALON (19200 km) having average optical cross-sections of $0.65 \times 10^6 m^2$, $7 \times 10^6 m^2$ and $60 \times 10^6 m^2$ respectively (Degnan, 1993). The diameter of these satellites is larger dependant on the orbital height in order to place more retroreflectors and increase the cross-

section.

For spherical satellites the on-axis (no angle of incidence), or maximum optical cross-section can be expressed by (Degnan, 1993):

$$\sigma = \frac{\sigma_{cc} N}{2}[1 - \frac{\sin^2(\frac{\theta_{max}}{2})}{(\frac{\theta_{max}}{2})^2}] \tag{2.15}$$

where, σ_{cc} is the on-axis optical cross-section of the retroreflector/s used on the satellite, N is the number of retroreflectors mounted on the satellite, and σ_{max} is the maximum angle of incidence on the retroreflectors that will give an optical cross-section (see figure 2.11).

Equation 2.15 will over estimate the satellite optical cross-section as it does not factor in the velocity abberation.

In order to estimate the average number of photoelectrons produced by a stations detector (MCP, SPAD etc) the satellite optical cross-section, the optics of the SLR, and the atmospheric conditions need to be taken into account.

Radar link equation

The radar link equation is used to estimate the photoelectron average. This figure allows system designers to determine if it will be possible to actually perform laser ranging. If the photoelectron average is lower than the noise or detection threshold of the conditioning electronics, then it will not be possible to detect a return from a satellite.

The radar link equation is expressed as (Degnan, 1993):

$$n_{pe} = \eta_q (E_T \frac{\lambda}{hc}) \eta_t G_t \sigma (\frac{1}{4\pi R^2})^2 A_r \eta_r T_a^2 T_c^2 \tag{2.16}$$

where η_q is the detector quantum efficiency, E_T is the laser pulse energy, λ is the laser wavelength, h is Planck's constant, c is the speed of light in a vacuum, η_t is the transmit optics efficiency, G_t is the transmitter gain, σ is the satellite optical cross section (from equation 2.15), R is the slant range to the target, A_r is the effective area of the receiver telescope aperture, η_r is the efficiency of the receive

optics, T_a is the one-way atmospheric transmission, T_c is the one-way transmissivity of cirrus clouds (if present).

The slant range is given by (Degnan, 1993):

$$\begin{aligned} R = & -(R_E + h_t)\cos\theta_{zen} \\ & + \sqrt{(R_E + h_t)^2\cos^2\theta_{zen} + 2R_E(h_s - h_t) + h_s^2 - h_t^2} \end{aligned} \tag{2.17}$$

where R_E is the radius of the Earth, h_t is the station height above sea level, h_s is the satellite altitude above sea level and θ_{zen} is the angle between the elevation value and zenith.

The transmitter gain $G_t(\theta)$ is based on the quasi-gaussian beam profile produced by most SLR lasers (including the PSLR laser) and is expressed as:

$$G_t(\theta) = \frac{8}{\theta_t^2} exp[-2(\frac{\theta}{\theta_t})^2] \tag{2.18}$$

where θ_t is the far field divergence half-angle between the beam centre and the $\frac{1}{e^2}$ intensity point and θ is the beam pointing error. As the beam pointing error is generally far smaller than the beam wander induced by atmospheric turbulence, θ is often replaced with this angle when determining transmitter gain (Wettzell, 2003).

The transmitted beam is generally truncated by an output aperture or obscured by a secondary mirror. If the output telescope is also the receive telescope (Cassegrain) there will be an obscuration of the beam and if there is a separate output telescope (refractive) then it will radially truncate the beam. If the beam is obscured by a secondary mirror it will cause a transfer of energy from the central lobe to the outer rings of the gaussian profile and refractive telescopes tend to concentrate the energy in the central lobe. The transmitter gain used in the radar link equation (2.16) should reflect these effects.

The effective receiver area is a result of the area of the primary mirror, the obscuration ratio (secondary radius (b_r) divided by the primary radius (a_r)) and a term that accounts for a spatial filter (pin hole) in the optical path or the detector. This is expressed as (Degnan, 1993):

$$A_r = A_p(1 - \gamma_r^2)\eta_D(\gamma_r, \frac{kR_D}{2F_s}) \tag{2.19}$$

where A_p is the area of the primary mirror (assuming it was a complete mirror i.e. no central hole), γ_r is obscuration ratio $\frac{b_r}{a_r}$ and,

$$\eta_D(\gamma_r, \frac{kR_D}{2F_s}) \tag{2.20}$$

represents the fraction of the incoming light intercepted by the detector of radius R_D.

If the detector diameter is sufficiently large and there is no limiting aperture, then η_D is approximately 1.

Atmospheric attenuation T_a^2 is a complex subject and beyond the scope of this dissertation. It depends on wavelength, slant path through the atmosphere and atmospheric constituents. Attenuation is a result of absorption of the beam by atmospheric constituents such as ozone, carbon dioxide and water vapour and scattering. The Mie scattering (by aerosols which are approximately the same size as the light wavelength) is more prevalent.

Cirrus cloud cover (high wispy cloud) is often present in the sky even if it is barely visible. It has been experimentally verified that the cirrus cloud transmission T_c can be expressed as (Degnan, 1993):

$$t_c = exp[-.14(t \sec\theta_{zen})^2] \tag{2.21}$$

where, t is the cirrus cloud thickness and θ_{zen} is the zenith angle at the telescope pointing direction.

The expected number of photoelectrons produced at the input of a detector can now be computed. This figure will determine if the system is capable of effective satellite laser ranging.

As an example of the calculation of the link budget, the number of estimated photoelectrons produced by the PSLR detector when fired at LAGEOS at zenith and with almost perfect visibility would be 262 (with some assumptions made) . This figure was produced with an online calculator (Wettzell, 2003) that is based upon the radar link equation. The MOBLAS systems would produce 612 photoelectrons for the same satellite and conditions (Degnan, 1993).

2.4.1.4 Target satellites and mission types

Many types of satellite are tracked by SLRs for a number of purposes. The most common types tracked are geodetic, Earth sensing, positional (GPS, Glonass (GLObal'naya Navigatsionnay Sputnikovaya Sistema)), and experimental instrumentation. Consequently, there are a number of designs of retroreflector arrays. The position of these arrays on the space vehicles needs to be accurately known as the range is always taken to the satellites centre of mass.

The geodetic satellites are easily recognisable as they resemble a "disco ball". They are small, dense, round and are studded with retroreflectors. The LAGEOS (LASer GEOdynamic) satellites are a good examples of this type; see figure 2.13 These satellites are placed in inclined orbits (measured from the East) with LAGEOS-1 at $109^o.84$ and LAGEOS-2 at $52^o.64$ and at an approximate distance from the Earth's surface of 6000km. They are classed as passive satellites as they have no means of propulsion, no on-board power or any sort of detector. The orbits that these satellites are placed in are very stable. The combination of these factors allows the acquired tracking data to be used to establish a terrestrial reference frame. In effect the position of the satellite is taken as perfectly known and the surface of the Earth is plotted against it. This also allows the change in position of an SLR station, due to tectonic motion, to be determined over time. As this shift is

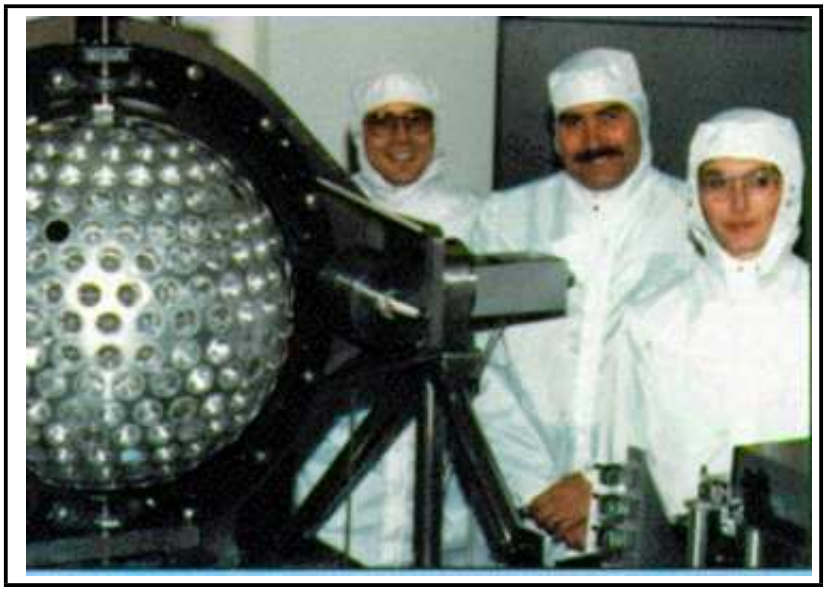

Figure 2.13: Photo of the as yet unlaunched LAGEOS 3 satellite. This satellite is all but identical to LAGEOS 1 and 2.

only a few millimetres a year, SLR is the most precise method of determination although the various radiometric techniques [GPS, Very Long Baseline Interferometry (VLBI)] also maintain a very high standard. Small perturbations in the orbit of geodetic satellites will also map the gravitational profile of the Earth. High mass areas (mountain ranges) will cause dips in the satellite orbit which can be extracted from SLR data. It can also be used to detect the changing mass/gravity profile due to the circulation of the Earth's oceans.

Altimetry satellites are designed to measure surface heights using a satellite based, down looking active instrument (see figure 2.14)(NASA/JPL, 2002). An example of a altimetry satellite is TOPEX/Poseiden. It uses a microwave pulse round trip elapsed time to measure the sea surface height. It uses a time of flight method to measure the distance from the satellite to the surface of the sea. In order to determine the height of the sea surface, the position of the satellite must be known precisely. This precise position is determined using SLR data. The altimetry data is especially accurate if multiple SLR stations are simultaneously ranging to the satellite while the altimeter measures the sea height.

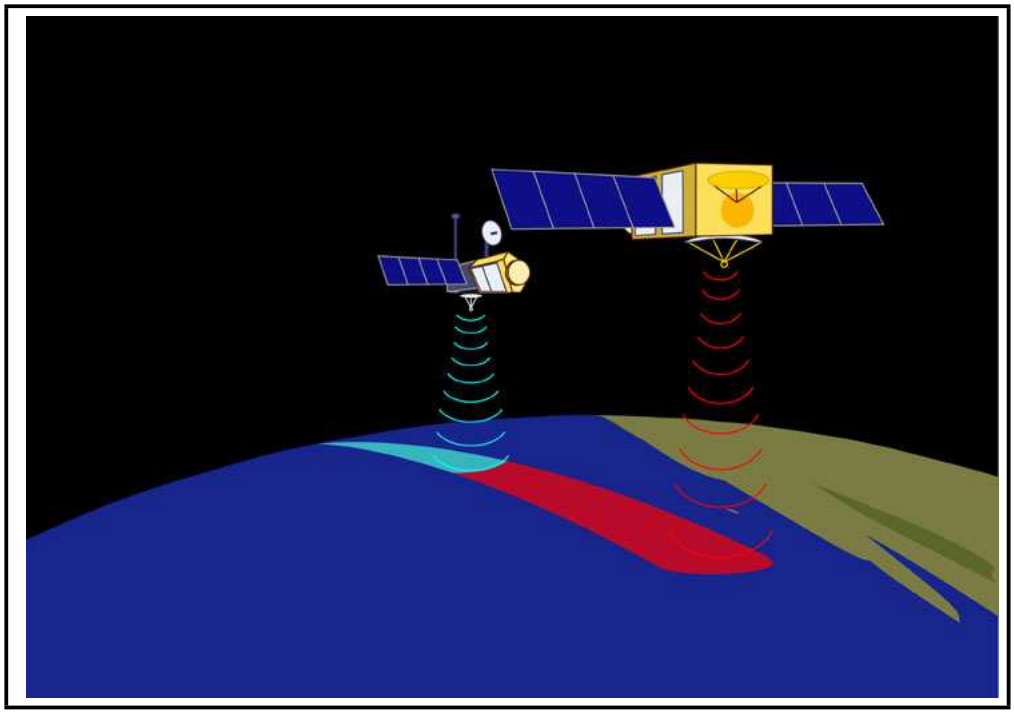

Figure 2.14: Illustration of the Jason 1 altimeter operating in the same orbit but a few kilometers ahead of the Topex/Poseidon altimeter.

The term positional satellites refers to GPS or Glonass satellites. These types of satellites are high orbiting (around $>$ 20,000 km orbital radius) and form part of a structured network. Each satellite broadcasts a radio signal which can be used by a ground based detector to triangulate its position and to calibrate the onboard clock. These satellites are placed in a number of carefully selected orbits and are spaced in these orbits so that any ground based user with an unobstructed sky view will always have a line-of-sight to at least three satellites. At worst this will allow the ground based detector to determine its position to within 100 m. With care, the best equipment, and use of the non-degraded GPS signal, this can be reduced to the millimeter level over a period of time. SLR plays a role in calibrating the radiometric ranging measurements performed by GPS by collocating with receivers at SLR stations and comparing the data sets. All of the Glonass satellites have retroreflector arrays but only two GPS satellites are similarly equipped. These type of satellite are not heavily tracked as they are capable of self-positional determination

and the altitude of the satellites makes them impossible to track for many SLR systems.

Experimental or specialist missions cover anything that is not included in the other categories. SLR support for such missions may be for calibration of onboard position finders, precise time related/full rate orbital positioning for science applications or as the principal orbital determination method if the satellite based system fails. One such example of an experimental mission supported by SLR tracking is the Gravity Recovery and Climate Experiment (GRACE) (see figure 2.15 (GFZ, 2000)).

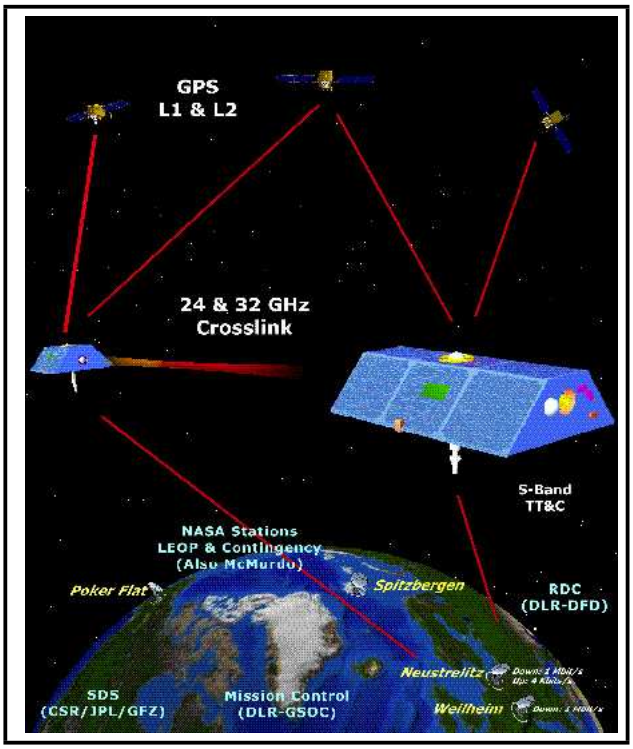

Figure 2.15: Illustration of the orientation and instrument payload of the GRACE mission.

This consists of two space vehicles in exactly the same orbit but separated by a distance of a few hundred kilometers.

Each space craft is almost identical and contains accelerometers, a GPS receiver, a star camera, a K-band (radar) ranger and a retroreflector array (see figure 2.16 (GFZ, 2000)).

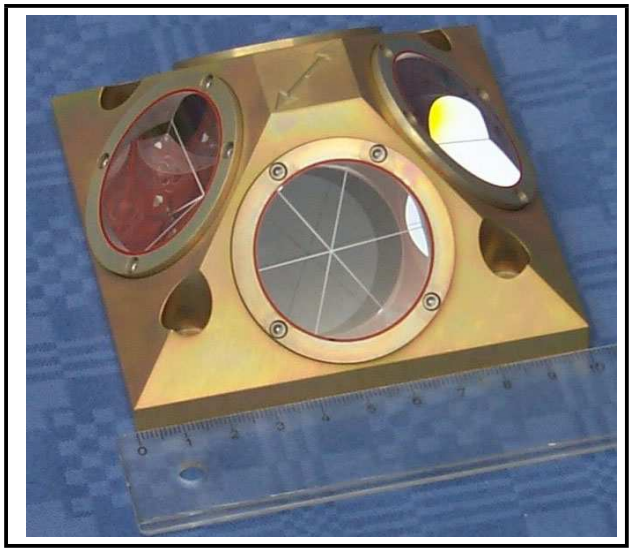

Figure 2.16: Image of the retroreflector array fixed to the GRACE space vehicles. As the retroreflector array is always at nadir, at least one retro will be visible to SLR stations.

The K-band ranger measures the distance between the satellites, the star cameras are used to measure the satellite orientations, the positions of the satellites are determined by GPS and locked in using SLR data. Since the two satellites are in the same orbit and separated by only a few hundred kilometers any perturbations in the gravitational field of the Earth will effect each satellite at slightly different phases. This sensitivity to smaller gravity variations by a comparison of the orbits of two satellites will allow higher frequency terms to be included in the Earth's gravitational field model.

Once the signal from any satellite target has reflected from the corner cube reflector (CCR) and it has completed the return journey through the atmosphere, it is collected and directed to a very sensitive detection device.

2.4.2 Return detectors

There are two types of commonly used detectors in the SLR community, photo tube (PMT, MCP) and semiconductor (PIN diode, SPAD). PMTs consist of an evacuated glass tube, a front plate made of metal, some sort of electron multiplication stage, and a collector at the rear end. The front plate, the electron multiplier elements and the collector are all electrically connected and have a voltage applied which creates a voltage gradient from the front plate to the collector. When light is incident on the front plate electrons are produced by the photoelectric effect. These electrons are then focused into the electron multiplication stage (EMS) of the detector. In a standard PMT (such as the type used with the PSLR) the EMS consists of a series of focused metal dishes. As electrons strike the metal dishes more electrons are removed. Each dish (or dynode) is focused so that the electrons that leave are focused onto subsequent dynodes. The Microchannel plate (MCP) EMS used quite extensively by SLRs works on the same principle. Instead of a series of focused dynodes a multiple set of small tubular channels are placed between the front plate and collector. Electrons are focused into the channels and progress down the tubes under the pull of the electric field gradient. As electrons strike the walls of the channel more electrons are knocked off and continue down the tube. These secondary electrons produced by the EMS eventually hit the collector. The collector is connected across a load so when the stream of electrons hit a voltage pulse is produced as the electrons proceed to earth. This pulse is used to stop a timer.

Semiconductor detectors used in SLR are based on the most simple of semiconductor devices, the diode. A diode is a two-element device that has two wafers of either silicon or germanium, with each wafer doped with a different material giving rise to a positive potential and a negative potential wafer. This produces a potential barrier in the centre of the device. These devices can be operated in "forward" or "reverse" biased condition. When reversed biased there is only a very small amount of current flowing across the diode. If a photon enters the device, electrons can be produced, jump the potential barrier and result in a detectable pulse.

PIN diodes are a variation on the basic design where a central wafer of undoped or intrinsic material (either silicon or germanium) is placed between the doped wafers. This aids in signal detection as it speeds up the signal transit time through the diode.

If the design of the diode is altered yet again by adding other wafers of differently doped material in to the diode structure, it is possible to produce avalanche regions within the device. This means that a produced photoelectron when it journeys to the avalanche region reacts with the lattice to produce 2 or more electrons. These electrons repeat this process and produce an avalanche of electrons from a single photoelectron. The SPAD (single photon avalanche diode) is a special case of the avalanche diode in that it requires only one photon to produce that first photoelectron and instigate the avalanche pulse. These devices are becoming more and more popular in the SLR community.

The choice of which device to use is based on a number of factors. These include, size, cost, pulse and gain characteristics, active area and average return signal strength. Each of the return detector devices mentioned have advantages so the choice of which to use is determined by the SLR system design.

2.4.3 Event/Interval timing

Interval counters are commonly used through out the SLR community. Interval counters work much the same as a normal-stop watch. One event starts the timer and one event stops the timer. The time interval is then recorded by the timer. They have many function that are not available with the common stopwatch. The SR620 time interval counter used with the PSLR is able to time with an accuracy of 25 ps RMS (about the time it takes light to move 7.5 mm) and can repeat this at a rate of 100 Mhz. As well as a start input and a stop input, they have an external gate input. This can be configured to improve the timing performance using a specially generated "hold-off" pulse. This pulse will produce the following action (see figure 2.17):

1. When the front edge of the pulse is detected, arm the start input.

2. When the start input receives a pulse from the laser start detector, start the timer.

3. Arm the stop input when the gate input detects the rear edge of the "hold-off" pulse.

4. Stop the timer when the stop input receives a signal from the return detector.

This type of precaution in necessary when using a time interval counter for determining laser pulse time of flight, especially during the day. As the return detectors used in SLR are so sensitive, it is common for stray photons to trigger the detector even after careful filtering.

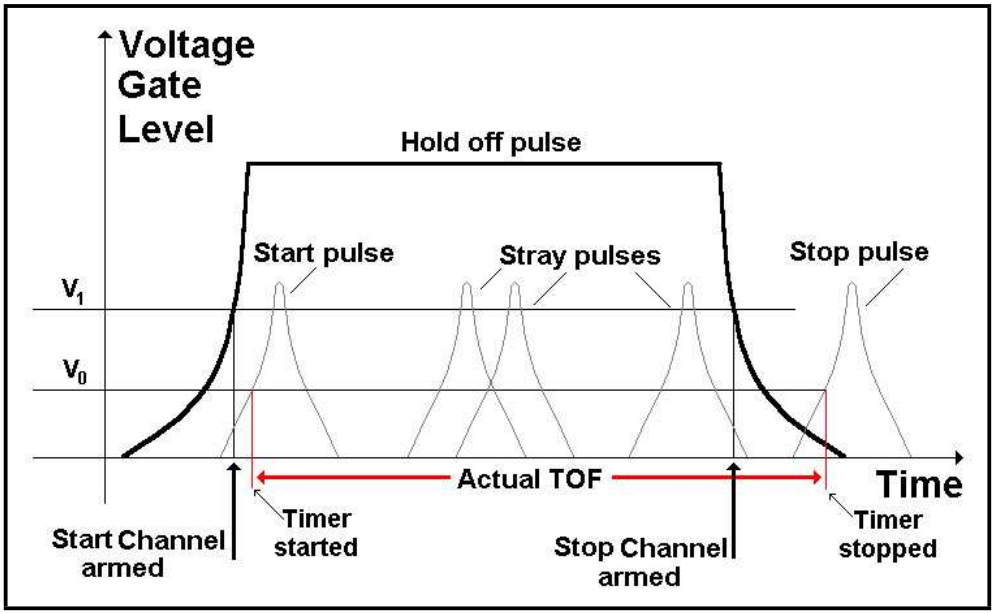

Figure 2.17: Example of the operation an interval counter in hold off/external mode. The start channel is armed when the hold-off pulse exceeds voltage level V_1 and the stop channel is armed when the pulse drops below this level. The timer is started by the first pulse to exceed V_0 at the start channel after arming and the timer is stopped by the first pulse to exceed V_0 at the stop channel after arming. All other pulses are ignored.

After the raw pulses from the "start" and "stop" detector are passed through a discriminator stage in an effort to remove any noise pulses and to condition the pulses sent to the interval counter, it is possible to produce very accurate "time of flight" readings for the round trip time from station to satellite.

2.4.4 Station timing

Positional determination for SLR requires very precise information about a satellite's orbit. This determination is generally done at each SLR station using an orbital model for the particular satellite of interest. In order to accurately calculate the orbit, a set of inter-range vectors (IRVs) are supplied for each satellite. These provide a velocity, a position, and the time for that position. These IRVs give this positional information in a terrestrial reference frame which is valid for any position on Earth with time given in a similar universal time frame. This time is called universal coordinated time (UTC). The stations need some method of keeping their clocks locked to UTC so that the orbital calculations will be valid in the universal reference frame. UTC is kept by a series of caesium atomic clocks.

Many SLR stations have local caesium or rubidium atomic clocks to register UTC. Even if it were feasible to take the local unit to the bank of clocks used to generate UTC and set it by these clocks the local unit time would eventually drift away from true time. Some method of transferring time from the UTC clock to the station clock constantly and remotely is needed. The GPS network is ideal for this purpose.

As GPS is also a satellite tracking method so it requires absolute position and time. Position is determined by calculating distances to a number of satellites. Distance is calculated by measuring the time interval between the sending of a signal from a GPS satellite and a receiver. The signal from the satellite is timed stamped so that the actual time in UTC of transmission from the satellite is known. If a series of satellites all send time stamped signals to a receiver, the receiver can calculate actual UTC time and set its own clock accordingly. The beauty of this

system is it is almost free of drift as the GPS receiver time is constantly updated. Each GPS satellite is constantly updated by ground stations so it maintains correct time and this is passed onto the station based receivers.

Station time, as well as being essential for correct satellite positioning, is required for good data analysis. Many stations use the UTC second to fire their laser. If a station has a fire repetition rate of 5hz it will fire the first shot exactly on the second with a 200ms period before the next shot and the 5th shot will occur exactly on the next second. All of the returns are now calibrated exactly with UTC. In some ranging applications this is essential as a satellite may be being tracked by multiple stations simultaneously (especially in Europe where there is high station density). If all of the stations fire on the second and at the same rate, individual returns from each station can be directly compared.

Given that all of the timing applications are adequately take care of, the directing of the laser pulse to the target requires that the orbital determination precision is matched by the accuracy of the opto-mechanical systems of station.

2.4.5 Satellite tracking/mount positioning

To hit a satellite with a laser beam, some knowledge of where the satellite is and a means of steering the laser beam to that point are needed. The first step is to determine where the satellite is. This process is a cooperative effort between the SLR station and the data analysis centres that provide the IRVs used to determine the satellite track. The analysis centres use the satellite data to improve the orbital calculations for the target satellites so that they can generate better IRVs. The better the IRVs are then the better the tracking data. For some satellites, new IRVs may need to be generated and sent to the SLR stations more than once a day and the tracking data sent back to calculate the next set of IRVs and so on.

The IRVs from the data centers are integrated into a geopotential field model for the satellite orbit type and this is transformed to station coordinates. The resulting calculation provides a set of coordinates and tracking velocities for the axes of the

station telescope. These take the form of an elevation (0° - 90°) and an azimuth (0° - 360° with due north being 0°/360°). The velocity will be an angular velocity and depends on the particular drive system for the telescopes. Many telescopes use positional motors to drive the telescope axes. A positional motor has some method of moving a set rotation rather than continually revolving. The two main types are servo and stepper motors.

The positional motors position the axes but some method of accurately registering the mount orientation is needed. Optical encoders are ideal for this purpose. There are many types of optical encoder but they all have a light source, a detector and a scaled grating. The scaled grating moves past the detector or the detector moves past the grating depending on which is connected to the moving parts. The light illuminates the grating and the detector in the encoder counts the transitions from light to dark as the grating moves past the detector. As the grating is scaled, either in angle, relative or absolute position, information on position can now be provided. Mounting encoders so that they move with the axes will provide the required orientation information. The change in mount orientation over time can be inferred using the encoders, giving a method of following the path of a satellite through the sky.

To track a satellite the telescope initially points to the position of the satellite at the current time and then moves to the next calculated point at the calculated velocity. The position is marked by the encoders connected to the axes and the velocity of the axes is determined by the speed of rotation of the motors or positional change per unit time of the axes encoders. If the axes are not at the next position at the correct time as measured by the axes encoders, the motor speed can be increased by the control program. If the hardware and control program are well designed then satellite tracking will proceed smoothly.

The only other concern is the actual seeing direction of the telescope. While the encoders on the axes may indicate that the telescope is looking in a particular direction, the actual looking direction is affected by several factors. It is impossible

to fabricate a telescope or mount that is perfect. Imperfection in fabrication can cause seeing errors dependent on the orientation of the telescope. This could be the result of 'bumps' in the axis tracks, non-orthogonality of the axes or tilt in either axis, problems with the optics, or sag of the telescope due to the mass distribution. The seeing direction is also largely affected by the atmospheric conditions. The fabrication error can be quantified for orientation of the telescope by pointing at a series of stars. If a star's position is well known and the telescope is pointed at the expected position then moved until the star is centred in the field of view, the difference in position can be recorded. If this is repeated for a number of stars (100 or so) at several positions in the full range of orientation, then a pointing profile can be constructed. This can be modelled to give offset equations that can be applied to all pointing coordinates. The path of a laser beam (and all light) through the atmosphere bends due to refraction. This path can be corrected by applying a model based on local atmospheric readings (see section 2.4.1.2, page 22).

Even with the corrections to the pointing direction of the telescope to achieve the correct seeing direction, it is still not always possible to track a satellite straight away. Occasionally the telescope needs to be corrected either by software or a human operator. Assuming that the seeing direction is very close to the actual direction, the telescope is nudged toward or away from the direction of travel until returns are received. Once the satellite is located the system should be able to remain locked to the satellite. At times many adjustments to the pointing direction must be made to track a satellite during a pass. It is not common to track satellites below an elevation of 20^o as the increase of the path through the atmosphere is difficult to pierce with a laser beam and the increased refraction makes correction of the actual direction to the seeing direction very difficult especially as many of the atmospheric correction models become erratic at low elevations.

When returns are received from a satellite and data is collected on the time of flight, pointing direction, station time, ground target calibration, and atmospheric data, this has to be turned into tracking information.

2.4.6 Data Analysis

SLR systems have many inherent areas of uncertainty in the range determination. Some of these errors are systematic and can be corrected in the data (permanent range or time biases). Additionally there is a great deal of random uncertainty introduced because of laser beam jitter, detector efficiency (due to environmental effects) and from atmospheric interactions.

These errors are reduced using a statistical approach. The raw or single-shot data error is far larger than the "Normal Point" reduced data. The MOBLAS-5 SLR at Yarragadee reports a single-shot RMS uncertainty of 10 mm and a normal point RMS uncertainty of 2 mm to LAGEOS satellites (Allied Signals, 1999).

The data are reduced to normal point format in the following way based on the Herstmonceux normal point recommendation (Sinclair, 1997).

1. Using high precision range predictions, a set of prediction residuals PR is generated using $PR = observation - prediction$

2. Using a suitable window, remove large outliers which may adversely affect the calculations.

3. Solving for a set of orbital parameters to produce a trend function f with the value $f(PR)$ at the epoch of the residual PR. This is fitted to the prediction residuals to remove any systematic trends.

4. Compute fit residuals FR using $FR = PR - f(PR)$. Compute the RMS of the fit residuals and identify outliers using a rejection level of $n \times (RMS)$. This rejection level is determined by the type of return beam detection. For multiple photon detection systems $n = 3.0$ and for first or single photon detection systems $n = 2.5$. This lower rejection levels for single photon systems is due to these being prone to skewness towards longer ranges.

5. Iterate steps 3 and 4 until the process converges. Previously rejected data should be re-included at step 4 for each iteration.

This set of steps reduces the data set by rejecting data which is obviously well outside the expected RMS range. Once this has been done the normal point data can be produced.

1. Sub-divide the range data points into appropriate bins. The bin sizes are determined for each satellite and depend on orbital characteristics, where stable orbits (i.e. LAGEOS) allow larger bins.

2. Compute the mean value of the fit residuals $\overline{FR}$ and the mean epoch (or time of occurrence of the mean value) for each bin.

3. Locate the observation O with its fit residual FR, whose observational epoch t is nearest to the mean epoch for each bin.

4. The normal point is now calculated as

$$NP = O - FR + \overline{FR}. \tag{2.22}$$

5. Compute the RMS of the accepted fit residuals in each bin by

$$RMS = \sqrt{\frac{1}{n}\sum(FR_j - \overline{FR})^2}, \tag{2.23}$$

   where the summation over j is over the accepted points within the bin.

The result of this process and the normal point formation is the fit residual for the particular point (which is basically the random error of the single shot) is subtracted from the point and the mean of the fit residuals is added. This reduces the random error of the normal point to the random error of the bin. If the trend function is well fitted, then this value should be almost zero (or at worst a few millimeters).

The normal point scheme is used as the range measurement instead of the mean as the detector-satellite range is generally skewed so the data are not symmetrical about the mean. The normal point is a much better estimate of the real range value.

Once the data has been collected and processed by the SLR station it needs to be distributed to the user community so that it can be applied to all manner of scientific investigation. This process has been greatly simplified with the introduction of internet based communication just a few short years ago.

2.4.7 Communication

The SLR network, consisting of the stations, data centres and the user community require a method of distributing data. With the advent of internet communication this process has become streamlined, fast and to a large extent automatic.

The stations are grouped into three networks; NASA, European laser tracking network (Eurolas), and the Western Pacific Laser Tracking Network (WPLTN). The NASA stations deliver data to the NASA data centre, the European stations deliver data to the European data centre and WPLTN stations deliver to both. This data is quality controlled, archived, shared with other data centres and sent to other analysis centres. The analysis centres provide IRVs and time bias (TB) information that is eventually sent back to the tracking stations. End users (geodetic, atmospheric and gravitational scientists etc) can retrieve data from the analysis centres. The data flow channels are illustrated in figure 2.18.

All of this data transfer is conducted either through e-mail or FTP sites and is mostly automated. Many stations are now providing daily data and are updating IRV files at the same rate. Some stations send data many times a day and update IRV predictions more than once. This is especially important for low satellites as their orbits change quite rapidly due to high atmosphere drag. Many of the earth sensing satellites undergo maneuvers during their lifetime and after each move new IRVs need to be provided. The advent of the internet and rapid data dissemination have improved the quality of SLR tracking data.

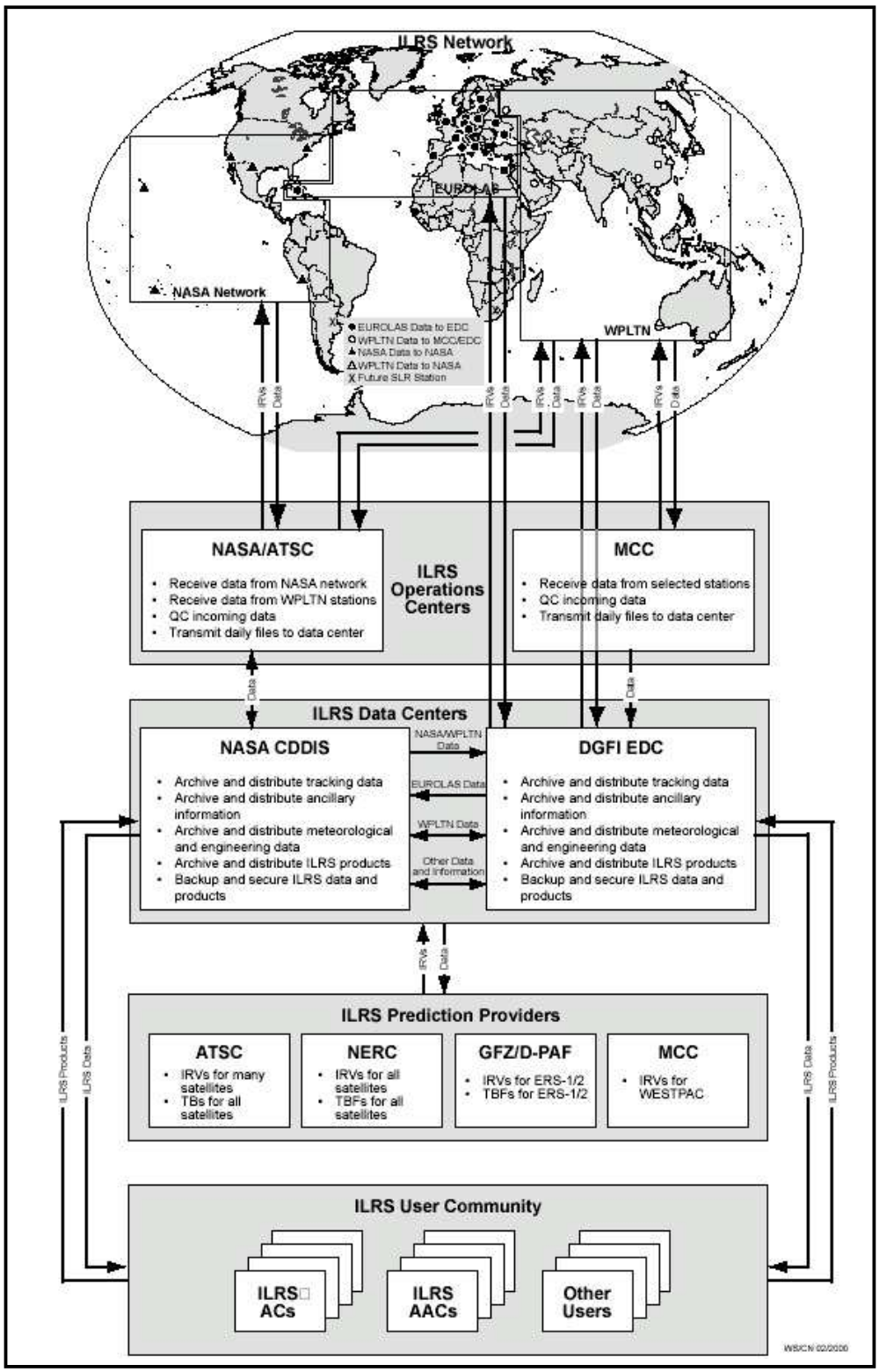

Figure 2.18: Data flow scheme employed by the ILRS.

(ILRS, 2003)

2.4.8 Conclusion

All of these processes are required to provide high quality data to a wider scientific community. SLR involves the integration of a number of sub-systems and components to achieve the exceptional ranging accuracy not available with any other sort of tracking. Equipment and alterations to various methods mentioned in this chapter are constantly changing. The basics for laser tracking of satellites still remain the same; a laser source, a telescope and detector, a timer, and a collection of equipment that ensure all of these components work together in the right order.

This chapter discussed, in a very broad sense, the process of tracking a satellite using optical communication. This thesis concentrates on the development of a such process, with the PSLR instrument. It concentrates on the operation and uses of a range of equipment as it pertains to the development of a SLR process. This is achieved by examining the relevant literature and the manufacturer's manuals or brochures. A great deal of useful information was obtained from the ILRS web site and the internet in general. Lastly it represents the investigation and testing of several of the key sub-systems by the PSLR project team at the Bentley Campus of Curtin University.

Chapter 3

SLR and PSLR components

3.1 Introduction

SLR is a prime example of an applied science which draws from a number of different fields. It makes use of elements from astronomy, optics, mechatronics, radiographic positioning and high speed electronics. A majority of the equipment used with SLR stations is designed to be used as stand alone equipment performing its own specific scientific function (this is evident with the GPS unit, meteorologic equipment, etc). Most of the other equipment is not specifically designed for the purpose it is required to perform with the SLR station (SR620 timer, caesium frequency standard, PMT tube, etc).Very few of the components used with a standard SLR station are restricted to the use they have been employed for within an SLR station.

With the improvements in manufacturing of scientific equipment, coupled with the improvement in electronic data communication, it is possible to order off the shelf equipment or have equipment modified to specification. This equipment could be shipped to almost any location and assembled to create an instrument capable of SLR. Of all of the equipment required to assemble a laser ranging system, only the laser and telescope may require some modification to allow successful use with an SLR.

The skill or science of SLR is in the choice of the available equipment and the

way in which the equipment is used collectively. It is this melding of the appropriate functionality of each piece of equipment and the sequencing of desired events that allows the laser tracking of satellites.

In order to allow this melding and sequencing, it is essential that the performance and limitations of each piece of the SLR station equipment is well understood. Given that the standard design of SLR stations has just about reached the limit of precision, the equipment operation must be optimal. If there is any degradation in the data quality, it is easy to identify the responsible piece of equipment with an optimised system.

To optimise the use of each piece of equipment in an SLR station, it is necessary to understand, in general, the principal of operation of each piece of equipment and, specifically, how this equipment is operated.

This chapter will deal with many of the major components and sub-systems which are assembled to build a satellite laser ranging station. The basic sub-systems can be divided as follows.

1. Laser
2. Detection
3. Filtering : Temporal, Spectral, Spatial, Amplitude
4. Pulse conditioning electronics
5. Event timers
6. Station clock/GPS
7. Telescope, optics and mount (covered in chapter 4, page 170)
8. Mount motion control

The operation of these sub-systems may be the result of one or many components. The operation of many of the individual components will be dealt with in detail

including the specific functions of these instruments which make them suitable for satellite laser ranging.

The general design of SLR systems tends to be fairly constant with all stations requiring all of the sub-systems mention in the previous list, however, there is some variation in the approach and equipment used by each SLR systems. This document is biased to equipment used with the PSLR system or equipment of a similar nature, and will deal with alternative types of equipment where there is common use of this equipment within the wider SLR community.

It will examine the function and specifications of the equipment used with the PSLR to determine how each piece of equipment performs its task within the desired operational parameters for a portable satellite laser ranging system. These operational parameters include:

1. accuracy/precision - is the equipment capable of producing an adequate level of performance (i.e. is this piece of equipment the limiting factor to the PSLR performance),

2. reliability - use in remote locations would require a high degree of reliability,

3. ease of use - for a system to be classified as portable, it must be able to be moved and setup quickly, must be easy to maintain and be simple to repair,

4. commercial substitution - using equipment that is commercially available will facilitate ease of use as replacements and technical support is available.

The suitability of the equipment used with the PSLR will be stated and recommendations as to the desired replacements will be made.

3.2 An Introduction to the laser

The laser is the most obvious component of SLR systems and the development of SLR over the years has closely followed the development of laser technology.

The type of laser used for laser ranging is not at first so self explanatory. The expectation of laser ranging systems to produce unparalleled levels of single shot accuracy requires the laser to produce an accurate and precise beam every time and over time. The laser beam must be able to hit the target constantly and with sufficient energy so that a return is received at the detector. Accurate timing has allowed the use of ultra-fast pulsed lasers. The first laser used for satellite laser ranging was a flashlamp pumped ruby laser and the general use of optically pumped solid state lasers for SLR has continued to this day. The type of laser most used by the SLR stations around the world is the Nd:YAG (Neodymium : Yttrium-Aluminium Garnet) laser. This type of laser has many advantages over other laser types for laser ranging applications.

This section will deal with some of the important theory of laser operation and will concentrate on the operation and properties of Nd:YAG lasers with special emphasis on the EKSPLA SL212 (See http://www.ekspla.com) laser used with the PSLR.

3.2.1 Laser basics and theory

The acronym laser stands for Light Amplification through the Stimulated Emission of Radiation. This rather accurate explanation encompasses the true nature of a laser. Lasers are simply put, light transformers and amplification devices. They take supplied energy, convert it to light then selectively amplify a specific type of produced light.

The production of light, selective amplification and the output of a coherent light beam require several conditions to be met. The three essential ingredients for effective laser product are stimulated emission, population inversion and a suitable lasing cavity. These ingredients and other factors which play a part in the production of a laser beam will be discussed in the following sections.

3.2.2 Stimulated Emission

Stimulated emission was first proposed by Albert Einstein in his 1917 paper "On the Quantum theory of Radiation". Unlike spontaneous emission where an atom in an exited state releases a photon in a random manner, stimulated emission is induced by interaction with a photon. If an excited atom is stimulated by an appropriate photon already produced by an equivalent atom, then the produced photon will be coherent with the stimulating photon (see figure 3.1).

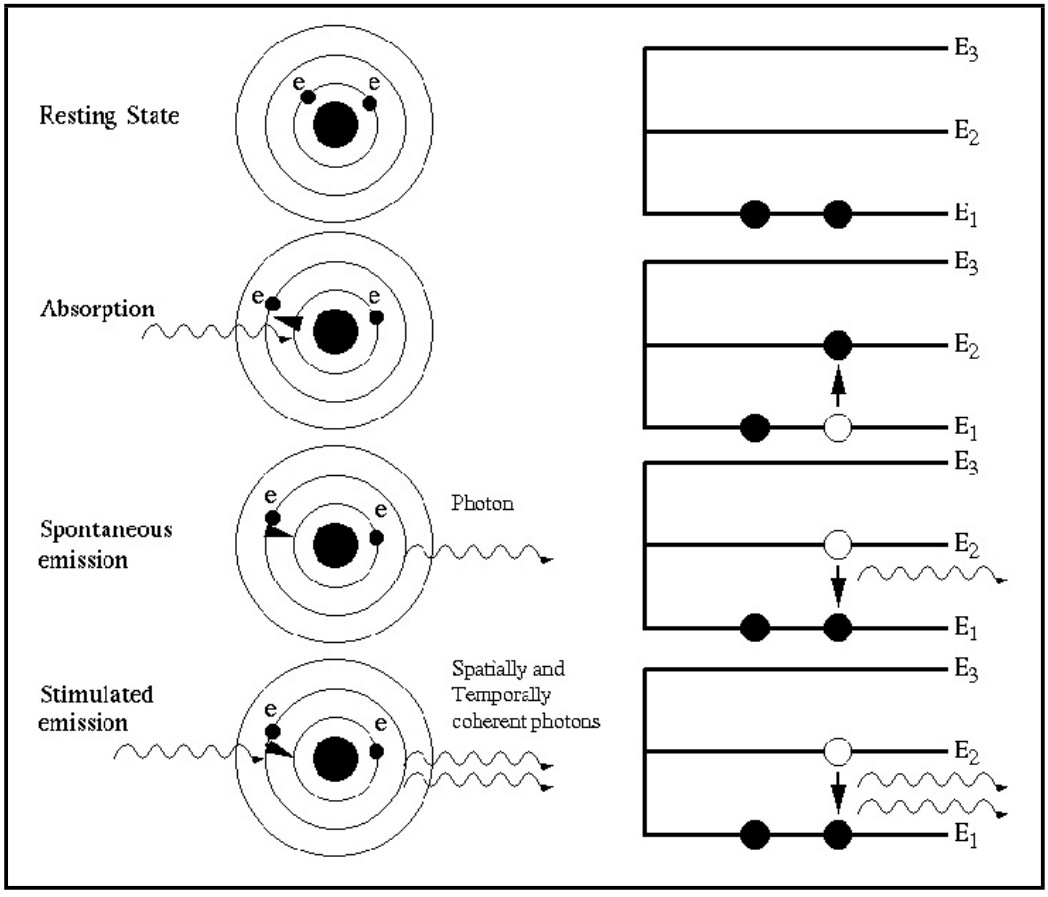

Figure 3.1: Spontaneous and Stimulated emission

This process can continue with the two coherent photons producing four coherent photons and so on until there is a huge population of coherent photons. The process is not quite this simple.

The complication is that for stimulated emission to occur there must be the exact

types of atoms which are all in exactly the same energy state so that photons are able to stimulate emission. In any population of atoms most will not be in an appropriate energy state. As an example the PSLR laser produces a primary pulse energy of 250 mJ. In the Nd:YAG laser the Nd atoms undergo the desired laser transition. This is a shell transition and has an ionisation energy of 5.51 eV (Serway, 1992). This energy is released as a photon when the atom relaxes. This means that each photon contributes $5.51 \times 1.602 \times 10^{-19} = 8.83 \times 10^{-19}$ J to the pulse. If the pulse energy is 250 mJ then there must be at least $250 \div 8.83 \times 10^{-19} = 2.83 \times 10^{17}$ atoms which produce coherent photons. As this process is not very efficient, the number of atoms in the correct energy state must be far greater than the actual number of photons produced. Many either do not react with other atoms but are included in the final pulse, or are off-axis to the beam direction and pass out of the resonant cavity (lasing cavity). Many of the photons are quenched or re-absorbed in the medium and do not contribute to the output beam. All of this is due to the fact that the Nd atoms are doped into a YAG lattice and form only a very small percentage of the total number of atoms present, generally around 1 % (Hecht, 1994). As the rod is relatively transparent to allow the flashlamp optical pulse in, the produced characteristic photons are able to escape.

3.2.3 Population inversion

All lasers require stimulated emission to produce coherent photons. In a pumped laser medium there will be atoms in both excited and relaxed states. Eventually a pumped medium will establish an equilibrium. If there were even numbers of excited and relaxed atoms in a medium then little or no beam would be produced as a photon has as much chance of being re-absorbed as producing stimulated emissions. This problem can be overcome by careful selection of lasing medium.

In every lasing system there is an excitation and relaxation phase. Figure 3.2 represents a four level lasing system. The lasing species is excited to level E_3 and passes through 2 other levels while returning to the ground state E_0. The desired

laser transition takes place between E_2 and E_1 so a photon is always emitted during this transition. If the species state is E_2 when it interacts with an appropriate photon, stimulated emission occurs. In the case of figure 3.2 the chances of this occurring are greatly increased because of a population inversion. The transition system represented in figure 3.2 refers to an excited system. If all of the transitions apart from the actual lasing transition ($E_2 \rightarrow E_1$) are fast and the medium is pumped then eventually a great deal of the atoms will be in energy state E_2. The population of atoms is inverted from the normal state where almost all atoms are at energy level E_0. The result of all of this is that any emitted photon has a much higher chance of causing stimulated emission because there is a large population of atoms at the required energy level. This manipulation to a shifted equilibrium is especially important for Nd:YAG lasers due to their relatively poor efficiency.

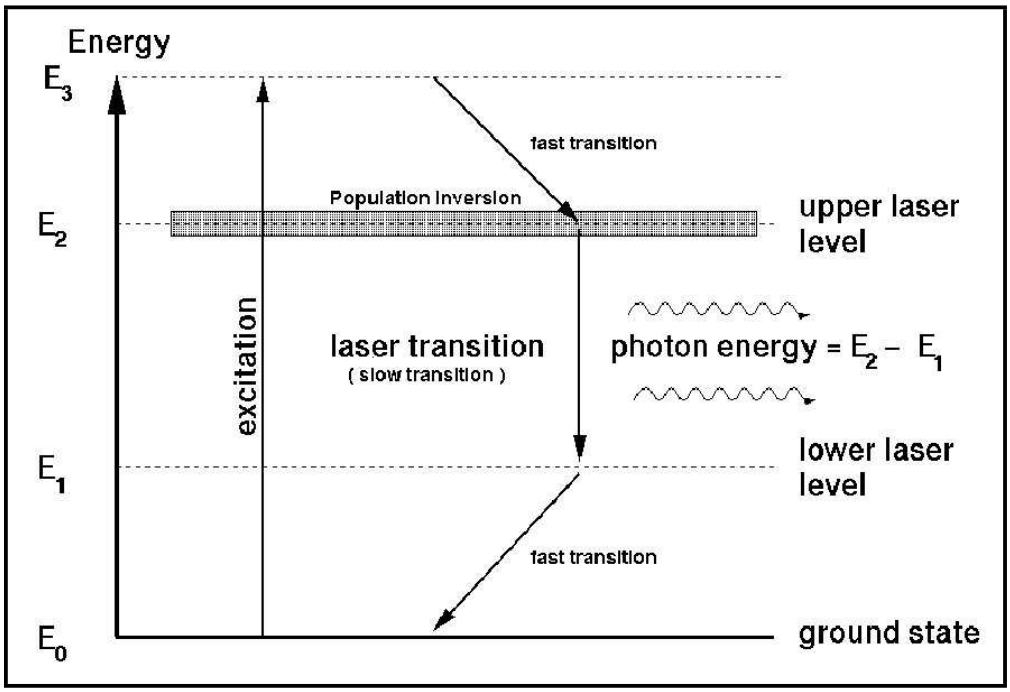

Figure 3.2: Four level lasing system showing a population inversion

3.2.4 Laser cavities

The last essential element of a successful laser system is a properly designed laser cavity. A laser is simplistically speaking an energy transducer and amplification system. The cavity plays the part of a tuned amplifier which has specific gain characteristics. A well designed cavity allows the laser beam to transit through a volume containing excited atoms, amplifying the laser beam while maintaining directional coherence. There are many different cavity designs. This section will deal primarily with the types of cavities used in laser ranging applications and specifically the PSLR.

A laser cavity is essentially a rod or tube of lasing medium encompassed at either end by inward facing mirrors. These mirrors direct the laser light back through the medium within the cavity where the characteristic photons are able to stimulate other emissions. There are several different designs of laser cavity. A laser cavity or resonator is generally defined in terms of the types of mirrors used to enclose the cavity and the spacing between the mirrors. Figure 3.3 (Pressley, 1977) shows a typical resonator cavity with the laser beam path within the cavity shown as the shaded region.

The stability of a resonator refers to the amount of energy lost from the resonator on each beam traverse of the cavity. In an unstable resonator a majority of the energy within the cavity is lost in each pass. Stable resonator cavities are only essential if the gain per unit displacement through the lasing medium is small. For effective laser production several tens of passes may be required. If the gain is high then one or two passes may be more than sufficient to achieve the same output.

A resonator is stable if it satisfies the following condition,

$$0 < q_1 q_2 < 1. \tag{3.1}$$

where $q_1 = (1 - \frac{d}{R_1})$ and $q_2 = (1 - \frac{d}{R_2})$ where the parameters d, R_1 and R_2 relate to figure 3.3.

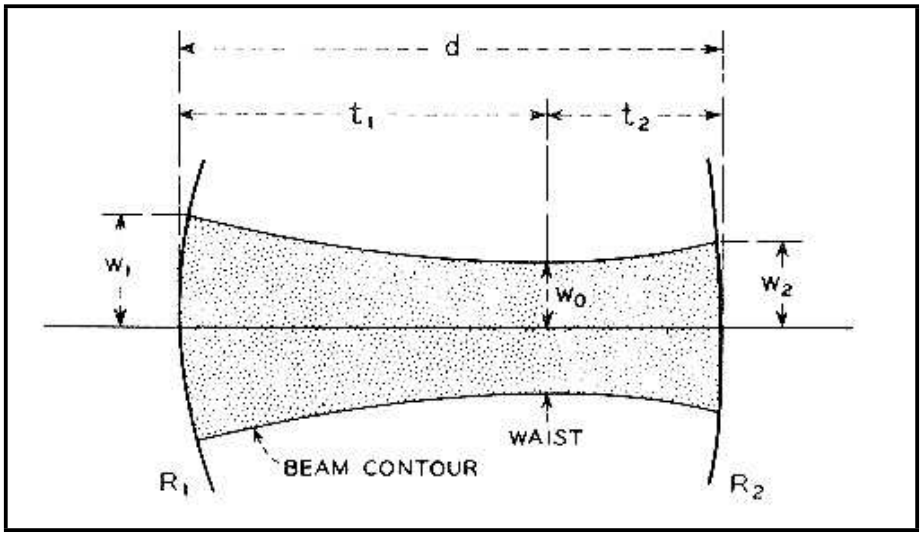

Figure 3.3: Resonator parameters, where $R_{1,2}$ are mirror radii, d is the cavity length, $t_{1,2}$ are the lengths to minimum beam width from each mirror, and $w_{1,2}$ are the beam radii.

Figure 3.4 (Hecht, 1994) shows several different types of resonators. These resonators are all stable (apart from (f))when they obey one of the following conditions:

1. Confocal $R_1 = R_2 = d$
2. Plane parallel $R_1 = R_2 = \infty$
3. Concentric $R_1 = R_2 = \frac{d}{2}$
4. Hemispherical $R_1 = \infty, R_2 = d$

The laser resonator must meet one more condition for effective laser production. Twice the cavity length must equal an integral number of wavelengths of the specific laser frequency,

$$N\lambda = 2 \times L_{cavity}. \tag{3.2}$$

This will ensure, especially in a many-pass laser, that subsequent waves will constructively interfere to increase the laser amplitude or output. As most resonant cavities are many times larger than the wavelengths of the light that they are trying

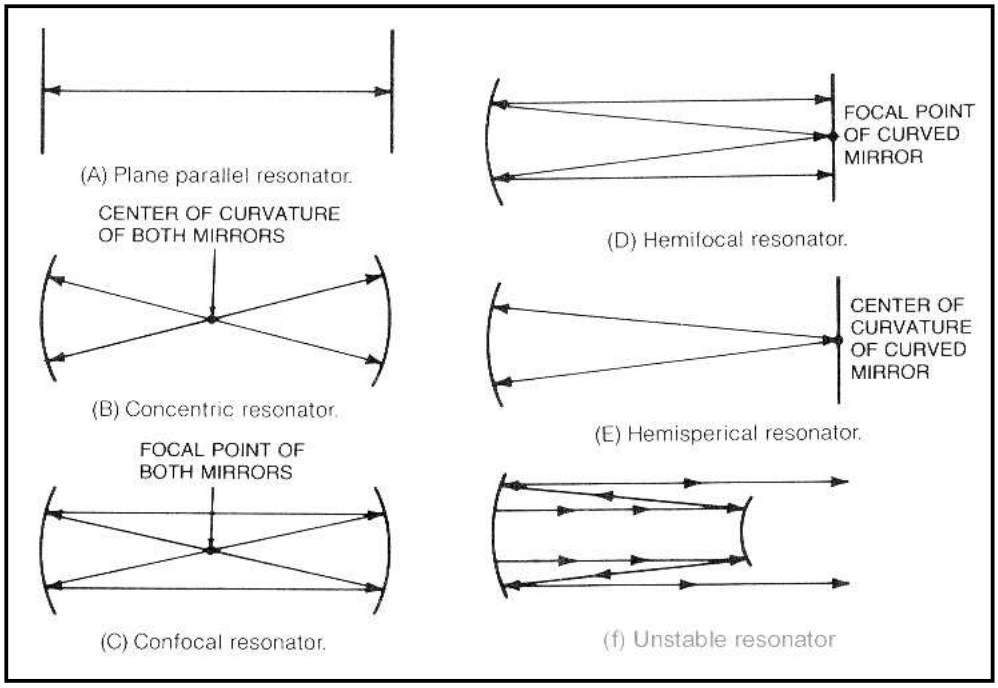

Figure 3.4: A selection of resonator types

to amplify, and laser transitions tend to be smeared and produce photons of many different wavelengths, these wavelengths may also satisfy the conditions of equation 3.2. Resonant cavities have a gain bandwidth or a range of wavelengths which they will effectively amplify (see figure 3.5 (Hecht, 1994)). Figure 3.6 (Arecchi and Schulz-Dubois, 1972a) shows transitions for excited state Nd^{3+} to lower energy states after pumping. The thick vertical line shows the major transition which produces the 1064nm output (when doped into a YAG lattice), but the transition from the ${}^4F_{\frac{3}{2}}$ to ${}^4I_{\frac{9}{2}}$ still represents a quarter of total transitions in an Nd:YAG and, as such, will be strongly amplified in the resonator cavity. Table 3.1 shows the transitions and wavelengths of the emitted radiation from figure 3.6 and the number of wavelengths which satisfy equation 3.2. This shows that the cavity length of 65 mm does not exactly satisfy equation 3.2 for the desired wavelength (1.064 μm). The wavelength shown in table 3.1 (1.0640039 μm) is as close to the desired wavelength so as not to make a great deal of difference. For the PSLR cavity to exactly satisfy equation 3.2 the cavity would have to be 24 μm smaller. The length of the cavity would in all

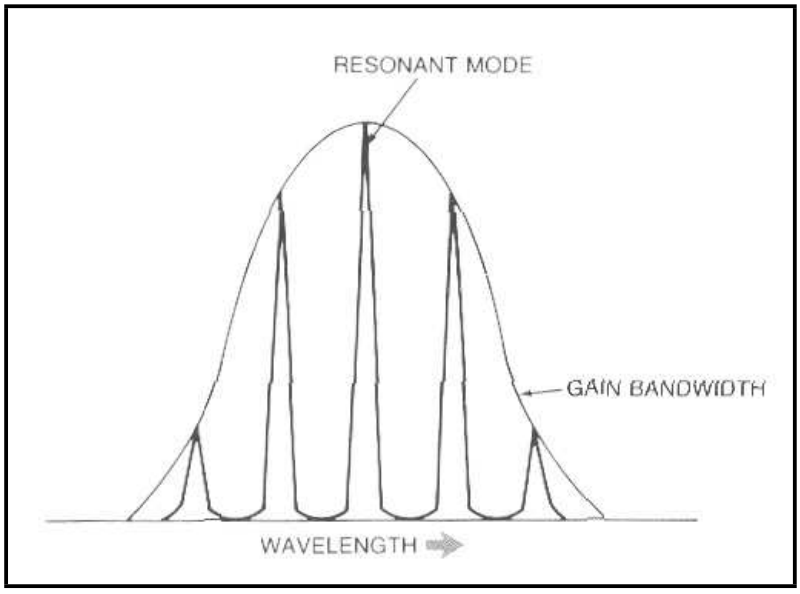

Figure 3.5: Illustration of the gain bandwidth of a resonator about the principal frequency

likelihood vary more than 24 μm due to heating of the cavity. As long as the cavity is >>> than the wavelength then it will be amplified by the cavity. The quality of the laser beam or the degree to which the output is monochromatic is largely dependent on the laser medium. If the medium produces a majority of the desired wavelength photons then the beam will be of good quality.

Transition	Wavelength that satisfies equation 3.2 in (μm)	Number of wavelengths
${}^4F_{\frac{3}{2}}$ - ${}^4I_{\frac{15}{2}}$	1.700013	76470
${}^4F_{\frac{3}{2}}$ to ${}^4I_{\frac{13}{2}}$	1.3	100000
${}^4F_{\frac{3}{2}}$ to ${}^4I_{\frac{9}{2}}$	0.939999	138298
${}^4F_{\frac{3}{2}}$ to ${}^4I_{\frac{11}{2}}$	1.604004	122180

Table 3.1: Comparison of the transitions from figure 3.6 and how many wavelengths satisfy equation 3.2 for effective amplification in a laser cavity of length 65mm (length of the PSLR oscillator)

The quality of the output beam can be improved by removing unwanted fre-

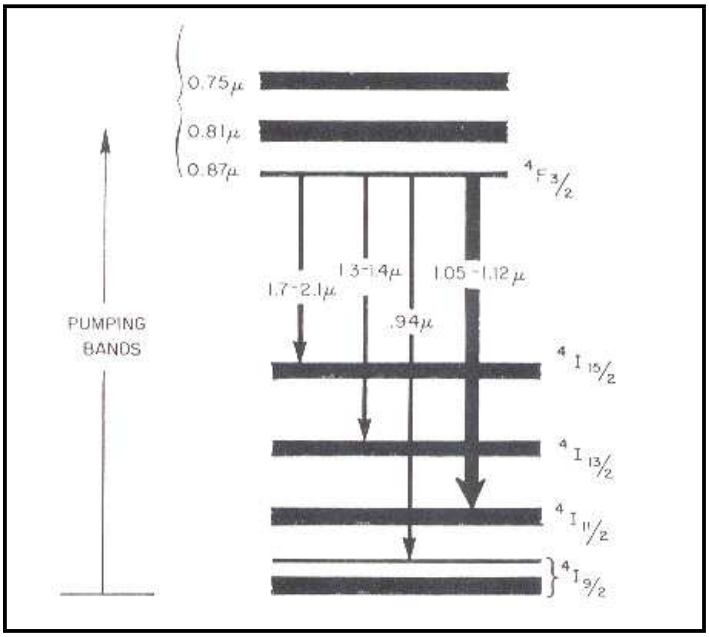

Figure 3.6: Diagram of the Nd^{3+} transition scheme. These levels will 'smear' when doped into different materials

quencies from the resonant cavity before they have a chance to be amplified. This can be accomplished in a number of ways. The most obvious method is to make the resonator cavity only a few wavelengths long so that it will satisfy equation 3.2 for only the desired wavelength. If the material used for the laser cavity is carefully chosen the gain bandwidth should only include the desired frequency. This approach is generally impractical as the laser cavity would be so small that an electron microscope would be needed to observe it and such a small resonator cavity would produce almost no gain at all so the output beam would be insignificant.

Another method is to place frequency-dependent filters within the oscillator. These filters are opaque to all but the desired frequency so while other wavelengths may be produced in the cavity, they will be quenched within the filter.

This method of removing spurious frequencies can be extended to create a tunable laser around the gain bandwidth of a resonator system. If a Fabry-Pérot or some other sort of angularly dependent filter or diffraction grating is used then a wavelength can be selected from the gain bandwidth of the resonator. An etalon

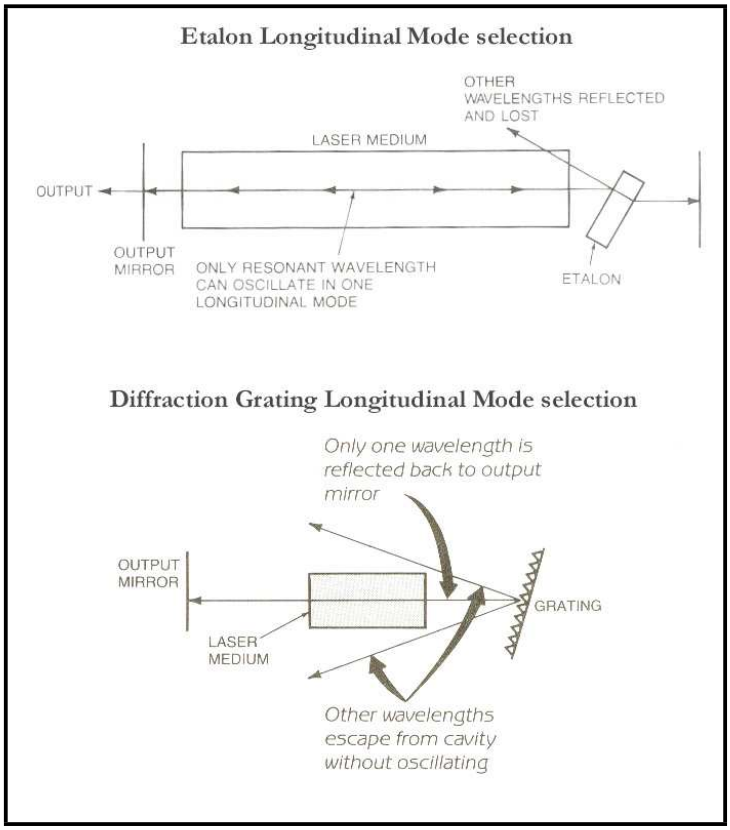

Figure 3.7: Two methods of selecting a longitudinal mode from a laser resonator

will allow the desired frequency to pass through it while reflecting all other frequencies out of the resonator. Similarly, a diffraction grating will reflect the appropriate wavelength back through the resonant cavity while removing all other frequencies. This is illustrated in figure 3.7 (Hecht, 1994).

There are many ways to construct effective resonator cavities. This section has dealt with only the basics and those types most relevant to laser ranging applications.

3.2.5 The PSLR Laser and application to Laser ranging

The PSLR laser is an example of the type of laser commonly used in SLR. SLR lasers are generally solid state lasers, with a majority of these being Nd:YAG. Neodymium is the lasing species and is doped into a crystal lattice of $Y_3AL_5O_{12}$, which is similar to the crystal structure of garnet, hence the name. The YAG lattice is transparent to

visible light and takes on a slight purple tinge with the Neodymium doping. Nd:YAG rods can be used in both the oscillator and amplifier stages but this need not be the case for all lasers as some use a slightly different host material. While the lasing species in other laser systems will be Nd, the host materials may be something like YLF(Yttrium lithium fluoride). This will alter the output wavelength for the same transition. The YAG lattice also alters the output wavelength which is 'smeared' by the host crystal structure (see figure 3.6). Doping Nd atoms into other materials will change the output wavelength due to the effect its crystal structure will have on the energy transitions that produce photons. For example Nd:YAG principal output λ is 1064 nm, Nd:YLF outputs at 1047 nm and 1053 nm and Nd-Glass lasers will emit frequencies dependent on the type of glass; 1054 nm for phosphate glass and 1080 nm for fused silica. Regardless of the host material the operation of the laser is nearly identical.

The PSLR laser has many components that are similar to other SLR systems. Some of the components are less common and the function of these rarer laser elements will be explained in the subsequent sections.

The PSLR employs a three stage method for production of the primary beam. The requirements for SLR are for a beam with well defined properties (beam profile, mode, divergence, pulse width) and high power. The laser oscillator stage uses several processes (Q-switching, mode selection, etc) to produce a beam of high quality but lacking the required power. The beam is then compressed in width, with a small increase in power and with the same beam qualities. The beam is then passed through the amplifier where the power is increased substantially. The only effect that the amplifier is required to have on the beam is power amplification. This results in a beam that has well defined properties and high power.

3.2.5.1 PSLR Oscillator

The PSLR oscillator (see figure 3.8 (Michailovas, 1997)) contains a 3 mm diameter by 65 mm length rod of Nd:YAG, a passive Q-switch, a polariser, a TEM mode

selector and is enclosed at one end with a 100 percent reflective mirror and at the other end, a Fabry-Pérot etalon.

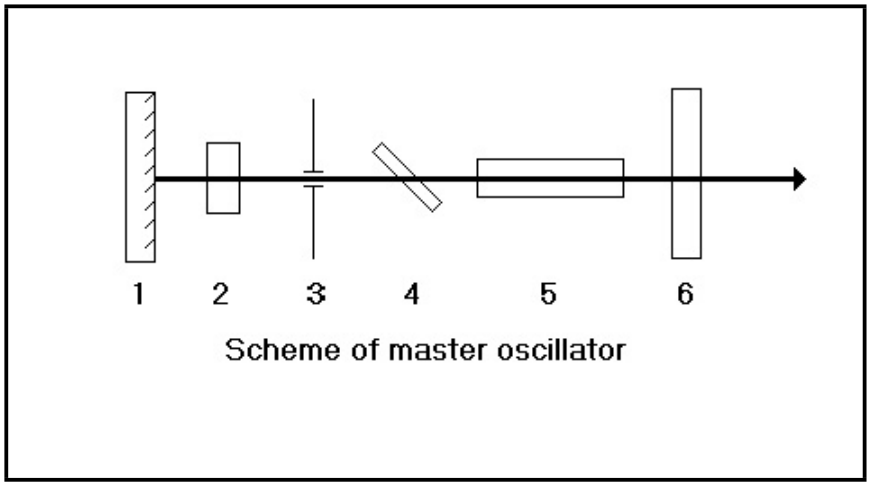

Figure 3.8: Representation of the PSLR resonator cavity

The numbers in figure 3.8 refer to the following components:

1. 100 percent reflective mirror
2. Passive Q-switch GSCG:CR crystal
3. TEM_{00} mode selector
4. Polariser
5. Nd:YAG rod
6. Uncoated glass Fabry-Pérot etalon

The oscillator is optically pumped using a single Xenon arc discharge lamp. The voltage to the tube and the repetition rate of flash can be selected. The oscillator flashtube voltage needs to be set at a level which will produce stable generation. As the flashtube wears out this voltage will need to be increased. As a general rule the laser is started and the oscillator tube voltage is increased to the point where stable generation has just been reached. The voltage is then increased by a further

10v to ensure fault free operation. This ensures the maximum flashtube operational lifetime. Increasing the oscillator voltage beyond this point does not increase the oscillator output as the Q-switch principally controls the energy build up in the oscillator rod.

Q-switched lasers are ideal for SLR applications as Q-switching produces high power with very short pulse lengths. For example the PSLR laser generates a beam within the oscillator of 3.5 mJ with a duration of ≈2 ns. This is equivalent to an output power of 1.75 kW. Q-switching is so called because it is employed with lasing rod material which have a low Q or quality factor. Q factor refers to the ability of a material to store energy per pump cycle,

$$Q = \frac{2\pi \times E_S}{E_D} \tag{3.3}$$

Where E_S is the energy stored per unit cycle and E_D is the energy dissipated per unit cycle in equation 3.3.

Low Q materials are ideal for pulsed lasers. As the materials lose energy quite rapidly it means that energy can be extracted from the material quickly and replenished very quickly. Low Q materials can generally store more energy than materials with a higher quality factor. When the lasing medium is pumped it very quickly saturates with energy. When the Q-switch is activated, almost all of the energy is dumped from the rod. High Q materials do not give up as much energy in such a short period of time and are therefore not as useful with such a short laser pulse. A Q-switch also controls the properties of the beam from the oscillator. It appears opaque to the primary laser frequency until the flux intensity within the rod has reached the switch threshold. At the switch threshold the beam is free to pass through and be reflected back through the cavity. This threshold (in the case of the passive Q-switch (a GSCG:CR crystal) used with the SL212) is always constant. Once the Q-switch has activated there is always only 2 full passes of the beam through the rod. As long as the oscillator cavity is well designed, then every

single beam emitted will have the exact same properties. This shot-to-shot stability is essential for precise laser ranging.

The oscillation process is actually quite simple in the passive Q-switching method utilised with the SL212 laser. A voltage pulse is sent from the SL212 power supply which causes an arc to be produced in the oscillator flashlamp. The resultant polychromatic light pulse is differentially absorbed within the Nd:YAG rod and stimulated emission occurs. When the energy stored within the rod exceeds the designed level of the passive Q-switch, it becomes saturated and is effectively bleached and transparent to light at the fundamental frequency (1024 nm). Photons are free to travel through the rod and reflect off the rear mirror (element 1 from figure 3.8). The resultant beam travels back through the rod stimulating more emission and extracting almost all of the energy stored in the rod. The beam passes through the Fabry-P*é*rot etalon where any unwanted frequencies are directed away from the optical path through the rest of the laser. In this way only one longitudinal mode or wavelength is selected. The beam has also made two passes through the pinhole aperture designated as element 3 from figure 3.8. This aperture selects the TEM_{00} (Transverse Electro-Magnetic) mode which ensures the beam has a gaussian profile. The TEM_{00} mode is selected as it will diverge less through the atmosphere than other TEM modes even though other TEM modes extract additional energy. The output beam needs only 2 passes through the rod to extract the maximum amount of energy, with one longitudinal and one TEM mode selected.

3.2.5.2 SL212 laser - From pulse compression to harmonic generation

The master oscillator produces a primary beam with a pulse length of ≈2ns, output energy of 3.5 mJ and λ 1064 nm. The final output beam (after passing through the amplifier and second harmonic generation stages) has a pulse length of 130 ps, an output energy of 130 mJ - 150 mJ, and a wavelength of 532 nm. The full optical scheme of the SL212 laser can be seen in figure 3.9 (Michailovas, 1997).

The final output beam characteristics are the result of three different processes:

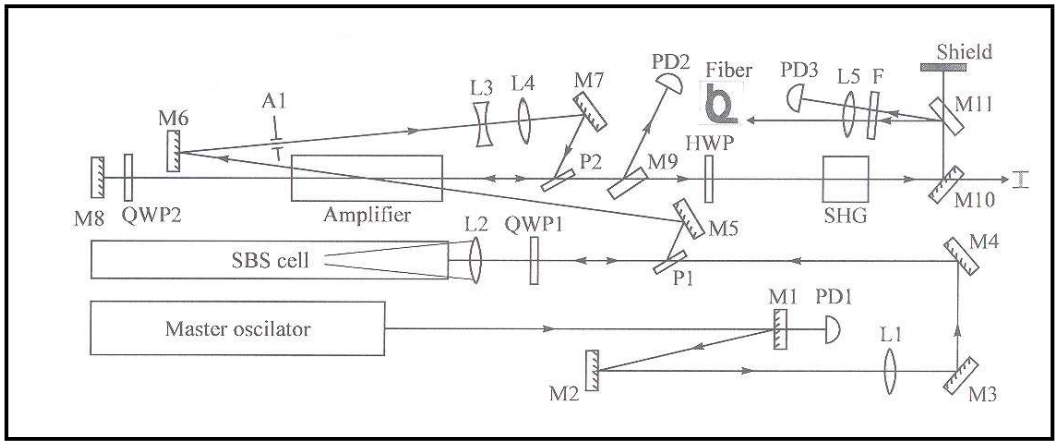

Figure 3.9: Representation of the PSLR laser optical scheme

pulse compression, amplification and second harmonic generation coupled with various filtering and polarisation processes.

3.2.5.3 Pulse compression

The primary pulse produced by the master oscillator is compressed to a pulse length of ≈ 130 ps within the component shown as SBS cell in figure 3.9. This cell contains carbon tetrachloride (common dry cleaning fluid) which passively compresses the pulse by backward Stimulated Brillouin Scattering (SBS).

Rayleigh scattering of light in materials is well known and is a result of minor differences in refractive index in inhomogeneous media. This scattering happens in all directions and is a result of the intrinsic properties of the media. There are two types or scattering which are the result of an acoustic wave induced in a material due to the interaction of light with the medium. These scattering processes are Raman and Brillouin. Many of the properties of these scattering phenomena are similar with the major difference being that Brillouin scattering (BS) occurs in a small cone in the opposite direction to the input light wave. The acoustic wave is induced in the material by a process known as electrostriction. The medium is in effect constricted and expanded as the electric field of a light wave traverses through. The acoustic wave follows the very high intensity electric field of the light source.

The acoustic wave has the effect of causing periodic differences in refractive index within the material. This mimics the behavior of a bulk grating, scattering photons at specific angles. The superposition of the scattered photons forms what is known as a Stokes wave, and in the case of spontaneous Brillouin scattering is of a lower frequency. Energy is conserved as the remaining energy $\triangle\hbar\lambda$ produces phonons in the material which increase the acoustic wave. This is represented in figure 3.10 (Fellay, 1998).

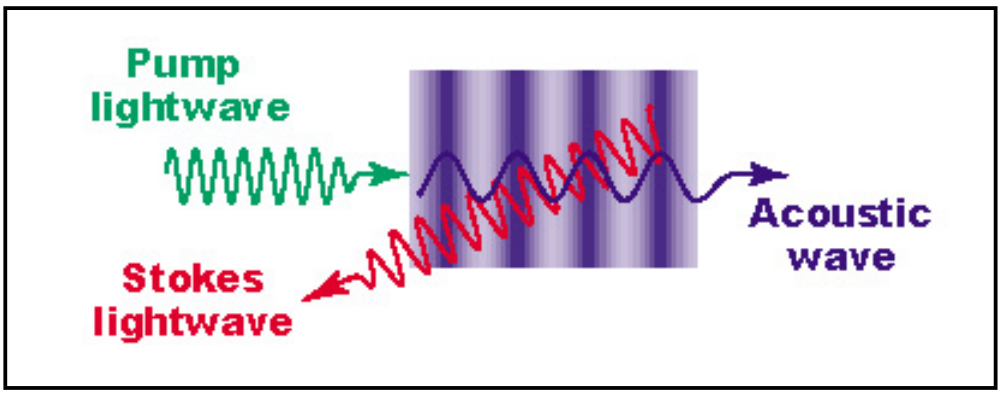

Figure 3.10: Spontaneous Brillouin scattering

With stimulated Brillouin scattering pulse compression a number of unique conditions occur. If the electric field of the light wave is sufficient $10^6 < I_L < 10^9$ Wcm^{-1} (Arecchi and Schulz-Dubois, 1972b) it will produce a Stokes pulse which is the conjugate of the incident light pulse. As the incident light pulse continues to enter the medium it will increase the amplitude of the Stokes pulse. The Stokes pulse and the initial pulse constructively interfere and the electric field strength increases. This in turn increases the acoustic wave. If the interaction of the two light waves produces a high enough electric field strength then an effective reflective barrier will be produced in the medium. All incident light will be reflected from this point as a Stokes wave. The Stokes pulse will quickly deplete the incident light pulse. As no extra energy is provided to the system and say, for example, the Stokes pulse has doubled in amplitude from the initial light pulse, then conservation of energy concludes that the pulse must be half as long. In a steady state system (a constant

wave laser for example) this process would act as an amplifier. With a pulsed wave this amplification process results in pulse compression.

The SL212 pulse compression system is often referred to as an SBS generator as it initiates its own SBS reaction. The incident pulse is focused at a point within the SBS cell. Eventually the electric field of the beam is increased to a point when SBS is initiated and the Stokes wave is generated at the front of the input laser pulse. The Stokes wave sweeps back through the medium constructively interfering with the input laser beam. This amplification of the Stokes wave further increases the SBS reaction within the medium. As the Stokes wave traverses back through the medium the SBS reaction is increased until the incident beam is depleted. This is illustrated in figure 3.11 (Veltchev, 2001). If the right medium is used, namely, one in which there is little energy lost in the SBS process, a great deal of compression can be achieved.

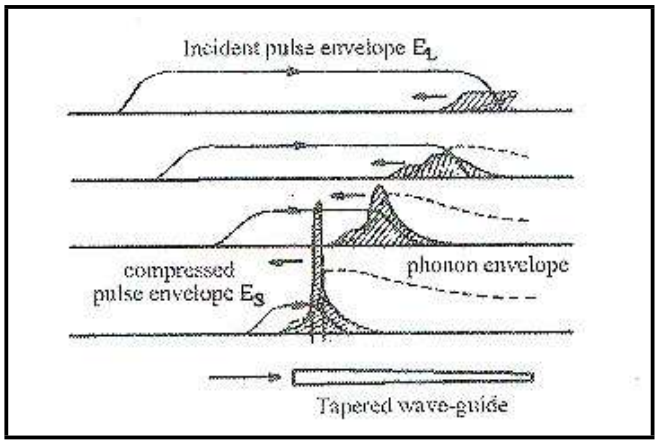

Figure 3.11: Brillouin scattering generation process used in the SL212 laser

In the SL212 laser the beam from the primary oscillator is linearly polarised before it reaches quarter wave plate (QWP1) indicated in figure 3.9. The beam takes on circular polarisation before it is focused into the SBS cell. The pulse is compressed and repeats the path of the of the oscillator beam, expanding into lens L2 where it is collimated again. It passes through QWP1 where it is once again linearly polarised but perpendicular to the original beam polarisation. The resultant

beam is then directed into the amplifier stage.

3.2.5.4 Amplifier stage

The amplification of the primary beam is a result of three passes through a second Nd:YAG rod. The primary beam stimulates emissions as it passes through the rod, increasing the intensity with each pass. The first pass through the amplifier is off axis with the eventual output beam but as the beam diameter is still small in comparison to the diameter of the amplifier rod it passes through easily. The 3 mm diameter beam is directed by mirrors through an aperture, then through lenses L3 and L4. These lenses expand the beam to 10 mm diameter which ensures the maximum amount of energy extraction from the 10mm diameter amplifier Nd:YAG rod. This produces some fringe interference with the end of the rod, which is carried through the system. This feature is obvious in near field observations but in the far field the beam has a Gaussian profile. The expanded beam passes through the amplifier twice before entering the second harmonic generation stage. This process extracts the maximum feasible amount of energy from the amplifier rod.

The amplifier is pumped by two flashlamps where the supply voltage and current supply can be controlled by the power supply. There is also a time delay control which can be adjusted so that the amplifier lamps flash at the correct time (some set time after the primary beam has departed the oscillator stage). These two modes of control (the voltage control has by far the greater effect) allow the final output to be varied greatly; from ≈3.5 mJ (if the amplifier is off) to 250 mJ at the primary frequency of 1064 nm at maximum amplifier voltage.

3.2.5.5 Second harmonic generation

Second and higher order harmonic generation has extended the usefulness of many laser systems as it allows the production of light frequencies for which a suitable generation scheme may not be available. The large drawback with harmonic generation is that it requires very high laser power to accomplish as it is the result of

very high field strengths. The use of harmonic generation with pulse lasers is well established due to the high powers obtainable with pulsed lasers. A majority of the SLR systems use Nd:YAG pulsed lasers with a second harmonic generation stage to produce the 532nm output as this is a more useful frequency for SLR systems.

Second harmonic generation is a result of non-linear optical phenomena which are generally only observed where there are very strong electric fields, as in a laser beam and specifically in pulsed beams.

If light enters a crystal the polarisation of the lattice is affected by the polarisation of the light and is proportional to the electric field as (Hecht and Zajac, 1974),

$$\rho = \varepsilon_0 \chi E \sin \omega t \tag{3.4}$$

where χ is the linear electric susceptibility of a material, ε_0 is the electric permittivity of a vacuum, E is the maximum electric field strength, and ρ is the resultant polarisation.

Equation 3.4 is valid for small values of electric field strength as the linear susceptibility χ is much greater than the susceptibility for higher order terms thus (Hecht and Zajac, 1974),

$$\begin{aligned} \rho = \varepsilon_0 \chi E \sin \omega t + \varepsilon_0 \chi^2 E^2 \sin^2 \omega t \\ + \varepsilon_0 \chi^3 E^3 \sin^3 \omega t + ... \end{aligned} \tag{3.5}$$

Equation 3.5, shows a truer picture of the polarisation effect. As the higher order electrical susceptibilities are very small, a modest electrical field will mean the higher order terms in equation 3.5 will effectively be non-zero.

As the electric field strength increases to the values obtainable with pulsed lasers, the huge values of E affect the higher order terms such that they start to contribute greatly to the polarisation.

If equation 3.5 is now rewritten (Hecht and Zajac, 1974),

$$\rho = \varepsilon_0 \chi E \sin \omega t + \frac{\varepsilon_0 \chi^2}{2} E^2 (1 - \cos 2\omega t) + \frac{\varepsilon_0 \chi^3}{4} E^3 (3 \sin \omega t - \sin 3\omega t) + ... \tag{3.6}$$

it shows that the second term in the series has a polarisation term which varies as 2ω, twice the original frequency. If ρ is proportional to $E + E^2 + E^3 + ...En$ then this would indicate that an electric field is produced in the material which also varies as $2\omega, 3\omega, ...n\omega$. With sufficient electrical field strength and the correct crystal, it is possible to produce radiation at harmonics of the original laser frequency. In the case of the SL212 laser this produces a green output beam at 532nm, twice the frequency of the original 1064 nm beam.

The other important consideration in effective harmonic generation is the concept of phase matching. As a primary beam and a generated beam will have slightly different speeds in a medium the production of the second harmonic will eventually shift out of phase with the primary wave. In order to produce a sizable second harmonic wave it is necessary to pass the primary beam through a large width of material (with respect to the wavelength of the light). Generally the effective coherence length is $20\lambda_0$ (Hecht and Zajac, 1974) which would find the second harmonic only periodically in phase with the primary wave where constructive interference could occur. This effect can be overcome by phase matching the second harmonic material to the input beam wavelength.

If the appropriate crystal and orientation are used, (see figure 3.12 (Hecht and Zajac, 1974)) it is possible to arrange for the refractive index of the material to be equal for both wavelengths $n_\omega = n_{2\omega}$. Both waves will now propagate in the crystal at the same rate and the secondary harmonic output will be increased due to constructive interference as generation and propagation occur at the same rate.

The SL212 laser uses a KD*P (potassium dideuterium phosphate) crystal which is temperature stabilised using an oven designed to keep the crystal at $41°C$ to stablise the conversion process. This produces a beam at 532 nm with an output

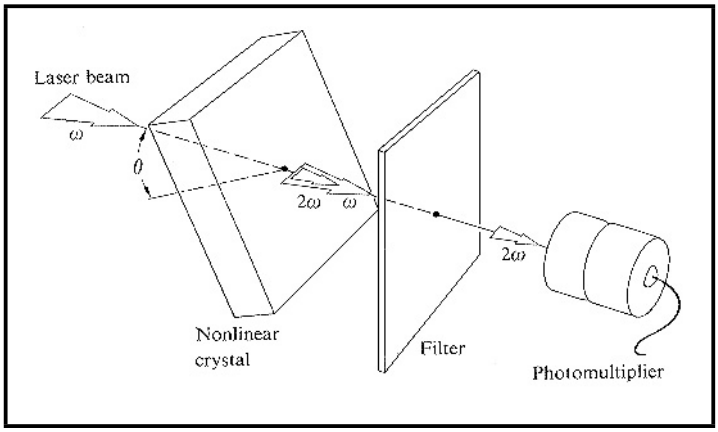

Figure 3.12: Phase matching using a selected crystal and orientation

energy of ≈ 125 mJ. The fundamental energy output is ≈ 250 mJ giving a conversion ratio of 0.5. The fundamental wave, as well as a small amount of the secondary is removed by a dichroic mirror M10 (shown in figure 3.9). The primary beam is quenched by a shield. Some of the secondary beam that was stripped by mirror M10 is directed into a fiber-optic lead which is connected to the PSLR start detector. The majority of the output beam is unhindered by M10 and is directed into the PSLR output optics and directed as required.

3.3 Laser ranging detectors

There are two classes or detectors used with current SLR systems. These are either electron tube or solid state detectors. Electron tube products use the photo-electric effect and electron multiplication to generate a signal whereas solid state devices use photon capture and reverse biased junctions for signal amplification. While detectors vary in design and function, they may be classified as either one or the other. The subsequent sections discuss the design, operation and function of current SLR detectors a with a more detailed examination of the detector used with the PSLR.

3.3.1 Purpose of detectors

With the range accuracy for current SLR systems expected to be less than 10 mm RMS, modern detectors must achieve the following results:

- ultra-fast timing,
- well defined transit times,
- good operational stability,
- linearity with photon flux
- good signal to noise ratio, and
- high gain especially for single photon detection.

A good detector must optimise all of these attributes so that it can provide the most accurate indication of the presents of a signal. In today's rush toward sub-millimeter accuracy even a few picoseconds of error can affect the final ranging result.

3.3.2 Photomultiplier tube

3.3.2.1 Introduction

Photomultiplier tubes (PMT) are widely used for photon detection applications. They have the advantages of a very high gain with a very high signal to noise ratio. This is very important with SLR as return signal strengths are generally very low and may in some cases consist of a single photon.

The PMT uses a photocathode which ejects photoelectrons as a result of the interaction of a photoemissive material (a metal alloy)and incoming photons. The photocathode is generally a thin plate held at a high negative potential ($>$ -1000 v). This is known as the photoelectric effect. The photocathode produces primary

photoelectrons with an energy determined by the type of material and the frequency of the incident light where,

$$K_{max} = hf - \phi, \text{ and} \tag{3.7}$$

ϕ is known as the work function of the photocathode material.

The work function represents the amount of energy needed to remove an electron from the photocathode material. Typically this requirement restricts the wavelength range of photon detection of PMTs below the near infra-red (≈1200 nm). PMT tubes are also restricted in their use by the type of glass used to enclose the tube in front of the photocathode window because most types of glass are opaque at ultraviolet frequencies. The spectral response (working range) of a particular tube is a result of these two factors and tubes can be designed for different purposes by careful selection of the materials (see figures 3.15 and 3.16).

Given that the correct tube has been selected for the desired wavelength range, and the tube is exposed to light, primary photoelectrons are ejected from the photocathode. The primary photoelectrons are accelerated under the influence of an electrical gradient to a set of secondary plates called dynodes. These dynodes eject two or more electrons (secondary emission) for an incident electron. Amplification through the PMT is achieved by the use of many dynode plates (see figure 3.13 (Hamamatsu Photonics, 1998)) which gives gains in the order of $10^5 - 10^8$. Each dynode in the dynode chain is electrically connected by a resistive element to the next element in the chain. This means that each successive dynode will be at a higher electrical potential than the last. Each dynode stage will then attract the secondary electrons from the previous stage due to the electrical potential gradient. Each stage produces more secondary emissions as a result of the previous stage's secondary electrons. The resultant voltage pulse is collected at the end of the dynode chain by an anode.

The Hamamatsu Photomultiplier guide shows two main types of photomultiplier

tube construction; head-on and side-on. The head-on type consist of a vacuum tube which contains a spectrally transparent window, a photocathode, an electron multiplier stage and a collection anode, which are all aligned from top to bottom. The side on type has a different architecture with the window being located in the side of the tube and the other sections of the apparatus being arranged in a circular manner rather than linearly (see figure 3.14 (Hamamatsu Photonics, 1998)).

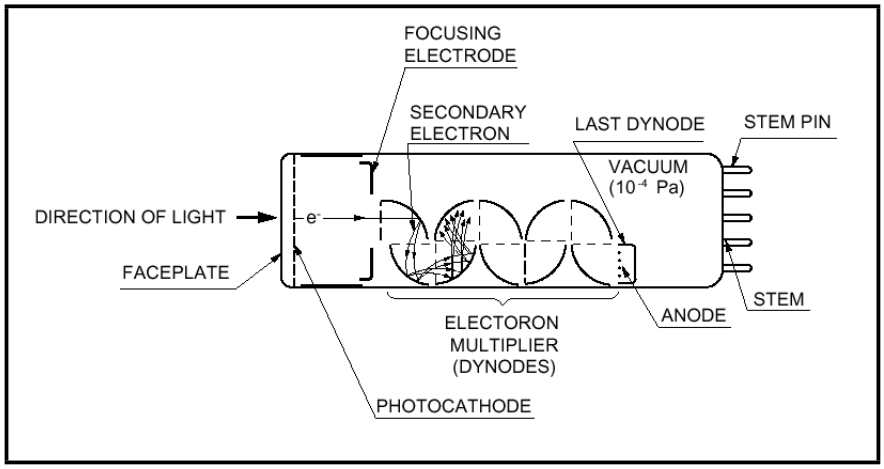

Figure 3.13: Cross section of a head on type PMT showing placement of the dynode chain as well as the processes of primary and secondary emmision.

3.3.2.2 Important characteristics of PMTs

PMTs, like all detectors, have certain characteristics determine their suitability for various applications. PMT and other types of electron tube detectors are very versatile due to the large size of the active detection area (compared with solid state detectors)and their relative simplicity.

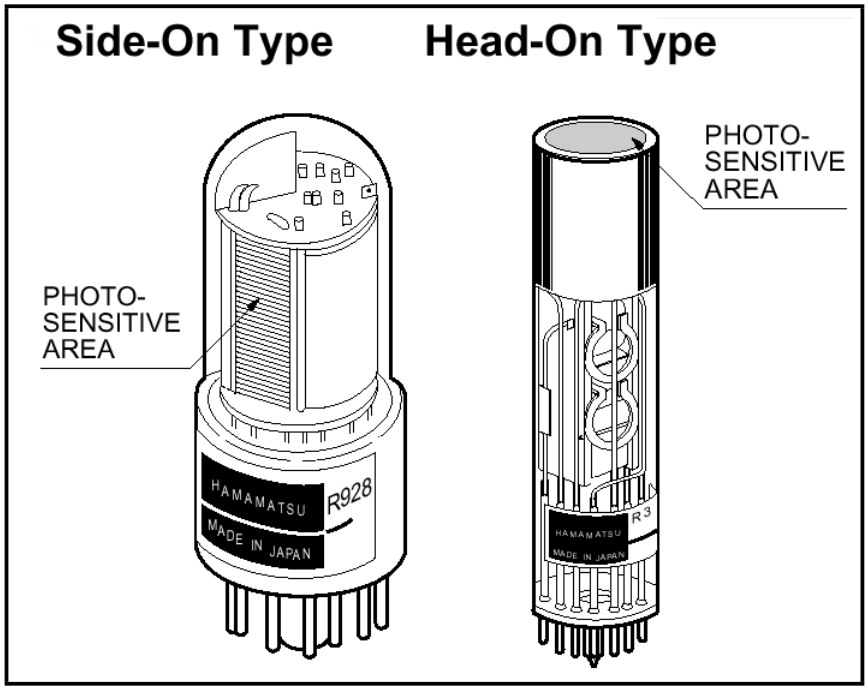

Figure 3.14: Two main types of PMT tubes

This allows a great deal of choice for the detector designer who is able to target detectors to applications by the correct selection of the following:

1. Window material.
2. Photocathode material.
3. Electron multiplier type.
4. Voltage divider construction.
5. Tube construction(length, diameter, head on or side on).
6. Current gain.

3.3.2.3 Window material

As mentioned in section 3.3.2.1, the window material is one of the limiting factors on the spectral range of PMT detectors. Glass is generally opaque at ultraviolet

wavelengths but there are materials which are transparent at least some way into the ultraviolet region.

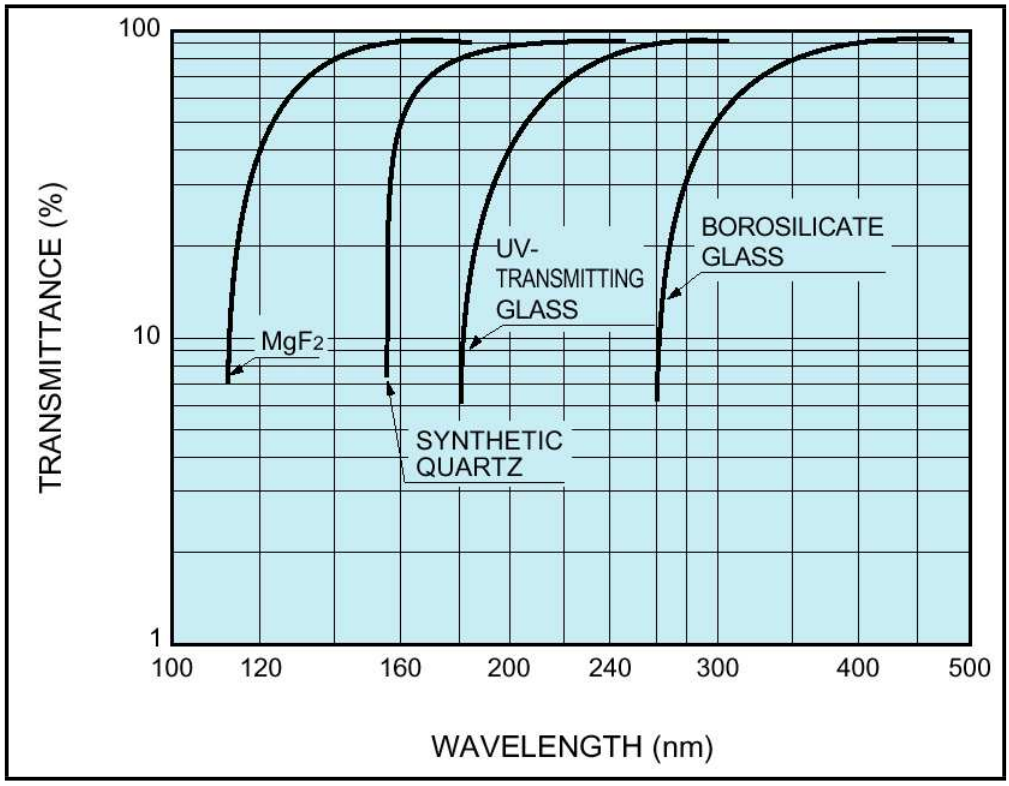

Figure 3.15: Transmittance at UV frequencies of common types of window material. These materials are almost totally transparent in the visible region.

Figure 3.15 (Hamamatsu Photonics, 1998) shows the percentage transmission through four different materials at UV wavelengths. The ability to transmit light at these lower wavelengths is only of importance in applications such as spectroscopy or where a UV laser may be in use. As single colour laser ranging is conducted with visible laser light, such considerations are unnecessary.

3.3.2.4 Photocathode type

The photocathode material determines the other extreme of spectral response as all the metals used have a specific work function(see equation 3.7). This spectral susceptibility of photocathode materials limits the use of PMT tubes to wavelengths

shorter than the near IR ($\approx$ 1200 nm). The Hamamatsu product catalog lists several different types of materials used as photocathodes. These typically contain alkali metals which have low work functions. The PSLR PMT detector (Hamamatsu R4124) has a bialkali (Sb-Rb-CS (antimony-rubidium-caesium) or Sb-K-Cs (antimony-potassium-caesium)) photocathode. This material operates efficiently over the range of 300 nm - 650 nm.

Photocathode materials are often characterised using the following terms:

1. Radiant sensitivity.
2. Quantum efficiency.
3. Luminous sensitivity.
4. Blue sensitivity.

Radiant sensitivity is the current produced at the photocathode per unit radiant power at a specific wavelength. Quantum efficiency is the number of photoelectrons produced at the photocathode per incident photon at a specific frequency.

Figure 3.16 (Hamamatsu Photonics, 1998) indicates that the radiant sensitivity of the R4124 photocathode is approximately 50 mA/W and has a quantum efficiency slightly above 10 percent at 532 nm (the wavelength of the PSLR laser). These are typical response curves for different types of tubes.

Hamamatsu provide a test sheet with each PMT tube purchase. As it is impractical to test each tube for spectral response and quantum efficiency, test sheets include figures for cathode and anode luminous sensitivity, anode dark current and cathode blue sensitivity or red/white ratio.

Cathode luminous sensitivity is the photoelectric current produced at the cathode when exposed to a tungsten filament lamp operated at a distribution temperature of 2856 K. Anode luminous sensitivity is the photoelectric current produced after dynode chain amplification at the anode when exposed to the same light (Hamamatsu Photonics, 1998). This is expressed as ampere per lumen with the

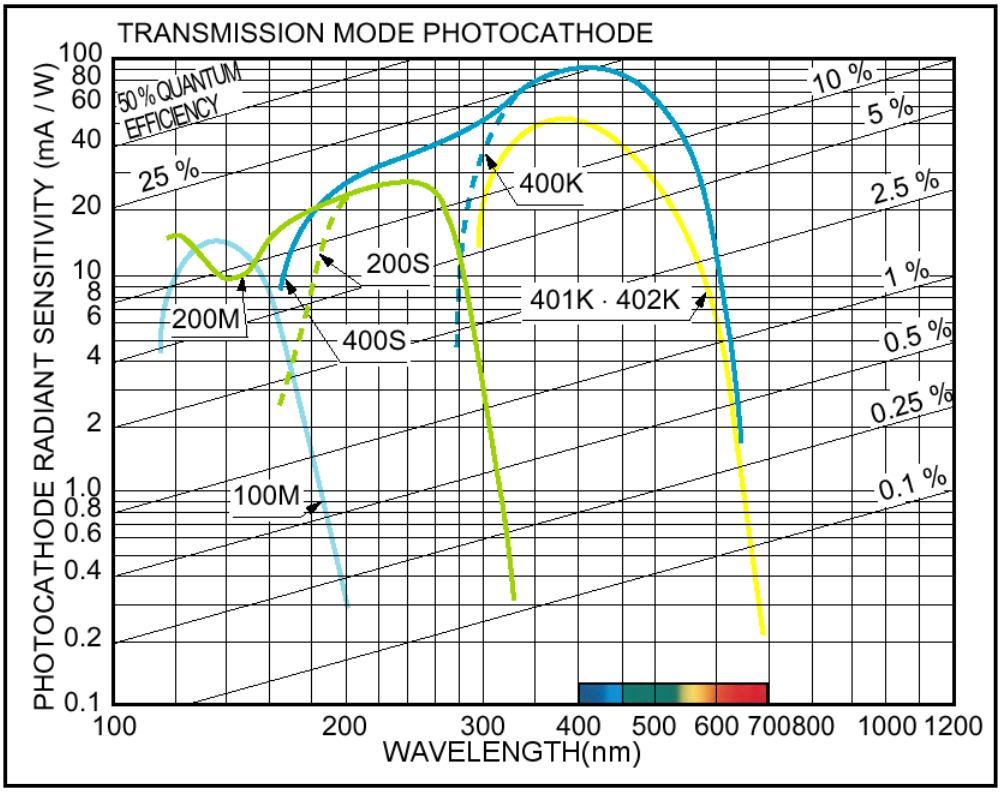

Figure 3.16: Spectral response of the R4124 photocathode is indicated as plot 400K in the figure

tests carried out in the range of 10^{-10} to 10^{-2} lumen, depending on the type of tube tested.

Cathode blue sensitivity is tested by passing light from a tungsten tube operated at 2856 K through a blue filter (Corning CS No. 5-58 polished to half stock thickness) (Hamamatsu Photonics, 1998). This expressed as ampere per lumen-blue and is useful for determining the response of the tube at the lower end of the visible spectrum, or close to the ultraviolet region.

Red/white ratio is determined by measuring the luminous sensitivity at the photocathode, after passing light from the tungsten tube through a red filter (Toshiba IR-D80A or R-68), and dividing it by the luminous sensitivity. This ratio is used for tubes that are responsive in the near IR.

Serial Number	Cathode Luminous Sens.($\mu A/lm$)	Anode Luminous Sens.(A/lm)	Anode Dark Current(nA)	Cathode blue Sens. Index
LA1944	95.3	169.0	1.72	9.97

Table 3.2: Final test sheet data for the R4124 PMT tube currently used as the return detector with the PSLR. The tube was operated at 1000 V using the standard voltage distribution ratio listed in the Hamamatsu PMT catalog (see section 3.3.2.6).

3.3.2.5 Electron Multiplier Stage (EMS)

The electron multiplier section of a PMT is essential in allowing the detection of extremely small signals. The photocathode produces a graded response to input light and the EMS must amplify this response without destroying the properties of that response. The most important considerations with SLR are output pulse rise time and low noise so that very small signals can be detected. While there are a number of EMS types, the two that will be mentioned here are the linear focused type [see figure 3.17 (Hamamatsu Photonics, 1998)] (this is the type used in the PSLR PMT), and the Microchannel plate (MCP) [see figure 3.18 (Hamamatsu Photonics, 1998)] as these are commonly used in SLR and have a number of desirable characteristics.

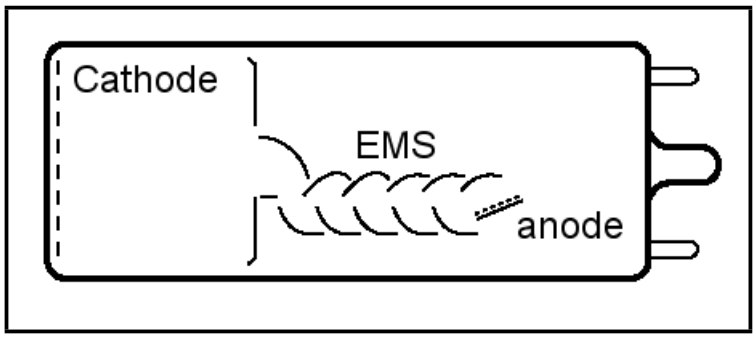

Figure 3.17: Illustration of the linear focused electron multiplier stage used in the R4124 PMT tube.

The construction of the dynode chain and the arrangement of the voltage gradient

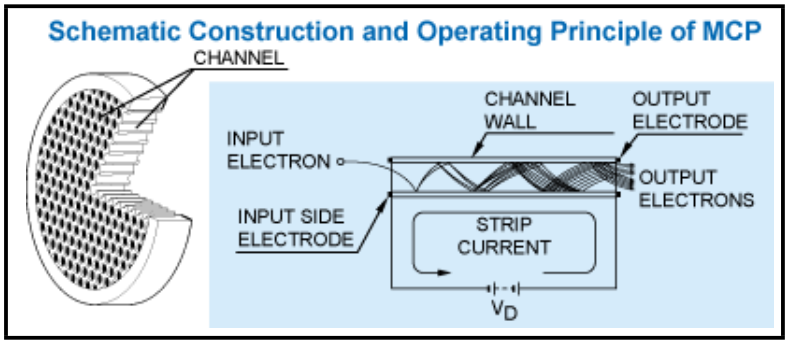

Figure 3.18: Illustration of the microchannel plate electron multiplier stage commonly used in SLR applications.

between the chain elements will be covered in detail in section 3.3.2.6. The linear focused EMS has the advantages of a very fast response time and good pulse linearity or the ability to closely match the characteristics of the input pulse. As pulses from SLR lasers are generally less than 200 ps and the fastest PMTs have rise times of 300 ps or more, this will always result in the output pulse from the tube being 'stretched' in comparison to the laser pulse. If the throughput from the tube matches the shape of the input pulse, it is possible to glean more information from the pulse rather than simple time resolution.

The other important feature of the EMS is the pulse amplification or gain. This is a function of the voltage applied to the dynode chain and the length of the dynode chain. These considerations will be dealt with in detail in section 3.3.2.6. The length of the dynode chain will determine the transit time or the time from receival of the light pulse at the cathode to generation of a pulse at the anode. The longer the dynode chain then the longer the transit time. The PSLR tube has a specified rise time of 1.1 ns and a transit time of 12 ns. The test carried out at the Curtin University test facility showed that the rise time was close to the 1.1 ns claimed by Hamamatsu. Figure 3.19 shows the outputs from the start detector (yellow trace) and the R4124 PMT tube (blue trace). The image is a screen capture from a Tektronix TDS3052 digital phosphor oscilloscope. This unit has a bandwidth of 500MHz, a sample rate of 5GS/s and a minimum timebase of 1ns.

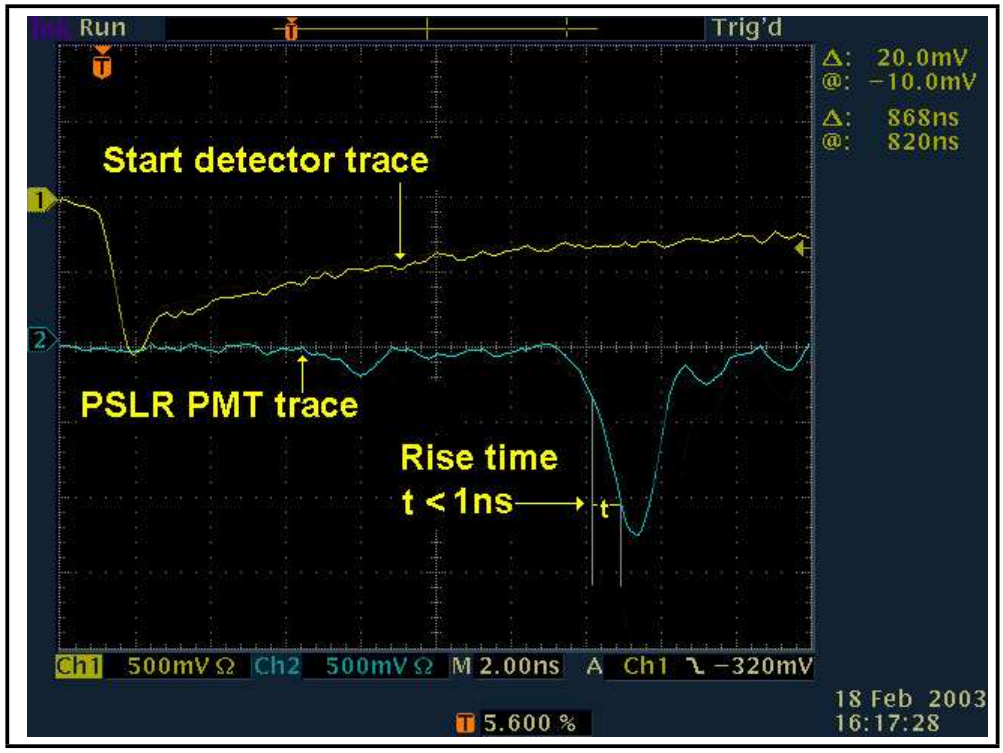

Figure 3.19: Screen capture from the TDS3052 oscilloscope showing both the start detector trace and the PMT trace. The timebase of 2ns per division indicates that the rise time of the PMT trace is less than 1ns.

No tests were undertaken to determine the PMT transit time. The rise time and transit time of the R4124 tube from Hamamatsu do not make it ideal for laser ranging. The best results are achieved when the properties of the detection apparatus and back-end electronics/pulse conditioning equipment match as closely as possible the input light pulse. With these considerations in mind, a PMT with a microchannel plate (MCP) EMS is definitely preferable.

The construction of the MCP-PMT can be seen in figure 3.18. The basic principle is the same as the linear focused type with a voltage being induced between the cathode and anode with a graded potential difference along the dynode path. In this case the dynode path is a small tube (typically 15-50 μm diameter) (Knoll, 1989) constructed of glass with a potential difference between the tube ends. Secondary electrons are attracted to the sides of the tubes where further secondary emissions

occur. The final electrons are collected at the anode. By placing many thousands of micro-tubes together, a significant amount of gain can be achieved. The timing specifications for MCP-PMTs are quite impressive. The Hamamatsu product guide quotes rise time figures of 150 ps and transit times of 0.55 to 1 ns, which is much closer to the pulse duration of modern SLR lasers (the SL212 laser has a pulse duration of 130 ps).

3.3.2.6 Voltage divider types and properties

The voltage divider components used with a PMT are generally external as tube construction brings all of the dynode connections to the base of the tube. This allows the end user to tailor the voltage division and dynode setup to individual needs.

The primary task of the PMT tube dynode chain is to amplify an incident signal by secondary electron generation. Each successive dynode is set at a higher electrical potential (with respect to the cathode voltage) than the last, firstly so that a greater number of electrons are produced per stage as the pulse proceeds down the chain, and secondly the increase in potential between stages attracts electrons towards the next dynode. The graded potential from dynode-to-dynode is easily created by placing the dynodes between resistors wired in series so there will be a voltage drop across each resistor. If dynodes are placed on either side of a series resistor then each dynode will be at a different voltage potential and thus a potential slope will be evident down the dynode chain. Simple schematics of this method are displayed in figure 3.20. These examples show a high negative potential (typically around -1000 v) applied at the cathode with the anode connected to ground. Electrons produced by the cathode are attracted by the potential gradient to the first dynode. The first set of secondary electrons produced are thus attracted to the next dynode by the more positive potential, and so on until the signal reaches the anode.

The PSLR multiplier chain configuration and resistor values are shown in figure 3.21. The resistors are chosen principally to satisfy two requirements. The current

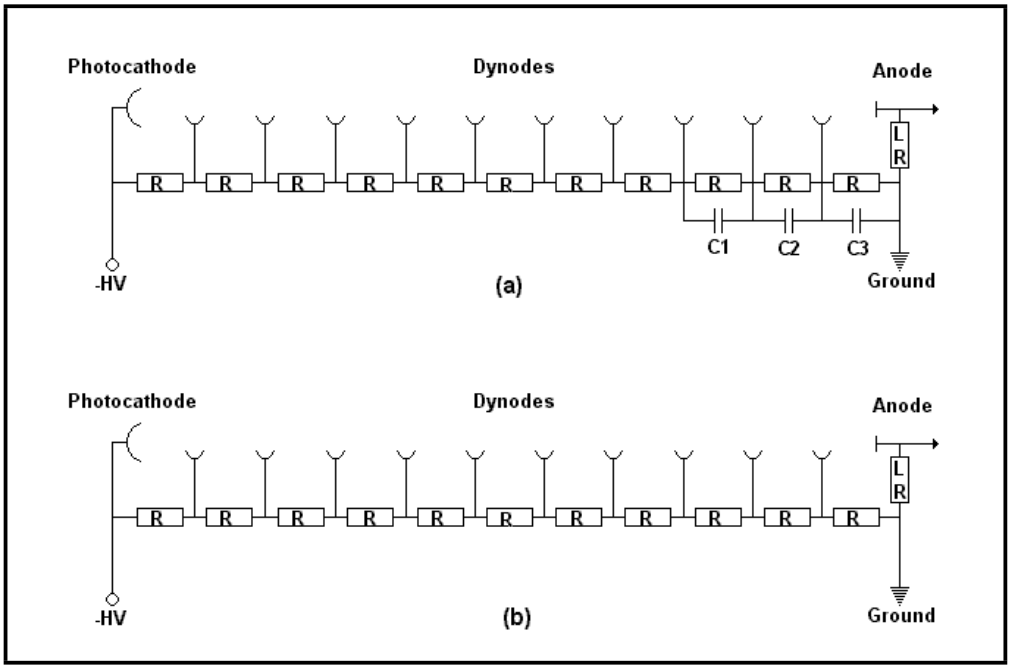

Figure 3.20: Voltage divider scheme used with PMT tubes. (a) represents a circuit that may be used with pulsed operation and (b) shows a circuit that would be utilised for DC operation.

passing through the tube must not exceed the tolerance of the tube or the power supply. It is also recommended that the dynode chain current be kept at least 20 times higher than the anode output current. If these values approach one another, the last few stages of the dynode chain tend to become saturated. The output in these last few stages is flattened out so pulse information is lost in a DC like signal. It is also desirable to keep dynode current to a minimum so that heat dissipation in the tube is low, thus operating temperature will be low and spurious thermionic emissions are reduced. If it is not possible to ensure that the dynode current is sufficiently high compared to the anode current, it is possible to compensate by using capacitors as shown in example (a) in figure 3.20. The capacitors are able to discharge over and above the level imposed by saturation.

There are no requirements for dynode chain electronics with MCP-PMTs as the amplification stage is made up of many small tubes which have a graded voltage

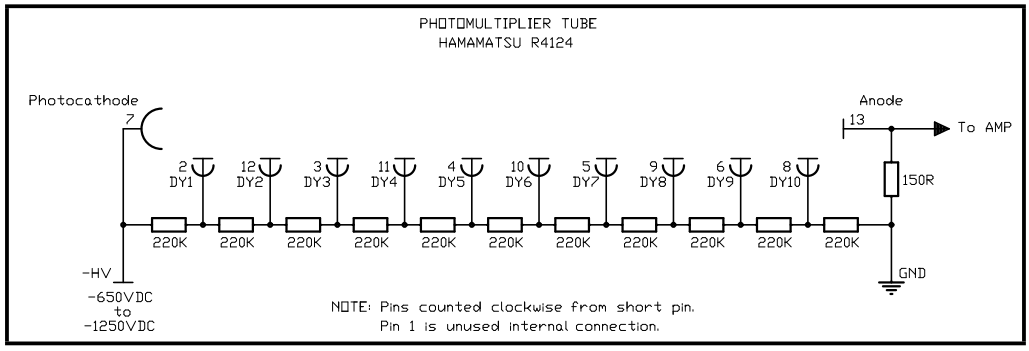

Figure 3.21: Voltage divider scheme used with the PSLR PMT detector.

differential along the tubes. The potential across these tubes is generally over 2000V so a great deal of care must be taken with proper enclosure and space charge effect. Care also has to be taken in the design of the microchannel arrangement as positive ions are often produced and accelerated in the opposite direction. If these positive ions are reabsorbed by a microchannel, they can produce secondary electrons if enough energy is supplied through electromagnetic acceleration, thus altering the shape of the original pulse. If the microchannels have a bend included in the path then there is not enough of a path to achieve sufficient acceleration before reabsorption.

3.3.2.7 Current gain values in PMT tubes

The PMT dynode chain is primarily a current amplifier. For a PMT, the current gain is the ratio of photocathode output current to anode output current. The gain is a result of the secondary emissions from the dynodes. Each dynode contributes to the overall gain which can be expressed as δ^n, for n dynodes. The gain of each dynode is a result of the voltage drop across the stage and the dynode material type and the structure of the dynode. This is expressed in the Hamamatsu product guide as (Hamamatsu Photonics, 1998),

$$\mu = \delta^n = [A.E^{\alpha}]^n \tag{3.8}$$

where μ is the overall current gain, A is a constant, E is the potential difference across the stage, α is a coefficient determined by the dynode material and the chain structure, and typically has a value from 0.7 to 0.8. Therefore,

$$\mu = [A.(\frac{V}{n+1})^{\alpha}]^{n} = \frac{A^n}{(n+1)^{\alpha n}}.V^{\alpha n} = K.V^{\alpha n}. \tag{3.9}$$

The Hamamatsu R4124 tube used as the PSLR detector has a typical gain of 1.1×10^6 and an average anode current of 0.03 mA. The Hamamatsu guide has a number of MCP-PMT's listed which all have a characteristic gain of a factor of 10 less than the R4124. The lower gain available with MCP-PMTs is a result of the construction of the electron multiplier region which is designed principally for fast rise times and fast electron transit times (see section 3.3.2.5).

3.3.3 Semiconductor detectors

Semiconductor-based detectors are becoming more popular as photon detectors in SLR applications. This is due to a number of factors such as high quantum efficiency, ease of use (simplified power supply, lower voltage), fast transit and rise times and the small size. PIN diodes or PN diodes are commonly used as "start detectors" and are activated by a laser fire event. Avalanche photodiodes (APDs) or single photon avalanche photodiodes (SPADs) are commonly used as stop detectors and are activated by satellite retroreflector returns.

3.3.4 The Photodiode diode

The photodiode is a widely used photon detector in the modern world. It has a wide variety of constructions and applications. This section will discuss those that relate to photon detection and in particular the PIN diode and the avalanche photodiode. The operation of PN diodes will be examined initially as comparison to these devices best describes the function of PIN and APDs

3.3.4.1 P type, N type materials and PN diode structure

Diode intrinsic material is generally either Silicon or germanium (4 valence electrons), the N type material is the same material but is 'doped' with low concentration of atoms having 5 valence electrons. The P type material is once again the same base material with very low concentrations of atoms having 3 valence electrons inserted into the crystal lattice. If an atom with five valence electrons is doped into a valence 4 material it has the effect of partially releasing one of the valence 5 atom's electrons. This electron is not as tightly bound to the doped atom as the atom tends to emulate the behaviour of the intrinsic material in the crystal lattice (ie four bound electrons). The lattice becomes suffused with a number of 'free' electrons which can act as charge carriers.

If a valence 3 type material is doped into a valence 4 material the opposite effect is produced. The valence 3 atoms once again emulate the behaviour of the host material and act as valence 4 atoms. This creates a deficiency in charge in the lattice that will readily accept a negative charge. This localised charge deficiency is typically termed a hole.

If an N type material and a P type material (doped in the same intrinsic material) are joined together, the donor material or N type will give up the loosely bound electrons to the P type material. Free charge is swept from the N type material near the junction. The N type material becomes suffused with donated electrons which fills the 'holes' near the junction. The region between the two materials is now completely depleted of any sort of charge carriers, hence the common name given to this region as the depletion zone. This depletion zone is the key to the operation of diode based semiconductor devices.

This depletion zone can be affected by applying an external potential difference across the diode junction. If the diode is forward biased (negative potential on the N type material, positive on the P type), the depletion zone will shrink as available electrons in the N material fill the holes and provided holes to the P type material join with the excess electrons. Once all of the charge carriers have been bonded the

depletion zone will disappear. Any increase in voltage will cause current to flow.

If the applied potential difference is reversed so that the negative voltage is supplied to the P type material, the diode is said to be reverse biased. This has the effect of supplying extra charge carriers to the regions near the depletion zone to join with the opposite polarity excess charge carriers still free in the lattice. This further empties the depletion zone of free charge carriers so the depletion zone expands. No current can flow in this situation until the diode is completely depleted. This effect is called break over and results in run away current throughput at the break over potential.

The PN diode can be operated as a photo emitter (LED), a photovoltaic or photoamperic cell, or as a photon detector by selecting the correct operating voltage. This is represented in figure 3.22 (Chaimowicz, 1992). The characteristic curves displayed in figure 3.22 are divided into 3 quadrants. The third quadrant, where the diode is reverse biased, is the region of most interest for photon detection.

When light is directed into the PN diode (see figure 3.23 (Chaimowicz, 1992)) a photon may liberate an electron within the depletion zone. The photon must have sufficient energy to impart to an electron so that it can transition the energy gap between the valence band and the conduction band.

In the case of photons, the energy is a result of the wavelength of the photon, namely,

$$E = \frac{hc}{\lambda} \tag{3.10}$$

For example, frequency doubled light from an Nd:YAG laser at 532nm has an energy per photon of $\approx 3.73 \times 10^{-19}$ J (2.33 eV). The band gap of a typical semi-conductor is $\approx 1.60 \times 10^{-19}$ J (1.0 eV) (Rosenberg, 1995). The primary Nd:YAG wavelength photons have an energy of $\approx 1.87 \times 10^{-19}$ J (1.17 eV) so the chance that they will be able to promote an electron across the band gap is not as likely it would be for a higher energy photon. The reaction could be said to generate an electron-hole

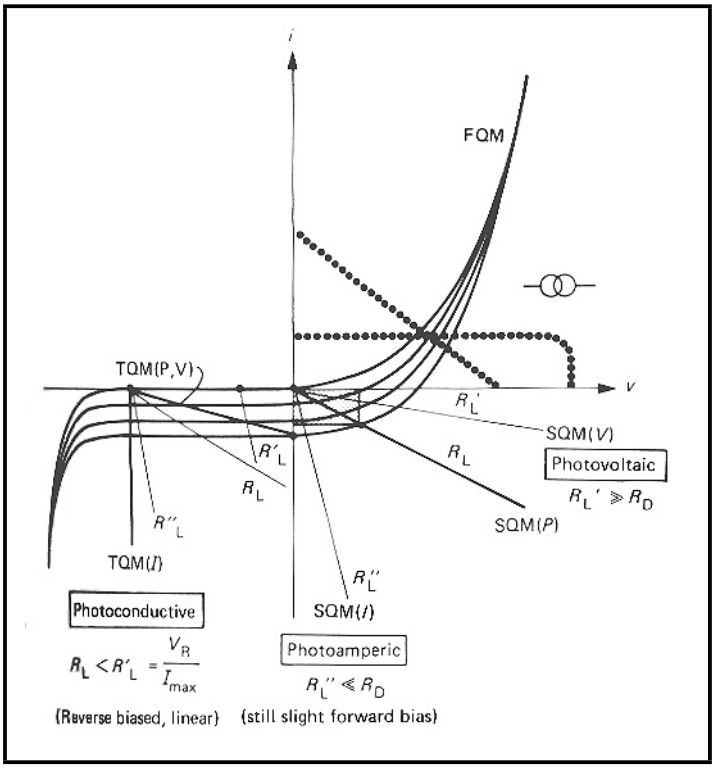

Figure 3.22: This diagram shows characteristic curves for diodes subject to various light levels. PN diodes operated at different voltage levels can be operated as either photon emitter, power source or photon detector.

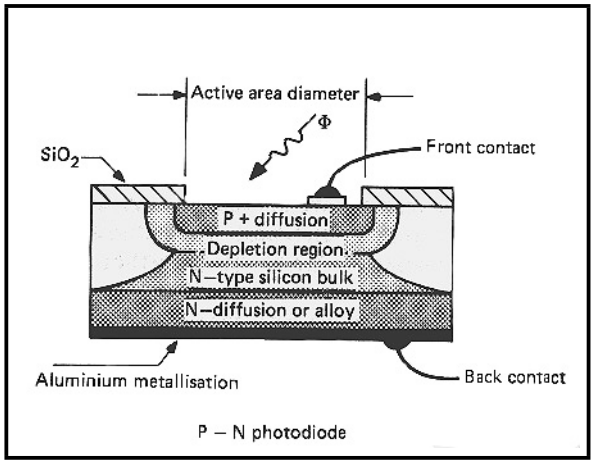

Figure 3.23: Simplified structure of a PN photodiode.

pair as the electron and the hole both migrate from the depletion zone under the influence of the strong localised electric field. In the case of a reverse biased diode

the current flow is mostly due to the incident light flux rather than the applied potential as is the case in forward biased conditions. Each characteristic curve in figure 3.22 shows a slight negative slope in the reversed biased direction (before the break-over point) that is due to the increased applied potential across the junction. Careful selection of the output load resistance will allow use of the diode as either a current generator or a voltage generator.

3.3.4.2 PN diode properties and characteristics

The photodiode is not an ideal detector and, as such, it is important to know the operating properties. These properties will include such things as spectral response, quantum efficiency, radiant sensitivity, noise and response time.

1. **Spectral response**

   This simply put is the current output per unit watt of incident light on a photodiode for a specific wavelength. Silicon photodiodes exhibit typical values of 0.5-0.6 $\mu A \mu W^{-1}$ at the peak λ of $\approx$ 900 nm.

2. **Quantum efficiency**

   The quantum efficiency, generally given as a percentage, represents the number of photoelectrons produced compared with the number of incident photons. This is always less than 100 percent as some electrons do not penetrate far enough into the device to generate photoelectrons and some generated photoelectrons recombine before they are registered by detection electronics.

3. **Radiant sensitivity**

   Radiant or irradiant sensitivity is the ratio of photo-current produced (in A) to the irradiance (in Wm^{-2}). This is generally expressed as Am^2W^{-1}.

4. **Noise**

   Diode detectors have two distinguishable types of intrinsic noise called shot or Schottky noise and thermal or Johnson noise (Chaimowicz, 1992). The shot

noise is a combination of the dark current and extraneous ambient illumination current or current produced by unwanted background light. The dark current is present even in the absence of illumination and is the result of random effects within the lattice and random generation-recombination of electron-hole pairs. This effect is largely influenced by the bias voltage applied to the diode junction. This can be expressed as (Chaimowicz, 1992),

$$\overline{(\Delta {i_d}^2)^{\frac{1}{2}}} = (2ei_dB)^{\frac{1}{2}}, \tag{3.11}$$

where e is the charge on an electron, i_d is the dark current, and B is the detection bandwidth.
The total shot noise is then (Chaimowicz, 1992),

$$\overline{(\Delta {i_s}^2)^{\frac{1}{2}}} = \sqrt{\overline{(\Delta {i_d}^2)^{\frac{1}{2}}} + \overline{(\Delta {i_i}^2)^{\frac{1}{2}}}}, \tag{3.12}$$

where i_i is the extraneous ambient illumination current.

The Johnson noise or thermal noise is a result of the random motion of free charge and is intrinsic to every material at a finite temperature. As temperature increases, more free charge is produced as thermal energy allows more electrons to be liberated from outer shells. This parameter can be expressed as (Chaimowicz, 1992),

$$\overline{(\Delta {i_j}^2)^{\frac{1}{2}}} = (\frac{4kTB}{r})^{\frac{1}{2}}, \tag{3.13}$$

where i_j is the Johnson current, k is the Boltzman constant, T is the temperature in Kelvin, and r is the circuit resistance in ohms.

It is obvious from equation 3.13 that thermal noise can be minimised by either lowering the temperature or increasing the resistance. Unless the temperature

is dropped to close to absolute zero the effect on the thermal noise is not as pronounced as increasing the circuit resistance. Conversely, this has the effect of increasing the rise time or time response of the detection assembly (see equation 3.16). If high speed detection with very low optical input signals is required then cooling of the detector assembly may be the only option. The total noise associated with a semiconductor junction detector is then (Chaimowicz, 1992),

$$i_T = [\overline{(\Delta {i_s}^2)} + \overline{(\Delta {i_j}^2)}]^{\frac{1}{2}}. \tag{3.14}$$

5. **Time response**

In a PN junction diode the response time is a result of the time it takes for a charge carrier (electron or hole) to diffuse through to the depletion layer after it has been produced by a photon absorbed in either the P or N layer, and the transit time of the charge carrier across the depletion layer. The transit time can be expressed as (Jones, 1987),

$$t_{st} = \frac{W}{v_{sat}}, \tag{3.15}$$

where t_{st} is the transit time at saturation, W is the width of the depletion layer in the diode and v_{sat} is the charge carrier velocity at saturation.

The carrier velocity is a result of the electric field strength. As the velocity increases, the charge carriers increase temperature. The higher the temperature, the greater the amount of energy deposited into the lattice. Eventually all of the energy is deposited into the lattice and the carrier is effectively re-absorbed. Transit times for PN diodes can be as low as tens of picoseconds.

The rise time τ for a PN detector is calculated as an RC time constant so,

$$\tau = RC, \tag{3.16}$$

where R is the load resistance of the external detector circuit and C is the capacitance of the diode junction.

The capacitance, C_j of the diode junction can be expressed as (Jones, 1987) ,

$$C_j = \frac{\epsilon A}{W}, \tag{3.17}$$

where ϵ is the electric permittivity of the material, A is the active surface area of the detector and W is the depletion zone width.

If a high speed detector has a capacitance of $\approx$ 1 pF (Jones, 1987), and this is terminated into a 50 Ω load, this would give a rise time around 50ps.

3.3.5 The PIN diode detector

The PIN diode (P-type, Intrinsic, N-type) diode differs from the common PN diode as it has a layer of intrinsic material between the P and N doped materials. The intrinsic material is the same base material as the N and P type material without any doping (see figure 3.24 (Chaimowicz, 1992)). This has two distinct advantages. The creation of electron-hole pairs (EHP) occurs closer to the depletion layer as the intrinsic (I) substrate can make up most of the bulk of the detector and the collection substrate (either N or P), where the EHP generation occurs, can now be very thin. Diffusion of the principle charge carriers to the depletion zone is far quicker. As the negative and positive charges are separated by the I type material the junction capacitance is reduced. This increases the detector time response as indicated by equation 3.16. The transit time through the diode is increased however as the depletion layer is wider than in the PN diode (see equation 5). The electric

field strength which is normally very high in the depletion zone of a PN diode is reduced by the separation of the charges due to the I material. The electric field determines the velocity of the charge carriers through the detector. This can be increased by increasing the bias voltage.

In general the increase in transit time is insignificant compared with the reduction of the junction capacitance as this decreases the rise time. (Chaimowicz, 1992) shows two calculations, one for a PN diode, the other for a PIN diode under the same conditions. The transit time in the PN diode was 50 ps and the rise time was 2.75 ns. The PIN diode had a transit time of 114 ps and a rise time of 1.38 ns. The PIN diode, even with more than twice the transit time of the PN diode has a time response 1.24 ns faster. This is an eternity in satellite laser ranging. PIN diodes are far harder to make due to the width of the layers and the precision required in their widths. They are for this reason a great deal more expensive than the average PN diode.

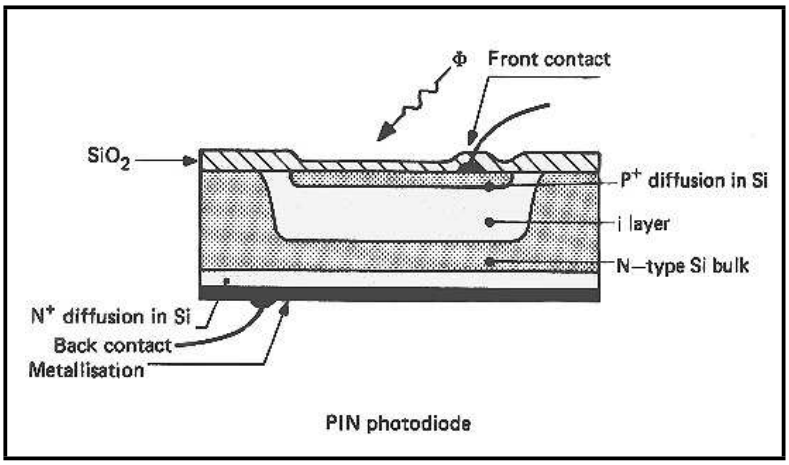

Figure 3.24: Simplified structure of a PIN photodiode.

3.3.6 The avalanche photodiode (APD)

The most distinctive advantage the APD (see figure 3.25 (Chaimowicz, 1992)) has over the PIN diode is the much higher gain. In a PN or PIN diode each photon at best will produce only one photo-electron. With a quantum efficiency or probability

that an incident photon will produce a photoelectron of around 30 percent, it is apparent that the gain of these diodes is quite small (less than one).

The APD, while no more likely to produce an initial photoelectron, will produce many more secondary electrons due to the structure and operating conditions. Essentially, a PIN diode could be used in avalanche mode. PIN diodes are

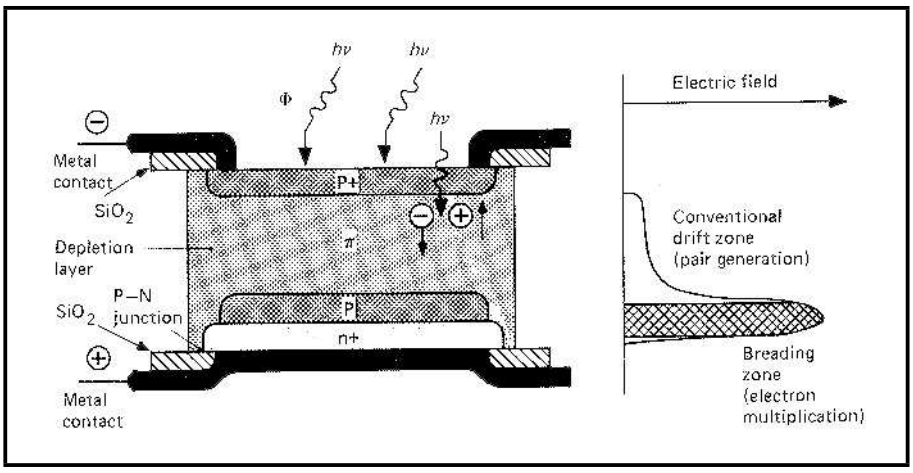

Figure 3.25: Simplified structure of an APD.

generally operated in reverse bias in the region known as third quadrant mode-photoconductive (see figure 3.22). If the reverse bias voltage is increased the characteristic curves drop sharply. This is known as the break over region and it is also the avalanche zone. The consequence of operating in this region is that photo-carriers (electrons or holes) experience high acceleration giving them enough inertial energy to 'knock' other charge carriers out of the lattice. If the energy gained by the photo-carrier is sufficient it may cause more than one such secondary generation and the secondary generations may themselves produce a further generation. The net result is a runaway or avalanche of charge carrier production. This increase in signal does not come at the expense of increasing the intrinsic noise level. The increase in noise is insignificant compared with the signal giving a far better signal to noise ratio than a simple PIN detector. This makes APDs especially attractive for the detection of weak optical signals.

The APD requires very careful treatment to achieve the best results. The gain

of the device is very sensitive to both operating voltage and temperature changes. Temperature increase perturbs the detector lattice making collision a great deal more likely. This will essentially dampen the output signal as more collisions will occur before the charge carriers have gained sufficient energy through acceleration. In many applications, especially SLR, the gain level is important, but the stability of the gain level is paramount. Many APD devices are temperature compensated so increases in incident light and ambient temperature have little effect on the device temperature so the operating characteristics will not change. This generally means cooling the device because this has the added advantage of increasing the gain. If the device was used with a high level of incident light, or in conditions where there are large changes in temperature, it may be better to heat the device so that the temperature is well above the maximum ambient temperature.

APDs often employ what is called a 'reach through' structure, so called because the high electric field generated in the Pn^+ layer (see figure 3.25) reaches through into the depletion layer. This electric field collects the charge carriers (electrons principally in the case of figure 3.25), generated in the depletion zone and accelerates these towards the avalanche zone. Charge carriers may produce secondary carriers in the intrinsic layer but this is not likely. The avalanche zone has the structure of a normal diode with a high number of receptor sites. The photoelectrons enter this zone with a high acceleration and energy and the number of photoelectrons is large as the chance of recombination in the intrinsic (generation) layer is small. There is now a high probability that these high energy photoelectrons will result in the generation of many secondary electrons.

This structure allows the charge carriers to achieve high acceleration before there is much chance of interaction, giving a much greater chance that significant numbers of secondary electron will be produced.

3.3.7 Comparison of the different detector types

The pursuit of accuracy in satellite laser ranging has prompted ranging sites around the world to investigate the capabilities of many types of photon detectors. These tests principally cover MCP-PMTs, APDs and SPADs (Single Photon Avalanche Diodes). SPADs are a special type of APD which are able to effectively operate on a single photon. They require special treatment as they are very susceptible to noise sources. Many such devices are temperature compensated (cooled) as even the chance of a spontaneous internal electron can cause an unwanted avalanche reaction. Many devices are specifically designed to work at specific temperatures. These are called C-SPADs (Compensated SPADs). The PSLR uses a standard PMT detector, a type not as commonly used by other SLR stations.

The PSLR detector has the advantages of being relatively inexpensive, easy to use, and the tube and power supply are small. It does not match the other detector types in terms of accuracy, time response, or quantum efficiency. Table 3.3 and table 3.4 show comparisons of the performance of various detectors at the SLR facilities; mobile station MTLRS-1, and fixed station 7836 Potsdam.

These tables show that each type of detector has advantages over the other types. The APD style detectors have high QEs, good accuracy and low timing jitter (or standard deviation from a known time). These types of detectors have very small active areas, and can be noisy. The tables indicate that APD type detectors have the best timing resolution. This performance must be weighed against the ease of use of such devices.

PMT based detectors do not have such good timing resolution but are less susceptible to induced noise, have far larger active areas and tend to be far easier to use as the treatment of the detectors need not be as strict.

The PSLR R4124 PMT tube and power supply are small which allows mounting on the portable telescope without taking up valuable space. The performance of this detector is only barely adequate for laser ranging applications and not up to the performance of the other types of detector.

	APD RCA C30902S	**APD** SPAD	**PMT** RCA 8850	**PMT** Hamamatsu H5023
Precision Single shot(RMS)	2.0-2.5cm	1.0-1.5cm	3cm	1.2-1.5cm
Quantum efficiency	20%-40%	10%-20%	14%	8%
Noise	$< KHz$	$0.1 - 1MHz$	$< KHz$	100hz
Active area	0.5mm	0.1 (0.2)mm	8mm	10mm
Supply voltage	$200V, 60V$	$< 50V$	$2000V$	$2000V$
Gating	$20\mu sec$	$2\mu sec$	no	no

Table 3.3: Detector comparisons carried out at MTLRS-1 (Sperber et al., 1994)

Detector type	**Sensitive area**	**QE@ 532nm**	**QE@ 1064nm**	**Timing jitter**	**Thermal noise**
RCA C30902 S-TC ($@T = 0^0C$)	small ($500\mu m$)	30%	2%	medium (150ps)	very low ($< 100Hz$)
SPAD ($@T = 20^0C$)	very small ($100\mu m$)	20%	1%	very low (30ps)	high ($> 100KHz$)
PMT H5023	very large ($> 1cm$)	8%	-	low (60ps)	low ($< 2KHz$)

Table 3.4: Detector comparisons carried out at Potsdam SLR station (Grunwaldt and Fischer, 1994)

The parameters listed in table 3.5 are for tests conducted at Curtin University using two fixed targets. In all cases the figures were recorded using an SR620 time interval counter, a purpose built pre-amplifier and an Ortec model 9307 pico-timing

Detector type	**Accuracy in cm**	**QE@ 532nm**	**Active area**	**Timing jitter**
Hamamatsu R4124	To fixed targets typically 1 - 3cm	(calculated from equ'n 3.18) $\approx 11.65\%$	13mm diameter tube	To fixed targets 100 - 300ps

Table 3.5: PSLR R4124 PMT detector behaviorial parameters.

discriminator.

The quantum efficiency (QE) as previously mentioned is the number of photoelectrons produced by the primary detection process (photocathode, electron-hole photogeneration) per incident number of photons. Quantum efficiency for the PSLR detector can be expressed in terms of the radiant sensitivity at a specific wavelength. Radiant sensitivity is the photocathode current divided by the incident radiant power of the light on the photocathode (expressed as $(\frac{A}{W})$ with the wavelength λ in nm) as (Hamamatsu Photonics, 1998),

$$QE = \frac{S \times 1240}{\lambda} \times 100\% \tag{3.18}$$

The quantum efficiency ultimately determines the design and operational modes of an SLR system. The PSLR, which has a high powered laser and a large area primary telescope can afford to have a detector with a lower QE, however with higher QE "fainter" ranging targets can be "seen". The quantum efficiency of the PSLR detector is shown in figure 3.26 (Hamamatsu Photonics, 1998). However the large primary mirror, high powered laser and associated equipment reduce the portability of the PSLR.

The ranging tests at Curtin University were conducted to two fixed targets at ranges of $\approx$ 17 m and $\approx$ 65 m.

The range timing jitter (actual time - expected time) varied from 100 - 300 ps RMS in all but the very first tests conducted at Curtin University and was generally

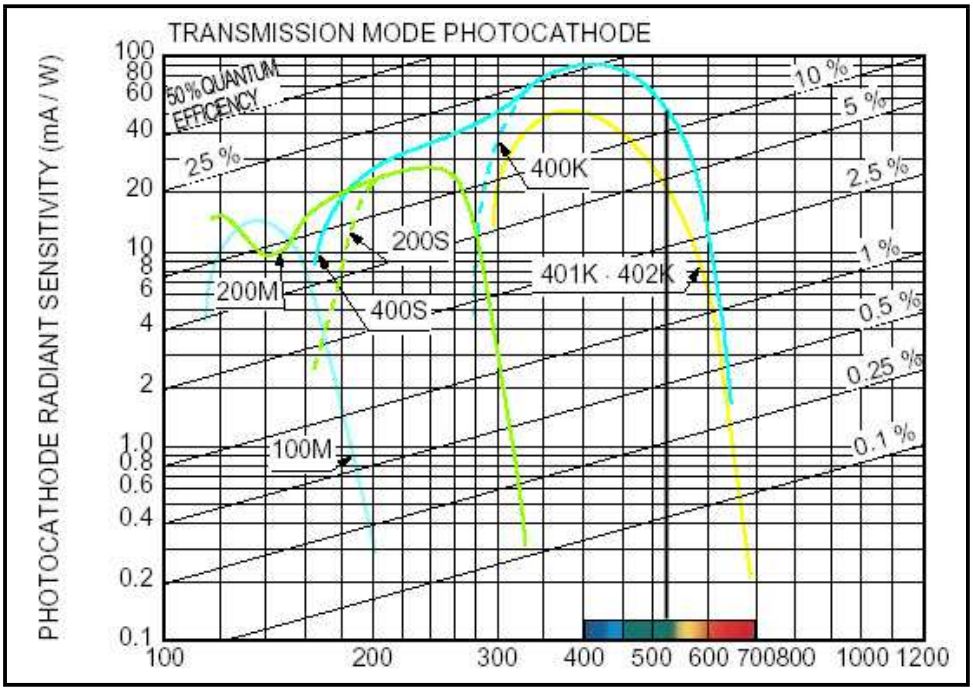

Figure 3.26: Spectral response and quantum efficiency for a number of Hamamatsu PMTs. The R4124 detector used with the PSLR is represented by the curve labelled 400 K. The vertical line added to the graph shows the approximate position of the PSLR laser operating wavelength (532 nm). This indicates that the QE for the PSLR detector at the ranging wavelength is just above 10%.

slightly smaller for the longer range. This is thought to be mostly attributable to a much larger return signal from the closer target.

The testing of the detector at Curtin University was not ideal. At the time the tests were conducted the main telescope and return detection optical path were not properly collimated and the power supply for the PMT was discovered to be very noisy. It is believed that the results achieved could be improved after some of these problems were resolved. These problems, results and description of the testing of the detector are covered in chapter 5.

3.4 Pulse conditioning electronics

3.4.1 The purpose of timing Discriminators

A majority of the detectors used for SLR applications are linear detectors (this is especially true for PMTs and MCP PMTs). This simply means that the output signal level from the detector is directly proportional to the number of photons received at the detector per unit time. For timing or counting applications this type of signal is too random for precise results. For this reason, a discriminator is used. The discriminator's basic function is to reject detector noise while enabling the linear or analogue signal to be to converted to a time correlated digital pulse which can be used to increment a counter or stop a timing unit. The discriminator, as indicated by its name can discriminate between low level background noise produced by the detector, and a genuine signal.

3.4.2 Fast-Timing discriminators

Traditionally, SLR systems have used constant fraction discriminators. This is principally to compensate for time-walk due to varying signal strength due to laser jitter, atmospheric effects and satellite retroreflector signature.

The purpose of a constant fraction discriminator is to use the input signal to set the threshold level. This is done by generation of a second signal. This second signal is delayed and then compared with the first signal. The second signal is attenuated so that it is half the original amplitude. This is generally added to a DC offset which is required to prevent a comparator from oscillating. The two signals are then fed into a comparator which will switch when they reach the same voltage level. This effect can be seen in figure 3.27 (Cova et al., 1996).

Another method is employed by the EG & G Ortec 935 Quad 200-MHz Constant-Fraction Discriminator (CFD). This produces a second signal which is treated similarly to the comparative discriminator in that it is also delayed. The delay is taken as the period of time taken for the original signal to rise from 20% to 100% of the

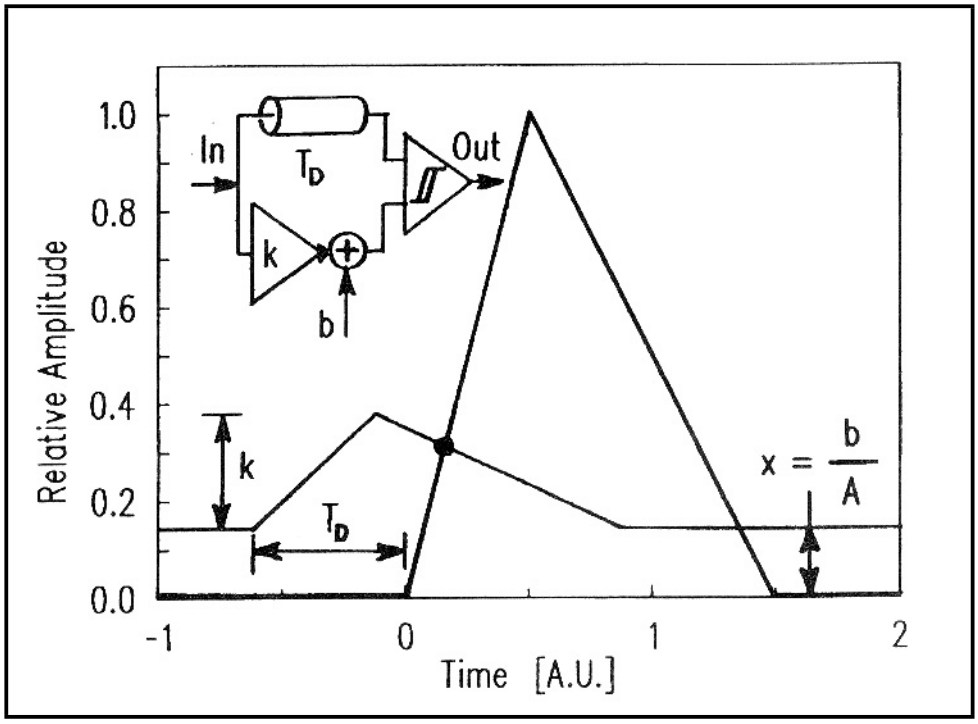

Figure 3.27: Constant fraction discriminator signal with comparator switching. As the signal is compared with a signal synthesised from itself, the switching of the comparator occurs at some fraction of the original input signal. This fraction is constant for each input signal so the switching is independent of signal level.

maximum signal strength. This pulse is now inverted. The original signal is attenuated to approximately half of its amplitude. These signals are added together producing a waveform of the type seen in figure 3.28 (ORTEC, 2001). The CFD tests this signal until it reaches the waveform zero crossing point. The CFD then produces an output pulse. Pulse conditioning of this type is very resilient to time walk.

3.4.2.1 Limitations of timing discriminators

There are three main limitations to the absolute functional accuracy of timing discriminators. These are: jitter, walk and drift. These properties are inherent in all electronic discriminators to a greater or lesser extent. Timing discriminators like all pulse conditioning electronics attempt to reduce these effects to a minimum.

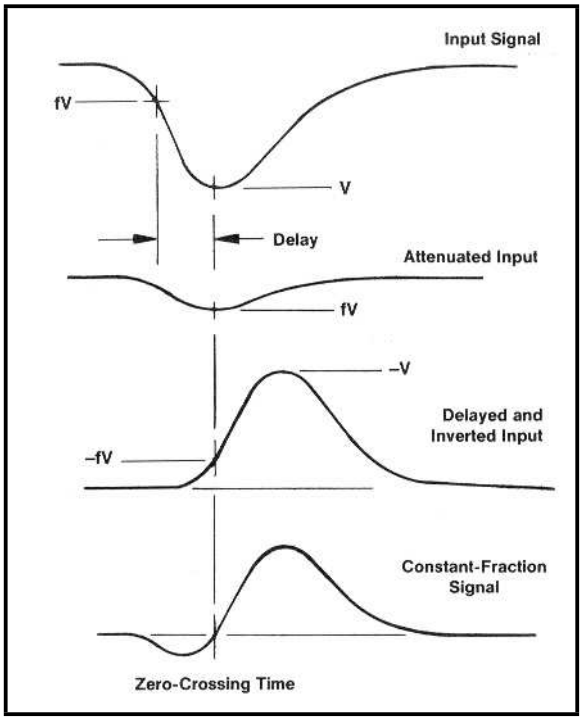

Figure 3.28: Constant fraction discriminator signal with zero crossing threshold switching

Jitter is a result of inherent electronic or white noise which is superimposed on the primary input signal.

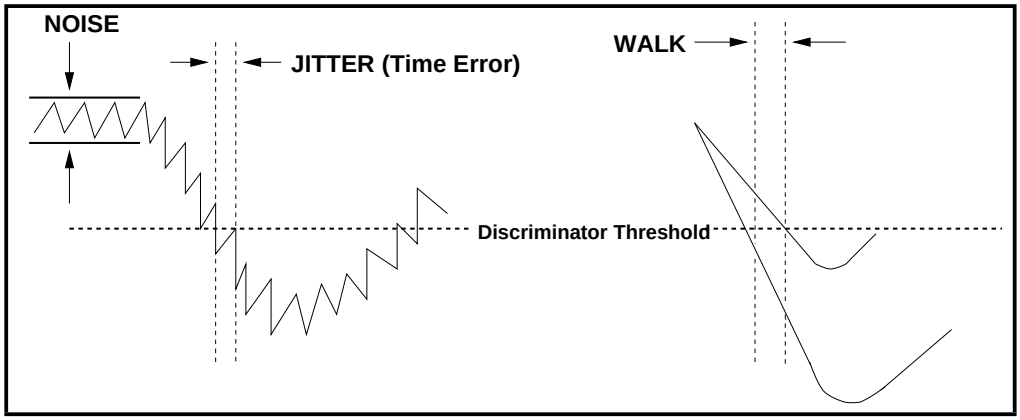

Figure 3.29: Factors effecting the absolute accuracy of discriminators

The illustration in figure 3.29 (ORTEC, 2001), shows a threshold level used to activate an output logic pulse from the discriminator. The pulse is activated when

the input signal exceeds the threshold level and is de-activated when the input signal drops below the threshold. Figure 3.29 shows the jitter or uncertainty in the start of the logic pulse as a variation in possible threshold crossing due to the noise on the signal.

The jitter can be quantified by the following equation (ORTEC, 2001),

$$Timingjitter = \frac{e_n}{dV/dt}, \tag{3.19}$$

where e_n is the amplitude of the voltage of the noise superimposed on the input signal, and $\frac{dV}{dt}$ is the slope of the leading edge of the input signal (neglecting the noise) when it crosses the discriminator threshold .

To reduce the timing jitter, the discriminator threshold should be set so that the input signal crosses the set level at the point were it has the maximum slope. This will decrease the jitter by reducing the number of possible threshold crosses by a noisy signal.

Walk or Time-walk is the greatest limitation of discriminators and timing electronics as it is difficult to remove this effect. It is a result of use of a preset discriminator level with pulses of different amplitudes received at the discriminator from a detector. This is clearly seen in figure 3.29. The right hand side of this figure shows two similar shaped pulses with the lower pulse having a greater amplitude. This pulse crosses the discriminator threshold earlier than the lower amplitude pulse, which would, with a simple threshold switching arrangement, cause the device to switch earlier than the smaller pulse. Timing accuracy would be compromised with such a simple threshold switching system.

While jitter is inherent to the system and can be compensated for, walk effects are more a result of the phenomenon being measured. In SLR, where there is great variation in signal strength due to atmospheric effects, target satellites, laser jitter and pointing accuracy etc, walk can pose a major problem.

Drift is a systematic effect which is somewhat harder to correct for. Drift is the

degradation in the timing accuracy over a period of time, either during a sampling run or over an extended period. Short term drift may be the result of temperature variations over the period of a satellite track. Long term drift may be the result of degradation of electronic components.

Most of the detectors used in SLR systems have a low to medium quantum efficiency. Put simply, quantum efficiency is the measure of the number of output electrons from a detector per number of input photons (before detector amplification). With low quantum efficiencies, large numbers of photons are required to produce good output signals. If this quantum efficiency is reduced then the output signal from the detectors will degrade and the accuracy of the timing will be reduced.

Sample-to-sample drift can be attributed to changes in detector quantum efficiency (due mainly to temperature variations). Long term drift results from detector materials gradually degrading through use.

Drift in event timing can also be caused by all of the other electronic equipment, including discriminators. Long term drift can, to some extent be compensated for by regular calibration of SLR systems. The short term drift is best compensated for by suitable climate control around vital SLR components.

3.4.2.2 The ORTEC 9307 pico-Timing^{TM} Discriminator

This particular model is used with the PSLR. The following deals with several of the characteristics and properties associated with the 9307 discriminator. This information was obtained from an ORTEC product sheet (ORTEC, 2001).

The pico-timing discriminator (PTD) is, according to the product manual, optimum for single-photon measurement with most electron tube products. It has a very small bandwidth, accepting pulses from 400 ps to 5 ns FWHM, with input amplitudes from -50 mV to -5 V. It incorporates ultra-fast timing circuits which minimise time-walk. It is claimed that input amplitudes can vary as much as 1:100 without significant error due to walk. There is an adjustment which will allow fine

tuning of the slewing compensation depending on the detector used. The following specifications are included in the product manual.

Performance

- **Time-walk(Slewing)**

  $<\pm$ 20 ps shift in the timing output for input signal amplitudes from -150 mV to -1.5 V. (Typically $<\pm$ 50 ps for signal amplitude from -50 mV to 5 V). Measured using a 1 ns wide input pulse with 350 ps rise and fall times.

- **Pulse pair resolution** $<$ 10 ns at the negative NIM outputs.

- **Maximum input/Output rate** Accepts bursts of up to 100 MHz.

- **Operating temperature range** 0 to 50 ^0C.

- **Threshold Temperature Sensitivity** $<\pm$ 0.1 $mV/^0C$ (0 - 50 ^0C).

The PSLR uses two ORTEC 9307 pico-Timing^{TM} Discriminators, one each for the stop and start detectors. Assuming that any laser jitter (variation in the laser output amplitude, pulse duration) should be seen in both the start and stop detectors, the identical treatment of two discriminators should eliminate the effect equally. Both PSLR detectors use a preamplifier to boost the signal before each is fed into the discriminators.

3.4.3 Preamplifiers and their operation

Even though photomultiplier tubes provide a great deal of amplification due to the number of dynode stages, low return signal strengths from satellites will still produce a very weak output signal from the detector. In an effort to improve the performance of the discriminator, the signal from the detector must be amplified so that it is well above the intrinsic noise level. This requires a pre-amplifier stage which increases the signal without significantly affecting the signal to noise ratio.

3.4.3.1 Choosing the right pre-amplifier

For SLR applications, ultra-fast timing is required for millimeter range accuracies. For optimum discriminator performance the pre-amplifier should have the following characteristics:

- fast rise time,
- impedance matching to the detector and discriminator, and
- good signal to noise ratio.

As well as these general characteristics there is one other major consideration. The largest source of error in timing resolution with PMTs is fluctuations in electron transit times through the tube (ORTEC, 2001). If the signal is small then a pre-amplifier can add significant timing jitter to the signal input to the timing discriminator. In general a pre-amplifier should be chosen which has a pulse rise time as close to the rise time of the detector as possible (ORTEC, 2001). This is disputed somewhat in the paper by (Cova et al., 1996) which states that the higher bandwidth pre-amplifiers often used with ultra-fast detectors (such as MCP PMTs) to match rise times, can add more jitter than it removes. This paper found a broad minimum which was centered around an optimum bandwidth value B_{Aopt} which in all cases was below 2 GHz and was generally closer to 1 GHz. This article concluded that the best results could be obtained by using pre-amplifiers constructed using fast bipolar junction transistors (BJT), rather than types employing ultra-fast metal oxide semiconductor field-effect transistors (MOSFETs). MOSFETs, while reducing the input current noise, contribute more to timing jitter due to a greater noise contribution in the lower frequencies of the noise spectrum. The BJT does have a larger noise component in the higher frequency end of the noise spectrum but this tends to increase the slope or rise time of the timing pulse which actually reduces jitter. The paper by (Cova et al., 1996) states that with the correct choice of pre-amplifier,

timing jitter due to circuit noise can be kept below 5 ps FWHM which produces an uncertainty in distance measurement of 0.75 mm.

3.4.3.2 Preamplifier types

There are three basic preamplifier types:

- current-sensitive,
- parasitic-capacitance, and
- charge-sensitive.

Each of these is suited to particular applications. For example the parasitic-capacitance type is used with MCP-PMTs for pulse-amplitude measurements and spectroscopy work where the resulting signal from the preamplifier is proportional to the total charge in the detector pulse. The rise time of the preamplifier pulse is matched to that of the detector. Charge-sensitive preamplifiers are used for spectroscopy with semi-conductor detectors as parasitic-capacitance types are sensitive to capacitance fluctuations often experienced by these detectors.

For SLR applications, where pulse rise time and jitter are the main concerns, current-sensitive preamplifiers are preferred (see figure 3.30 (ORTEC, 2001)). These use a properly terminated cable with a fixed resistance of 50 Ω which will allow the preamplifier to develop a corresponding output pulse, the voltage of which is proportional to the preamplifier output current.

The output pulse voltage V_{out} can be estimated using (ORTEC, 2001),

$$V_{out} = 50 I_{in} A. \tag{3.20}$$

Preamplifiers are often essential when down stream electronic devices are connected to detectors that do not produce large output signals. Pushing a signal through a length of cable requires that there is some current capacity from the signal generator. The types of detectors commonly used with SLR do not have a great

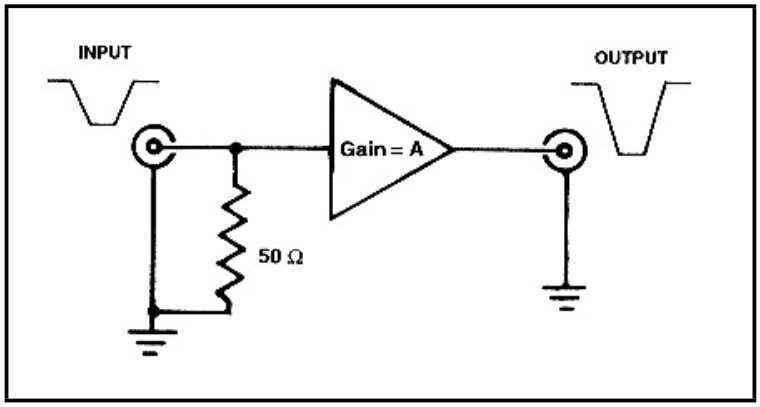

Figure 3.30: Simple schematic of a current-sensitive preamplifier

deal of current capacity so pre-amplification is required to push the signal through the cable. It is considered a good practice to have the preamplifier as close to the detector as possible since the preamplifier as placing it at the end of a cable could result in the preamplifier increasing not only the detector signal but also noise introduced in transmission along the cable. This will degrade the signal to noise ratio of the signal supplied to the amplifier/discriminator.

3.5 Time interval acquisition

3.5.1 Methods of time interval acquisition

Accurate event timing is crucial for modern laser ranging applications. Modern timing devices are capable of timing resolutions of just a few picoseconds. This level of timing resolution requires not only sophisticated equipment but intelligent techniques.

Most electronic timing devices operate by digital principles where an analogue phenomenon is measured using a discretised system. How is a time interval, which is an analogue phenomenon, measured electronically? A digital system can determine elapsed time if there is some periodic change of state. It can count time by registering a number of periodic changes of state. The result is a count of a number of packets

of time over an interval. If the packets of time can be made as close to identical as possible then multiplying the time packet interval by a number of counts will yield a total time interval.

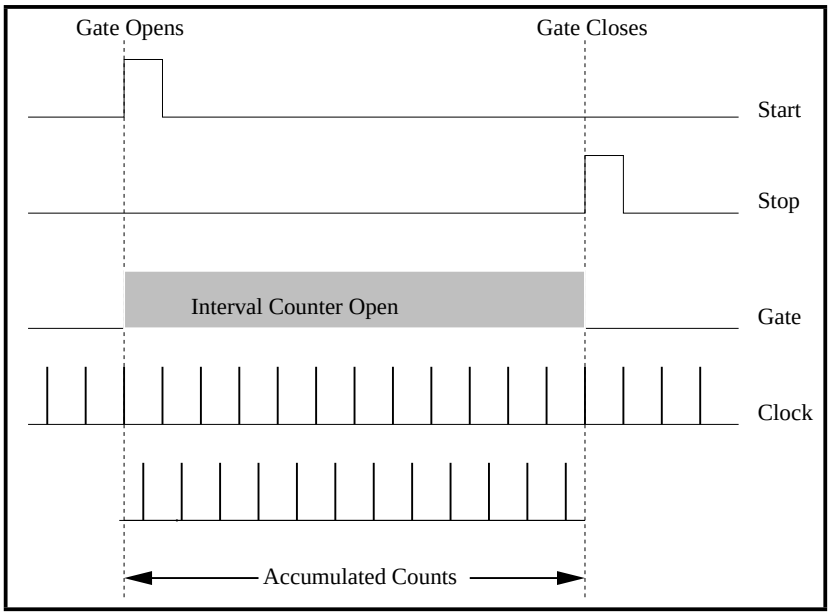

Figure 3.31: Representation of measuring a time interval by counting a number of periodic pulses.

Precise time interval pulses are produced today by two main schemes. The first and most commonly used, due to its relatively low cost and versatility, is based on the quartz crystal oscillator. Quartz crystal can be made to oscillate by applying an alternating electric current. The frequency and mode of vibration is determined by the size and shape of the quartz crystal. In general the smaller the size of the quartz crystal then the higher the frequency of vibration. Modern crystal oscillators can be made to oscillate with stable frequencies in the MHz range.

The second type is the atomic frequency standard. This relies on the discrete energy levels associated with electron states. In general alkali metals or group (I) elements are chosen because they have very tightly bonded inner shell electrons with a single outer shell electron which is easy to excite. In general, the material chosen is bombarded with microwave radiation which causes an electronic energy transition

to occur. The frequency of oscillation is a result of the difference in energy in the particular transition and can be measured by,

$$f_1 = \frac{\Delta E}{h}, \tag{3.21}$$

where h is Planck's constant.

The frequency standard most commonly used today is the Caesium frequency standard. This uses the hyperfine transitions in the electronic and nuclear spin orbitals of the ^{133}Cs atom to resonantly tune to a frequency of 9192631770 Hz, which gives a period slightly longer than 100 ps. The frequency standard uses crystal oscillators (which are slaved to the primary frequency) to produce normally 5 MHz and/or 10 MHz output frequencies. This type of atomic clock is stable to 2 to 3 parts in 10^{14} and will lose only 2 ns per day (Breakiron, 1999).

Regardless of the type of oscillator used, this method of time interval determination is fairly straightforward. The appropriate oscillator circuitry will produce electrical pulses at a frequency (f_{TB}) determined by the time base (either quartz crystal or atomic). These pulses are used to increment a counter which will store the total counts corresponding to a time interval. The time interval can then be determined by multiplying the pulse counts by the reciprocal of the time base frequency,

$$TI = \text{Total Counts} \times \frac{1}{f_{TB}}. \tag{3.22}$$

The uncertainty associated with this timing scheme (neglecting delays associated with cable delays, rise times etc) and the smallest interval that can be measured is one time base interval. If the oscillator frequency is 500 MHz then the uncertainty or resolution is 2 ns. This single oscillator technique time resolution of 2 ns is about the maximum achievable accuracy with a single quartz crystal (HP, 1997).

SLR techniques require that timing resolutions are in the order of 30 ps for current single shot accuracy which is 2 orders of magnitude better than single oscillator

time resolution. To achieve the required resolution there are two main techniques, Time Interval (TI) averaging and Interpolation.

3.5.1.1 TI averaging

This is a purely statistical approach and requires that the type of measurements taken comply with the following requirements:

1. Each time measurement must be taken of exactly the same physical characteristic i.e pulse transit time through a length of cable.

2. The errors associated with the measurements must be random.

3. The frequency of measurement error must be greater than the clock frequency or the uncertainty in measurement must be less than the resolution of clock so that the least significant digits contain the random error.

If all of these conditions are met then averaging the timed results will improve the resolution. The uncertainty or resolution of a single measurement is the inverse of the oscillator frequency. For interval averaging, the uncertainty of the time interval (ΔTI) can be reduced to the single measurement resolution (SS) divided by the square root of the number of measurements taken (HP, 1997),

$$\Delta TI = \frac{\pm SS}{\sqrt{N}}. \tag{3.23}$$

So, for the maximum resolution of 2 ns available from an oscillator, if a million measurements are taken, this uncertainty can be reduced to 2 ps or improved by 3 orders of magnitude.

Unfortunately this technique is not applicable to SLR measurements for a number of reasons. The major reason is that it is impossible to take measurements that are exactly the same. As satellite orbits are elliptical, precess with respect to a fixed observer on Earth and the medium through which the laser beam travels is largely variable, each measurement is unique. Many of the uncertainties associated

with the measurements are not random in nature i.e range bias cause by a gradual increase in atmospheric pressure. For these reasons, another method of improving the estimate of accuracy in range resolution is required.

3.5.1.2 Interpolation

This method requires the use of three separate oscillators. The original time base oscillator is still required and is used as the reference oscillator as well as two slave oscillators, one used for marking the start of a time interval, and one to mark the end of the interval. The process involved is much like reading a vernier caliper and the start and stop oscillators are often called the 'verniers'. With a vernier caliper, two scales are used with differing levels of resolution and a reading is taken where the two scales coincide.

The dual vernier interpolation method employed with many timers uses the two slave oscillators to mark these coincidences. The start signal to the timer starts both the first slave oscillator and the associated counter (n_1) as well as the counter for the reference signal (n_m) which will start to count on the next reference pulse. The reference oscillator (timebase) always operates so the next references pulse will occur at some time after the starting process occurs. At the first instance of a coincident pulse from both the first slave oscillator and the reference oscillator (coincidence 1), the first slave oscillator count will cease. When the stop signal is received it will activate the second slave oscillator and associated counter (n_2) and cease the count on the reference oscillator at the next reference oscillator pulse. The second slave oscillator count will cease as soon as there is a coincident pulse between it and the reference oscillator (coincidence 2). This is more evident with reference to figure 3.32.

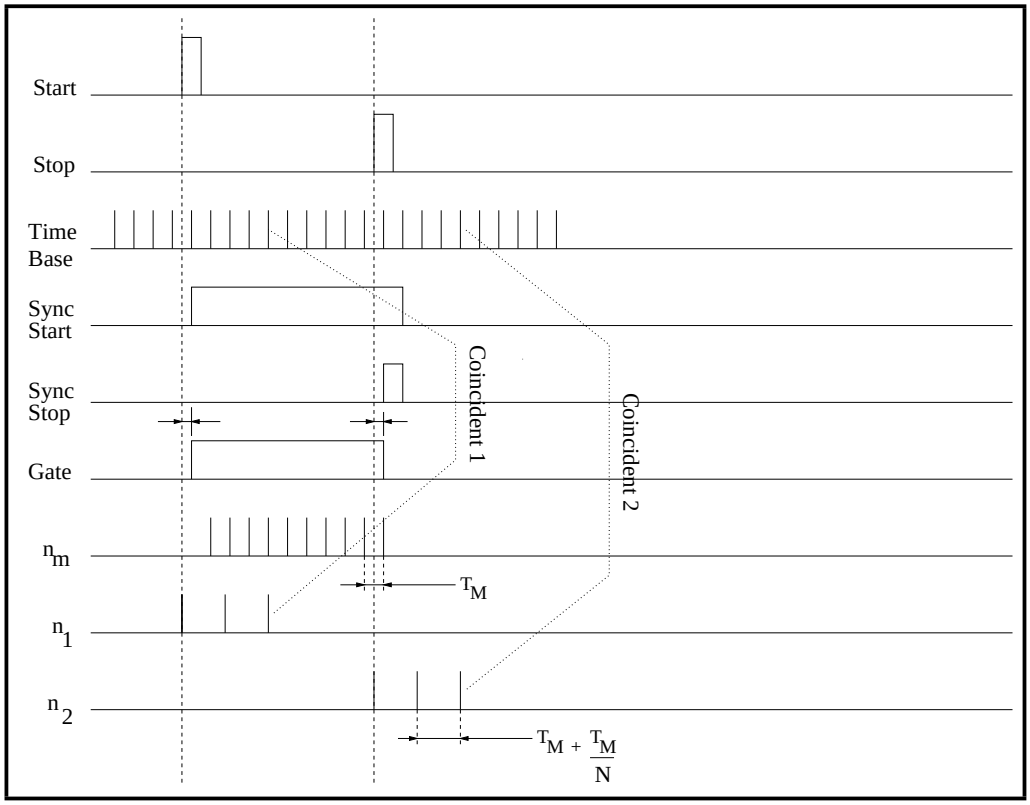

Figure 3.32: Interpolation technique using vernier slave oscillators to improve the time resolution without improving the oscillator resolution. The start and stop pulses shown in this figure start the appropriate oscillators and counters. The time interval is then determined by counting oscillator pulses and applying the appropriate interpolation factor.

This allows the following calculation to be carried out to determine the time interval, TI, where (HP, 1997),

$$TI = T_m[n_m + (1 + \frac{1}{N})(n_1 - n_2)], \tag{3.24}$$

T_m = Master oscillator period, n_m = Master pulse counts, N = Interpolation factor (T_m/(Slave oscillator period $- T_m$)), n_1 = Start slave oscillator pulse counts, and n_2 = Stop slave oscillator pulse counts.

This interpolation technique is very useful. It allows information about the arrival of start and stop impulses that arrive between the master oscillator pulses

to be noted. If the master oscillator has a pulse mark width of 5 ns and the slave oscillators have a pulse mark width of 5.02 ns (an interpolation factor of 256) then the 5 ns resolution is now increased to approximately 0.02 ns (20 ps). If the start pulse arrives at 0.5 ns past a master clock pulse and the start oscillator is activated, then there will be a coincident pulse 231 slave oscillator pulses later, which will correspond to 4.5 ns. This amount of time needs to be added to the time determined by the master clock pulses. The same situation occurs at the stop impulse. If the stop impulse arrives 2.22 ns after a master oscillator pulse then there will be a coincident pulse 145 slave oscillator pulses later. This amount of time needs to be subtracted from the time determined by the master oscillator clock pulses.This would be determined electronically by the time interval counter in the following way where,

$$TI = T_0 + T_1 - T_2, \tag{3.25}$$

$T_0 = n_m T_m$ (master oscillator time),
$T_1 = (T_m + \frac{T_m}{N})n_1$ (start oscillator time),
$T_2 = (T_m + \frac{T_m}{N})n_2$ (stop oscillator time), and
$(T_m + \frac{T_m}{N})$ = (slave oscillator period).

If values for T_0, T_1, T_2 are substituted into equation 3.25 then , as expected, equation 3.24 results:

$$\begin{aligned} TI &= n_m T_m + (T_m + \frac{T_m}{N})n_1 - (T_m + \frac{T_m}{N})n_2 \\ &= n_m T_m + T_m(1 + \frac{1}{n})(n_1 - n_2) \\ &= T_m[n_m + (1 + \frac{1}{N})(n_1 - n_2)]. \end{aligned} \tag{3.26}$$

While this method of improving resolution without producing an oscillator faster than 5 ns seems to lend itself to even better resolutions by selecting a large inter-

polation factor, there are limitations on this technique. If the inherent jitter in the system is around 35 ps, which is feasible for high quality electronics, then having an interpolated resolution substantially better than this will only lead to false triggering and a degradation of the acquired data. There is also the problem of marking the coincidences. This requires the use of a discriminator which will trigger at a rate faster than the resolution value or false coincidence marking will occur (ie it would miss the first coincidence) (HP, 1997).

3.5.1.3 Other factors affecting the precision and accuracy of time interval counters

This section will deal with other limitations associated with time interval measurements that reduce the resolution. This will deal principally with the Stanford Research Systems SR620 Time Interval Counter (TIC) which is the time interval counter used with the PSLR. These comments, however, are applicable to other time interval counters.

3.5.1.4 Resolution

The smallest time interval or time difference that a TIC can recognise is termed its resolution. It is determined by many different factors and parameters. The most important of these is the absolute resolution determined by the clock speed and interpolation factor as discussed in sections 3.5.1.1 - 3.5.1.3. Other factors such as, short-term timebase stability, internal noise and trigger noise will affect the resolution. These factors are mostly random in nature so these are added as RMS uncertainties. The absolute resolution is also expressed as an RMS value. The time resolution (δT_{SR}) of the SR620, without regard to the type of measurement made, is specified as (SRS, 1999),

$$\delta T_{SR} = \sqrt{(25ps)^2 + (\Delta t \times \text{short term stability})^2}. \tag{3.27}$$

In equation 3.27, Δt is the time interval over which the measurement is recorded with the resultant resolution expressed in ps RMS. The effect of short-term stability is mostly important for measurements over 125 ms for the standard SR620 oscillator, and 500 ms for the oven-stabilised oscillator because it will be the dominant factor in resolution for longer time periods (SRS, 1999). This is less important for SLR measurements as time intervals associated with most measurements are far less than 125 ms i.e LAGEOS time intervals are around 40 ms (round trip time to a LAGEOS satellite at 6000 km). For lunar laser ranging and ranging to GPS satellites (closer to 40 000 km round trip), this issue will need to be considered.

The timebase drift can be compensated by using an external signal to condition or steer the internal timebase. This signal can be supplied from a GPS time unit or a caesium frequency standard. These devices have better resilience to short term drift (these devices are explained in greater detail in section 3.7). The benefit of this is that the internal stability characteristics are also locked to the external signal. The figure 3.33 illustrates how a caesium clock is used to improve the stability of an internal timebase for the SR620.

For time interval, width, rise and fall time measurements the SR620 resolution, (T_{res}) and error, (T_{err}) are given as;

$$T_{res} = \pm\sqrt{\frac{(25ps)^2 + (\Delta t \times STS)^2 + (TJ_1)^2 + (TJ_2)^2}{N}}, \tag{3.28}$$

STS = Short-term stability,

TJ_1 = Start trigger jitter,

TJ_2 = stop trigger jitter, and

N = number of measurements if TI averaging is used.

$$T_{err} = \pm[Res + (TBE \times \Delta t) + TLE_1 + TLE_2 + 0.5ns], \tag{3.29}$$

TBE = Timebase error,

TLE_1 = start trigger level error, and

TLE_2 = stop trigger level error.

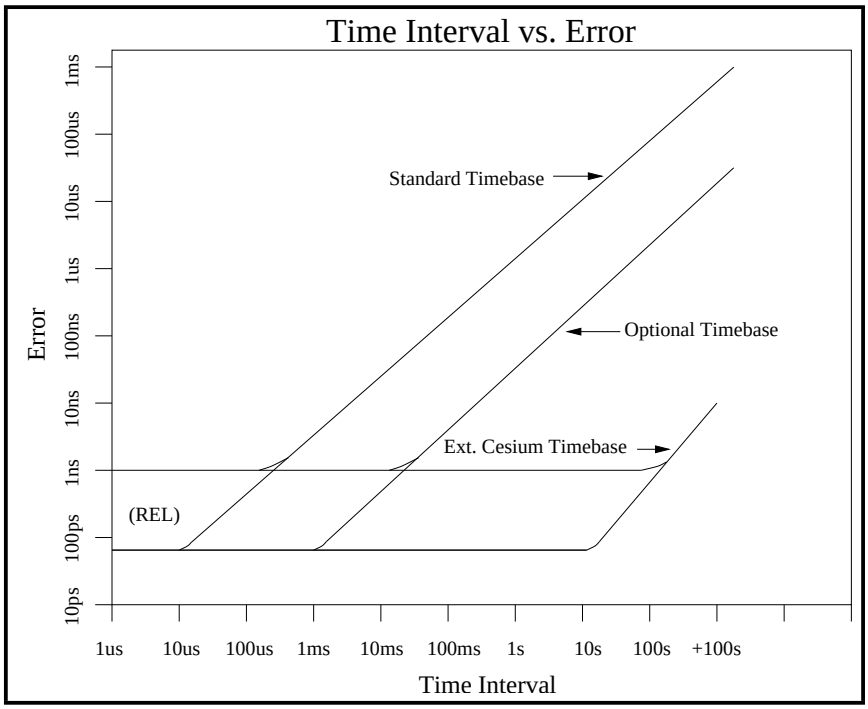

Figure 3.33: Illustration of the improvement in short term stability or timebase error for a standard and ovenised oscillator used with the SR620. The stability of both oscillators is improved over much longer time intervals with application of an external frequency.

3.5.1.5 Timebase error - Long term stability

The long-term stability of an oscillator is indicated by the amount of shift away from the starting frequency or period of the timebase over an extended period of time i.e day, week, year etc. This is a systematic error, which can be largely removed with careful calibration. The monitoring of long term drift is especially important with SLR measurements as many of the applications of SLR data (such as gravity measurements and continental drift), rely on long term data sets. It is essential that trends in data sets that run over many years show the actual long term property rather than long term measurement drift of the instrument.

The drift is caused by environmental factors such as temperature change and physical changes in the oscillator crystal along with component aging. Both the aging effect and the temperature effect drift rates are quoted as fractional frequency changes over a period of time. For the SR620 TIC these figures are quoted in table 3.6.

	Standard Oscillator	**Oven Oscillator**
Aging	$1.0 \times 10^{-6}/yr$	$5.0 \times 10^{-10}/day$
Temperature response	$1.0 \times 10^{-6}(0-50)^0C$	$5.0 \times 10^{-9}(0-50)^0C$

Table 3.6: SR620 fractional long-term stability drift rates.

The interval counter (or timing device) provides the most important SLR data as all subsequent products are derived from these measurements. The SR620 and the HP5370 are two of the oldest timers used in the current generation and still the most popular (still used by approximately 76 % of stations). SLR stations like MOBLAS-5 still use the HP timer and can achieve normal point (see section 2.4.6, page 49) RMS accuracies of a few millimeters. Table 3.7 contains a list of the timer specifications for timers commonly used by the SLR community. As can be seen from this table, the specifications for the MOBLAS-5 timer are at the poor end of the scale and still this station is among the most accurate throughout the world. This would indicate that with better time resolution, sub-millimeter accuracy is likely in the near future.

Many stations are adopting new approaches to ranging which require event timers. These type of timers do not measure an interval but time stamp received signals. If a high repetition laser is used it will note the return time of all of the pulses rather than the time interval for each laser pulse. The time of flight for each pulse is extracted from the sequentially recorded times during processing. This type of timer allows stations to increase the volume of data collection. Coupled with the resolution of the new breed of event timers being 1ps and below, normal point accuracies in the sub-millimeter range are achievable.

Timer	**Res^n (ps)**	**Jitter (ps)**	**Lin. (ps)**	**Stab. (ps/K)**	**Stab. (ps/h)**	**Max. rep. rate (Hz)**	**Max. TOF (sec)**
1	4	22	50	5		100	1000
2	20	35	20			10	10
3	10	20	2		2	80	0.209
4	100			40			NA
5	1.2	3.5	3	<0.3	<0.5	>100	NA
6	2	10	1		1	1000	NA
7	0.5	<2			0.5	2000	NA
8	1	10.8	<1	0.1	0.5	1000	NA

Table 3.7: Comparison of time of flight (TOF) devices used by the SLR community including: resolution, timing jitter, timing linearity, timing stability over time and temperature range, the maximum sampling rate, and the maximum recordable time period. The model, year of manufacture and the timing approach used are listed below:

1.) SR620 (1998) - interval counter,

2.) HP5370B (1982) - interval counter,

3.) Latvian University A013a (2002) - interval counter,

4.) Ortec TD811 (pre 1980) - event timer,

5.) PESO Consulting PET4 (1999) - event timer,

6.) EOS MRCS V.4 (1998) - event timer,

7.) HTSI MLRO (1998) - event timer,

8.) Latvian University A031-ET (2003) - interval counter and event timer.

(ILRS, 2003)

3.6 Filtering

Satellite laser ranging requires the ability to very precisely detect the epochs of the output of each laser pulse and the subsequent return. The optical signal (laser pulse)

is very small with respect to ambient sunlight so methods of optical filtering have been developed to increase the signal to background ratio. Even with the use of the optical filtering techniques it is not possible to completely remove the background from the signal. The next layer of filtering is electronic and occurs in the detection, pulse conditioning and timing electronics. These devices can be gated at specific times so that any unwanted optical signals will not cause a return or stop event to be registered before it is expected.

Both optical and electronics methods are used to control the amplitude of the return pulse. This is essential to reduce timing degradation due to time-walk.

3.6.1 Optical filtering

Optical filtering is employed on SLR systems in an attempt to:

1. ensure that all extraneous light (any light that hasn't originated from the stations laser) will not enter the detector and cause an unwanted triggering of the device,

2. and to ensure that the incoming light lands on the centre of the detector to reduce the chance of any edge effects (differing pulse lengths and shapes dependant on the position of the incoming light on the detector front).

3.6.1.1 Spectral Filtering

Spectral filtering as the name suggest relies on the spectral properties of light to restrict or remove the unwanted part of the spectrum. Laser ranging applications require that this restriction of the spectrum is total (for all parts of the spectrum which will trigger the detector) apart from a very small band, and that this band is centred at the station lasers wavelength.

The PSLR used a spectral filter which has a centre wavelength of 532 ± 2 nm, a full width half maximum (FWHM) value of 1.5 nm and a maximum transmission of 45% and almost complete blocking of all other wavelengths from 100 - 1200 nm.

A more appropriate filter for the PSLR would be the model 532FS02-25 from Andover Corporation. This filter has a centre wavelength of $532 + 0.2/-0$ nm, a total bandwidth of 1.0 ± 0.2 nm and a maximum transmission of 45% and will block all other wavelengths from x-rays to the far infrared. This filter is a two cavity filter and it's bandpass characteristics are represented in figure 3.34.

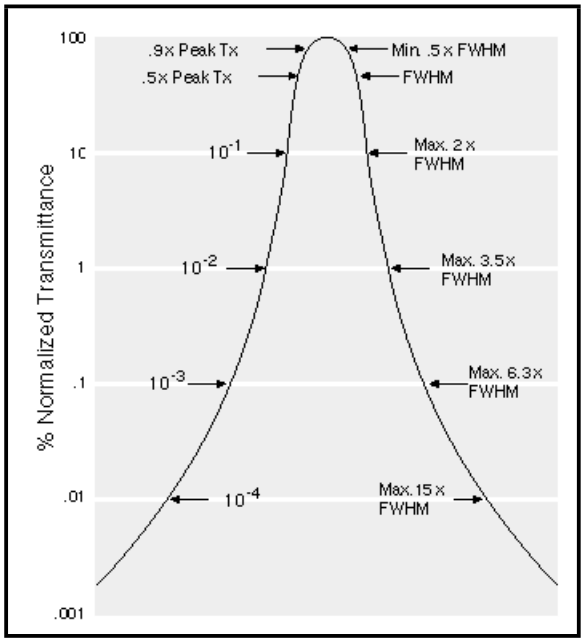

Figure 3.34: Example of a type 2 (two cavity) filter transmission band (Andover Corp., 2004b).

Each cavity in this filter consists of two Fabry-Perót etalons separated by a dielectric material. The etalons consist of alternating layers of high and low refractive index material. If the number of layers and/or the width of the dielectric is altered, it is possible to choose the central wavelength of transmission through the filter. The first cavity is designed to select the central wavelength but does not provide adequate blocking for the rest of the spectrum. This is accomplished by the second cavity.

The central wavelength of this type of filter is affected by temperature and the angle of incidence. As the temperature increases, the central wavelength will also increase. The central wavelength will decrease when the temperature drops so it

is essential to provide a stable temperature to the filter when high tolerances are required (as in SLR). The angle of incidence will also change the central wavelength of the filter with this value moving towards lower wavelengths with higher angles of incident.

The wavelength shift with the angle of incident can be expressed by (Andover Corp., 2004b):

$$\lambda_\theta = \lambda_0[1 - (\frac{N_e}{N^*})^2 \sin^2\theta]^{\frac{1}{2}} \tag{3.30}$$

where, λ_θ is the wavelength at the angle of incident, λ_0 is the wavelength at normal incidence, N_e is the refractive index of the external medium (i.e. air), N^* is the effective refractive index of the filter, and θ is the angle of incidence.

This property of the filter can be used to fine tune the central wavelength and to some degree compensate for the temperature shift.

If the spectral filtering is working properly it should provide significant protection against ambient light entering the detector. This is essential during daylight hours.

3.6.1.2 Spatial Filtering

It is possible to adjust the field of view of a telescope below the diffraction limited value by either placing an aperture stop or field stop in the optical train. The aperture stop is placed before the secondary mirror (from the direction of incoming light) and simply makes the incoming aperture smaller. As the apertures of most SLR primary telescopes are relatively large (diameters larger than .5m) it is not practical to use variable aperture stops to limit the field of view.

A field stop is placed just before the focal plane (in SLR applications, this is the detector) and is simply a plate with a circular hole (see figure 3.35).

The field of view of a telescope in steradians Ω_r can be evaluated by (Degnan, 1993):

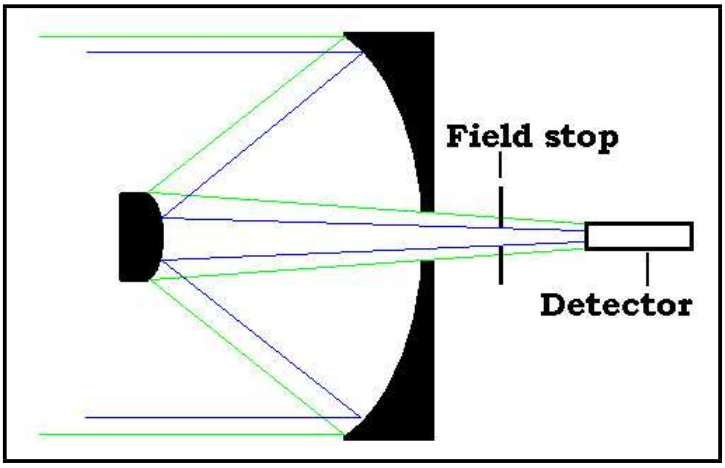

Figure 3.35: Illustration of the effect on the field of view of a reflecting telescope when a field stop is placed in the optical chain.

$$\Omega_r = \frac{\pi\theta_r^2}{4\pi} = (\frac{\theta_r}{2})^2 \tag{3.31}$$

given,

$$\theta_r = \frac{R_D}{f} = \frac{1}{ka_r}(\frac{kR_D}{2F_s}) \tag{3.32}$$

where, θ_r is the half angle of the the receiver or field stop field of view, f is the focal length of the telescope, $k = \frac{2\pi}{\lambda}$ with λ being the wavelength of interest, and F_s is the focal length to diameter ratio.

As can be seen from equations 3.31 and 3.32, the field stop diameter R_D (or the detector diameter if there is no field stop) can alter the field of view as would altering F_s. Altering F_s would require changing the diameter of the main mirror or adjusting the focal length of the telescope. This is completely impractical.

If the plate used as a field stop has a number of different diameter holes and these holes can be rotated in and out of the optical path, then it is possible to achieve a number of different fields of view very easily.

When the field of view is reduced from the diffraction limited value, the effective collecting area of the telescope is reduced. This will decrease the possibility of extraneous light from entering the detector as well as reducing the signal level. This then gives a simple method of signal filtering.

It is also possible to use this method to exploit the differences between Gaussian laser beams and uncollimated light. Gaussian beams can be focused to an incredibly small spot. The spot size of focused uncollimated light is far larger. If the gaussian beam is on-axis with a telescope this tight beam can be directed to the centre of the optical axis. If extraneous light is not on-axis it may still be focused but it will not be centred on the optical axis. If a small aperture or pin hole is placed at the focal point of the gaussian beam just large enough to allow the focused beam to pass, it will block both the on-axis and off-axis extraneous light. The gaussian beam can then be refocused to parallel with a majority of the extraneous light removed.

3.6.1.3 Optical Amplitude filtering

The control of the amplitude of optical energy allowed through to a detector is largely provided by neutral density filters (with the PSLR). Neutral density (ND) filters are designed to block all light in a given spectral range with little or no spectral dependance. This allows all light in the region of interest to be blocked and hence reduce the total transmitted radiant power to the detector. ND filters are classified by their optical density D as (Andover Corp., 2004a):

$$D = log_{10}\frac{1}{T} \tag{3.33}$$

where, T is the transmitted radiant power so $T = 10^{-D}$ so an optical density of 0.5 would give a transmittance of 31.6% and an optical density of 4.0 would give a transmittance of 0.01%.

Two main types of ND filters are absorptive and metallic. The absorptive type, as the name suggests, block light by absorbing energy in the substrate of the filter.

This of course causes heating of the filter so it is important to limit the amount of light being blocked. The metallic type use absorption and reflection to block light so do not heat up to the same extent as the purely absorptive type.

ND filters are essential for SLR as it allows ranging to be conducted during the day. The detectors would be swamped with extraneous light without ND filters and the return laser signal would be lost as the detector would be saturated.

3.6.2 Electronic Filtering

Once the laser pulse has passed through all of the optical components, electronic techniques are employed to complete the filtering story.

3.6.2.1 Temporal filtering

Temporal filtering refer to the application of gating to reduce the chance of a false triggering event. This is accomplished by only switching a device on just before the return laser pulse is expected. With interval counters this switching refers to the stop channel of the counter which is only activated by the falling edge of a hold-off pulse (see 2.17, section 2.4.3, 43 for a more complete explanation).

The other commonly used form of temporal filtering is to apply a range gate to the station detector. This is accomplished by turning the detector on just before an expected laser pulse return, and turning it off again at some time after the expected return. It is better to miss a true return than have the data corrupted by false triggering events.

The choice of the width of the range gate depends mostly on the accuracy of the orbital prediction for the satellite that is being tracked. Satellites with stable orbit and consequently very good orbital predictions (such as LAGEOS) can have very narrow range gates (0.1μsec to 1μsec (Degnan, 1993)) centred on the expected epoch of arrival.

Low Earth Orbit (LEO) satellites that experience high orbital drag or satellites that are frequently maneuvered may not have the most accurate of orbital predic-

tions. The range gate at the detector may need to be set to several microseconds centred on the epoch of the expected arrival. Once the satellite is located (this is generally obvious as the electronic pulse produced is far larger than any false trigger), it may be possible to reduce the size of the range gate.

3.6.2.2 Electronic Amplitude Filtering

This type of filtering is generally accomplished with some sort of discriminator (see section 3.4). These devices can be adjusted so that they trigger or pass a pulse that is of sufficient size (generally much higher than the pulses produced by background level radiation).

The size of the return pulse from a satellite is mostly a result of the satellite height (LEO satellite have larger return pulses than LAGEOS satellites). As a result it is possible to set the detection thresholds for LEO satellites much higher than the more distant satellites. This allows compensation for the larger range gates required for the LEO satellites.

3.6.3 Filtering - The big picture

The previous sections have dealt with the individual aspects of signal filtering (optical and electrical). All of these aspects of filtering need to be implemented to achieve the best results.

The highest level of filtering would require:

1. A very narrow band spectral filter (less than 0.1 nm about the central wavelength). In general the tighter the spectral bandwidth, the lower the transmission.

2. A very small field of view of the receive telescope. The smaller the telescope however the smaller the collecting area so the optical signal is reduced.

3. An ND filter with a very high optical density (>4.0) to block ambient light. This will also decrease the optical signal.

4. Very narrow range gates perhaps less than 0.1μsec. If the range gate is too small the return signal may not reach the detector inside the range gate and data will be lost.

5. The discriminator threshold needs to be set as high as possible. While this should prevent false triggering of the timing device from ambient light, it may also block the signal if the signal is not sufficiently large with respect to the background.

In general it is not always possible or desirable to set the filtering levels to a maximum. It is more likely there will be trade-offs within the filtering scheme to achieve the best results. One such trade-off situation is discussed with the LEO satellites above.

The other extreme where the satellite orbits approach LAGEOS distances (and above) require a different filtering setup. In general the orbital predictions for the satellites is very good so the range gate can be significantly reduced. The return optical pulse will be smaller so the discriminator threshold will need to be reduced. The field of view of the telescope (spatial filtering) needs to be balanced by the need to compensate for smaller optical signals and the reduced need to broaden the field of view because of uncertainty of the satellite position due to poor orbital prediction.

It is the balance of filtering levels, signal strength (optical and electrical) and tracking requirements that will ultimately determine the filtering setup for each SLR station for each satellite.

The final level of filtering is data filtering. If a false triggering event occurs so that a recorded range is short or long, it may be possible to remove this range from the final data. This is covered in section 2.4.6.

3.7 Station timers/GPS/Frequency Standards

3.7.1 Introduction

With good pointing accuracy required to continually track a satellite with a series of laser pulses, it is not only important to know where a satellite is but when it will be there. This information is contained within the Inter-Range Vectors (IRVs) used to calculate a satellite ephemeris. IRVs contain position and velocity vectors which are referenced to a known time. This time is provided in Universal Coordinated Time(UTC), in this case kept by a number of caesium primary frequency standards at the U.S. Naval Observatory (USNO). As all tracking stations and data centers which provide the IRVs use UTC, all are working from the same temporal reference frame.

A satellite laser ranging station requires a way of keeping time so that it agrees with UTC (as determined by the US Naval observatory GPS Master control station, see section 3.7.1.1), which since the removal of selective availability for domestic GPS receivers (this was a signal degradation imposed by the U.S. military to limit the effectiveness of civilian equipment), should agree to better than 100 ns. Some stations, (the PSLR included) have their own caesium or rubidium standard set to UTC. As there are always minor differences in the material and the construction of any device, these station clocks will 'drift away' from UTC. The use of a GPS unit can solve this problem by providing UTC time to the station clock. The station clock can effectively be slaved to the master clock at the USNO.

3.7.1.1 The components of the GPS system

The Global Positioning System can be divided conceptually into three segments, the space segment, the control segment and the user segment. The space segment consists of 24 satellites in one of six orbital planes, so there are four satellites in each plane. The satellites complete an orbit of the earth in 11h 58m with each satellite in the plane approximately four hours behind one satellite and four hours ahead of

another satellite. Each orbit is inclined at 55^0 to the equator with a 60^0 separation between each orbital plane. This ensures that, for any position on earth at any time, there should be at least 4 satellites with a line of sight to an observer. The satellites orbit at 20,200km with an almost circular orbit. This is especially important for very precise GPS measurements which require long term observations of the same satellites in very similar orientations.

The control segment consists of a master control station, monitoring stations and ground antennas which are located mostly in the U.S. but with overall global coverage. The locations and station type are shown in table 3.8. The monitoring stations receive information from the satellites which is transferred to the master control station. The master control station determines any ephemeris updates for the individual satellites, corrections to clock biases and any other data that may be required by the satellite. This information is relayed to the ground antennas and is uploaded to the satellites when they are in range of the ground antennas.

The user segment consists of anyone who can afford to purchases a GPS receiver (with the cost starting at a few hundred Australian dollars, this includes almost everyone in the western world). Most modern GPS units, from hand held units, to sophisticated sub-centimeter positioning systems, can track more than the required four satellites and produce time and position solutions using this more complicated array.

3.7.1.2 The theory of GPS

The Global Positioning System, as its name implies is principally concerned with positioning. Determining the location of a GPS receiver on the surface of the earth requires knowing the relative distances between the receiver and a number of satellites. In order to determine the relative distances, the time of transmission of a radio signal from the satellite to the receiver is noted. If the speed of transmission is known then the distance between the satellite and the receiver can be determined.

Master control station	Falcon Air force base Colorado Springs, CO
Master control station (backup)	Gaitheresburg, MD
Monitor station	Falcon Air force base Colorado Springs, CO
Remote monitor station	Cape Canaveral, FL
Remote monitor station	Hawaii
Remote monitor station	Ascension Island
Remote monitor station	Diego Garcia
Remote monitor station	Kwajalein
Ground antenna	Cape Canaveral, FL
Ground antenna	Ascension Island
Ground antenna	Diego Garcia
Ground antenna	Kwajalein

Table 3.8: Location of the components of the operational control segment (Farrell and Barth, 1999)

This method using time to generate a position is well described in the Hewlett Packard application note 1272 "GPS and Precision Timing Applications" (Hewlett Packard, 1996).

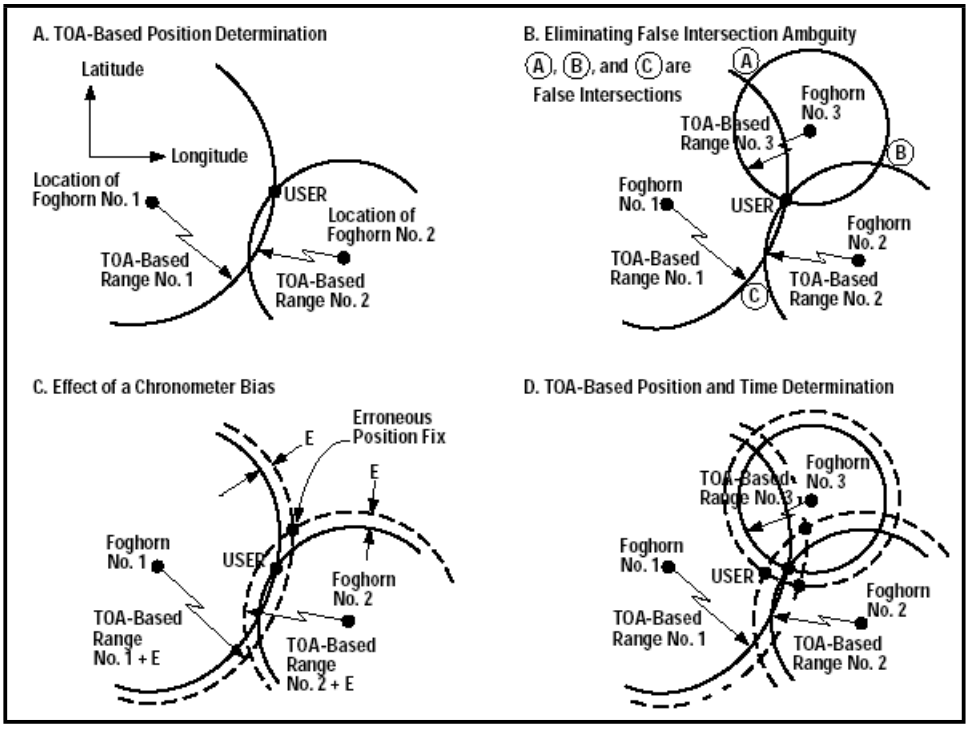

Figure 3.36: Example of position referencing using time of flight measurements from a number of sources

Figure 3.36(A.) (Hewlett Packard, 1996), represents a way of determining position using a remote signal (the foghorn), an accurate and well set chronometer, and the speed of travel of the signal. In this example the user notes the time of arrival of two foghorn signals which have been sent on the hour. Noting the approximate direction of the signal two arcs are drawn on the map at the distance from the user as determined by the time of arrival of the foghorn signals after the hour (distance is approximately 330 $\times$ time of arrival). These two arcs will intersect at least once, giving the position of the user. Depending on the geometry of the user to the foghorns, there may be two intersections of the distance circles. In this case the user would have to have a good idea of the their current location to discount the false

intersection. This uncertainty can be removed by using three foghorns. In figure 3.36(B.) there is only one intersection of all three foghorn signal. If the position of the three foghorns is known then the user can fix a very accurate position on a surface. Using at least three foghorns or signals also has the advantage of being able to correct for user chronometer bias. If the chronometer is fast then the signals will appear to arrive too soon and as a result the three distance circles will not intersect at a common point. If the chronometer is slow then the distance circles will overlap the true position giving multiple intersects. If the circles are adjusted evenly until a common intersect is found then not only is the position fixed but the chronometer time bias is found and can be removed. This is illustrated in 3.36(D.). This is the same approach used with GPS positioning except that the foghorn is replaced with a radio transmitter and one more satellite is needed to fix the observers position in three dimensions. Using this type of approach with the GPS receiver results in essentially, four equations with four unknowns.

$$\widetilde{\rho}^{(1)} = [(X^{(1)} - x)^2 + (Y^{(1)} - y)^2 + (Z^{(1)} - z)^2]^{\frac{1}{2}} + c\Delta t_r + \chi^{(1)} \tag{3.34}$$

$$\widetilde{\rho}^{(2)} = [(X^{(2)} - x)^2 + (Y^{(2)} - y)^2 + (Z^{(2)} - z)^2]^{\frac{1}{2}} + c\Delta t_r + \chi^{(2)} \tag{3.35}$$

$$\widetilde{\rho}^{(3)} = [(X^{(3)} - x)^2 + (Y^{(3)} - y)^2 + (Z^{(3)} - z)^2]^{\frac{1}{2}} + c\Delta t_r + \chi^{(3)} \tag{3.36}$$

$$\widetilde{\rho}^{(4)} = [(X^{(4)} - x)^2 + (Y^{(4)} - y)^2 + (Z^{(4)} - z)^2]^{\frac{1}{2}} + c\Delta t_r + \chi^{(4)}, \tag{3.37}$$

where, $\chi^{(i)} = c\Delta t_{sv}^{(i)} + c\Delta t_a^{(i)} + SA^{(i)} + E^{(i)} + MP^{(i)} + \eta^{(i)}$.

In equations 3.34 - 3.37, the values $\widetilde{\rho}^{(i):(i=1-4)}$, refer to the calculated pseudoranges to the four space vehicles (SV), ($X^{(i)}$,$Y^{(i)}$,$Z^{(i)}$) are the earth-centered earth-fixed coordinates (ECEF) of the SV, (x,y,z) are the ECEF coordinates of the receiver

antenna, Δt_r is the receiver clock bias, $\Delta t_{sv}^{(i)}$ is the clock bias of the SVs, $\Delta t_a^{(i)}$ is the atmospheric delay of the radio signal, $SA^{(i)}$ is the selective availability degradation applied to the signal, $E^{(i)}$ represents error in the satellite broadcasted ephemeris data, $MP^{(i)}$ is the multipath (atmospheric) error, $\eta^{(i)}$ represents receiver tracking error noise, and c is the speed of light (Farrell and Barth, 1999).

While the primary function of GPS is to determine position, it also allows the continuous transfer of time. The on-board clocks of each satellite are consistently updated by the remote monitoring station ground antennas when the satellites are in range. This information is sent as part of the GPS transmitted message. The receiver clock bias is estimated by comparison of the time messages sent by the tracked satellites.

3.7.1.3 GPS transmitted message

The signal from each GPS satellite is transmitted on what is known as L band radio frequency. This consists of two frequencies L_1 at 1575.42MHz and L_2 at 1227.60MHz. Each satellite is identified by a unique code which is transmitted within its broadcast sequence. The broadcast signal is called pseudo-random noise(PRN) as it would appear as white noise to any receiver, without a decoder tuned to one of the L band frequencies. Within the PRN a digital bit stream is sent. This is accomplished using a system known as binary phase shift keying(BPSK). The zeros or ones within the code are generated by either shifting the carrier phase either leading or lagging, one way for zeros and the other for a one.

In order for the GPS receiver to determine the range to the satellite the satellite must send a time mark as part of its message. A satellite's on-board clock time-stamps the start of the time signal or code that it sends. The receiver generates its own time signal which is an exact copy of each satellite's signal. The receiver then electronically shifts the self-generated signal so that it is in phase with the GPS signal. The amount of shift made by the receiver indicates the time of flight from the satellite to the antenna position of the receiver.

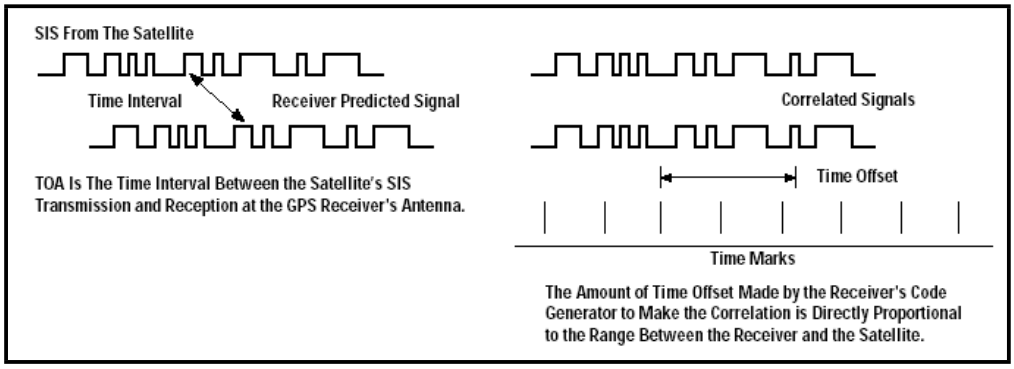

Figure 3.37: Determination of the range using signal correlation

This will give pseudorange information for use with equations such as 3.34 - 3.37. When the four equations are solved, the value of the user clock bias, a constant in these equations, is solved. This bias can still contain errors due to atmospheric delay. Some GPS units are able to eliminate much of the atmospheric delay in the receiver clock bias by doing dual frequency ranging (L_1 and L_2). The difference in propagation of the frequencies through the atmosphere will very accurately determine atmospheric delay.

Each GPS satellite also sends more information apart from the correlation clock signal. Both the selective availability and the precise code have a navigation message superimposed on the signal. This includes the time of transmission for range determination, clock bias information for the particular satellite, satellite ephemeris data for the particular satellite, messages from the control network, the satellite almanac for satellites not being tracked, and the ionospheric delay model. These data are transferred at a bit rate of 50 bits/s. The entire GPS message takes $12\frac{1}{2}$ minutes to download and is required when a GPS unit is started for the first time, if a master reset is done, or if for some other reason the receiver loses the almanac data. The navigation message is only valid for four hours so needs to be consistently downloaded from any of the GPS satellites.

The TM1 GPS time machine from Spectrum Instruments (see figures 3.38 and 3.39) is used with the PSLR system. This unit is small and lightweight while providing good timing resolution to UTC.

Figure 3.38: Front panel display of the TM1 GPS time machine.

Figure 3.39: Rear panel display of the TM1 GPS time machine.

It is able to provide a number of selectable frequencies as square wave output from a BNC connection on the rear panel as well as a 1 pulse per second (1PPS) output. The 1PPS is used to slave other timing devices (time code generation cards, primary frequency standards) to UTC. It is able to accomplish this to an accuracy of 50 ns if there is no delay/latency within the down-stream instrument. The selectable or programmable frequency option can be used to condition other devices (such as the SR620). This is an integral part of the PSLR system as it provides the only way to lock the PSLR station clock to UTC.

3.7.2 Primary frequency standards

Many SLR stations use a primary frequency standard to provide both UTC-locked 1PPS as well as reference frequencies (5 MHz, 10 MHz) for other station functions. While it is possible to operate without a frequency standard, they do provide backup

station time in the event of the failure of the GPS receiver. This method was employed with the PSLR (although only briefly) when the HP5071A caesium standard (from Hewlett Packard) was slaved to the TM1 GPS unit. The HP5071A time was manually set from the GPS display and was then conditioned using the 1PPS from the GPS unit. The HP5071A then provide its own 1PPS output, 10 MHz output, and user selected output.

The time card (based on information from the PSLR program operation manual (Zarins, 1996)), which was never delivered to Curtin University with the rest of the PSLR equipment, used both the 1PPS and the 10Mhz signal to provide station time. The new PSLR time card (the bc620AT from Datum Inc., see section 3.7.3) only requires the 1PPS for synchronisation to UTC so either the GPS or GPS + caesium clock can be used.

3.7.2.1 Principle of operation of the caesium clock

The operation of the HP5071A caesium primary frequency standard is based on the oscillation frequency of one of the hyperfine resonant frequencies of the ^{133}Cs atom in the ground state. The ^{133}Cs atoms are kept in a high vacuum to ensure that only the required species is subjected to the microwave beam. The microwave beam interacts with the electron located in the outermost ^{133}Cs atomic shell. The rest of the electrons are quite stable as they inhabit full shells and are more tightly bound. The microwave beam causes energy level transitions of this outer shell electron. This sets up a resonance between hyperfine transition states causing radiation emissions from the ^{133}Cs atoms in an extremely narrow spectral band.

At startup of the HP5071A, ^{133}Cs atoms are organised into a particle beam and then separated from any impurities using a mass spectrometer like magnetic separator. The resultant beam is then subjected to microwave radiation in the resonator cavity. The beam, (containing both excited and relaxed atoms) is separated by state selection magnets with the excited atoms directed into a detector. The microwave frequency is adjusted until the detector current is maximised. This has effectively

measured the resonant frequency of the ^{133}Cs transition (Breakiron, 1999). The value of the frequency is 9.19263177138 GHz, which according to the assembly level service manual (Hewlett Packard, 1997) "... the actual frequency of the resonance differs slightly from the nominal value of 9.192631770 GHz because of the applied magnetic field present, and the second-order Doppler shift resulting from the finite velocity of the atoms in the beam". This is illustrated in figure 3.40 (National Institute of Standards and Technology, 2003).

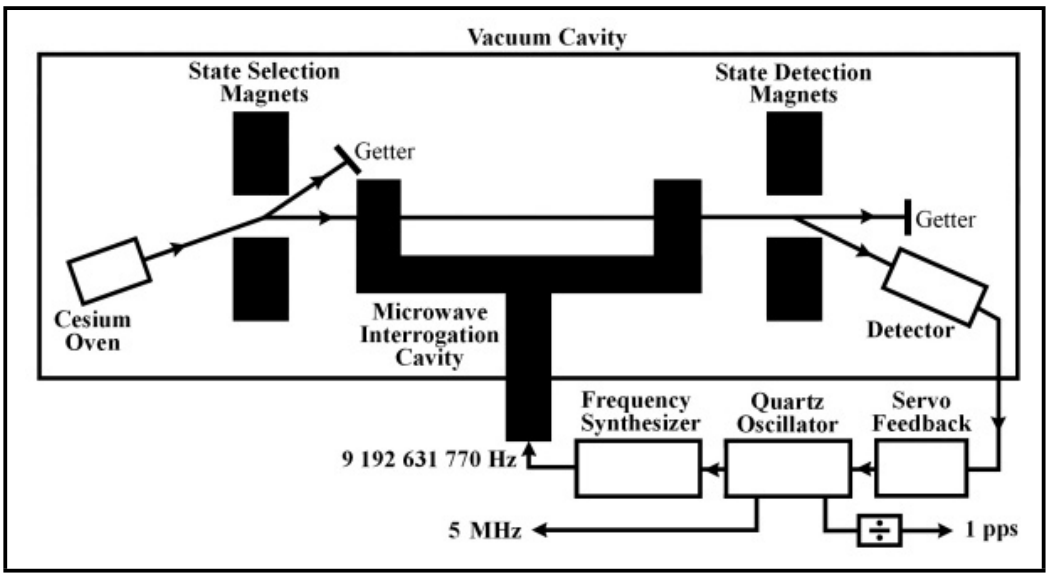

Figure 3.40: Illustration of the principle of operation of a caesium primary frequency standard.

The operation of the HP5071A is based on a frequency of 10MHz. A 10MHz quartz crystal oscillators output frequency is multiplied by a rational number to achieve by frequency synthesis a value as close as possible to the ^{133}Cs resonance. This frequency is compared to the actual resonance in the HP5071A caesium beam tube. The error between the two frequencies is fed back to the oscillator control circuitry to steer the generated frequency from the quartz crystal until the comparison between the two signals yield zero Hz. The quartz crystal should now be oscillating at $10MHz \pm 2 \times 10^{-4}Hz$ giving a time accuracy of $\pm$ 2ns per day. (Breakiron, 1999). The caesium frequency standard is still one of the most accurate time keeping

devices in use.

3.7.3 The bc620AT time and frequency processor card

The last step in the creation of the PSLR station time keeping system is the Datum Inc. bc620AT time and frequency processor. This is a ISA bus based card which provides a number of external functions as well as information to the ISA bus. The time card (TC) provides the following features (Datum Inc., 1996):

1. Time on demand, from days to microseconds with zero latency to request by the host computer

2. Event logging to $0.1\mu sec$ (100 ns) on receipt of a secondary bus request with the time latched on either the positive or negative edge of the request pulse

3. Four sources of synchronisation

Mode	**Source of Synchronisation**
0	Time code - IRIG A,B; XR3, 2137;NASA36
1	Free running - on board 10 Mhz oscillator (VXCO) used as reference
2	1PPS - synchronised to external one pulse per second
3	RTC - uses on board battery backed real time clock IC.

4. Provides an output clock set to the selected reference of either 1, 5, 10 MHZ TTL

5. Flywheel operation which will operate the time and frequency processor at the last used reference rate

6. Generation of IRIG B timecode, externally available

7. Five maskable interrupt sources are supported including external event input occurred and 1PPS has occurred

The PSLR station time is provided by synchronising the TC with either the 1PPS output from the GPS unit or the HP5071A primary frequency standard. As the PSLR is a portable system, all effort has been made to ensure correct operation of the station timing system without use of the HP5071A, as it is quite heavy and as such is not conducive to portability.

The event time tag output from the card is read by the PSLR control program through the bus theoretically giving a time of ± 100ns to UTC although this was not tested at the time of the writing of this thesis. Assuming an along-track orbital speed of LAGEOS-1 of $\approx 5.71 km.s^{-1}$ and a perfect orbital model, then ± 100 ns would relates to a cross track error in positioning, assuming perfect telescope pointing and zero laser jitter, of 0.571 mm. At the absolute best, the PSLR could point with an accuracy of ±0.33" on each axis or a minimum cross-track error of ≈ 3 m to LAGEOS-1. The timing system is more than capable of providing the precision required to follow satellites.

The station time system accuracy to UTC is far more important when the data from three or more stations is combined to trilateral the position of a satellite. If there is some time synchronisation error in the station time system then this will cause range measurement errors.

This can be explained by considering the tangential velocity of a satellite with respect to an SLR station. If the zenith position of a satellite at a station is considered then the tangential velocity v can be calculated by (Serway, 1992):

$$v = \sqrt{\frac{GM_e}{r}} \tag{3.38}$$

where, G is the universal gravitational constant, M_e is the mass of the earth, and r is the radius from the centre of the earth to the satellite.

If LAGEOS is considered then $r = 6000 + 6370 = 12370$ Km, given the radius of the earth is 6370 Km. If this is substituted into equation 3.38, it gives a velocity of 5.679 Km/sec or 5.679×10^6 mm/sec. In order to find how many seconds it takes for

each millimeter of tangential travel of the satellite the tangential velocity is inverted. This gives a time of 176×10^{-9} or 176 ns.

This means that in order to range to LAGEOS so that the position of the satellite (as determined from orbital elements fixed to UTC) is known within the orbit to less than or equal to 1 mm, the station clock must be synchronised to UTC to $\pm$ 176 ns.

This is important as each laser fire event is timed tagged by the station clock. The laser pulse diameter at LAGEOS distances is in the order of 30 m with the PSLR. If the laser pulse is fired off either early or late it will still hit the satellite and a return will be registered. Figure 3.41 shows a station ranging to a satellite. If the pulse leaves on time then it will intersect the black position as expected. If the pulse leaves late, it will intersect the grey position. Each return recorded at the station will look identical but due to the delay in firing the laser there will be a range error (R_e).

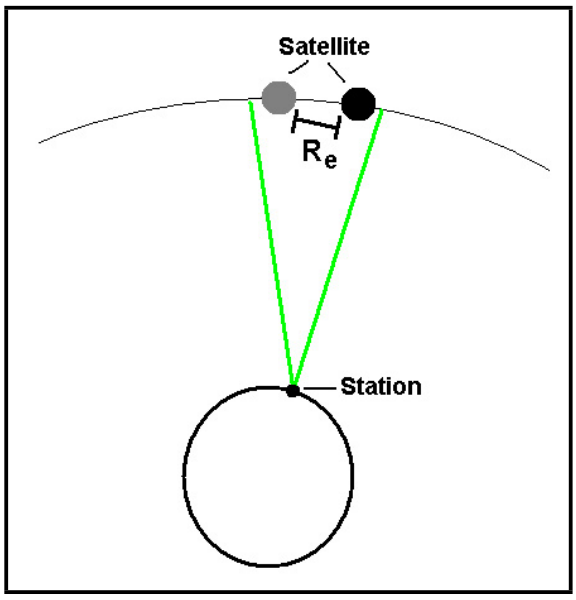

Figure 3.41: Illustration of how a laser pulse will be returned by a satellite even if the laser beam is fired off late.

This error can be reduced by providing the best synchronisation to UTC possible.

Most modern GPS units will enable UTC synchronisation to the points where the error associated with synchronisation is far less than other error sources. If a range error of 1 mm is taken as the benchmark, this can be compared with various satellite orbits and the synchronisation to UTC required to produce this level (see figure 3.42). This shows that the PSLR station timing system (which is an old system in terms of SLR) is capable of providing UTC synchronisation which will produce an along-track range error less than 1 mm for all satellites. Range errors of few mm are only produced by the best systems so the PSLR station timing system would be adequate even for these worlds best systems.

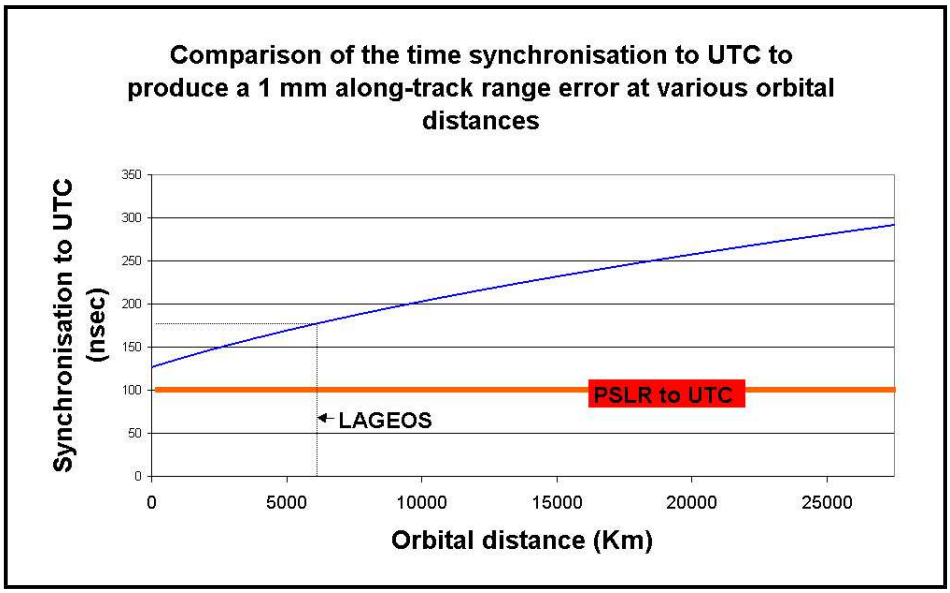

Figure 3.42: Plot of various satellite orbital distances and the time offset to UTC that will cause a 1 mm cross-track range error. LAGEOS orbital height and associated offset as well as the PSLR station offset to UTC are shown on the graph.

The along-track error is only an indication of the timing error concerns with laser ranging systems. The above discussion has ignored two important factors. The first of these is that the station velocity is ignored completely. The second is the position of the station with respect to the satellite. The graph in figure 3.42 represents the very special case where the satellite(s) will be directly over the SLR station and the velocity of the station is ignored. For a true calculation of the cross-

track error, the station velocity with respect to the satellite must be considered. The other consideration is of course the position of the satellite with respect to the station. This is important as the range between the satellite and the station is directly related to the position. The minimum distance will be when the satellite is directly overhead. This will increase to a maximum as the satellite approaches the station horizon. The rate of change of the station - satellite distance is known as the range rate and is one of the biggest limiting factors on the accuracy of laser ranging measurements. For a range rate of around 5 km/sec for the LAGEOS satellites this would mean that less than 1mm error in station - satellite range would be possible if the timing resolution of the station was less than 200 ns. Higher range rates would of course require better timing resolution. Range rates of various satellites are dependant on both the geographical location of the station, the orbital distance of the satellite in question and the orbital parameters (eccentricity, declination etc.). The range rates are determined by each SLR station as a matter of course when orbital parameters are calculated for satellite that are to be tracked. A complete treatment of this subject is outside the scope of this thesis and the reader is directed to consult the many on-line resources that deal with this issue in greater detail.

3.8 Telescope drive, control and mount position reporting

In order to produce tracking data using SLR, the telescope(s) must be able to point with a high degree of accuracy to a number of contiguous points in space in order for a laser beam to hit a remote target. This requires accurate relative positional information with respect to the station at a known time, and a precise method of driving and positioning reporting for the telescope(s).

3.8.1 Telescope drive

Telescope drive in the PSLR is initiated by the control program which runs on a standard desktop PC. The positional requirements from the control program are sent to the indexer card. The indexer card provides a direction and possibly several positional pulses to either of the two stepper motor drive units for elevation and azimuth. The stepper motor drive units then provide pulses to the stepper motors which move the required number of steps in either a clockwise or counter-clockwise direction. The stepper motors are coupled to simple reduction gearboxes which turn friction wheels. This friction wheel moves upon either the azimuth or elevation track and the telescope position changes.

This section will deal with the operation of the indexer card, the motor drive units and the stepper motors which control the pointing of the PSLR telescope.

3.8.1.1 Stepper motor basics and the Compumotor S57-51 stepper motor

Stepper motors are similar in construction to series universal motors with a permanent magnet rotor and wound stator. The operation of the two types of motors is identical in the respect that the permanent magnet rotor is made to follow a magnetic field generated by the stator. In a series universal motor the magnetic field is controlled by a split ring commutator which alternatively switches poles on the stator to either a north facing or south facing pole. The permanent magnet of the rotor is alternately attracted and then repelled from each pole as the magnetic field's direction is swapped. This in effect sets up a rotating magnetic field in the stator. The rotor will attempt to catch the rotating magnetic field, which results in constant rotation of the rotor. The construction and operation of these types of motors is quite simple. The switching of the poles in the motor is mechanically controlled by the rotation of the commutator as it is rigidly fixed to the rotor. Power simply needs to be supplied.

In figure 3.43, the operation of a commutated motor is illustrated on the left of

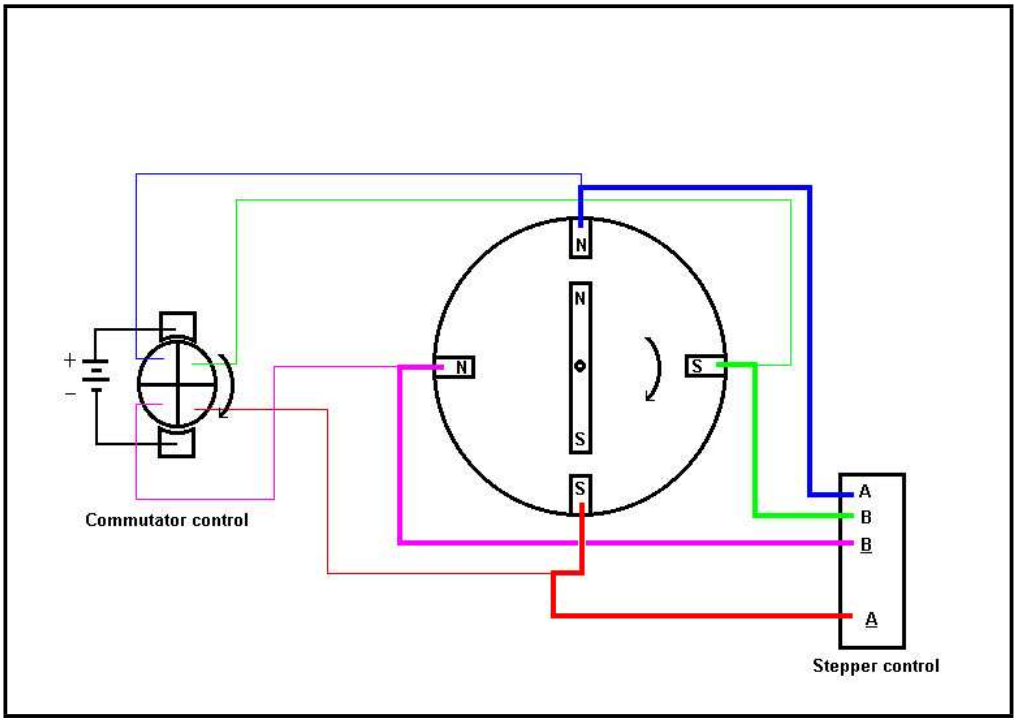

Figure 3.43: This figure represents the simple control of a series universal motor and how it compares to stepper control

the figure. The commutator segments are wired so that opposing poles will form magnetic dipoles. As the rotor rotates the polarity of the poles changes. This gives the effect of a rotating magnetic field. The heavier lines in figure 3.43 show how a stepper motor would be connected to a controller. The controller is now able to individually control each pole of the motor. If opposing poles in the stator are switched so that they are opposite dipoles, it is possible to fix the rotor in place. If the poles in the stator are now reversed then the rotor will be repelled until it encounters the next set of poles which will once again hold the rotor in place.

This type of control has the advantage that it is also possible to interpose the permanent magnet rotor between two poles. If the rotor is repelled from a set of poles and attracted to the other set of poles and the attracting poles are now reversed, it would mean that two adjacent poles are now of the same polarity. The permanent magnet of the rotor would move to the position of magnetic balance

between the adjacent poles. This is illustrated in figure 3.44. The motor diagram at the top left of the figure shows that the poles directly adjacent to the rotor are forcing the rotor to travel clockwise. Once the rotor has begun to move the polarity of this pole is reversed so that the two adjacent poles in the motor are opposite to that of the rotor. The rotor will then be held firmly in place as it finds the balance point between the two attractive poles. The top pole in the diagram is now switched back to the original polarity and the rotor is captured by the horizontal poles. The continuation of this process is demonstrated in the remaining diagrams in figure 3.44 with the rotor stepping $\frac{3}{8}$ of a full revolution. In this way, the position, direction and speed of revolution of the rotor can be tightly controlled.

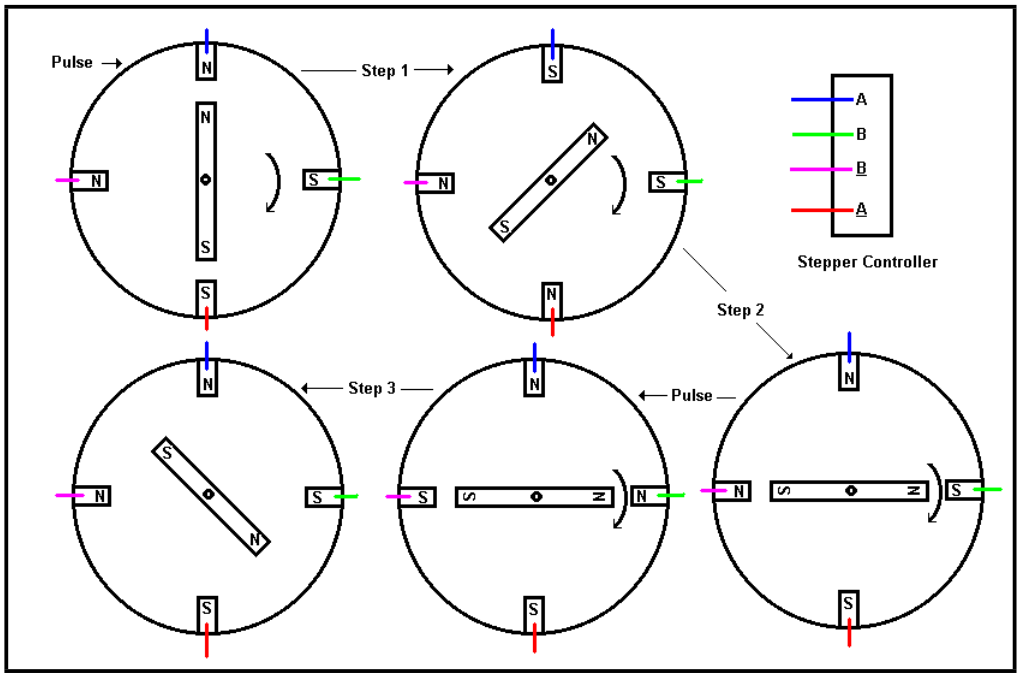

Figure 3.44: Stepping scheme where an interpolated step is performed between poles.

The PSLR telescope drive consists of two identical S57-51 motors, each mated to a reduction gearbox. These motors are small but are capable of moving the PSLR telescope at around 20^0 per second on each axis. Table 3.9 outlines the specifications of the PSLR motors.

Each motor is connected to its own S series microstep drive. The drive units

Current (amp)	**Peak shaft power (watt)**	**Peak total power (watt)**	**VA rating (VA)**
1.15	55	90	140
Resolution (steps/rev)	**Max speed (steps/sec)**	**Static Torque (Nm)**	
2000	100000	0.459	

Table 3.9: Common characteristics of the S57-51 when wired in series

power the motors and perform all of the switching of the stator windings to achieve motor stepping. Each drive is set for each motor or application using a series of DIP switches. This makes the drive unit versatile as it will work with a number of different types of motors. The drive unit acts as a very sophisticated amplifier. The actual stepping commands are issued from another device called an indexer. It provides step rate and direction signals to each drive unit. The drive unit in turn provides step pulses to the motors at the rate and in the direction (of rotation) as directed by the indexer pulses.

3.8.1.2 The PSLR motion controller

The DMC-1720 indexer is a PC card based indexer controller. The DMC-1720 is an Optima series controllers from Galil Motion Control Inc. These controllers can be either PC card based or stand alone units controlled through various PC ports (ethernet, RS232 and USB). These controllers can be used as either servo-motor or stepper controllers and are configured using on-board jumpers and software. The LURE SLR facility at Haleakala, Hawaii has replaced their old motion control system with a DMC-2220 controller. This controller is rack mounted and controlled through an ethernet connection to the host computer. It is used to control two servo-motors. The PSLR uses the DMC-1720. This is an ISA bus PC card which communicates with the host computer through the ISA bus. It controls two stepper motors. These two controllers, while differing in appearance and approach, are essentially the same

DMC-1720	Value	PSLR requirement
Min update time	$250\mu sec$	$550\mu sec$
Position accuracy	$\pm$ 1 quad count	-
Velocity accuracy	.005%	-
Max Velocity	3×10^6 pulses/sec	1×10^5 pulses/sec
Velocity resolution	2 counts/sec	-
Max encoder velocity	12×10^6 quad counts	4000 quad counts

Table 3.10: Motion controller specifications for the PSLR

device.

3.8.1.3 The DMC-1720 indexer card

This card is ISA bus based. The 1700 series identifier specifies the type of bus or mounting (1800 series identifier specifies PCI bus) and the 20 added to the 1700 identifier specifies the number of axes controlled by the card (2). The DMC-1720 was chosen for the PSLR because the currently used control software was written for a Windows 3.1 environment and the control card that came with the PSLR was ISA bus based. The Optima series controllers are ideal for the PSLR as a system upgrade will mean the selection of a new controller is a matter of preference as all of the DMC controllers use the same software. Programs developed for the DMC-1720 will function equally well on a DMC-1820 or a DMC-2220.

The DMC-1720 also has many other features that make it appealing as the PSLR motion controller. The card provides connections for several types of encoders, it has 8 digital inputs, 8 digital outputs and 8 analogue inputs. These on-board I/O channels are all uncommitted and can be used for any number of applications. The card also provides a series of opto-isolated inputs for error control such as a "home" input, "forward" and "reverse" limits and an "abort" limit. The specifications of the card exceed the requirements of the remainder of the PSLR motion control system. As the DMC-1720 has vastly superior specifications to what is actually required

with the current PSLR motion control equipment, it will allow upgrade of these components at a later date without the need to purchase new indexer equipment.

3.8.1.4 Optima series programming language

The Optima series controllers are operated using a specifically designed programming language. This language allows the motion controller to be configured (as a stepper motor driver), specific applications programmed (such as joystick control of telescope movement), and I/O easily accessed (reading joystick position). Further, it has a number of in-built profiling functions such as circular interpolation and ramping.

The language consists of several two-word commands. These commands can be seen in figure 3.45. This language can be very powerful with some rather involved movement condensed to a few lines of code

Figure 3.46 shows one of the simple programs written in the Optima control language. This program reads the voltage from two of the analogue inputs available with the card. These inputs are connected to a joystick which supplies $\pm$ 10 volts depending on the position of the joystick. The commands:

- $X = @AN[7]$
- $Y = @AN[8]$

assign the value read from analogue input 7 and 8 to the variables X and Y. These values are then multiplied by a scaling factor (VEL) to achieve a range of stepping speeds for each axis:

- $VX = X * VEL$
- $VY = Y * VEL$

OPTIMA SERIES

DMC-1200, 13x8, 1600, 1700, 1800, 2000, 2100, 2200

INSTRUCTION SET

SERVO MOTOR COMMANDS

AF	Analog feedback
DV	Dual loop operation
FA	Acceleration feedforward
FV	Velocity feedforward
IL	Integrator limit
KD	Derivative constant
KI	Integrator constant
KP	Proportional constant
NB	Notch bandwidth
NF	Notch frequency
OF	Offset
PL	Pole
SH	Servo here
TL	Torque limit
TM	Sample time

STEPPER MOTOR COMMANDS

DE	Define encoder position
DP	Define reference position
KS	Stepper motor smoothing
MT	Motor type
RP	Report commanded position
TD	Step counts output
TP	Tell position of encoder

BRUSHLESS MOTOR COMMANDS

BA	Brushless axis
BB	Brushless phase
BC	Brushless calibration
BD	Brushless degrees
BI	Brushless inputs
BM	Brushless modulo
BO	Brushless offset
BS	Brushless setup
BZ	Brushless zero

I/O COMMANDS

AL	Arm latch
CB	Clear bit
CI	Communication interrupt**
CO	Configure I/O points
EI	Enable interrupts
II	Input interrupt
OB	Define output bit
OC	Output compare function
OP	Output port
SB	Set bit
UI	User interrupts*

* Supported on Bus-based products only.
** On serial port only

SYSTEM CONFIGURATION

AO	Analog output (DMC-2x00)
BN	Burn parameters
BP	Burn program
BV	Burn variables and arrays
CC	Configure auxiliary port
CE	Configure encoder type
CN	Configure switches
CO	Configure I/O points
CW	Data adjustment bit
DE	Define dual encoder position
DP	Define position
DR	DMA/FIFO update rate
DV	Dual velocity (dual loop)
EI	Enable interrupts*
EO	Echo off
IA	Set IP address (DMC-2x00)
IH	Internet handle (DMC-2x00)
IT	Independent smoothing
LZ	Leading zeros format
MB	ModBus (DMC-2x00)
MO	Motor off
MT	Motor type
PF	Position format
QD	Download array
QU	Upload array
RS	Reset
VF	Variable format

MATH/SPECIAL FUNCTIONS

@SIN[x]	Sine of x
@COS[x]	Cosine of x
@COM[x]	1's compliment of x
@ASIN[x]	Arc sine of x
@ACOS[x]	Arc cosine of x
@ATAN[x]	Arc tangent of x
@ABS[x]	Absolute value of x
@FRAC[x]	Fraction portion of x
@INT[x]	Integer portion of x
@RND[x]	Round of x
@SQR[x]	Square root of x
@IN[x]	State of digital input x
@OUT[x]	State of digital output x
@AN[x]	Value of analog input x

INTERROGATION COMMANDS

LA	List arrays
LL	List labels
LS	List program
LV	List variables
MG	Message command
QR	Data record
QZ	Return DMA information
RP	Report command position
RL	Report latch
'R 'V	Firmware revision information

INTERROGATION COMMANDS (Cont.)

SC	Stop code
TB	Tell status
TC	Tell error code
TD	Tell dual encoder
TE	Tell error
TI	Tell input
TP	Tell position
TR	Trace program
TS	Tell switches
TT	Tell torque
TV	Tell velocity

PROGRAMMING COMMANDS

DA	Deallocate variables/arrays
DL	Download program
DM	Dimension arrays
ED	Edit program
ELSE	Conditional statement
ENDIF	End of cond. statement
EN	End program
HX	Halt execution
IF	If statement
IN	Input variable
JP	Jump
JS	Jump to subroutine
NO	No-operation–for remarks
RA	Record array
RC	Record interval
RD	Record data
REM	Remark program
UI	User interrupt
UL	Upload program
ZS	Zero stack

ERROR CONTROL COMMANDS

BL	Backward software limit
ER	Error limit
FL	Forward software limit
OE	Off-on-error function
TL	Torque limit
TW	Timeout for in-position

TRIPPOINT COMMANDS

AD	After distance
AI	After input
AM	After motion profiler
AP	After absolute position
AR	After relative distance
AS	At speed
AT	After time
AV	After vector distance
MC	Motion complete
MF	After motion–forward
MR	After motion–reverse
WC	Wait for contour data
WT	Wait for time

INDEPENDENT MOTION COMMANDS

AB	Abort motion
AC	Acceleration
BG	Begin motion
DC	Deceleration
FE	Find edge
FI	Find index
HM	Home
IP	Increment position
IT	Smoothing time constant
JG	Jog mode
PA	Position absolute
PR	Position relative
SP	Speed
ST	Stop

CONTOUR MODE COMMANDS

CD	Contour data
CM	Contour mode
DT	Contour time interval
WC	Wait for contour data

ECAM/GEARING

EA	Ecam master
EB	Enable ECAM
EC	Ecam table index
EG	Ecam go
EM	ECAM cycle
EP	ECAM interval
EQ	Disengage ECAM
ET	Ecam table entry
GA	Master axis for gearing
GM	Gantry mode
GR	Gear ratio for gearing

VECTOR/LINEAR INTERPOLATION

CA	Define vector plane
CR	Circular interpolation move
CS	Clear motion sequence
ES	Ellipse scaling
LE	Linear interpolation end
LI	Linear interpolation segment
LM	Linear interpolation mode
ST	Stop motion
TN	Tangent
VA	Vector acceleration
VD	Vector deceleration
VE	Vector sequence end
VM	Coordinated motion mode
VP	Vector position
VR	Vector speed ratio
VS	Vector speed
VT	Smoothing time constant–vector

Figure 3.45: Command list from the Optima motion control language.

The axes are then directed to step or jog at this speed where the first value after the command JG is for the mount elevation axis, and the value after the comma is for the azimuth axis:

- $JGVX, VY$

```
#JOYSTIK
IN"HIT 1 FOR GROSS 2 FOR FINE",Q
IF(Q=1)
      VEL=-10000
ENDIF
       IF(Q=2)
      VEL=-100
ENDIF
JG0,0
BGXY

#LOOP
X=@AN[7]
Y=@AN[8]

JP #SLXLOOP,@ABS[X]<=0.5
#RETX
JP #SLYLOOP,@ABS[Y]<=0.5
#RETY

VX=X*VEL
VY=Y*VEL
JGVX,VY

JP#LOOP

#SLXLOOP
X=0
JP #RETX
#SLYLOOP
Y=0
JP #RETY
```

Figure 3.46: Simple joystick control program to move the PSLR mount.

One part of the program selects the scaling factor to set the speed range (the first 8 lines). The other part of the program checks the input voltage and if it is below a particular voltage, it stops the mount from moving. This was necessary as the resistor pots within the joystick were quite noisy and a deadband was required to prevent the mount from moving when not required. The commands,

- $JP\#SLXLOOP, @ABS[X] <= 0.5$, and
- $JP\#SLYLOOP, @ABS[Y] <= 0.5$,

cause a jump to the label $SLXLOOP$ or $SLYLOOP$ if the absolute value at the analogue inputs is less than 0.5 V. The code at the labels $SLXLOOP$ and $SLYLOOP$

sets the jog speed to zero so the mount will remain motionless. The analogue inputs are provided with a 12 bit analogue to digital converter. This allows the joystick program, shown in figure 3.46, to move each axis at less than 1 step per second, when the scaling factor is 100, and in increments of 24 steps a second when the scaling factor is 10000. A velocity of 24 steps a second relates to about $\frac{1}{2}$ an encoder position or .0025 of a degree per axis per second. It is theoretically possible to maintain this directional accuracy even at maximum speed as the controller updates the position twice per encoder division even when at the maximum speed of the stepper motors.

While this is a very simple program, it is quite powerful as it allows full motion control of the PSLR mount. Other more complicated programs have been written to try and automatically track stars. This is where the usefulness of the Optima software is severely limited. While the in-built functions can perform powerful tasks, the process control facilities of the programming language are limited. It is much more useful to read data in and out of the card and do all of the process control in another programming language (such as C). It is possible to store programs in the memory of the controller and to run these program independently of the host computer. It should be possible to have a resident program in the memory of the controller which will take input from a host computer instructing the controller on how many step pulses need to be completed for the next update cycle. Fudge factors and intelligent compensation for tracking error can then be handled by a control program which is much more versatile. If the required position, velocity and duration are calculated by other software, then the actual movement can be easily accomplished using a small resident program on-board the controller.

3.8.2 Encoder considerations

Using angle encoders for absolute reference is essential with the PSLR as the pointing direction of each axis must be known precisely. The angle encoders are solidly mounted to the rotation axis and will experience the same angular displacement as

the axis. The angular displacement, not the position, is reported by the encoders so the position is determined by counting a set of pulses from some known position.

The encoders output a quadrature signal. In the case of the RON 225 encoders used with the PSLR, this equates to two channel TTL output with one channel lagging the other channel by 90^0. This is illustrated in figure 3.47 (Heidenhain, 1999) which shows the two channels plus a reference pulse.

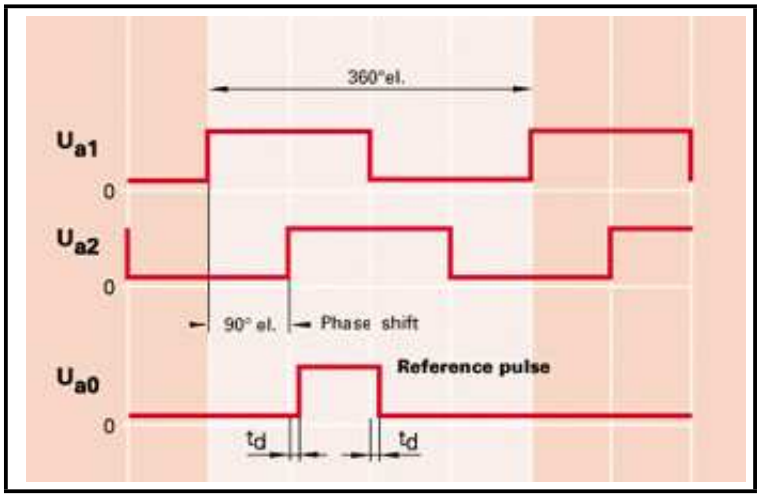

Figure 3.47: TTL quadrature output of the RON225 angle encoder, shown with reference pulse.

The production of pulses from the encoders involves a number of different components. The PSLR encoders utilise an optical scanning method as illustrated in figure 3.48 (Heidenhain, 1999). Parallel light is passed through a scanning reticle which contains the four principal scanning fields and a reference field. These reticles consist of a very fine grid which is alternately transparent and opaque. The lines on the reticles are arranged so that they are phase shifted by 90^0 with respect to each other. The generated signal is a result of the large graduated disk passing between the scanning reticles and the photovoltaic detectors of each reticle. As the disk turns (due to the movement of the mount) it produces light and dark periods on the detectors as the gaps in the scanning reticle are blocked and uncovered sequentially. This process occurs at each detector at a slightly different position of the disk as it

rotates due to the arrangement of the reticule lines. Each detector produces a sine wave due to the variation of the light intensity, and each sine wave is phase shifted 90^0 as a result of the reticle orientation and rotation of the graduated disk. The result of this type of reticle scanning can be seen in figure 3.49 (Heidenhain, 1999). The PSLR encoder output is represented by the two channel composite signals(red traces) at the bottom of figure 3.49. This type of output has two distinct advantages as,

1. the direction of movement is easily determined by a decoder as the output channels lag or lead each other (dependent on direction), and

2. since the channels are essentially electrically independent, it is unlikely that stray pulses will register on both channels at the correct time to cause the decoder to register a count.

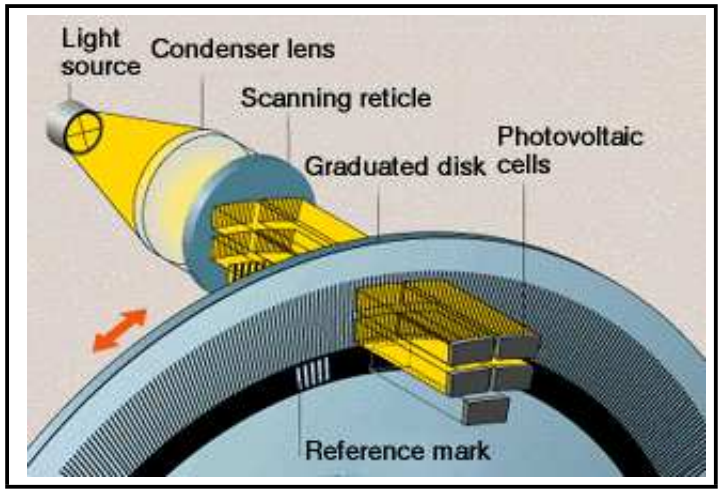

Figure 3.48: Optical scanning method used with the RON225 angle encoder.

The accuracy of the RON 225 angle encoder from Heidenhain Pty Ltd is quoted as being primarily influenced by the following conditions:

1. quality of the graduation,

2. quality of the scanning process,

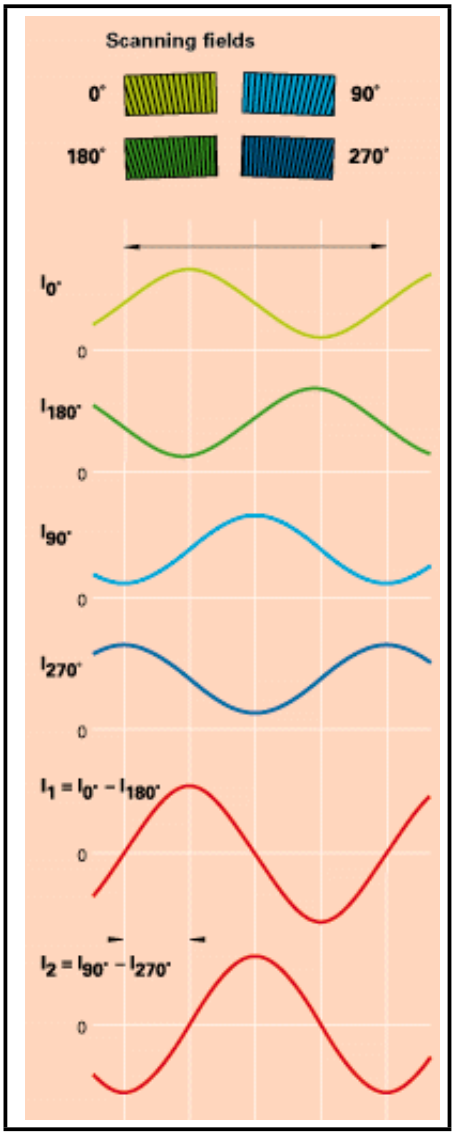

Figure 3.49: Output of the scanning reticle method used with the RON 225 encoder.

3. quality of the signal processing electronics,

4. eccentricity of the graduation to the bearing,

5. radial run out of the bearing,

6. elasticity of the encoder shaft and its coupling with the drive shaft, and

7. elasticity of the stator coupling.

Heidenhain provide a calibration chart for each RON encoder which takes into account the deviation of the encoder and the deviation caused by the coupling. This calibration accounts for all but point 3 (above).

The signal processing electronics are provided by the DMC 1720 dual axis controller. The DMC 1720 has two dedicated encoder inputs (one per channel) which are able to handle $12,000,000$ quadrature counts/sec. This relates to a rate of 3Mhz (full encoder cycle) so encoder line spacing and angular speed must not exceed this figure (Tal, 1999). At maximum permissible rotation rate of 4000rpm (Heidenhain, 1999) of the encoder, a frequency of 12 Mhz would be generated and would exceed the capacity of the motion controller. The maximum speed possible with the PSLR motors is 3000 rpm or 50 revolutions per second (100,000 steps/sec). As each encoder quadrature step requires at least 55 motors steps, this gives a maximum encoder frequency of less than 455 Hz ($100,000 \div 55 \div 4 = 454.\overline{54}$). This figure is far less than the capacity of the encoder inputs of the motion control card.

The PSLR telescope is able to move about its own axes at a rate greater than 39^0/sec, more than adequate for almost any conceivable tracking purpose.

Heidenhain claims that the measurement accuracy of the Ron 225 encoders over 1 signal period is typically less than $\pm 1\%$. As the RON 225 encoders have 18,000 lines this equates to a signal period of $360^0 \div 18,000 = 0.02^0$. With accuracy of $\pm 1\%$, the maximum accuracy over a period of $0^0 01' 12''$ is $\pm 0.72''$ and $\pm 5''$ over an entire encoder revolution.

3.8.3 Motion control methodology

The PSLR motion control system uses a quasi-digital approach to motion control. The stepper motors connected to each drive axis permit motion in discrete positions or steps. To position each axis, a number of steps of each motor need to be performed. In an ideal world, the axis in question should be able to be moved by $\pm$ 1 motor step. In the case of the PSLR which is driven through a reduction gearbox, this would amount to .5 of an arc second motion per axis. Unfortunately, the

PSLR drive system is not digital. Although the steppers have discrete positions, the reduction gearbox and the friction drives that move each axis are subject to slippage and hysteresis. This simply means that not every motor step will move the telescope axes by exactly the same amount. For an application such as laser tracking of satellites where positioning is all important some external form of position measurement is required. The PSLR uses an angle encoder on each axis. The one big drawback with the DMC-1720 indexer is the insistence on open loop operation for stepper motors.

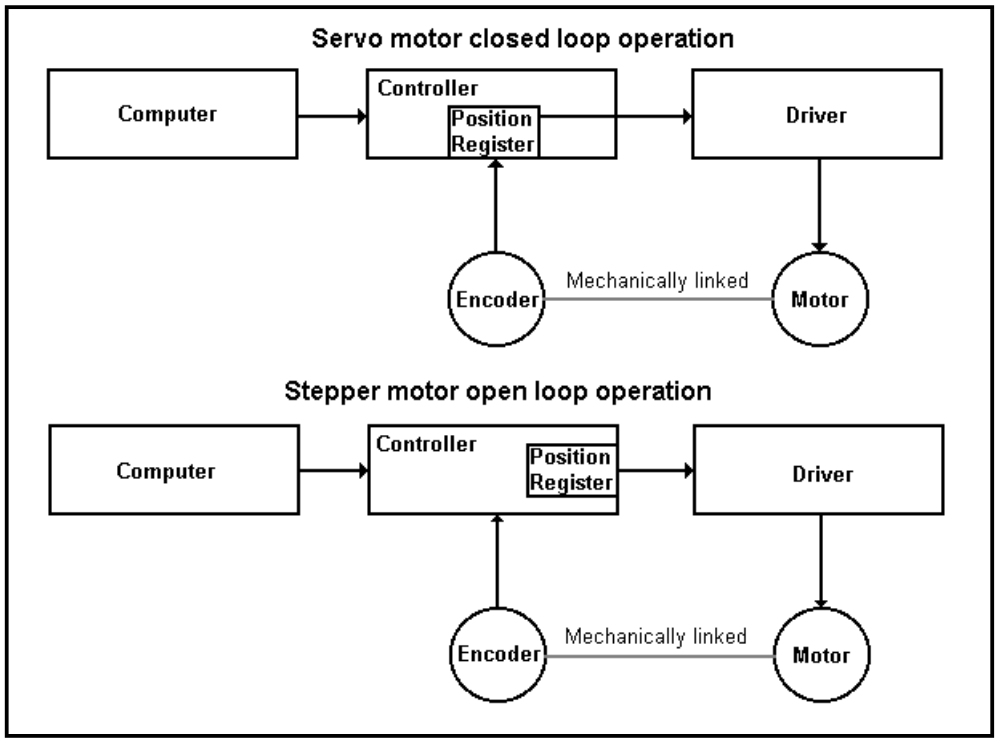

Figure 3.50: Illustration of closed loop and open loop motion control with the DMC-1720 indexer card.

The top half of figure 3.50 shows the closed loop tracking method often used with servo motors. This shows the encoder is attached to the load. If this type of approach was used with the PSLR, it would be attached to one of the telescope axes. When the servo motor is instructed to move, its position is monitored by the encoder. If a trip point was set within the controller; for example, in order for the

elevation mount to stop at 45^0, the motor would move and the position of the mount would be read from the encoder which as stated is attached to the mount. The motor would stop when the encoder on the mount registered the correct position.

The bottom half of figure 3.50 shows the setup for PSLR mount control. The controller, when set to drive stepper motors, registers the position according to the number of step pulses it has sent out to the drive unit. It assumes that stepper motors, due to the discrete positions within the motor, provide their own intrinsic positioning. If a particular position is required then the amount of steps required to move the mount to this location could be estimated and instructions sent to the controller to move the required number of steps. Due to inconsistencies of the gearbox, slippage of the friction drive and overrun due to mount momentum, there is very little chance of ever ending up in the correct position. It is possible using the DMC-1720 to read the encoder mounted to the axes but it is not possible to use many of the in-built controller functions with this encoder position. All of the DMC-1720 functions that require positions, trip points, velocity, ramp functions and the in-built interpolation movements use the pre-registered step pulses generated from the card to determine the position and the appropriate movement. If the PSLR used servo motors these in-built motion profiling command would use the position registration provided by the encoders.

This limitation of the controller card has meant that many of the in-built functions are of little use to the PSLR control scheme. The only way to be entirely sure where the telescope is pointing is to interrogate the angle encoders. In order to track and position the PSLR mount, when any of the in-built functions are used to move the mount, the final position has to be determined using the encoders.

To locate a star of known position the method used is to give the controller a PR command. This command means position relative and indicates that the controller should move the motors to a position so many steps relative to the current position. The estimated number of steps required, assuming that there is perfect inertialess movement of the friction drives, is predetermined by the tracking program. This

value is multiplied by a fudge factor (generally between 1 and 2) so that the mount is instructed to cross the required position. The motors are stepped with "start" and "stop" ramp values to try and minimise slipping and inertia of the drive wheels and mount. The encoder position is read and when the required position is reached motion is halted, even if the PR move is still in effect. This will still mean that the axis in question will overshoot the mark due to inertia as the initial movements are generally executed at close to maximum speed. The axis in question is moved back to the required encoder position at much lower speed so that there is no inertial overrun on cessation of the motor drive. If it were possible to use the closed loop tracking functions of the DMC-1720 indexer, all of the ramping and stopping at the correct position would be achieved automatically and would save a great deal of time when locating a position.

It would be possible to achieve closed loop tracking using purpose written software to achieve all of the functions of the DMC-1720 indexer. This would be achievable as the encoder position and motor speed can be read from the indexer card by a PC, even if there is some delay. Reactive programs could be written that would be able to adjust the motor speed by calculating the real speed from counting encoder steps over time. This would allow the motors to be ramped up and down so that finding a position could be accomplished in only one move. This is a task that, in retrospect, would have been a better use of the PSLR programming personnel.

When using the mount to track slow moving objects, such as stars, the mount will track reasonably smoothly with very little slippage after initial acceleration of the mount to tracking speeds. As the PSLR control program is not operational, it is not currently possible to gauge the performance of the mount for the tracking of Low Earth Orbit satellites which require much faster tracking speeds.

3.8.4 Conclusion and recommendations

This chapter has attempted to give a broad overview of SLR components, their operation, and their application to SLR and the PSLR. Understanding the princi-

ples and method of operation of the afore mentioned equipment is essential when designing and/or building an SLR system. It is the application of the appropriate functionality of the individual equipment that makes the applied science of SLR possible. Without a high level of knowledge about each piece of equipment used with an SLR station it is not possible to produce optimal data. The precision levels of standard SLR stations has almost reached the acme of possibility, due in part to collected experience but principally because of optimal equipment function.

The focus of this chapter has been on the equipment used with the PSLR and similar systems. In times past, most of the equipment used by SLR stations was not freely available. The requirement for precision meant that equipment was either one off or so prohibitively expensive that very few units were ever made. As technology has improved, specifically in the manufacture of electronic equipment, it has become possible to purchase many of the components required for SLR off-the-shelf. Many other uses have been found for high precision timing and positioning, and lasers have developed over the years so the prices for these items have greatly decreased. It is now entirely possible to assemble a laser ranger, including optical, electronic, and mechanical systems, from commercially available components without the need for their extensive modification. The ultimate goal for the PSLR instrument is that its design would evolve so that it would consist almost exclusively of commercially available components.

If portable satellite laser ranging is to be more than an expensive experiment, it would need first of all to define its operating parameters. Secondly, it would need to be significantly cheaper than a fully functional fixed system. The intelligent use of commercially available equipment can accomplish much towards this cost cutting goal.

The PSLR, as a portable system, is required to perform all of the functions of a fixed system (with a comparable level of accuracy) while maintaining good portability (must be able to be relocated and setup quickly). The performance of the PSLR equipment mentioned in this chapter and any recommendations for the

replacement of this equipment to better suit the requirements of a portable system are listed below.

- **Laser** - the PSLR uses a Ekspla SL212 Nd:YAG pulsed laser. It has a separate Q-switch controlled oscillator and amplifier stage as well as a second harmonic generator, equipment that is very common in other SLR lasers. It has a SBS pulse compression unit which is not at all common. The second harmonic output is at 532 nm with pulse duration 130 ± 20 ps and a maximum energy per pulse of 125 mJ.

  The stability of the laser output energy appeared to be poor. This was inferred from the observation of the pulse shapes produced on the Tektronix TDS3052 oscilloscope by the laser "start" detector and the R4124 PMT.

  Recommendation - given the large size of the primary mirror and the desire to reduce the weight of a portable system, such a large and powerful laser is not recommended. A smaller laser with shorter pulse duration and lower energy and better stability would produce better results. Another approach would be to use a high repetition laser ($>$ 1000Hz) and an event timer (see section 7.1.4, 294).

- **Detector** - the PSLR uses a Hamamatsu R4124 PMT. This detector has a quantum efficiency of approximately 12%, a gain of 1.1×10^6, a rise time of 1.1 ns and a transit time of 12 ns .

  The detector and Latvian built preamplifier unit proved to be very noisy when the PMT was operated above 700 V. The discriminator was not able to separate actual return pulses from the noise pulses when operated at the recommended voltage (1000 V). It was not possible to attribute the large spread in the time of flight values for the fixed target ranging tests conducted (see chapter 5) specifically to the PMT tube without independent corroboration,

although is appears to be a major contributing factor.

Recommendation - replacing the PMT detector with a SPAD would allow a reduction in the size/capacity of the laser, while improving the detector sensitivity, rise and transit times. As the active area of a SPAD is small compared with the R4124 PMT, it may be useful to retain the PMT for signal acquisition when tracking.

- **Pulse conditioning electronics** - The pulse conditioning electronics were generally good. The Latvian built preamplifier units specifications were unknown and may have contributed to spurious noise pulses when the PMT tube voltage exceeded 700 v. The Ortec 9306 preamplifier had excellent rise time specifications (350 ps) and operated to expectations. The Ortec Pico-timing discriminators also had excellent rise time specifications (350 ps). One of the units in operation was less sensitive than the other and would not trigger on small input pulses.

  Recommendation - Removal of the Latvian built preamplifier would reduce the spurious noise pulses. Replacing this unit with another 9306 preamplifier would not only exceed the parameters of the current PMT detector but match the discriminator unit. The discriminators require factory maintenance to address the loss of sensitivity in one of the units. If the PMT detector was not replaced, the pulse conditioning electronics in use are more than adequate.

- **Time interval counter** - The SR620 is still one of the most widely used interval counter in SLR as it is capable of excellent resolution (25 ps RMS), and can be operated in various timing modes (i.e. external/time hold-off).

  Recommendation - The initial ranging tests at Curtin University were conducted without supplying the unit with an external timebase frequency. The external timebase frequency (supplied by GPS) governs the SR620 oscillator

and reduces long-term measurement drift. This should be corrected for any further testing.

A paper (Gibbs, 2002) presented at the 13^{th} International Workshop on Laser Ranging, in Washington D.C. in 2002, states that SR620 timers can have range dependant biases of up to 100 ps. It also states that these biases are very stable, even after a unit has been returned to the manufacturer for repair. It would be beneficial to establish any range biases in the PSLR interval timer by direct comparison with other timers of know bias.

- **Station timing** - PSLR station time is supplied by the bc620AT time and frequency processor card slaved to the TM1 GPS unit. The GPS unit is capable of maintaining its lock to UTC to within 100 ns (with good satellite geometry). The bc620AT card can be synchronised to the GPS with almost zero latency.

  Recommendation - Station time keeping exceeds the capacity of the PSLR to utilise. As an example, a satellite orbiting at 6000 km has an orbital velocity of 5670 m/s. In 100 ns it only travels 0.5 mm. The maximum theoretical pointing accuracy of the PSLR is around 9 m at this orbital distance (this assumes a pointing accuracy of 0.3", although this is wildly optimistic).

  The time tagging of laser pulses determines the usefulness of the station data when calculating a satellite orbit from combined stations. In this respect, the more accurate the synchronisation to UTC, the better the data. The PSLR station timing system is adequate so there is no real justification for replacement.

- **Telescope drive and positioning** - The telescope drive system uses stepper motors driven through a reduction gearbox and controlled by a programmable indexer card. The indexer card card is capable of 3 million steps per second with a resolution of $\pm$ 2 steps/sec. The stepper motors are only capable of stepping at 150,000 steps per second. The angular encoders on the PSLR have

a resolution of $0.005° \pm 0.0025°$. Each step should advance the axis by $0.33"$ making this figure the maximum possible angular resolution.

Recommendation - The telescope drive system is capable of adequate tracking and positioning. Higher resolution encoders would be of benefit as the beam spread at LAGEOS distances is only 15 - 16 m (see page 179, section 4.2.1) and the current encoder resolution gives a difference of 523 m between each position at LAGEOS distances. It is coupled to a friction drive system on a mount that has far too much inertia to suit a friction drive system. Consequently the telescope drive experiences "drive slip" at the instigation of a movement, and mount "run on" when ceasing movement. The telescope drive system requires a better designed drive system and a reduction in the mass of the telescope system.

SLR is an applied science utilising a variety of equipment that was not specifically designed for use within the SLR field. The increasing demands for millimeter accuracy or better require that this equipment is operated at the very limits of its specifications. This requires that the function and behavior of each component in an SLR system be very well understood. This chapter has therefore concentrated on discussing most of the commonly used SLR components with the aim of developing such an understanding.

Chapter 4

PSLR optical design and features

4.1 Introduction

The PSLR instrument is primarily a research instrument although it was intended to be a prototype for possible commercial development. Many of the design features are ad-hoc as one avenue of the design was abandoned in favour of a new approach. The instrument contains many fine adjustments essential for an instrument that requires good precision and that may be adversely affected by changes in mass distribution as a result of system redesign. The PSLR initially started as a coaxial system with the output and input optical systems separated by use of a flip mirror system. This was later changed to a parallel (paraxial) system with input and output optical systems completely separated. None of the research team at Curtin University had seen the PSLR in the coaxial configuration but there are indications of this configuration in the PSLR control program "users manual" produced by the original University of Latvia researchers. This manual is somewhat outdated as it refers to flip mirror control and the current configuration shows no evidence of having contained a flip mirror. An intermediate stage of the PSLR development is shown on the right hand side of Figure 4.1. This shows a much smaller aperture output telescope and slightly different counterweighting, but clearly shows the evolution from a coaxial system to the current design.

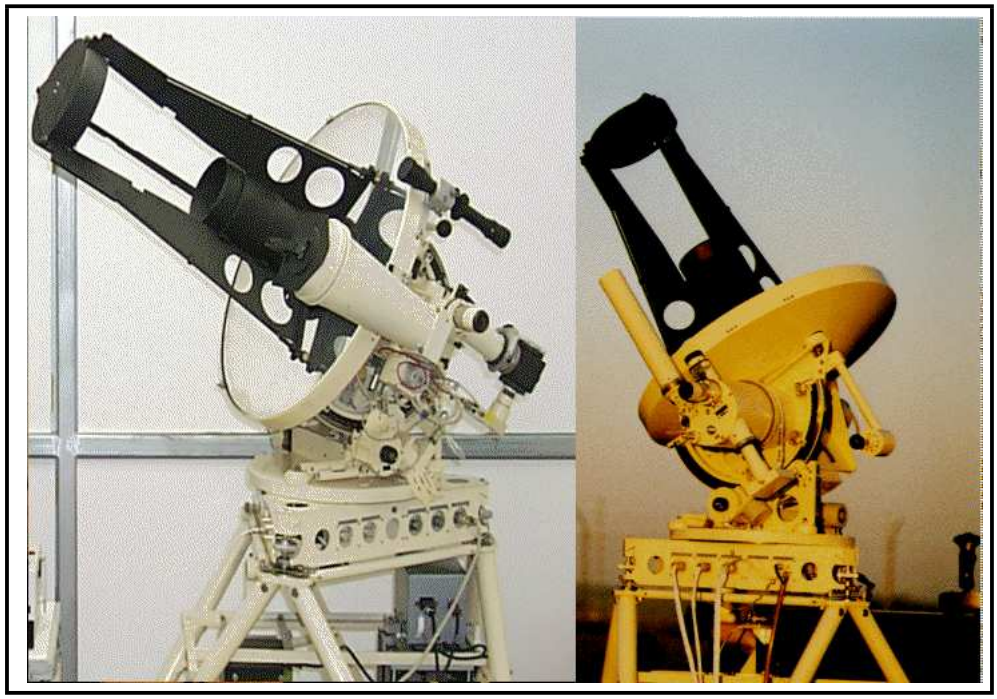

Figure 4.1: Two images of the PSLR at various design stages. The image on the left shows the current version.

As almost all of the design drawings, equipment specifications and descriptions were not made available when the PSLR was sent to Curtin University, and many of the test facilities are not available at the University to test many of the components, the discussion on the design of the PSLR is less specific than might be expected in normal circumstances. This chapter will deal with the opto-mechanical design features of the PSLR

4.2 Optical design and alignment considerations

The task of directing a laser beam to a specific point in space at a specific time requires that the PSLR performs to a high level of accuracy. The PSLR is designed to use optical elements to; (i) steer the laser beam through the mount to the transmit telescope and, (ii) to direct the returning photons to the PMT detector. These optical elements need to be of high quality (precise steering control, robust, minimal

signal loss) and able to handle the high thermal strain due to the high power laser propagation.

The individual optical elements need to be aligned with each other to produce a well defined optical path able to steer a laser beam with repeatable accuracy. This task is further compounded with only one of the PSLR optical elements in a completely static state during normal operation. All of the other optical components are attached to parts of the mount that are in motion during normal operation. The optical elements must remain precisely aligned for all orientations of the PSLR mount.

As mentioned, the PSLR has two separate optical systems, the laser beam transmitter optical system and the receiver optical or main telescope system. These two systems are completely separate and behave quite differently. The alignment of each system is approached separately so each system will be discussed in kind.

The alignment of the two optical systems to each other was never seriously tested due to the multitude of problems with the individual systems. As these problems were not successfully solved, it was impossible to investigate the alignment for all orientations of the mount.

4.2.1 Laser transmitter optical system

The laser output optical system consists of; two 45^0 prisms, one flat mirror, two matched sets of lenses for beam expansion and of course the laser. The laser is fixed to a small optical table and enclosed by a weather proof insulated cover. This sits on its own mount which is adjustable for alignment purposes (see figure 4.3). The mount is fully adjustable, over a limited range, in three dimensions. The output of the laser is aimed at the only optical element that is stationary during normal operation, a 45° prism labelled as M4 in figure 4.2. The laser's adjustment allows it to be directed onto prism M4 with any required orientation.

Prism M4 is mounted in an adjustable apparatus which sits under the coaxial telescope systems. This apparatus consists of a tube which houses the prism M4,

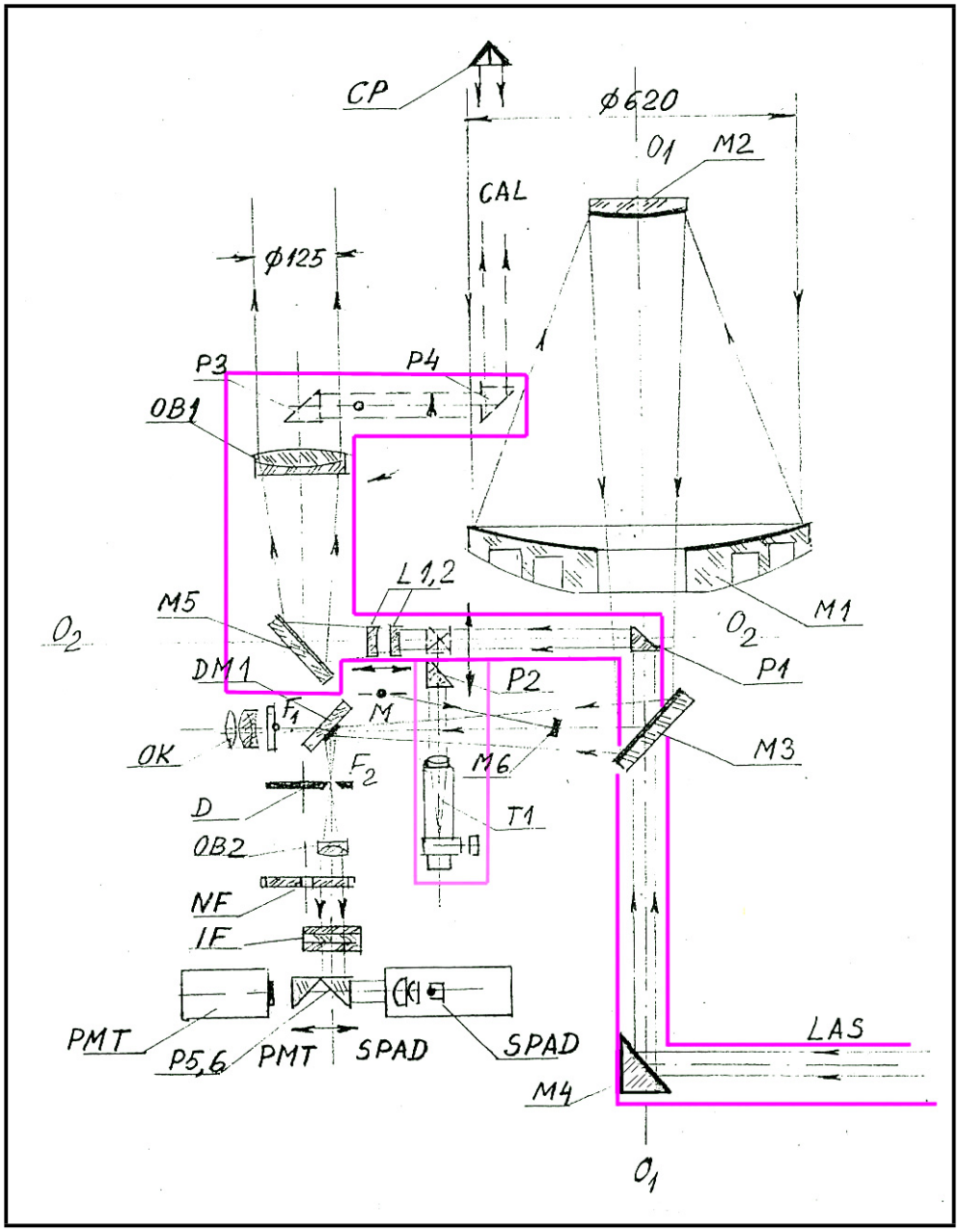

Figure 4.2: The PSLR optical systems. The transmit path and components are outlined in pink.

pivoted within another tube. The location where the inner tube is connected to the outer tube by the pivot can be seen in figure 4.4. The hex nut on the side of the outer tube of mounting apparatus is used to adjust the tension on the pivot. The prism is located at the right hand end of the inner tube (as indicated in figure 4.4),

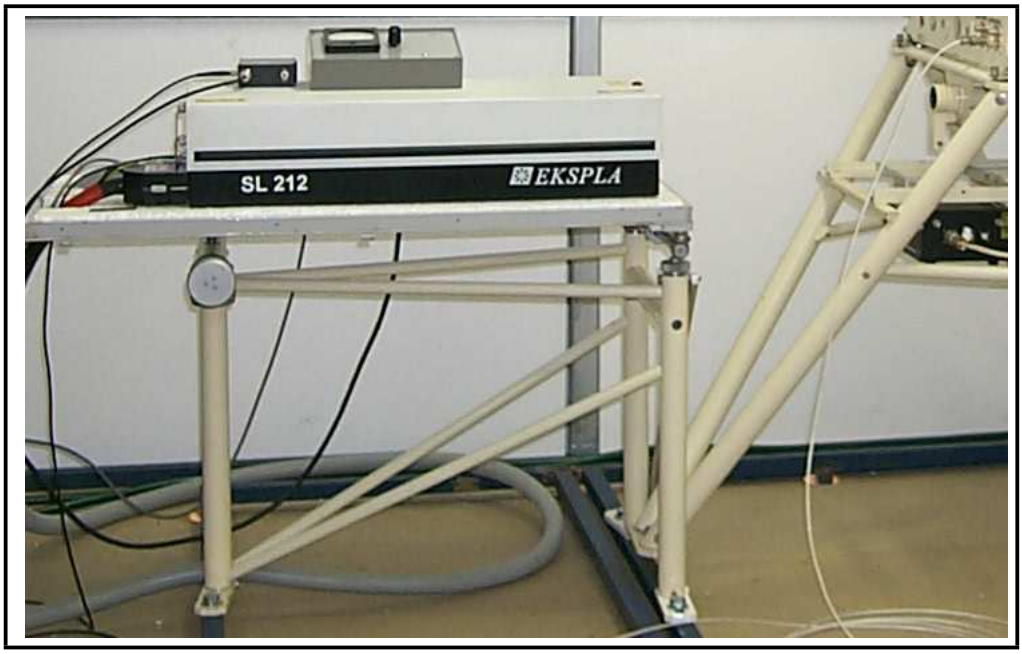

Figure 4.3: PSLR laser and laser mount.

inside the prism mount. The prism mount can be rotated about the inner tube of the apparatus, it can slide in or out of the inner tube (left to right in figure 4.4), and the inner tube can be moved in all directions around the pivot (within a limited range of movement). There are no adjusting screws or other devices for the rotation or sliding of the prism mount about the pivoted tube. This must be adjusted by hand and then locked by clamping screws. There is no calibration for the adjustments so the positioning of the prism mount is mostly guess work. The inner tube is moved about the pivot by use of three screw adjustments mounted on the outer tube at the end opposite to the prism.

These adjusting screws are visible in figure 4.5. The top adjusting screw rests upon the inner tube of the apparatus and pushes the tube against a spring. Adjusting this screw will rotate the prism around a horizontal axis through the pivot point. The other two screw adjustments nudge the spring which holds the inner tube in place. This has the effect of rotating the inner tube either clockwise or counter clockwise around a vertical axis through the pivot point. These adjustments are quite imprecise without the use of micrometers and tends to cause unwanted move-

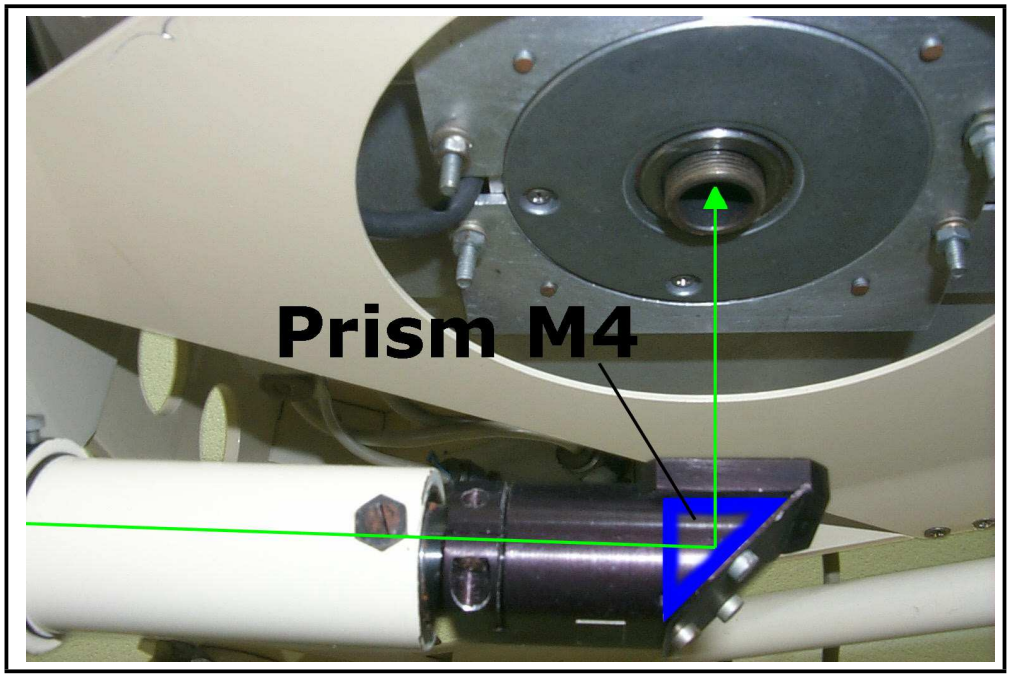

Figure 4.4: Prism M4 mounting apparatus.

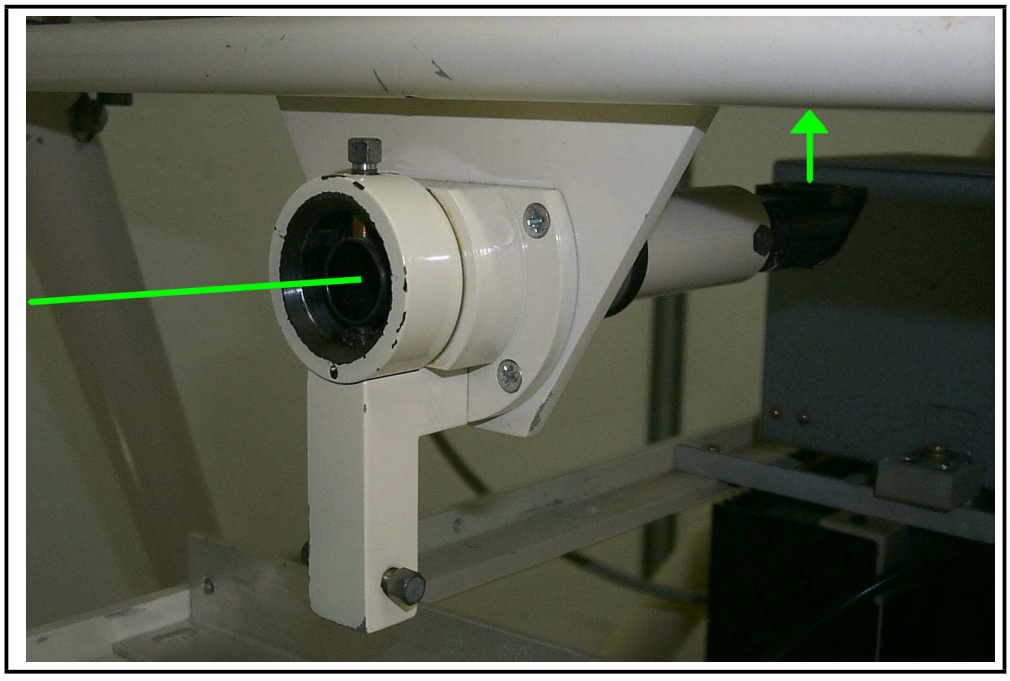

Figure 4.5: The adjustment screws used to position prism M4.

ment in the other adjustment plane. The top screw adjustment has the flat of the end of the screw sitting on the inner tube. When the screw is turned, as well as the

inner tube being forced down, there is a tendency for the tube to be pushed either left or right depending on the direction of turning of the screw. The two horizontal adjusting screws can move the tube to compensate for this motion but because the inner tube is cylindrical, when the tube is not gripped in the exact centre, the tube moves up (see figure 4.6) .

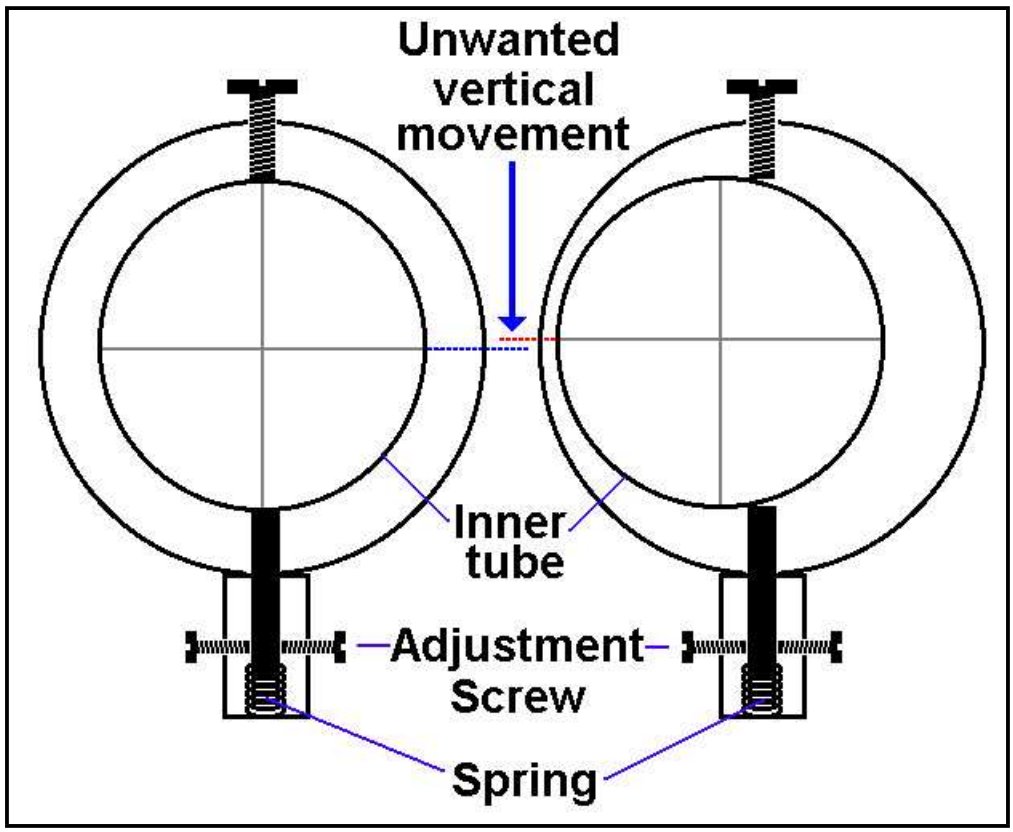

Figure 4.6: Illustration of the affect of side adjustment on the position of the inner tube. The top screw is the principal height adjustment with the horizontal screws causing side adjustment. As the inner tube is moved off centre, the spring loading causes unwanted upward movement.

As both the prism M4 and the laser table are adjustable, it is possible to find the correct alignment so that the laser beam is directed up through the mount in the correct orientation, although given the required propagation distance of the laser beam, it is not easy to do this accurately. The center of the mount axis of rotation needs to be concentric with the laser beam's vertical path. As the laser and prism

M4 remain stationary at all times during normal mount operation, this alignment is not affected by the alignment of any rotating mechanical equipment.

Prism M4 directs the laser beam up through the mount to prism P1. Prism P1 is intended to direct the laser beam through the mount horizontally so that the direction of the laser beam is exactly coincident with the rotation of the elevation axis. This prism is the most critical optical element in the laser transmit optical system as it is at the intersection of the axes of rotation (this is the point to which all distance readings are referenced) and it has the greatest effect of all of the optical elements on the final direction of the transmitted laser beam.

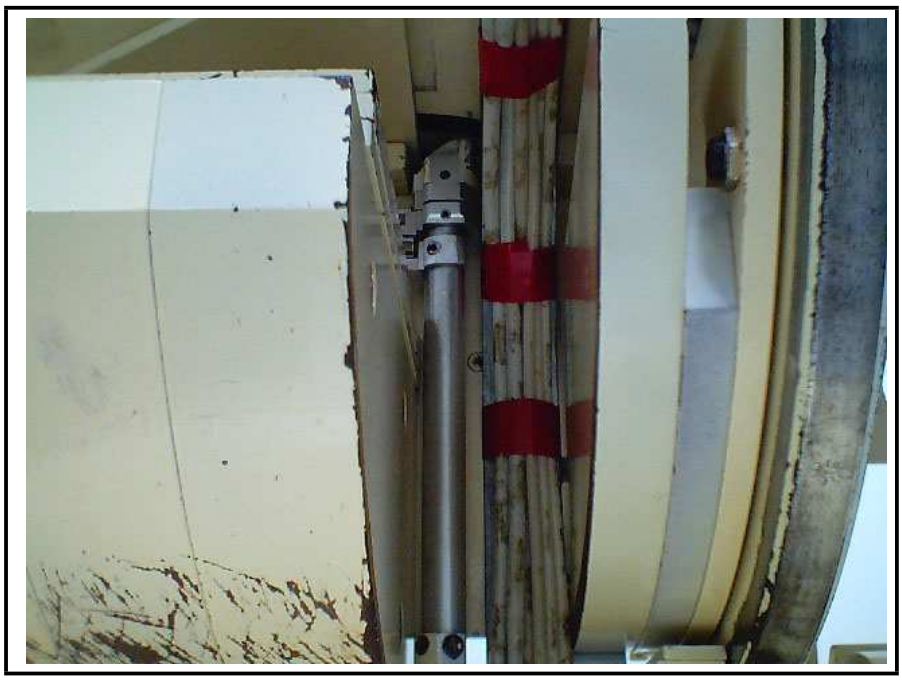

Figure 4.7: Position of the periscope that contains prism M1

This prism is mounted on an $\approx$ 15cm long tube which in turn is mounted on the azimuth turntable. The turntable rests on two rollers and the azimuth drive wheel. The rollers and drive wheel are borne upon a solid steel track which is fixed to the non-moving part of the mount. This means that, as the prism is essentially fixed to the azimuth turntable, any motion inconsistencies or biases in the turntable arrangement will be transferred to the prism. Prism P1 must rotate about the exact

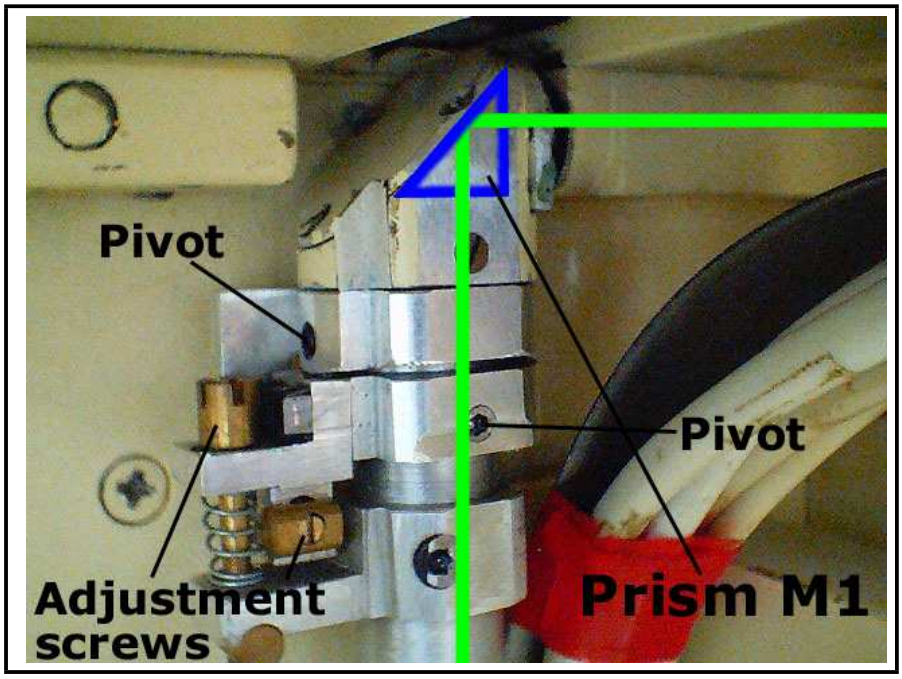

Figure 4.8: Top of the periscope which contains prism M1 which shows two of the adjustments for the prism. Each plane of adjustment has a separate pivot point.

centre of the transmitted laser beam with a consistent angle of incidence between the laser beam and the reflective surface of the prism. If this angle of incidence changes due to rotation of the azimuth table then the output laser beam from prism P1 will precess about the elevation axis. The orientation of the prism can be altered in any direction, for a limited range of movement, using the adjustments on the prism mount (see figure 4.8). This will always allow the laser beam to be directed precisely along the elevation axis in static mode. If the orientation of the prism is affected by the rotation of the azimuth table then this precise directional alignment will be lost. Unlike the receive optics, where a mount error model can compensate for alignment inconsistencies due to mount fabrication errors, it can do nothing to solve the problem of the directional error of the transmitted laser beam arising from the rotation of the mount.

The output from prism P1 is directed to optical elements labelled L1, L2 in figure 4.2. This is a compound lens constructed from lenses L1 and L2. This lens

arrangement expands the laser beam. The expanded laser beam is then incident on mirror M5 (see figure 4.10). This is a front coated plane mirror placed at 45^0 to the laser beam and is adjusted principally by three adjustment screws located at three separate corners of the mirror. This allows the three degrees of freedom needed to direct the laser beam at the correct orientation to the objective lens OB1. The lens OB1 is matched to the compound arrangement L1,L2 and collimates the expanded beam so that the final output leaves essentially as a parallel laser beam. The last optical component in the transmit system is a flip periscope arrangement (see figure 4.10) used when firing to calibration retroreflectors, labelled as P3 and P4 in figure 4.2. The flip periscope is mounted on top of a cover that is hinged to the end of the output laser telescope. During calibration to retroreflector target, the cover is flipped over the aperture of the output laser telescope with the very centre of the laser beam directed through the periscope.

The key elements of this design is the expansion of the laser beam by the matched compound lenses and the flip periscope. The indication is that these changes in design (as compared to the intermediate model viewed at the right hand side of figure 4.1) were an effort to make the PSLR more eye safe. There is, due to the changes in design, little chance of serious eye damage from scattered or diffuse reflection from the PSLR in normal operation. Direct exposure to the output would still prove hazardous to ocular tissue.

Expansion of the beam in this manner can also be used to reduce the divergence of the beam. The divergence of the beam will effect the beam intensity and spread at satellite distances. This in turn will affect the return beam intensity and the required pointing precision of the telescope system.

The divergence (θ) of the beam from a laser is result of the beam waist radius(ω_o)(see figure 3.3, page 62) and can be expressed by (Melles Griot, 2004):

$$\theta = \frac{\lambda}{\pi\omega_o} \tag{4.1}$$

where, λ is the wavelength of the laser beam.

From the beam waist it is possible to determine the waist radius at a distance ω_z by (Melles Griot, 2004):

$$\omega(z) = \omega_o[1 + (\frac{\lambda z}{\pi\omega_o^2})^2]^{\frac{1}{2}} \tag{4.2}$$

where, z is the distance along the optical axis in the direction of beam propagation.

The beam waist, divergence and the focal lengths of a galilean expander are related by:

$$\frac{\omega_2}{\omega_1} = \frac{\theta_1}{\theta_2} = \frac{f_2}{f_1} \tag{4.3}$$

where, ω_1 is the beam waist radius of the laser beam, ω_2 is the beam waist radius at the objective lens, θ_1 is the divergence of the laser, θ_2 is the divergence after the objective, and f_1 and f_2 are the lengths indicated in figure 4.9.

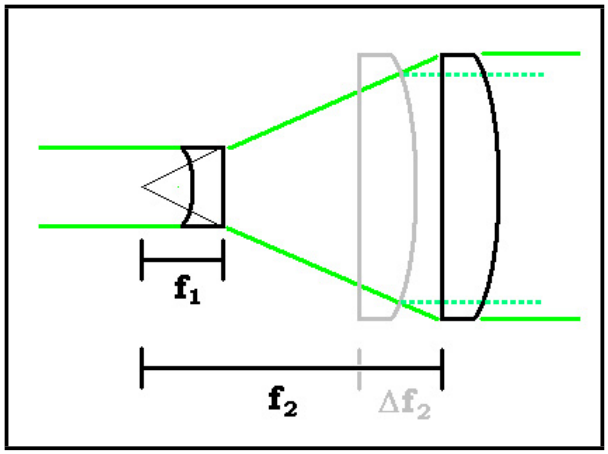

Figure 4.9: Illustration of the Galilean expander system used with the PSLR. Focal length f_1 indicates the focal length of the lens doublet L1,2 and focal length f_2 indicates the distance from objective lens OB1 to the focal point of L1,2 (see figure 4.2)

This then shows a method of controlling the divergence of a beam and the spot size at a distance.

$$\omega_2 = (\frac{f_2 \pm \Delta f_2}{f_1})\omega_1 \tag{4.4}$$

$$\theta_2 = (\frac{f_1}{f_2 \pm \Delta f_2})\theta_1 \tag{4.5}$$

To put all of this in perspective the approximate measurements of the PSLR beam expansion system can be used. The output beam from the PSLR laser (SL212) is 10 mm so the beam waist radius is assumed to be half of this value. Using equations 4.1 and 4.2 the raw laser beam would have a divergence of 33.8 μrad and the beam waist radius at LAGEOS distance (6000 km) would be 201.6 m.

Using equations 4.4 and 4.5 where f_1 is 50 mm and f_2 is 650 mm it can be shown that the divergence from the expander is now 2.6 μrad and the beam radius at LAGEOS is 15.6 m.

The raw beam will produce a beam at LAGEOS with a cross-sectional area of 126923 m^2 whereas the divergence limited beam will have a cross-section of 764 m^2. This means that there will be 167 times more photon per square metre at LAGEOS by reducing the divergence.

The PSLR has the ability to adjust the focal length f_2 (see figure 4.9) to fine tune the divergence and the beam waist radius. Focal length $f_2 \pm \Delta f_2$ can be adjusted from approximately 635 - 665 mm by a worm drive that houses the lens doublet L1,2. This gives a range of divergences from 2.55 - 2.67 μrad and beam radii ranging from 15.3 to 16.0 m at LAGEOS distances. This has very little effect on the final beam radius. It is more likely that the adjustment of L1,2 is used to focus the telescope (rather than control the divergence) for star viewing when the separate optical systems are aligned to each other.

These figures for the beam radii at satellite distances do not take into account beam spreading by refraction in the atmosphere due to localised turbulence. Atmospheric turbulence is a complicated subject as is the effect on Gaussian beam propagation. A good introduction can be found in (Degnan, 1993).

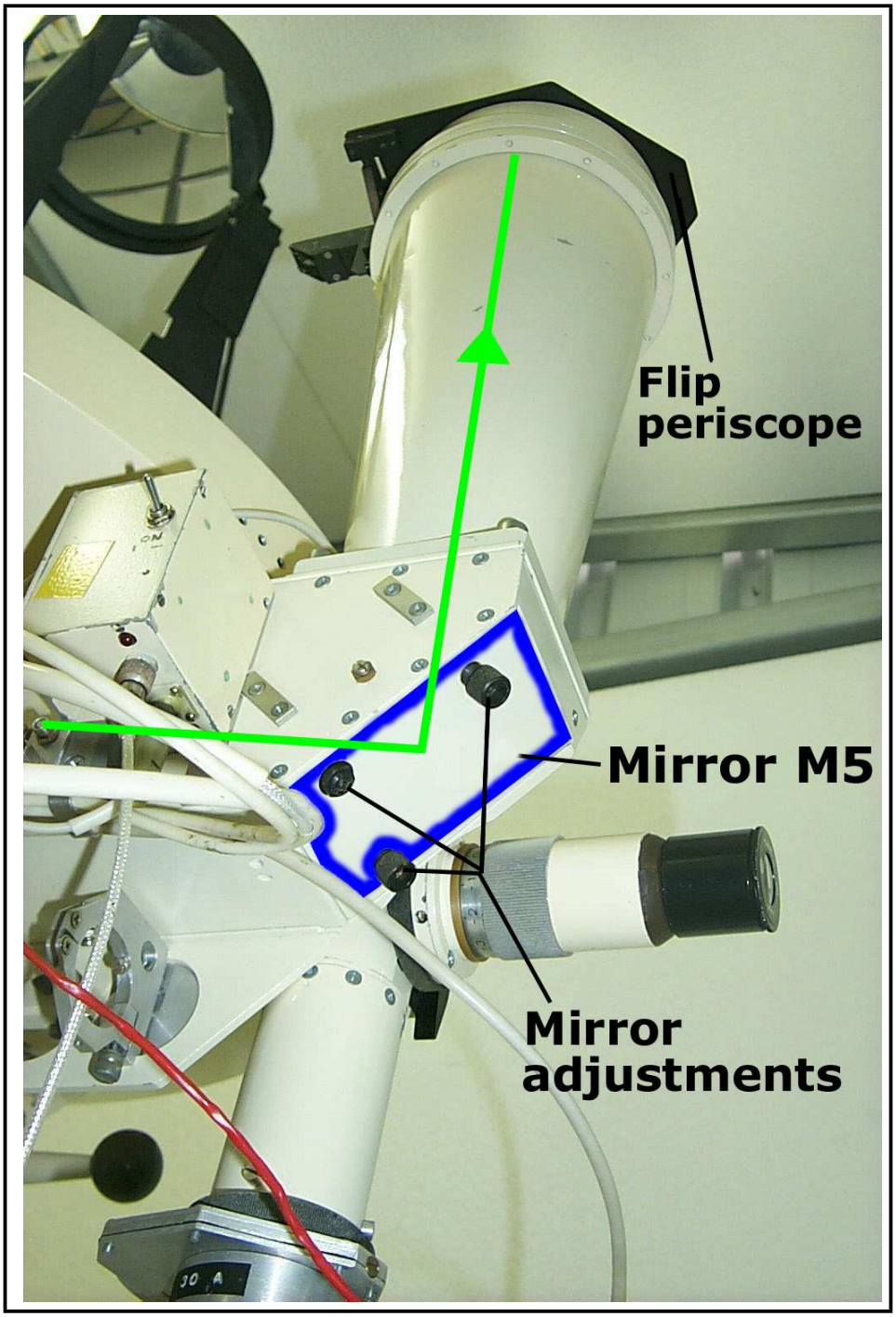

Figure 4.10: The output telescope showing the flip periscope apparatus and the adjustments for mirror M5.

The optical elements placed after prism P1 in the optical chain are all located in an arm mounted under and to the side of the main mirror. This is shown in figure

4.10. This arm is fixed to the elevation axis. This means that optical element L1,L2 and mirror M5 will rotate in a plane about the laser beam. As with prism P1, it is essential for these elements to rotate precisely about an axis. The mechanical axis of rotation and the optical axis need to remain aligned for all angles of elevation and azimuth. If this is not the case then the final output from the laser telescope will precess around the centre of the pointing coordinates of the main receive telescope. As the output beam then would be off angle with the pointing direction, the laser beam could be hundreds of kilometers off target at satellite ranges, as even a discrepancy of 1^0 at the height of the LAGEOS satellites will give over a hundred kilometers in cross track or along track error.

Prism P2 and telescope T1 indicated in 4.2 are able to be inserted into the output optical path by vertically translating prism P2 into the path. This prism enables viewing in either the output direction or towards the laser entry point by a 180° rotation about the axis of symmetry of prism P2. Telescope T1 is variable focus so it can be trained on particular elements in the optical chain. If the apparatus containing prism M4 is removed, then the horizontal surface on which the PSLR is situated can be bought into focus. This facility makes it easy to set the PSLR accurately over a datum point in much the same way as a surveyor would position a theodolite. This facility is also designed to aid in the alignment of the optical path. If prism P2 is used as a reference point and the optical path in either direction is aligned to prism P2, then presumably the entire optical path should be in alignment when prism P2 is flipped out of the optical path. It is also possible to use this facility with the final output lens (OB1) as a telescope. Celestial object can be viewed in conjunction with the main receive telescope. This not only provides a means of co-aligning the two optical systems but gives a way of measuring differential flexure between the two systems in various orientations.

4.2.1.1 Alignment of the output optical system

The achievement of alignment of the PSLR transmit optical system has proven to be very time consuming. The major reason for this is when one of the many adjustments was changed, the only way to observe the impact was to move the telescope and watch the movement of the laser beam within the field of view of the output telescope (lens OB1). If another adjustment was made, the telescope again was moved and the laser beam transit was compared with the last observation. A decision was made if this was better or worse aligned, and more adjustments were made. This process proved to be highly counter-intuitive due to the 23 mechanical adjustments directly able to alter the alignment of the axis of rotation and the optical axis. The effect of each adjustment was not predictable and the result, while appearing to improve the alignment, may have been only compensating a problem with one of the other adjustments.

Various methods were used to measure the effect of changes made to the PSLR adjustments. These ranged from simple observation of the orientation of the ranging laser as it exited element OB1, use of prism P2 and telescope T1 to observe the relative movement of optical elements during mount movement, and the use of a lower power CW laser trained through the optical chain to observe its direction and orientation.

One such observational method involved the use of a low cost USB based digital camera (web cam). This camera was mated with a variable focus telescope and mounted under the PSLR (see figure 4.11). This allowed an image of the PSLR laser transmit optical path to be viewed on a nearby computer screen. The variable focus telescope made it possible to view through the entire transmit optical path and focus on sections of interest, such as the top of the laser transmit periscope (prism P1). This proved to be a very powerful alignment tool as it was instantly obvious where many of the misalignments were located when the first images were taken. As the telescope was rotated or tilted, the centre of rotation or tilt could be seen to move away from the centre of the optical axis (which was at the centre of

the image displayed on the computer screen). The effects of adjustments could now be observed as they were made. This proved to be very useful for gross adjustment of the mechanical axis of rotation so that it remained coincident with the optical axis at all times.

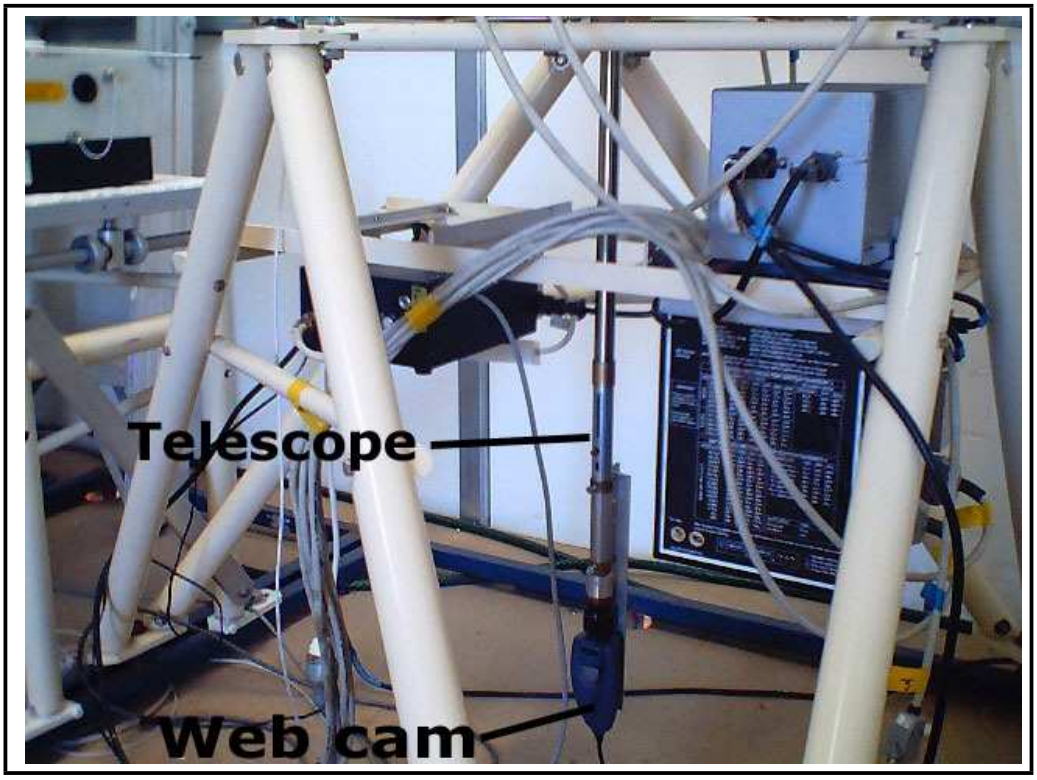

Figure 4.11: This image shows the camera, almost on the floor, looking up through the laser output optical system.

The misalignment of the mechanical axis to the optical axis, when the telescope was rotated in elevation, was not obvious from casual observation. It became clear when the camera was focused slightly past the rear horizontal surface of prism P1. The image showed the intrusion of an aperture through the elevation track mount. (the elevation track mount is fastened to a semi-circular track which principally rides upon the elevation motor drive wheel and is where motive force is applied to elevate and declinate the PSLR telescopes). This aperture allows the laser beam to pass through and eventually out to the transmit telescope. The evidence from the

camera suggested that the elevation mount was not rotating around the appropriate axis as the image of the edge of the aperture was not concentric with the periscope aperture edge and the position of the centre of eccentricity changed as the mount was tilted (see figure 4.12). This meant that the axis of rotation of the elevation mount changed as the mount was moved. This also indicated that the optical elements within the elevation mount were not rotating but precessing about the elevation axis. It essentially was impossible to correctly align the optical path as the path was changing when the mount was moved.

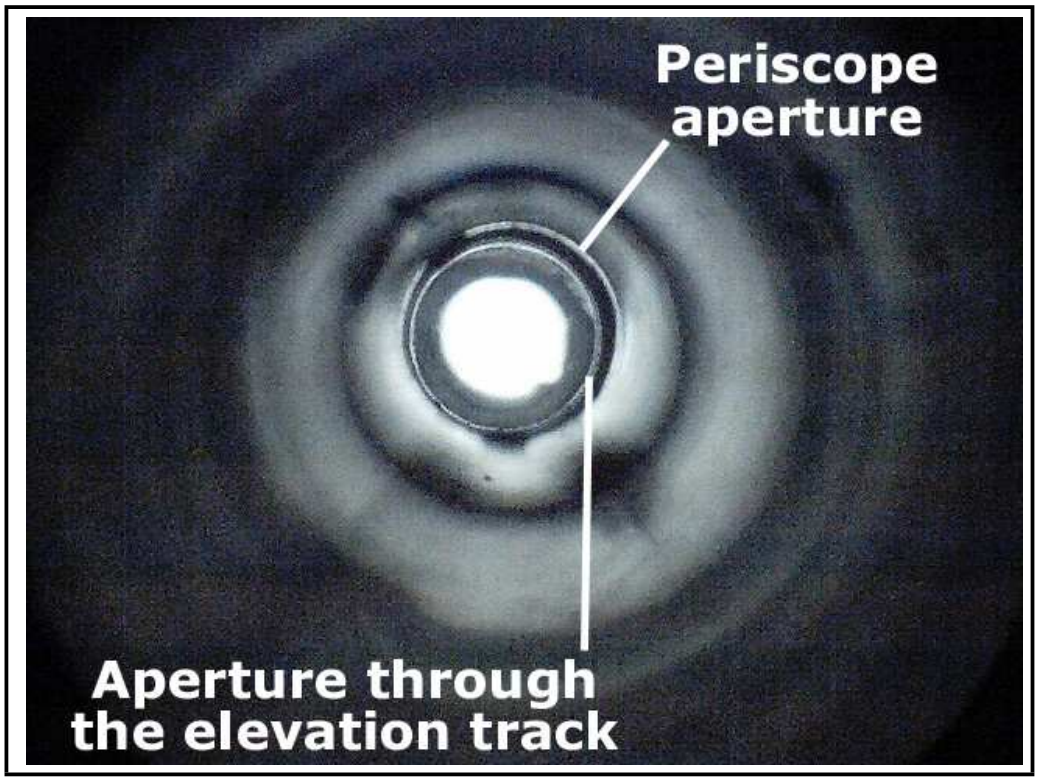

Figure 4.12: Image from the webcam were the focal point is in front of the horizontal surface of prism P1. The aperture of the periscope of prism P1 is clearly non-concentric with the aperture through the elevation mount. Subsequent images showed these apertures precess with respect to each other.

Following this exercise, the elevation mount was checked using a dial gauge and solid metal insert. This process is shown in figure 4.13. The elevation mount was shown to be offset with the elevation drive track so that the aperture through the

elevation mount was precessing about the centre of the elevation axis. Adjustments were made so that the metal insert inside the aperture was rotating concentrically with the elevation axis. The adjustments were made until the dial gauge readings were at the tolerance of the machining of the rod.

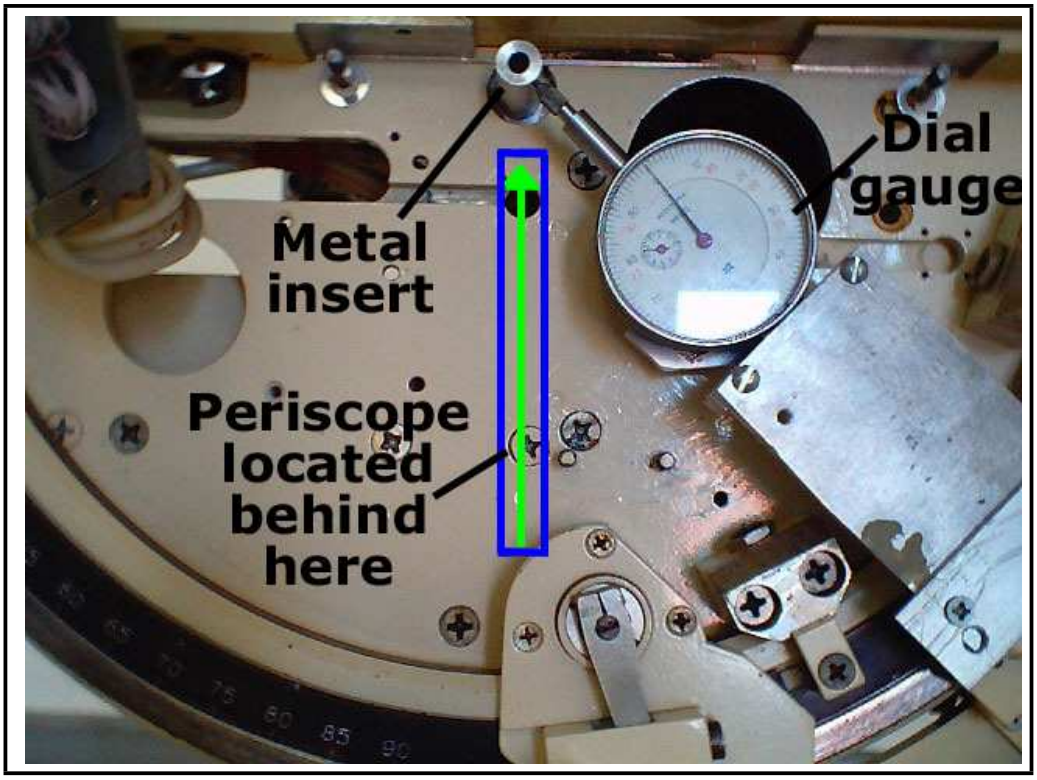

Figure 4.13: The dial gauge is fixed to the azimuth rotation table and trained upon an insert in the egress hole. This aperture should rotate concentrically with the elevation axis.

After several adjustments were made, the dial gauge showed a maximum deviation of 0.05mm when the mount was rotated from fully elevated to horizontal. This range was over a millimeter when the dial gauge was first used. This offset indicates that the axis of mechanical rotation was changing by up to a millimeter and, as such all, of the optical elements located after P1 in the transmit optical path were moving in accordance with the changing axis. This was certainly borne out by efforts to align the laser with the optical path before the adjustments to the elevation axis were made as it was not possible to keep alignment when the mount

was tilted. After the mount was adjusted so that the centre was within 0.05mm it was possible to keep the laser aligned when the mount was tilted. This alignment was tested further with a low power CW laser and then the SL212 in a process that will be explained subsequently.

Once there was confidence that the elevation mount and the optical elements designed to move with the mount were behaving properly, the next task was to align those elements that were affected by the azimuth mount movement. This included the SL212 laser, prism M4 and prism P1. Although the laser and prism M4 remain static when the mount is moved, these elements have to be properly aligned to the azimuth mechanical and optical rotation axes. The azimuth mount rests upon the azimuth drive motor wheel and two free-wheeling rollers, all 120^0 apart (see figure 6.4, section 6.2.1, page 267). These three points sit upon a solid steel track which is fixed to the PSLR tripod.

Given the level of precision required to track satellites it is surprising that the designers of the PSLR decided not to use a meshed gear drive system. It would still be possible to rest the mass of the mount on the azimuth drive wheel and give positive drive (and precise braking) if both the drive wheel and track were cut as gears. It would even be possible to include this positive drive meshed gear system on the inside edge of the azimuth track and drive wheel without a great deal of remanufacturing of the PSLR mount.

Both the rollers and the motor are adjustable, each able to be raised or lowered with respect to the track. The separation of each element or angle around the circular track can be altered slightly. The expectation is that the azimuth rotation occurs around a completely horizontal base. If there is some tilt in the base then as long as the azimuth rotation stage is adjusted (so it will maintain the same tilt) then the effect of the tilt can be removed by mount error modelling. This is the purpose of the adjustments on the motor and the rollers. If, as was the case initially, the base and the rotation stage have different tilt planes then it is impossible to align the transmit optical path. This is due to the mounting position of prism P1.

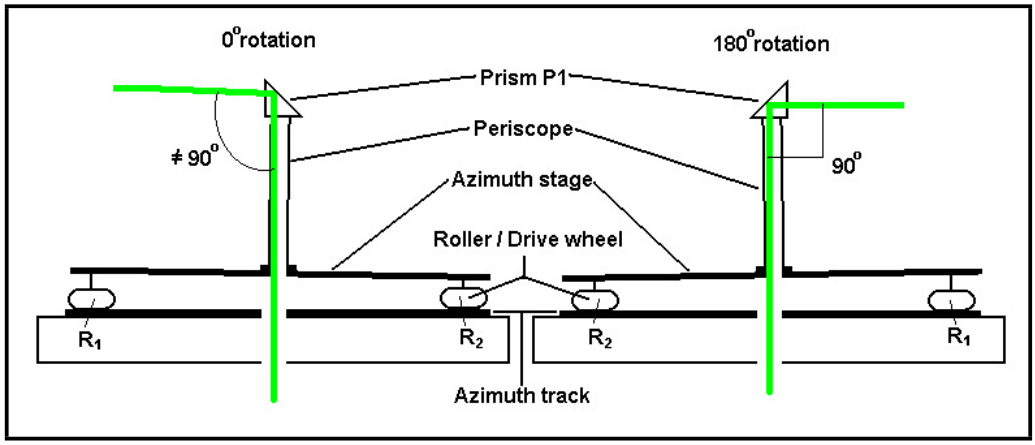

Figure 4.14: Illustration of the effect of differences in the tilt plane of the azimuth stage and the azimuth drive track. This represents the path of the laser at different azimuth orientations. It shows that the alignment between the laser beam and prism P1 is altered if the azimuth rotation stage and the drive track are not parallel.

Prism P1 is located at the top of a 15cm long tube which is rigidly fixed to the azimuth stage. The tube and prism P1 need to rotate about the input laser beam (reflected from prism M4) so that there is no change is the angle of incidence on prism P1. The effect of this is illustrated in figure 4.14. If there is any inconsistency between the azimuth stage and track then the output direction of the laser from prism P1 will not be constant over the full range of azimuth orientations.

In an effort to correctly align the azimuth mechanical rotation axis with the optical path a number of steps were taken. The first step was to completely remove the mount from the support tripod and ensure, to the level of capability of the instrument used (a builders spirit level), that the base for the PSLR mount was level. The PSLR mount was disassembled so that the azimuth rotation track was completely accessible. This was fixed to the tripod base and levelled with the adjustments located at the apexes of the triangular mount base. The track was checked over the entire circumference using a very sensitive engineers spirit level (placing a cigarette paper at one end of the spirit level on a level optical table caused the air bubble to move completely to the end of the spirit tube) until the track was level. The

azimuth rotation stage has two spirit levels permanently mounted near the edges of the stage and arranged at right angles with respect to each another. These levels are also very sensitive and are adjustable. The rotation stage with the levels attached was taken to a laboratory based optical table and placed upon a level surface, once again checked with the sensitive spirit level. The spirit levels on the rotation stages were subsequently adjusted so that they also read as level. The azimuth rotation stage was replaced on the azimuth rotation track in the expectation that the spirit levels located on the rotation stage would allow the stage to be levelled with the rotation track.

The PSLR was completely re-assembled and the azimuth motor and idler rollers were adjusted. The mount was rotated and the spirit levels were examined so that the tilt plane of the azimuth mount could be investigated for all orientations. It was expected that once the three major factors affecting the tilt plane (tripod/base, rotation track, azimuth stage and motor/rollers) were levelled, that the adjustments to the motor and rollers in any azimuth position to achieve level would ensure that the mount stayed level in any azimuth orientation. This was not the case. There was always some small movement in the spirit levels regardless of how often the motor and roller adjustments were changed.

It was thought that this was caused by the entire mount and tripod tilting slightly. This seemed the most logical explanation as this entire system was mounted to a floating frame. The frame was designed to rest upon the rooftop below the test facility. The facility is mounted on a raised platform. This isolated the PSLR from any vibration caused by walking around the test facility or the platform (there is a discussion on the vibration isolation frame in section 5.2.3, page 220). The laser and its mount were fixed on the same floating frame so the tilt caused by the loading of the frame would not affect the relative alignment.

The next step in the azimuth alignment procedure was to use a low powered CW laser to define the impact of the various adjustments to establish what effect these had, and to determine when the optical path was correctly aligned. The CW laser

was positioned behind the SL212 ranging laser so that it was able to be directed through the centre of the laser amplifier rod and follow the output path of the SL212 laser. The SL212 had previously been directed through the PSLR transmit optical path and directed onto a screen ≈4 m from the calibration output prism P4. The centre of the output beam was marked on the screen. The CW laser was then directed through the laser and output optical path and adjusted until it was centred on the same position marked previously using the SL212. The PSLR telescope mount was moved through 90^0 azimuth and the positioning process repeated. As the SL212 and the CW laser images on the screen were still concentric, the CW laser was now concentric with the ranging laser and could now be used to align the output optical path from ranging laser to final output.

As there are three 90^0 changes in direction of the transmit beam facilitated by the moveable optical elements in the PSLR, and the axis of rotation of both the mechanical axes needed to be aligned with the optical axes, a set of machined centres were designed and fabricated (see figure 4.15). These were able fitted between prism M4 and P1, between prism P1 and mirror M5 and at the output of the telescope before element OB1. The first and last centres were made from aluminium and were 5mm thick with a 1mm hole drilled through the centre. The middle element was 5cm long, also made from aluminium with the same size 1mm hole drilled through the centre. Using the CW laser that was previously aligned with the output of the SL212 laser, the laser mount, and optical element M4, P1, M5 were adjusted until a path for the CW laser was established through all the centres. The PSLR azimuth axis was rotated and the CW laser was observed to determine if it was still able to pass through all of the centres. It was found that there was still some movement of the alignment laser away from the middle and far centres when the PSLR was moved in azimuth. Several days of tedious adjustment of the optical elements and the mechanical axes improved the alignment to the point where any movement of the alignment laser from the holes in the centres was impossible to perceive by eye.

This process proved to be tedious for two main reasons. Firstly, many of the

Figure 4.15: The bottom and middle centres used for alignment of the output optical system.

adjustments of both the optical elements and the mechanical rotation axes produced movement in more than one plane. When the PSLR was rotated, it was possible to see how the alignment laser location moved away from the holes in the fitted centres. If an adjustment was made to direct the alignment laser back through one of the holes, it quite often moved it away from one of the other holes in a new direction. This would often mean that one adjustment required several others to compensate for the first. The second problem stemmed from the lack of any sort of measurement or calibrated scale on any of the PSLR adjustments. All of the adjustments are made by turning screws or bolts with screwdrivers or spanners. Clearly micrometer adjustments would have been preferable. However, they could not be retro-fitted due to the physical constraints imposed by the original design. If parts of the PSLR were disassembled (as undertaken on one occasion when the arm housing the output telescope had to be unbolted to remove a spider from the middle of the optical path that was otherwise reluctant to move, even when the ranging

laser was fired at full power), much of the alignment process had to be repeated as there was no way to reset the adjustments to precisely the same registration.

Once the azimuth axis and optical path were adjusted so that the alignment laser passed cleanly through the inserted centres for any orientation of azimuth, a final check of the elevation axis was performed using the same process. Once again, several days of careful adjustment were required until the alignment laser was able to pass cleanly through the middle and last centres.

The centres were removed and the ranging laser was fired through the optical path. Previously, when the output of the ranging laser was examined as it exited the final compound lens (OB1), (prior to the many days of careful alignment adjustment), it could be seen to wander around the aperture as the axes were rotated. Once there was no movement discernible to the naked eye, the alignment procedure was terminated.

This level of alignment was deemed adequate for fixed target laser ranging but, as was previously mentioned in this chapter, even a small alignment error can produce kilometers of pointing error at satellite distances. The best practical way to test the alignment would be to fire the laser over a long distances to fixed ground based targets for several mount orientations or to attempt actual laser ranging. These methods were not possible at the Curtin University campus as there is limited range available because of surrounding buildings and local topography and atmospheric firing of the laser contravenes Civil Aviation and Safety Authority rules.

A further approach for improving the alignment accuracy was investigated. It was essentially the same process, moving the axes and examining any movement of the laser beam away from the centre, but instead of a human eye, a CCD camera was used. The CCD image is produced by an array of elements that record an intensity. As the project CW laser output was TEM_{00} mode, the intensity of the laser beam was maximum in the centre of the beam and falls off with radius in a gaussian. If this change in intensity could be measured by a CCD image then it gives an easy way to identify image coordinates corresponding to the centre of a

laser beam. This could be achieved to within a couple of pixels and would provide a means of quantifying small alignment discrepancies.

To test this approach a Kodak DVC325 digital video camera was purchased. This camera was low cost and had a maximum resolution of 640 x 480 pixels. At the point of closest focus (approx. 1cm) the camera images an area of 1.5 x 2.0 cm. If it was possible to centralise the laser beam to one pixel accuracy then this would give a resolution of ± 0.03 of a mm in both directions. If the height from the prism P1 to the proposed camera position is taken as approximately 1.5m, this gives an angular resolution of $1.19 \times 10^{-3^{\circ}}$ (or $4.30^{"}$), which is approximately 4 times better than could be measured by the PSLR encoders.

In the short series of tests conducted, the low powered CW laser was directed through the transmit optical path from the output telescope down through optical elements M5 and P1. Components OB1, L1,2 and M4 were removed. The camera was placed under the PSLR viewing upward from the bottom of the PSLR mount. The laser was directed onto a screen (a neutral density (ND) filter) and the camera was focused on the image made by the laser on the top side of the screen. The ND filter reduces the intensity of the laser beam so that the light directed into the camera does not exceed the dynamic range of the CCD array. Ideally the intensity of the centroid of the laser beam should be close to the maximum input intensity of the CCD.

The result of finding the centroid of the image produced by this method can be seen in figures 4.16, 4.17, 4.18. These images are screen outputs from IDL, a graphics analysis program, using code written by Leon Majewski (PSLR project software developer). Figure 4.18 shows the intensity vs position of the laser spot produced on the ND screen and imaged by the Kodak camera. The actual spot is highly visible as a huge peak in the centre of a collection of smaller subsidiary peaks. These smaller peaks in Figure 4.18 are noise within the original image due largely to scattering within the PSLR optical path and by the ND screen surface that had been badly scratched. This reflected some of the laser speckle from the

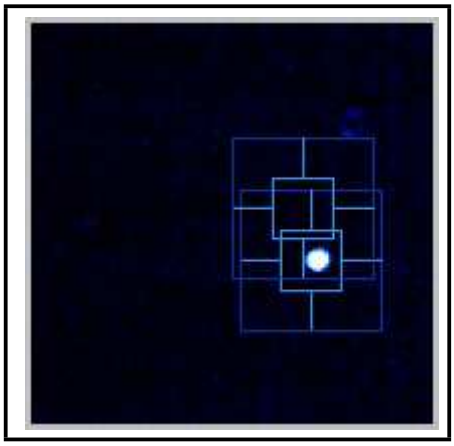

Figure 4.16: Raw image of the CW laser on the neutral density screen.

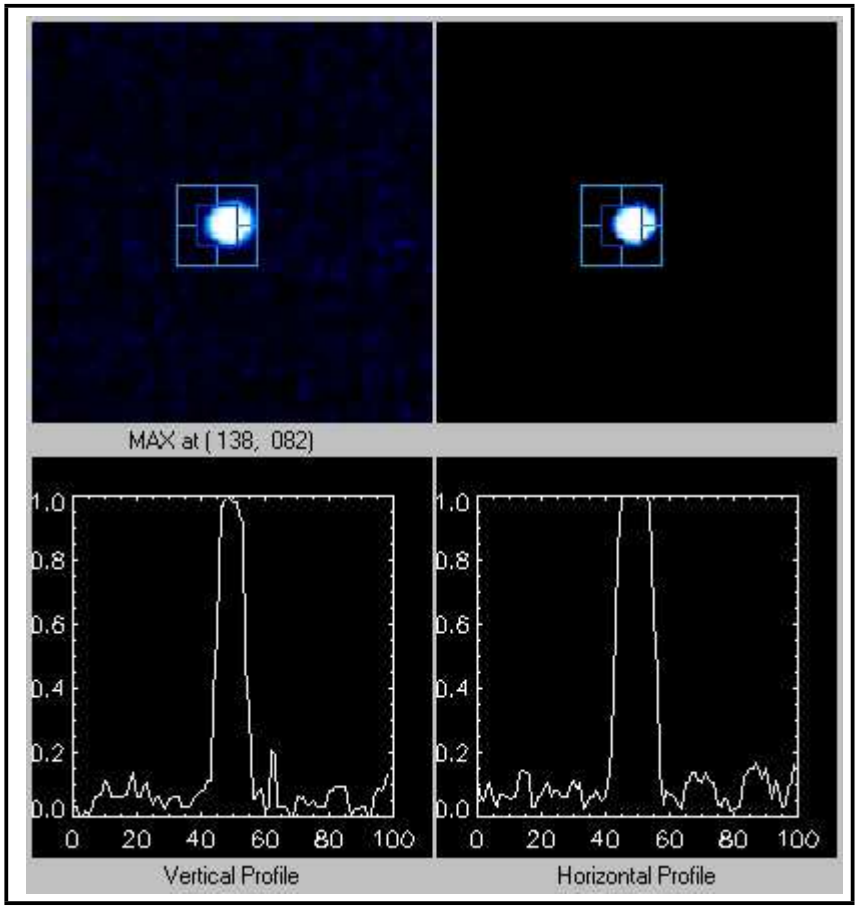

Figure 4.17: Maxima determination in the vertical and horizontal of the image in figure 4.16.

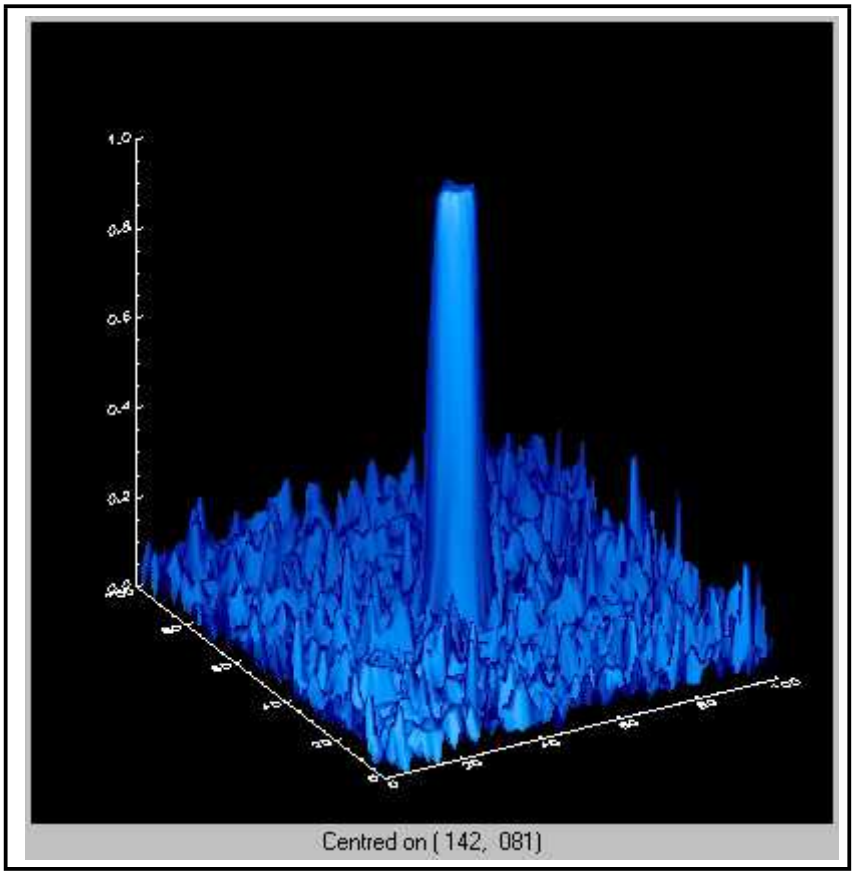

Figure 4.18: 3 dimensional representation of the position and intensity of the laser image in figure 4.16.

top of the ND screen onto the CCD. The other obvious problem with the image shown in Figure 4.18 is the size and shape of the large peak. This is due to the saturation of the pixel elements of the CCD affected by the laser beam. This would be corrected by a camera with a higher dynamic range and very selective filtering (screen selection) so that the maximum intensity of the laser image on the ND screen was sufficiently bright without exceeding the camera's dynamic range. Several other images were analysed with varying results. Not all of the images yielded the same shape as the image in Figure 4.18 with some showing less than a gaussian-like profile. The error was not with the method but rather with the hardware. It was possible to show that there was some movement of the centroid of the laser beam when the PSLR mount was moved. Unfortunately, this area of investigation was halted

due to other project commitments. In the event that the PSLR was configured to commence satellite laser ranging, this alignment method could be re-examined as it showed that, given the sensitivity of the approach, there is still some room for improvement.

The alignment of the PSLR transmit optical system was complicated, the adjustments difficult to use and the results often unexpected or undesired. This somewhat defeated the purpose of a portable instrument as it must be sufficiently robust and able to be disassembled, transported, reassembled and setup in the new location promptly. If the setup can not be accomplished efficiently and simply then moving locations becomes a major impediment.

It is recommended, for any future versions of the PSLR, to remove most of the adjustments by better design specifications and construction. There should be no more than one mechanical adjustment on each rotation axis and probably one adjustment for the ranging laser with the location of other optical elements correctly designed and accurately placed within the instrument. Once the transmit optical system is fixed at the point of manufacture, there should be no need to adjust it. The greatest problem is prism P1, which is the point where the outgoing laser beam is translated from vertical to horizontal, and is the location of the intersection of the axes. Azimuth rotation moves this prism and elevation rotation moves other optical elements about an axis centred on this prism. Any mechanical rotation errors are therefore transmitted to misalignment of the optical path as a result of prism P1. The first step in any redesign would be to remove the reliance of the transmit optical path on the mechanical axes. It is very difficult to guarantee that the mechanical axes are precise for all orientations but this can be corrected for in software. It is not possible to correct for alignment errors in the optical output path in software.

4.2.2 Receiver optical system

The receive optical system is basically a *coudé-Cassegrain* telescope with special filtering and detection apparatus added to the objective end of the telescope.

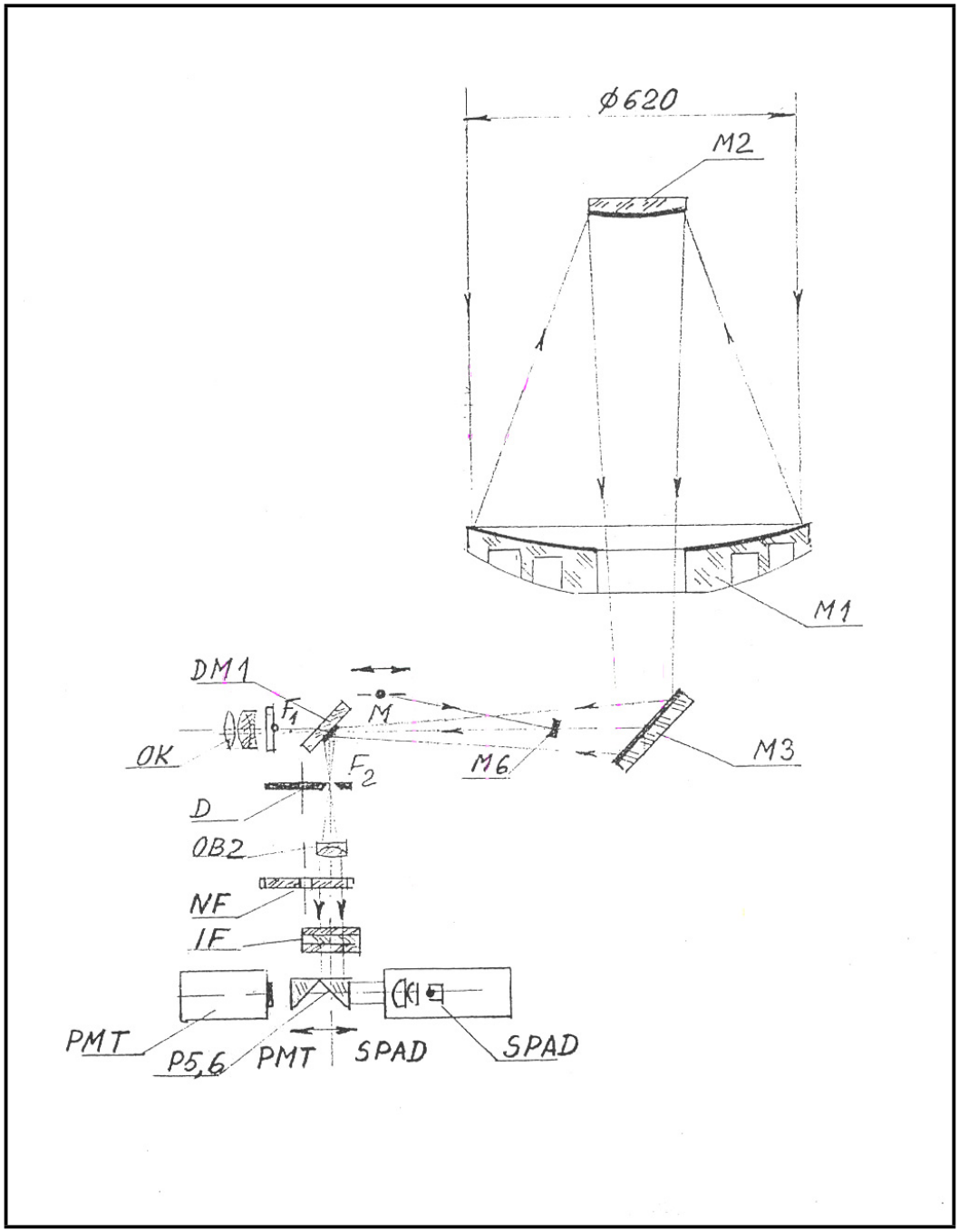

Figure 4.19: Illustration of the PSLR input optical system.

The primary mirror of the telescope has a diameter of 620 mm which is almost as large as the MOBLAS telescopes and larger than the aperture of the principal telescope at the Perth observatory, Western Australia. This relatively large size

has some advantages over other portable systems but these advantages come with drawbacks.

The large primary mirror and the powerful ranging laser (> 130 mJ per pulse) ensure that there will be a large return optical signal at the return detector from all but the furthermost satellites. This large return signal means that all sorts of detectors will work with the PSLR. It would also allow the system to be configured to work as a LIDAR (LIght Direction And Ranging) and as the name suggests is very similar to RADAR except that it uses light rather than radio wavelength radiation. The system could be configured to do this separately or in conjunction with laser ranging. The disadvantages are; greater care is required to avoid exposure to the sun/moon, and the problem of steering and stabilising such a large mass on a small mount. Mount inertia and wind loading will effect the PSLR a good deal more than smaller portable systems such as the French Transportable Laser Ranging System (FTLRS) which has only a single telescope of aperture 130 mm.

The main telescope (see figure 4.19) is an uncovered (uncorrected) *coudé-Cassegrain* consisting of the primary mirror M1, secondary mirror M2, 45^0 mirror M3, eye piece objective OK, dichroic mirror DM1, field stop D and objective lens element OB2. Figure 4.19 also shows a variable ND filter wheel (NF) and spectral filter (IF). While these elements do not form part of the telescope optical scheme, they are essential for laser ranging. These elements control the amount and wavelength of light transmitted to the return detector (see section 3.6, page 125).

The primary mirror M1 is mounted on the elevation swing mount and fixed at three positions, equidistant about the outer edge. The bottom of the mirror has three brass sockets permanently attached to the mirror. These sockets sit on three brass ball hinges that are free to pivot on the elevation swing mount. The ball hinges are held by a fine threaded nut which allows the height of each ball to be adjusted by screwing in or out along the thread. This is evident in figures 4.20 and 4.21. The orientation of the main mirror is obtained using the three ball and socket adjustments. The adjustment of the main mirror is relatively simple (compared with

the rest of the instrument) as a required adjustment direction is effected by at most two of the mirror adjustments.

The main mirror is held in place by the secondary mirror mount. This consists of a central column (which also acts as a light excluder) that is fixed to the elevation swing mount, three support arms mounted to the central column, and a spring loaded holder. The holder contains three simple leaf springs which press on the back of the secondary mirror (see figure 4.21). The front of the secondary mirror sits upon three pins which are connected to three levers. The levers run down the support arms through collets and rest upon the secondary mirror exactly above the main mirror ball and socket adjustments. If the main mirror is moved, the lever is moved and this is transferred to the secondary mirror which also moves. The secondary mirror is adjusted by a hex nut which moves the lever it is attached to either up or down. Collimation is achieved when primary and secondary mirror axes of symmetry are parallel and ideally coincident. The PSLR secondary mirror, which essentially floats between pin and spring can also be adjusted around the centre of the optical axis. This is achieved by three pins which screw through the top of the support arms and push on the side of the secondary mirror. As the secondary mirror is hyperbolic rather than spherical, it must be located exactly central with the optical axis. This makes the job of collimating the main telescope rather more difficult.

The lever system is designed to ensures that once the main and secondary mirror are collimated, any adjustment of the primary mirror will not result in a loss of collimation. This has two distinct advantages with the PSLR system,

1. adjusting the main mirror is the principal method of focus for the telescope, and

2. it is preferable to align the transmit optical system first then align the main telescope against it. If some change is made to the output optical system, then there is no need to re-align and collimate the main telescope.

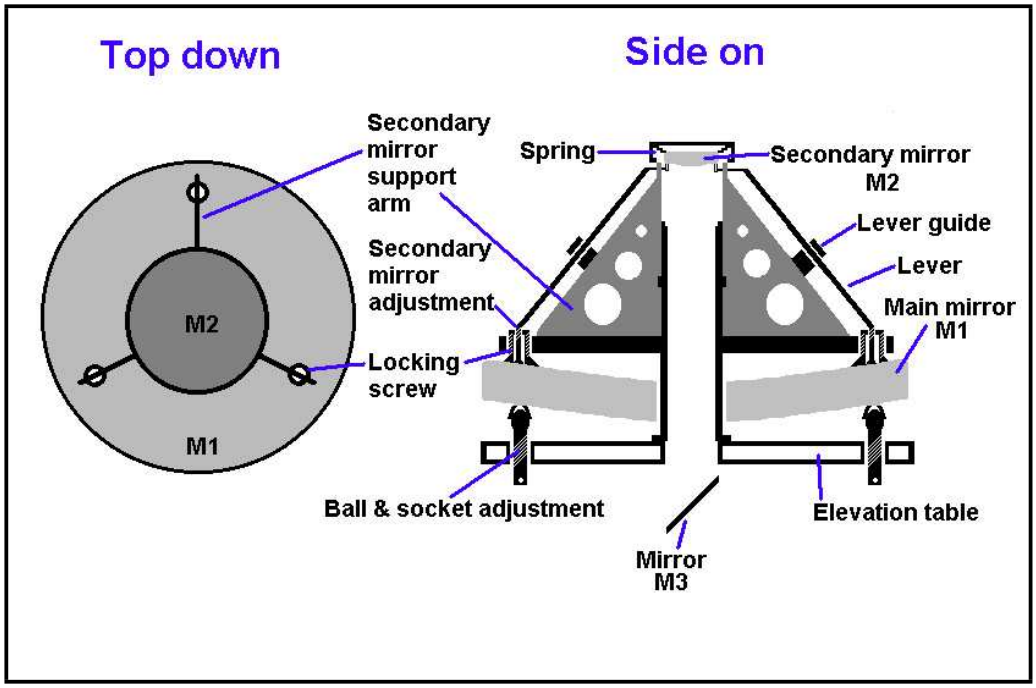

Figure 4.20: Stylised illustration of the main telescope construction and features.

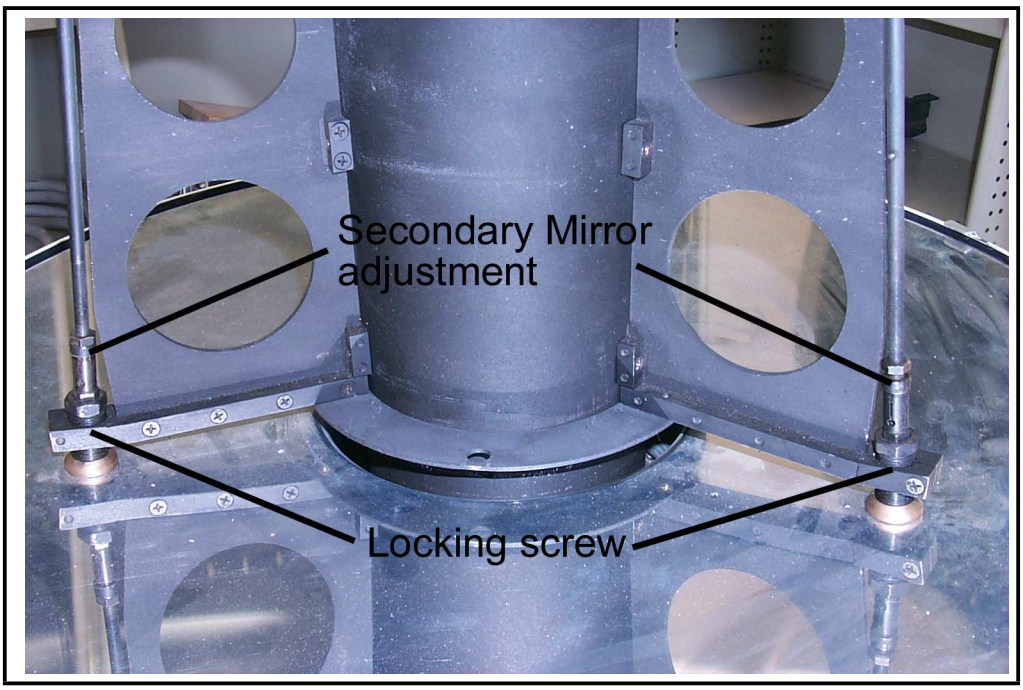

Figure 4.21: Picture of the lock screw and secondary mirror adjustment arrangement used with the PSLR.

Mirror M3, 45^0 with respect to the optical axis of the main mirror is used to direct light into the rest of the receive optical system. The aperture, filtering and detection apparatus constitute the rest of the system. These elements are all located in a removable L-shaped tube (see figure 4.22).

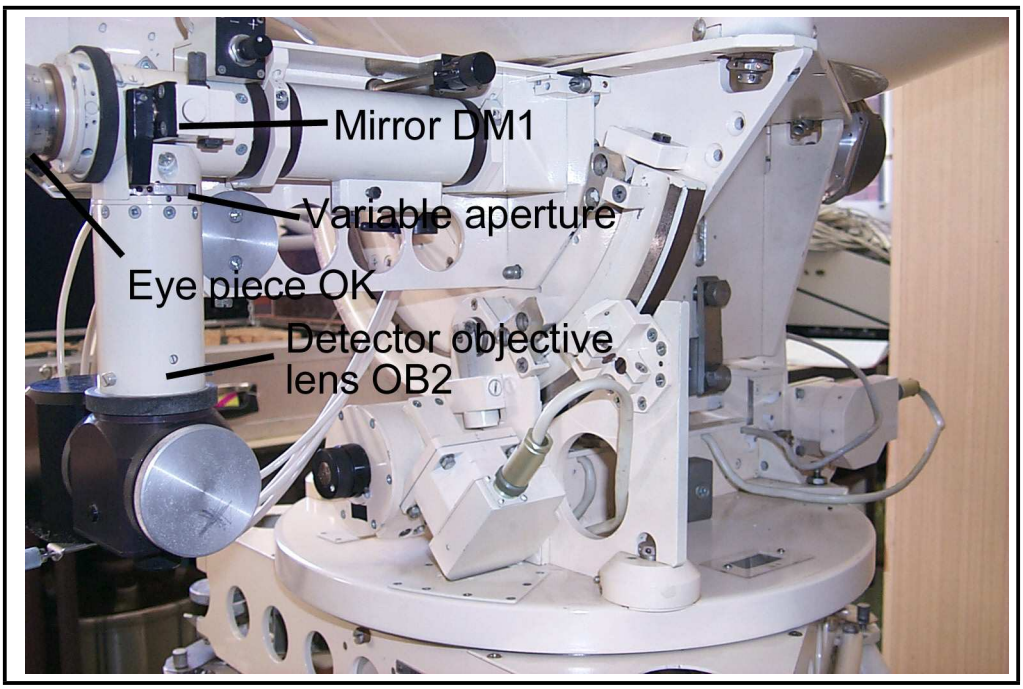

Figure 4.22: L-shaped tube holding the filtering and detection optics.

The detector/s, ND filter NF, the colour filter IF and the translation prisms P5,P6 can be configured in several different ways as they are mounted in the optical path using screw and collar connections. Figure 4.22 shows the translation prism housing under the objective lens OB2. The filter apparatus would normally sit between the objective and the translation prisms with the detector mounted on either side of the translation housing. The translation housing can be removed with the filter and detector mounted directly to the L-shaped arm.

4.2.2.1 Alignment of the receive optical system

The alignment of the input optical system required 2 steps;

1. collimate the main telescope (mirrors M1 and M2), and

2. adjusting mirror M3.

The rest of the optics located in the L-shaped arm did not require any adjustment as these elements are all fixed into position.

The adjustment of mirror M3 was a trivial task as it essentially centres the telescope image in the eyepiece field of view. This mirror is held in its housing by the corners with spring loaded pins. Three of these holding positions have screw adjustments located at the rear face of the mirror. These screws are adjusted until the telescope image is centred in the eye piece field of view. Once this is set, it need not be changed unless the main telescope components are altered.

The collimation of the main telescope is more complicated. In order for the telescope to be perfectly collimated, the secondary mirror must be configured with its optical axis parallel and coincident with that of the main telescope.

Centering the secondary mirror with the optical axis of the telescope is not easy. Most basic books on telescope collimation assume that the secondary mirror is always centred and simply requires the optical planes of primary and secondary mirrors be made coplanar. As a result it is difficult to speculate on how an uncentred mirror will affect the final image quality.

The method used to centre the secondary mirror may not have been the intended method of the Latvian developers but it seemed to work adequately.

The secondary mirror and the cover that holds the springs that back onto the mirror M2 both contain holes of roughly the same diameter. The cover has a mostly opaque filter over the hole which will permit the entry of some light. Mirror M6 is a small circular mirror which is designed to be in the centre of the optical axis. This can be adjusted. To ensure that it is centred, a light source (labelled M in figure 4.19) is trained onto the mirror. When viewed in the telescope eye piece it appears as two red lines as the light emanates from a double slit and mirror M6 is tinted. These red lines appear oriented at 90° to two similar lines permanently visible in the

eyepiece as they are engraved on filter F1, which unlike the lenses in the eyepiece, does not rotate when focusing. The mirror will be centred in the optical axis when the red lines and the engraved lines give the appearance of a cross hair (see figure 4.23).

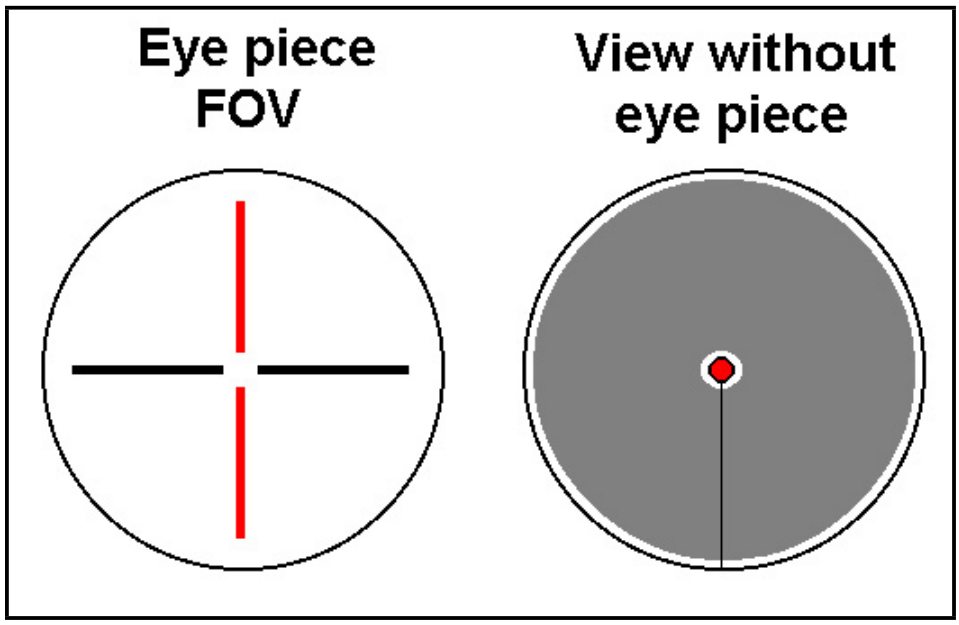

Figure 4.23: The image on the left shows the image in the eye piece when mirror M6 is centred with the optical axis. The image on the right illustrates what would be seen up the optical path, without the eye piece when the secondary mirror is centred in the optical axis.

The eyepiece was then removed so that by moving to the correct position, a view of mirror M2, similar to the illustration in figure 4.23, can be seen. The correct position to view up the optical axis (toward the incoming optical signal) is obtained when a reflection can be seen from mirror M6 (appears as a dull red light) and the outer edge of mirror M2 can just be seen contained within the field of view. The idea is to ensure that the eye always sees the red light (as this will be the centre of the field of view with the eyepiece attached). The position of the secondary mirror is adjusted until the hole in it is concentric with mirror M6. The outside edge of the mirror will also appear concentric with the part of the L-shaped housing that

contains mirror M6. Once the view up the optical path is the same as the illustration on the right hand side in figure 4.23, mirror M2 is very closely aligned to the centre of the optical axis of the main telescope.

It was not possible to ensure the positioning of the secondary mirror M2 was perfect without further tests and apparatus. Some discussion of proposed tests is contained later in this section.

The collimation of the main mirror involved a two step process. Following advice from (Verveer, 2001) from the Perth Observatory, Bickley, Western Australia, a "virtual" star was assembled. This 'virtual' star consisted of a small but bright incandescent light bulb (although a bright LED would have been better), a simple condenser lens with a focal length of 20 cm, and a telescope eyepiece with a focal length of 6 mm.

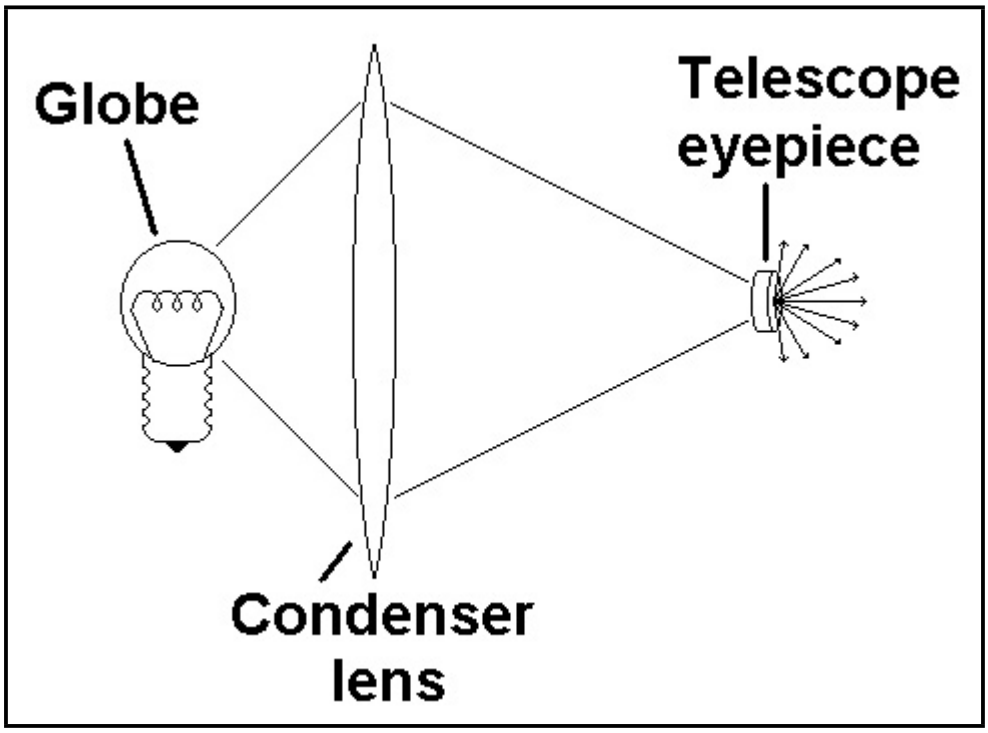

Figure 4.24: Representation of the virtual star constructed to aid in the collimation of the PSLR main telescope.

The placement of these elements can be seen in figure 4.24. The small globe and condenser lens are arranged so the image of the globe element is focused as close to a point as possible. The eyepiece is then placed back to front at the point of focus so that light passes backwards through the eyepiece. The effect of this is very similar to viewing a light through a pin hole except that it is a good deal brighter. The advantage of the virtual star is it can be viewed at a distance and some way off centre of the eyepiece optical axis while maintaining the point source appearance. In this respect it resembles the light from a star.

The virtual star was placed about 50 m from the PSLR telescope and the telescope pointed at this "star". The point of closest focus for the PSLR telescope is several hundred meters using the current setup and eyepiece. The virtual star being so close produced a series of concentric rings around a central occlusion when viewed through the telescope. The rings were skewed or elongated about the central occlusion which was not centred in the field of view. The primary mirror was adjusted slightly and the secondary mirror adjusted substantially until the rings were concentric with the centre occlusion, round, and in the centre of the field of view, as shown by the image on the right hand side of figure 4.25.

The telescope was subsequently pointed at a bright star. The star was left out of focus and the telescope adjusted again until the rings around the central occlusion were concentric. The star was then bought into focus until a sharp image of the star could be seen. The secondary needed some slight adjustment at this stage to sharpen up the image.

The final image was still a little blurry around the edges due to the degradation of the coating of the mirrored surfaces, especially that of the main mirror M1. As the main telescope, which includes the main and secondary mirrors, is unprotected from the elements during normal operation, it is very susceptible to dust build up, moisture penetration and direct UV radiation. The main mirror especially gathers a lot of dust as it generally faces vertically. The front coating applied to the mirror was very delicate and almost impossible to clean without scratching the surface. The

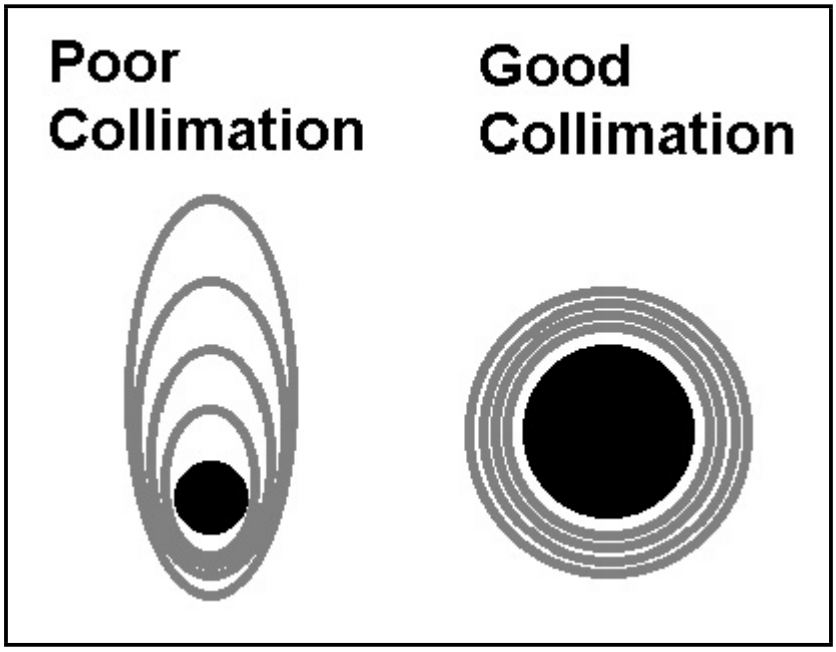

Figure 4.25: Representation of the view through the telescope eyepiece during the virtual star collimation process.

coatings used on the mirrored elements of the PSLR is unknown. If the PSLR was ever to become operational it would be imperative that the coating on the primary and secondary mirrors is far more robust than the current coating as these mirrors are exposed to the elements and require frequent cleaning.

With the purchase of a fair quality CCD camera so that visual tracking could be simplified and star images could be taken, the Perth Observatory offered the use of a software package from the Santa Barbara Instrument Group (SBIG). This software used Hartmann masks and a ray tracing regime to indicate collimation problems with telescopes. The Hartmann masks are basically a screen (with holes cut out in specific locations) that is placed over the front aperture of the telescope.

The mask shown in figure 4.26 (Holmes, 1999) is generally used to aid telescope collimation. Two images of a bright star are taken, one with focus achieved before the image plane (inside focus), the other beyond the image plane (outside focus). These images will resemble the right hand side of figure 4.26. The program requires the focal length of the telescope as this is used in the ray tracing calculations. Each

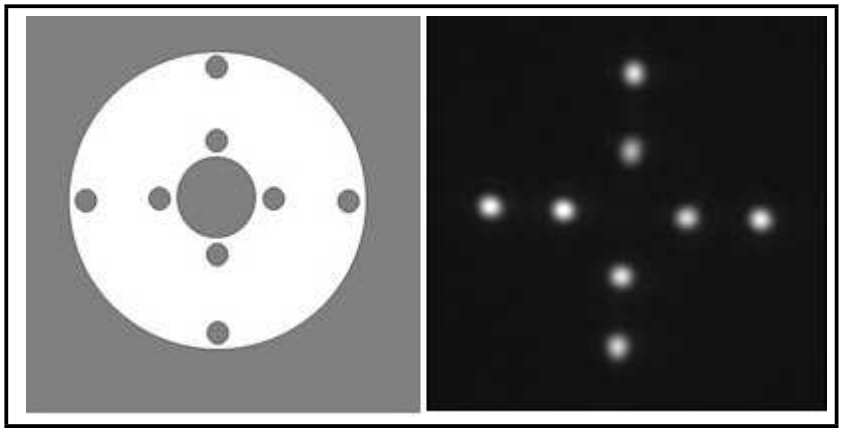

Figure 4.26: Hartmann mask on the left showing the location of the holes in the mask. The right hand side shows the out of focus image of the Hartmann mask.

of the images for the star (near and far) will have local foci. The centroid positions of the foci on the images are calculated. Each focus on one image corresponds to one of the foci on the other image. The images are inverted with respect to one another. The program will trace rays between corresponding foci, through the true image plane (see figure 4.27 (Holmes, 1999)). The position of this plane is determined by the focal length of the telescope provided to the program.

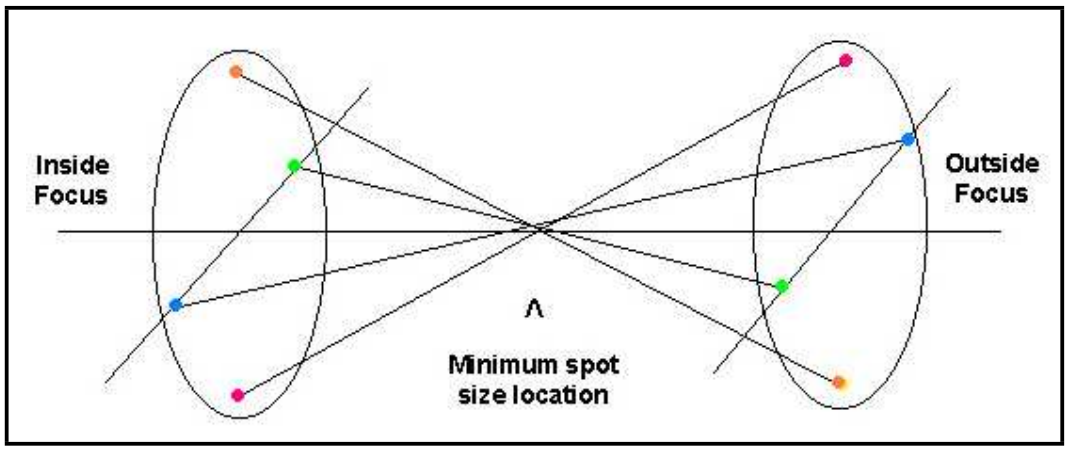

Figure 4.27: Illustration of the ray tracing method used to examine the focus or collimation with the true image plane.

If the telescope is collimated correctly the rays all trace through the centre of the image plane. If the spots produced on the image plane (by the rays tracked

through it) do not all occupy the same point then some estimate of the particular disfunction of the telescope collimation can be given. According to (Holmes, 1999) the three major disfunctions of the collimation can be identified thus;

1. If the outer ring of spots focus in a different optical plane then the telescope has spherical aberration.

2. If the outer spots form a centre displaced from a centre formed by the inner dots then the telescope has coma.

3. If the vertical rows of spots form a centre displaced from the centre formed by the horizontal rows of spots then the telescope has astigmatism.

Unfortunately the software does not give any real indication of how to fix problems that are identified, only an indication that they exist. If images are taken and specific adjustments are made then the effect can be seen in the analysis. This suggests whether a particular adjustment made the situation better or worse. By monitoring the effect of many adjustments it should be possible to eventually arrive at perfect collimation. It should also give some indication of how any future degradation of collimation can be removed quickly.

Due to time constraints, the project was not able to fully utilise the Hartmann mask software. This is principally due to an incompatibility of the Hartmann mask software with normal image formats. The Hartmann mask software only works with SBIG CCD camera images. The CCD camera purchased for the project was used with a USB graphics adaptor to form jpeg images. Some attempt was made to reverse engineer these jpeg images into the SBIG format but it proved to be too time-consuming. The Perth Observatory offered to lend the PSLR project a spare SBIG camera but the large physical size of this camera prohibited easy mating with the telescope.

To allow the PSLR to operate effectively as a portable system it must be able to be quickly assembled and setup in a new location. In its current state, such a simple software-based alignment tool would be essential for fast collimation.

4.3 Conclusion

The PSLR optical systems, on the whole, are simple. There are small numbers of optical elements in both the input and output optical paths. Given that the PSLR has many components of the optical systems moving in relation to each other, this simplicity is essential.

These optical components are moved in conjunction with the mechanical axes of rotation. In order for the optical elements to remain in constant alignment, the mechanical rotation must be very precise. As the PSLR is primarily a test model or prototype, it provides several adjustments to both the mechanical rotation axes and the optical elements contained within. None of these adjustments has any fixed reference point or indication of their position. Many of the adjustments cause relative movement in more than one plane and on more than one axis. When all of these factors are combined it makes the process of aligning the output optical system cumbersome, non-intuitive, tedious and almost impossible to accomplish quickly if the instrument is relocated and reassembled. This severely detracts from the primary goal of the system; namely, to be highly portable. In its current form, once the system was setup and aligned, subsequent users would be loath to move the instrument.

The receive optical system was certainly more user friendly. However it also has far too many adjustments and consumed a considerable amount of time to collimate and align. The ancillary optics (involved in the final directing of the optical signal onto the detector) do not require any alignment as they are fabricated into the input optical axis and there is no relative movement of any of the optical elements in this axis. Ideally the main telescope should not be disassembled once it is collimated but due to the large size of the telescope, shipping it intact was impractical.

The majority of the problems experienced by the PSLR project personnel had to do with establishing and maintaining accurate alignment of the optical elements and the appropriate mechanical axes. The major recommendation to stem from

the project would be a complete redesign and re-engineering of the opto-mechanical system. This would involve modularising the entire system. Presently, the PSLR system is shipped as hundreds of individual components. It would be far simpler to ship the system as a small number of modules that fit together with positive location fittings. All of the optical elements in the modules for such a system could be aligned on the bench and fixed in position. Any alignment that needed to be done could be accomplished by properly realised adjustments on the modules. This would greatly simplify the setup process and drastically reduce the setup time. This seems to have been the intention of the designers for the instrument in its next incarnation.

Chapter 5

Fixed target laser ranging

5.1 Introduction

The purpose of the PSLR project at Curtin University was to:

1. assess the status of the instrument with respect to completeness of hardware and software provided,
2. acquire appropriate components and software to replace any missing items,
3. assess the functionality of systems and their appropriateness for SLR tasks,
4. identify system weaknesses and strengths,
5. evaluate the instrument's accuracy as a SLR and the origin of any inaccuracies,
6. determine the robustness of the system for development as a portable instrument,
7. if possible, return the instrument to full operational capacity, and
8. as required, keep the project sponsors informed in writing of the progress with items 1 to 7.

This involved ranging to fixed targets on campus leading to collocated ranging to satellite targets along side the MOBLAS-5 system at Yarragadee, Western Australia. The above steps required that many system parameters were tested once the appropriate equipment had been replaced or repaired. One of the most important parameters of any satellite laser ranging system is the absolute accuracy of the ranging system. This includes; the laser, detectors, conditioning electronics and timing devices. All of these devices working together allow the range to a distant object to be determined. In order to first of all check the operation of the equipment and then to determine the accuracy of the system, a testing program was required that did not involve a satellite target as the permission to track satellites was not available.

This chapter discusses the approach, experimental setup, results and draws conclusions based on the results of the testing of the PSLR laser ranging equipment conducted at the Curtin University facility.

5.2 Experimental Methodology

To test the accuracy of the ranging performance of the PSLR, a target at a known range is required. The laser ranging system could then be used to determine the range and be compared with the known value.

The measured time of flight T_f of the laser beam from the PSLR instrument to the target and back would yield the required range R,

$$R = \frac{T_f c}{2}, \tag{5.1}$$

where c is the speed of light.

Equation 5.1 does not however, allow for internal transmission delays inherent to the ranging system. There is a delay between the firing of the laser, detection of the outgoing beam by the start photodiode, generation of an electrical signal, electronic

signal transmission, signal discrimination, receipt at the interval counter, and the eventual registration of a start event. There is a similar chain of events involved in the registration of a stop event, as well as atmospheric transmission delay. If there is a known system delay then this can be removed from the time of flight recorded by the timer to get an accurate range reading R, where

$$R = \frac{(T_f - delay)c}{2}. \tag{5.2}$$

The system delay could be measured directly by determining how each component in the ranging system contributed to the delay and adding these contributions to obtain the correct figure. This would not only be time consuming and very hard to achieve but be generally inaccurate as these delays are affected by environmental conditions, component aging and many other factors that cannot be corrected for without continual measurements. Rather than repeatedly measuring all of these factors separately and directly, there is a far simpler method of calculating system delay and removing it from ranging calculations.

If the range to a second target is determined with exactly the same system setup and with as little time delay as possible between making ranging measurements to each target, then it can be safely assumed that the system delay of the two samples will be almost identical. There will be some extra delay due to propagation delay in the atmosphere for the farther target, although this will be negligible over the range of the testing and can be corrected for. If the range of the second target T_{f2} is known exactly, then the system delay in the measurement to the first target can be removed by taking the time of flight measurement of target 1 T_{f1} from target 2, and adding the known range back to the figure calculated as,

$$R_1 = \frac{(T_{f1} - T_{f2})C}{2} + R_2. \tag{5.3}$$

Using this method, when the time of flight from target 2 is subtracted from that of target 1, the system delay is also removed as noted. The system delay is indirectly

measured by this method for the current conditions. This method also allows for changes to the system setup (which may affect system delay) to be accounted for immediately.

5.2.1 Experimental setup

A roof top facility was constructed atop building 207 at the Bentley campus of Curtin University and was used to house the PSLR and associated equipment. From this vantage point it is possible to direct the laser beam from the PSLR to a limited number of possible target points. This was essential to comply with University and State safety regulations on irradiating apparatus.

The PSLR laser is a class IV laser, the most dangerous class of laser. In normal operating conditions the class IV rating would require that the laser was operated in a room that was optically sealed from the outside world. This room would need to display the appropriate signage indicating the presence of a class IV laser and the danger of ocular damage from direct or reflected beams. Indicator lights and laser power-off interlocks on the doors are also generally required. There are ways to reduce the power output of the PSLR laser such as running the unit with the amplifier off and expanding the primary beam. The PSLR primary oscillator and pulse compression system produce a beam of 3.5 mJ at a duration of 130 ps. If the energy conversion ration of 60% for the SHG remains the same for the oscillator only energy level then the output at the laser aperture is 2.1 mJ. After the beam passes through the output telescope the beam cross section is 130 mm. The energy density is then 2.1 mJ divided by 130 ps(pulse duration) divided by $\pi \times (\frac{130\times10^{-3}}{2})^2$. The value of the energy density is $3.04 \times 10^8 W.m^{-2}$. According to AS/NZS 2211.1:1997 laser safety standard tables 3 and 4 (Standards Australia, 1997) this reduces the classification of the laser to 3B. This is the second most dangerous type of laser and still requires significant safety protocols. Using the oscillator only may have been safer for the experimental team as this would have provided plenty of signal for fixed target ranging, but the start detector would not operate at such a low energy level.

The laser as a result was operated at the lowest level that would allow the correct operation of the start detector. This was the only method employed to reduce the output energy.

These elevated target locations were deemed to present no reasonable possibility of anyone (apart from the research team) from encountering a direct or reflected laser beam. The site, chosen principally for public safety, has a number of other features which were appropriate for testing purposes as;

- from this site it was possible to fire the laser horizontally to an elevated position at the wall of another building that had no facing windows,
- there are only two points of entry onto the roof so access could be restricted,
- the rooftop of building 207 has a large platform frame mounted on pylons away from the concrete roof so the facility could be easily fixed to this frame. Building regulation prohibited the facility being directly fixed to any of the concrete roofs at the University,
- the location is close to the Department of Applied Physics facilities, and
- the frame is mounted above the roof of the building, vibration is reduced (see below).

The facility was set up to allow all of the equipment to fit comfortably and allow the PSLR space to rotate and point at the targets. Figure 5.1 shows the positioning of the equipment in the rooftop facility.

The PSLR telescope and laser are mounted on a specially constructed frame which is labelled in figure 5.1. The frame is designed to reduce floor vibration transmission to the PSLR. If the PSLR was mounted directly to the floor of the facility it would experience considerable vibration and movement due to personnel movements. The platform, as mentioned previously, is mounted on pylons which are, in turn mounted to the concrete roof of the building. The platform is constructed of

Figure 5.1: PSLR equipment layout in the roof top test facility. The blue vibration damping frame is visible just above the floor of the facility.

RSJ or I-beams with the facility located at one corner (see figure 5.2). The platform has a set of steps allowing access to a walk way which runs up one side.

In an effort to monitor the amount of vibration on the platform, a 3-axis accelerometer was fixed to one of the beams in the approximate location of the PSLR before placement of the facility on the platform. A set of tests were conducted, such as walking along the frame, jumping up and down and kicking the platform to simulate extremes of working activity. The results of this showed that there was significant vibration that would be transferred to the PSLR if it was mounted directly to the platform (see figure 5.3). The mounting frame for the PSLR compensates for this unavoidable movement by isolating the PSLR from the facility. The frame is supported by a set of struts which extend through the floor of the facility. This effectively isolates the PSLR from the facility as the frame does not touch any part of the facility. The stilts are welded to a set of heavy steel beams which rest on the roof of building 207.

Figure 5.2: Curtin University of Technology PSLR test facility.

This situation is not ideal as the frame cannot be made absolutely rigid. Any significant amount of perturbation will cause noticeable harmonic motion although this is quickly damped. As the PSLR is shielded from the wind and all other sources of perturbation, this did not prove to be problematic.

In a field situation the instrument would ideally be solidly fixed to a concrete pad where the concrete pad was set as deep as possible into the earth and sitting on bedrock. Failing the presence of a convenient concrete pad complete with surveyed datum point, a reasonably large flat tank that could be dug into the ground and filled with water would suffice. This tank would still require a surveyed datum so that the PSLR could be fixed in the terrestrial reference frame.

5.2.2 Target Positioning

The targets were positioned to allow the PSLR to fire at them without causing any harm to the general public. The closest target was mounted on the wall of the facility

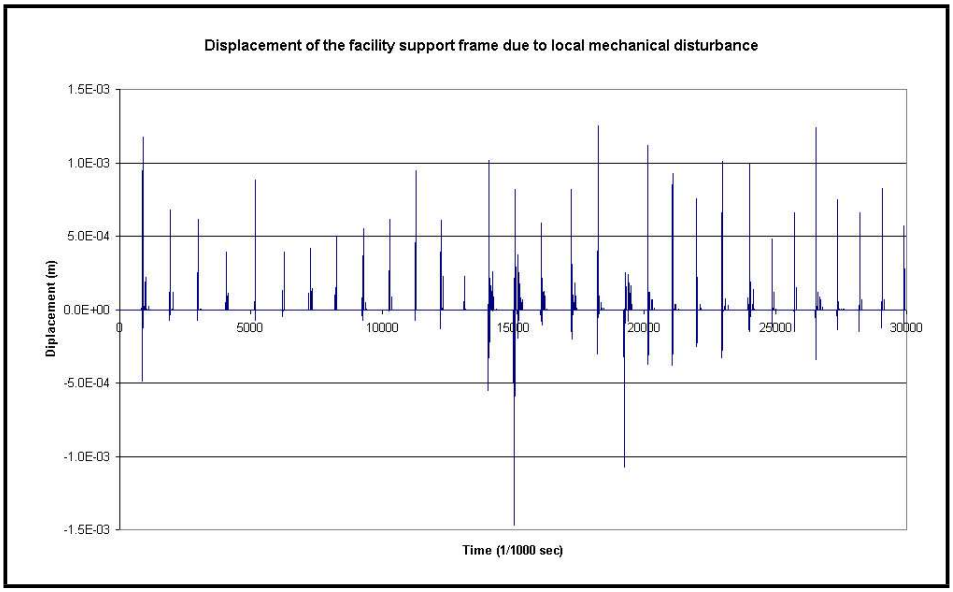

Figure 5.3: Determination of the vertical vibrational component of the frame used with the PSLR test facility. The displacement shown is due to a member of the research team jumping lightly on the frame at approximate 1 second intervals.

building (the Electrical Engineering building), with the far target mounted on the wall of the adjacent Geology building. To hit the Electrical Engineering target the laser was required to fire over a small section of the roof of the building. Hitting the Geology target required the beam to travel over a different type of roof and adjacent car park. As a result there was some concern about particulate matter and exhaust gases from traffic interfering with the beam, as well as thermal turbulence from hot bitumen. The car park is not particularly busy and the facility is 4 stories above the ground so these effects probably had little impact on the testing.

The targets used were retroreflectors so the positioning of the targets was not critical. They were placed on each wall so there was little chance of accidently firing the beam without it hitting the targets or being terminated by hitting the brick walls, even in the event of the output telescope suddenly moving. Figure 5.4 shows the general layout of the facility and the target position in relation to the position of the PSLR.

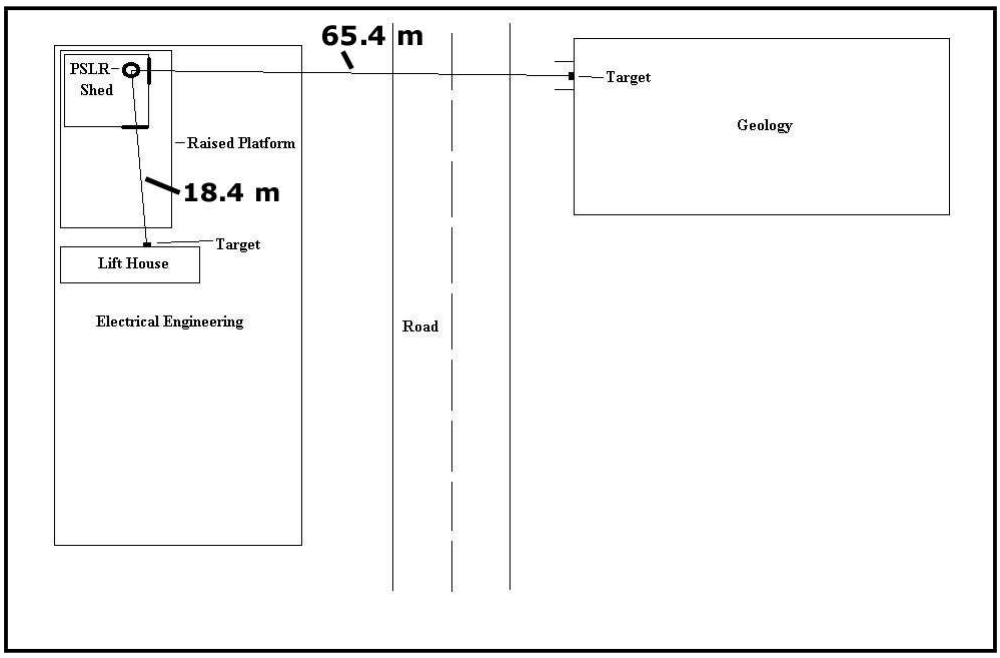

Figure 5.4: Illustration of the testing range atop Building 207 at Curtin University, showing the relative positions and distances to the targets.

5.2.3 Equipment setup

The first phase of testing at the Curtin University campus in Bentley was to establish the ranging accuracy of the PSLR, and to examine the mechanical, electronic, and optical sub-systems. As not all of the equipment to construct an operating system was received from Latvia, some modifications were necessary before any testing could be conducted. Theses modifications specifically involved replacement of the missing system time card and stepper motor drive card (or indexer card) and their integration with the system. It was possible to conduct testing without a time card, but it proved difficult without a stepper motor indexer.

As the PSLR control program does not operate properly with control cards missing, it was necessary to write software and change the way the hardware was configured so that a firing sequence could be established and ranging data collected.

This task required controlling the mount movement, the laser and the time interval equipment. The intention was to keep the process as close to the original

operational method as possible to simulate normal operation.

5.2.4 Original configuration

The original configuration required the control program to interface with three ISA bus mounted control cards and three hardware devices addressed through RS-232 ports. The control configuration is graphically represented in figure 5.5 (Zarins, 1996). The first card used an input frequency and a calibration pulse from a GPS clock to provide station time. The second card was used to provide index pulses to the PSLR motor drives to position the telescope. The final card (and the only card delivered with the PSLR) was used to read the angular encoders, provide fire control for the laser, and gate the SR620 timer.

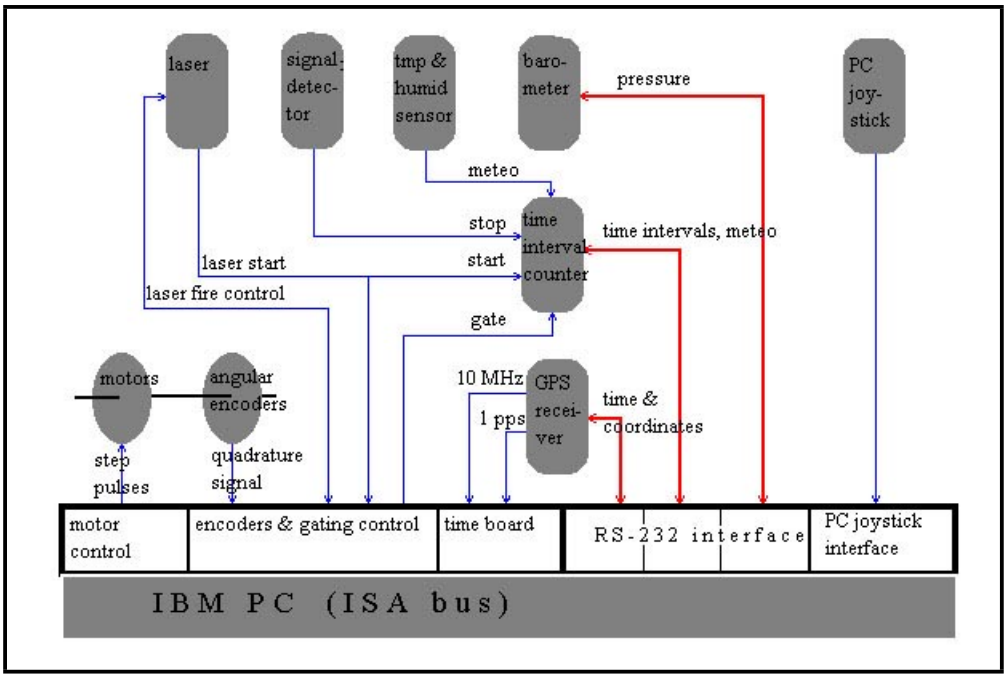

Figure 5.5: Original PSLR control configuration in operational status. This diagram shows the external components that input and are controlled by ISA bus expander cards (blue lines). Devices that are accessed by RS-232 ports are indicated by red lines.

The RS-232 ports interface with the SR620 timer (which also provides temperature and humidity through two devices connected to the two voltmeter channels),

the GPS time machine and the Druck barometer. The RS-232 interface allows control and data retrieval from all of the devices. There is also a joystick interface that can be used for manual control of the telescope drive system.

When the PSLR ranges, a series of steps occur for each range sample or laser shot. This is termed the original firing sequence in this document as it describes, as closely as can be determined from the PSLR control program operation manual, how ranging with the PSLR occured.

5.2.5 Original firing sequence

Once all of the preliminary functions were completed such as target selection and the telescope positioning, a fire pulse was produced by the encoder and gating control card (EGC card) which was directed to the laser. The EGC card also initiated the hold-off or gate pulse to the SR620. The leading edge of this pulse armed the start channel of the SR620. The hold off pulse remained high at this time. The laser then fires with a small portion of the output beam directed into the PRE-T start detector. This activates the PRE-T which produces an electronic pulse that feeds into one of the Ortec 9307 Pico-timing discriminators. The discriminator produces a conditioned fast NIM output pulse and triggers the start channel to initiate the SR620 timing. The return beam from the target CCRs is collected by the primary telescope where it is directed by the internal optics to the PMT detector. The stop PMT produces a pulse that is amplified by the home built preamplifier circuit built into the tube housing. This produces a pulse which feeds to the other pico-timing discriminator which in turn produces a fast NIM pulse that activates the SR620 stop channel. The stop channel will have been armed by this time as the hold off pulse will have gone low just before the arrival of the return pulse. The stop channel is triggered and the SR620 will register a time interval.

The SR620 was configured by computer interface before each ranging sequence but was commanded before each shot. The command sent to the SR620 before each shot made the unit ready and cleared the input buffer. The SR620 was configured

to wait for input from the start, stop and hold off channels and when it received all inputs and completed one range reading, it sends the reading back to the computer. This sequence of command, record and reply happens for every range sample to allow the hold-off pulse to control the gating functions of the timer so as to prevent false triggering and spurious readings.

All of the interval data (time interval, time of sample instigation, atmospheric data, etc) are written to a computer file. These data are recalled later to perform the normal point calculation and range determination.

5.2.6 Altered configuration

The altered configuration was designed to allow for ranging to at least two fixed targets. In all of the ranging test described in this chapter there were only two targets used. These targets were located approximately 90 degrees from each other (see figure 5.4) in the horizontal plane and a couple of degrees from each other in the vertical plane.

In order to test the accuracy of the ranging measurements, at least one known distance was required. The distances to the targets were determined by the PSLR personnel to ± 2 mm using a total station, a surveyors tool which contains a theodolite as well as optical range determination components. The distances between the targets and the azimuth axis of the PSLR were 18.403 m and 65.432 m respectively (although the 65.432 m target was later moved and a new distance of 65.488 m was measured, the early tests used the original target position). The targets were large solid retroreflectors which were solidly mounted to the walls of both buildings.

The PSLR was not functional when it arrived at Curtin University due to two missing control cards. One of these cards supplied station time and the other moved the telescope. Without the time card it was impossible to get the control program to work properly because it was constantly trying to update station time. The control program could not be used to program the hardware peripherals or receive information from them. This meant that new software needed to be written. There

was no real need for station time (UTC) as there was no need to track a moving target during these initial tests so the time card function could be ignored when writing new software. It was still necessary to move the telescope and position it reasonably precisely. This required the use of an indexer card to control the stepper motor drives. The original sequence used a hold-off pulse to control the channel gating. This was accomplished using the ECG card. This card was accessed through the non-functional control program so some other method of providing a hold-off pulse was required.

The project purchased two new pieces of equipment, a pulse generator capable of being triggered by an external pulse, and an indexer card that was capable of driving the Compumotor stepper motor drives. Two new programs were also written. A BASIC program was developed to control the SR620 timer and the Druck barometer and to store the data in files for use in later calculations. The other program utilised the Galil indexer card to drive the telescope to point at the targets, and to control the firing of the laser so that it only fired when stationary. These programs ran on different computers and are essentially independent. This altered configuration is represented in figure 5.6.

5.2.6.1 The BASIC program

The BASIC program controlled the SR620 time interval counter, the meteorologic probes and collected data from these components. It allowed the user a few options at the inception of the program run then configured the SR620 and collected data. While the program was simple, the ease of use of the SR620 allows powerful functionality with a small lexicon of commands. This program configured the SR620 to record a time interval using a hold-off pulse to control channel arming and gating. To initiate a timing sequence, a set of commands in ASCII was sent through an RS-232 port from a computer to the SR620. There were two lines of instructions sent to the timer. The first line configured the SR620 and was sent only once at the beginning of each ranging test. The commands while sent to the timer in a single

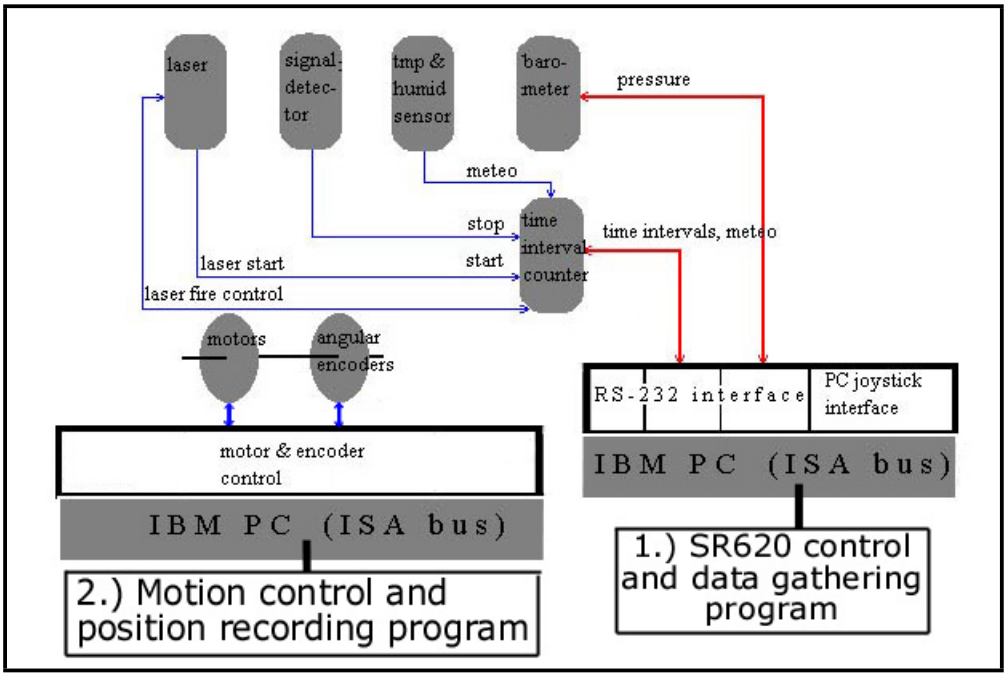

Figure 5.6: Altered configuration for ranging to fixed targets which shows how two computers and two programs are used to, 1.) gather range data and 2.) move the PSLR using the purchased indexer card.

line are actually a number of individual commands. Each command is separated from the next by a semicolon.

The actual command line from the BASIC program used in the laser ranging tests at Curtin University was:

```
480 PRINT ♯1 ,"MODE0;LEVL1,0.35;LEVL2,0.35;LEVL0,2.0;TSLP1,0
;TSLP2,0;TSLP0,0;TCLP0,0;TCLP1,0;TCLP2,0;TERM0,0;TERM1,1;TERM2,1
;ARMM8;AUTM0;SIZE1;SRCE0".
```

These commands have the following effect.

`MODE0` - Sets the SR620 to time between channels 1 (start) and 2 (stop),

`LEVL(1,2,0),(x)` - these commands set the trigger level for the three channels, the number 1 (start),2 (stop), 0 (gate) selects the channel and the number after the

comma sets the voltage level,

`TSLP(1,2,0),(0 or 1)` - sets the trigger slope for the three channels to either 0(positive going) or 1(negative going),

`TCLP(1,2,0),(0 or 1)` - sets the coupling of the channels to either 0(DC) of 1(AC),

`TERM(1,2,0),(0 or 1)` - sets the termination resistance of the channels to either 0(50Ω) or 1($1M\Omega$),

`ARMM8` - sets the arming mode of the SR620 to external arming triggered hold-off. The SR620 has several arming modes.,

`AUTOM0` - sets the automatic restart of measurements to off,

`SIZE1` - sets the number of samples to be measured by the SR620, which in this case is 1,

`SRCE0` - sets the measurement/start source to channel A, which is the start channel in this particular test configuration.

The second command line sent to the SR620 instigates the actual measurement. This command is sent for each measurement.

```
520 PRINT ♯1, "STOP;MEAS?0"
```

This command has the following effects:

`STOP` - Stops any current measurements that are incomplete or in progress,

`MEAS?0` - The `MEAS?` command starts a new measurement and will pause all other

input or output until it gets a result, the 0 switch at the end of the command will return the mean of the measurement to the computer. Selecting another number will return other parameters such as the maximum or minimum value, the trigger levels on each of the channels or the readings from the external voltmeter inputs.

The BASIC program could also be used to collect meteorological data from the barometer as well as temperature and humidity from the SR620. While temperature and humidity were not collected when most of the ranging tests were performed (as there were no probes for these measurements at the time) it was a simple matter to implement as these probes are connected to the SR620 voltmeter channels and the levels of these channels can be easily polled from the SR620 using the `MEAS?` command. The barometer was polled before each ranging sample run. The barometer was sent an ASCII space, `360 PRINT ♯2, " "`, which prompted the DP151 to return the current atmospheric pressure to the computer. In normal operation these readings were taken at regular intervals (every 30 sec or so) to allow for atmospheric correction of the range. This function was included in the BASIC program after most of the ranging tests were complete as a compatible temperature and humidity probe had not been purchased before this time. The output of the PSLR meteorological station can be seen in figures 5.7, 5.8 and 5.9.

At the execution of the BASIC program, the user can specify how many samples or individual shots are to be taken. The program will only record valid shots in the data file. The program has preset range of allowable time intervals and shots which are outside of this range are not stored. These ranges are quite broad and will only remove samples which are several orders of magnitude too small or large. This was necessary as at the very start of ranging to the fixed targets, there were many spurious readings due to faulty equipment and incorrectly configured equipment. Once the program has collected the appropriate number of valid samples, these are written to a file.

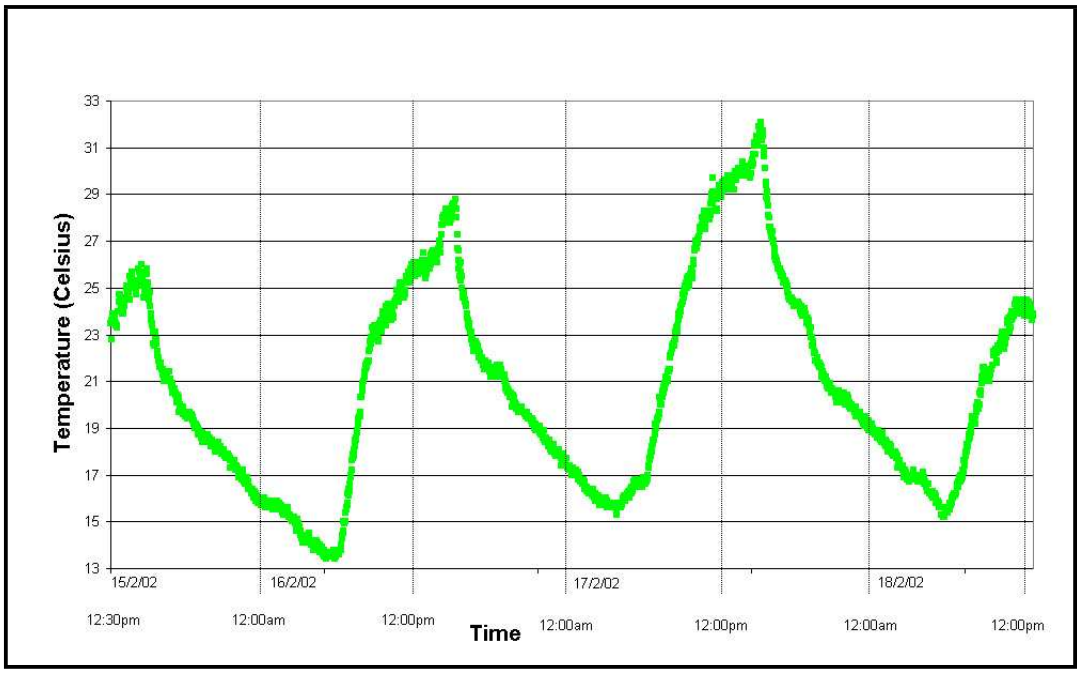

Figure 5.7: Output record from the PSLR temperature probe for a 72 hour period between February 15 - 18, 2002.

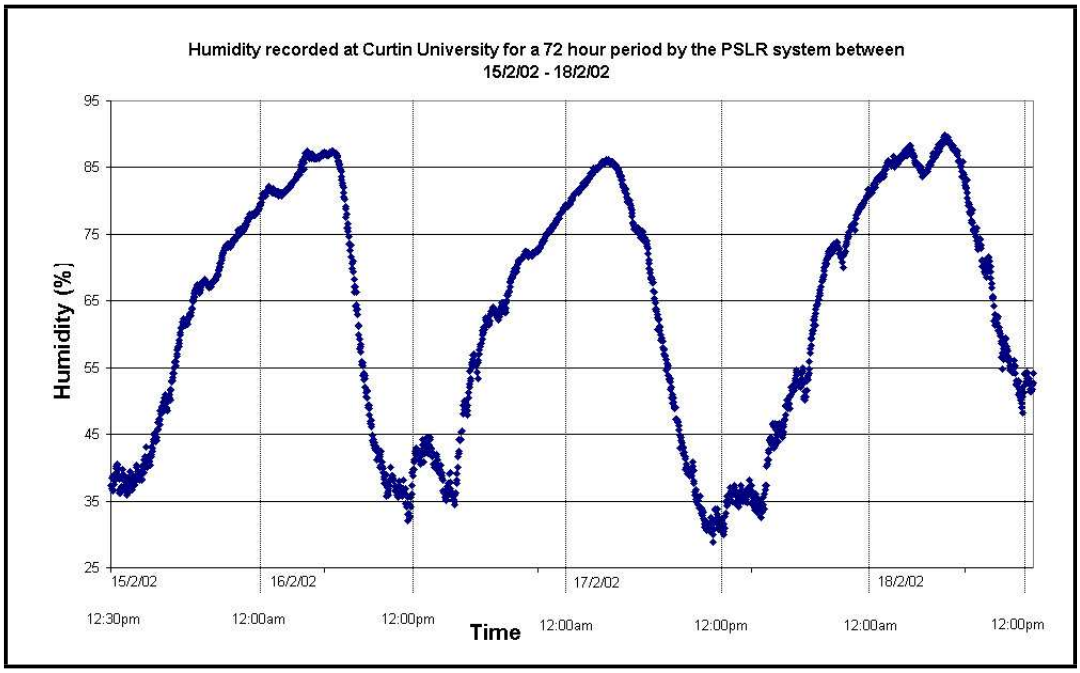

Figure 5.8: Output record from the PSLR humidity probe for a 72 hour period between February 15 - 18, 2002.

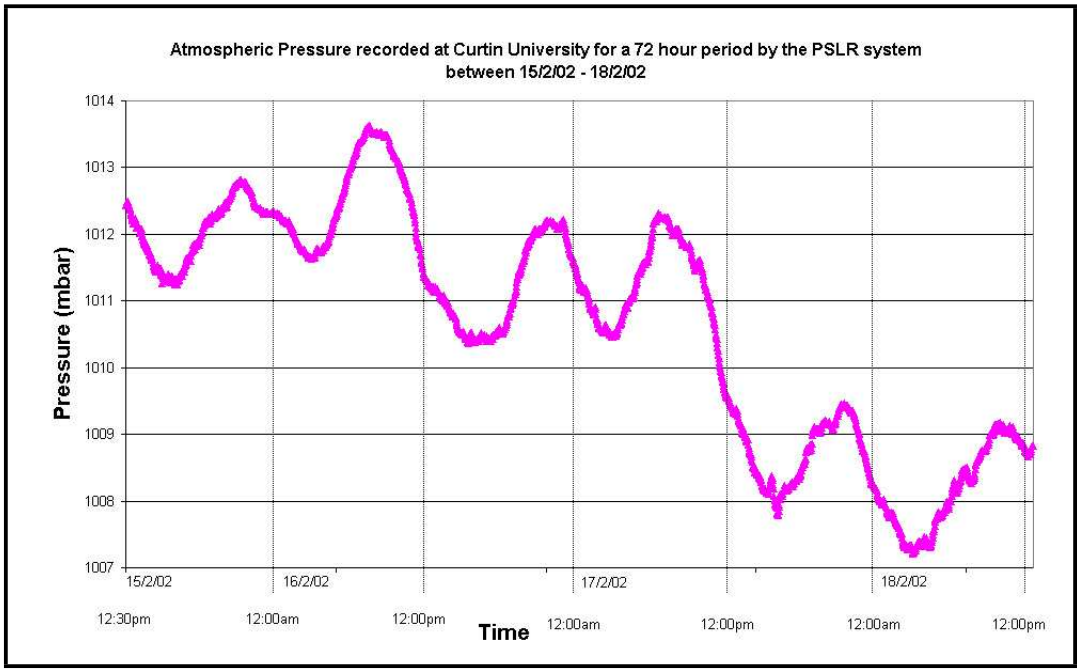

Figure 5.9: Output record from the PSLR barometer for a 72 hour period between February 15 - 18, 2002.

The program also displays the mean value, the range of values, and the standard deviation as a quick look at the the quality of the data before the next ranging run.

5.2.6.2 Galil program

The Galil program communicates with the ISA bus indexer card installed in the second computer. The indexer card interfaces with the Compumotor driver units which send step pulses to the drive motors and in turn moves and positions the telescope. The Galil card came complete with a text editor which provides an active interface with the card. This allowed commands to be entered and downloaded to the card one at a time or allowed a complete program to be downloaded and run from the text editor. Any program that was executed accepted data from the text editor and directed data to the text editor.

The Galil card uses a complete control language which comprises a set of two letter commands. These commands are quite intuitive with two letters essentially

indicating the function of the command. As an example, `AC` sets the acceleration, `SP` sets the speed in encoder counts per second and `JG` sets the jog speed in motor steps per second. This simple language makes it relatively easy to program complex movements. These commands are shown in figure 3.45, section 3.8.1.4, page 155.

The telescope was positioned so that the output from the calibration periscope hit one of the fixed targets and the PSLR electronics registered a steady sequence of returns. Initially this was done for the target mounted on the wall of the Geology building at Curtin University. The encoder position was set to zero on the DMC1720 card as the encoders use a relative position rather than an absolute position. This was accomplished by using the command `DE0,0` which means define encoder position for the x and y axes as 0. The telescope was then repositioned to point the laser beam output at the other target until a steady return signal was registered and the position noted. As the PSLR has relative encoders, as long as the relative position between each target is known it is a simple matter to direct the telescope from target to target.

The program called TARGETS had the previously determined relative positions of the fixed targets intrinsically written into the code and labelled as either the Geology target or the Engineering target. The user directed the program to point at a target of choice. As the telescope moved, the program monitored the encoder position, continuing to move until it read the appropriate position and ceased motion. The telescope had a certain amount of inertia due to the motion and ran past the target position. This was compensated for in the software by stopping forward motion before the target position was achieved so that the telescope only just ran past the required position. The direction of motion was reversed at a much slower speed so that when the target position was reached there was no overrun of the mount. This process was the same for both targets and for both axes.

The only other function of note controlled by the program was the setting and clearing of one of the digital outputs. This was connected to a small relay which shorted or open circuited the blocking input of the laser power supply. This deacti-

vated and reactivated the laser. When the mount moved, the laser was deactivated so that the risk of accidentally directing the laser out of the test area was prevented.

5.2.6.3 Conducting a ranging sample

In order to conduct a complete ranging cycle, both the BASIC and Galil program were required to operate simultaneously. The steps required to take a full ranging sample (both targets ranged in sequence for a set number of laser shots) is as follows:

1. Choose a target (Engineering or Geology) with the Galil program. The program will turn off the laser if it is on and point to the required target. When all motion has ceased, the laser is switched on.

2. The BASIC program is executed. It requests the user to specify which target is being ranged and then asks the number of range readings to be recorded.

3. Once the target and sample number are chosen, the BASIC program configures the SR620.

4. The SR620 buffer is cleared and the counter is instructed to wait for the hold-off pulse.

5. The GPS unit (which was previously configured to output a 5 Hz pulse on the UTC second) controls both the laser firing rate and the instigation of the hold-off pulse. The hold-off pulse is generated before the laser fire event so that the start channel is armed before it receives a start pulse.

6. The laser start detector is activated which starts the timer.

7. The hold-off pulse will cease with its trailing edge activating the stop channel.

8. The PMT is activated by the returning beam and stops the SR620.

9. The time interval is immediately sent to the computer which stores the result, clears the SR620 buffer which waits for the next hold-off pulse.

10. Steps 5 - 9 continue until the selected number of samples has been taken. The data storage ceases and the BASIC program requests if there will be any more samples taken.

11. If an affirmative answer is given then the program requests range sample numbers etc.

12. The Galil program once again is utilised by choosing the next target.

13. When the telescope has ceased motion and the laser is reactivated, the BASIC program can be instructed once again to accept input until the required number of samples are taken.

This constitutes a full ranging cycle. Generally, the Engineering target was ranged first and considered to be the known distance or calibration target. The Geology target was ranged last and treated as a 'satellite' or target at unknown range. All of the ranging results and subsequent results were determined using this approach.

5.3 Experimental results

The purpose of the designed experiment was to test the ability of the PSLR to range and to gauge the absolute accuracy of ranging. The initial ranging tests were conducted to prove that the experimental setup (control cards, control software, timing system, laser control) was able to produce data. Little or no care was taken with the alignment of the PSLR optics as long as a return signal could be detected and a range reading taken. As it became apparent that the PSLR was able to produce range results using the two fixed targets the emphasis of the testing was shifted to improve the quality of the data. This involved taking a great deal more care with the setup of the pulse capture and conditioning electronics and attempting to improve the alignment of the PSLR optics. This approach resulted in a marked improvement in the standard deviation and range of the data which can be largely attributed

to the improvements in the electronics setup. This was significantly enhanced by the purchase of an oscilloscope (Tektronix TDS3052) capable of displaying the fast pulses produced by the detection and conditioning electronics. The alignment of the PSLR laser output optics with the offset mechanical axis of rotation was shown to be grossly inadequate. At the time that the initial testing was conducted it was impossible to ensure that the output laser beam would maintain directional coherence with the pointing direction of the telescope. Consequently the return signal path varied for each of the targets. It is most likely that the return beam reflected off the internal surface of the receive optical path before triggering the PMT. The first set of ranging results are presented in the following section.

5.3.1 First Ranging Results

These first ranging results were produced using Microsoft Excel. The tables presented in the following figures are a product of the descriptive statistics package included in Excel. The information located at the bottom of each of the tables is calculated in the following way (see equation 5.2).

1. Time Diff(sec)- The mean time for the Electrical Engineering (EE) target is subtracted from the Geology (Geo) target mean time

2. Dist Off(m)- This is a product of half Time Diff times the speed of light in a vacuum ($299792458 m.s^{-1}$)

3. Cal Dist(m)- This is a sum of Dist Off and the known distance to the EE target

4. Error(m)- The Cal Dist is taken from the known distance to the Geo target

The uncertainty in the range measurement (Cal Dist) is determined using the sum of the calculated standard deviations for both targets.

The range of the data for both targets in the results shown in figure 5.10 is several nanoseconds. This relates to more than a meter of variation in the optical range.

Electrical Engineering target(18.403m)		*Geology target(65.432m)*	
Value	Time(ps)	Value	Time(ps)
Mean	145701.8594	Mean	458590.217
Standard Error	54.78515014	Standard Error	16.14063934
Median	145101	Median	458539
Mode	145068	Mode	458594
Standard Deviation	1728.990175	Standard Deviation	510.4118322
Sample Variance	2.98941E-06	Sample Variance	2.6052E-07
Kurtosis	6.214316085	Kurtosis	75.51476068
Skewness	2.60513383	Skewness	7.720575169
Range	10490	Range	6648
Minimum	144444	Minimum	457840
Maximum	154934	Maximum	464488
Sum	145119052	Sum	458590217
Count	996	Count	1000
Largest(1)	154934	Largest(1)	464488
Smallest(1)	144444	Smallest(1)	457840
Confidence Level(99.0%)	141.3885384	Confidence Level(99.0%)	41.65518056
TIME DIFF(ps)	DIST OFF(m)	CAL DIST(m)	ERROR(m)
312888.3576	46.9007849	65.3037 ± 0.3356	0.1282

Figure 5.10: Results of descriptive statistic data analysis of the unedited data from the first successful cycle of ranging tests to the Electrical Engineering target (distance 18.402 m) and the Geology target (distance 65.432 m). All figures are in (ps) except the rows indicated in red.

Examination of the graphs in figures 5.11 and 5.12 show that there are several large outliers in the data which has skewed the mean values. The range of the data and the standard deviation expressed in figure 5.13 are a result of a significant amount of data editing to remove these outlying values. There were many recorded range times which were well outside of two or three standard deviations. These data points were removed to produce the numbers in figure 5.13. The large spread in data was predominantly a result of the the misalignment of the receive optics. The photons that finally reached the detector were scattered off the internal surfaces of the optical path or by happenstance found a way straight along the optical path.

The range error from figure 5.13 of 0.0412 m in the data was attributed to;

1. An actual increase in path length produced by the misalignment of the output optics.

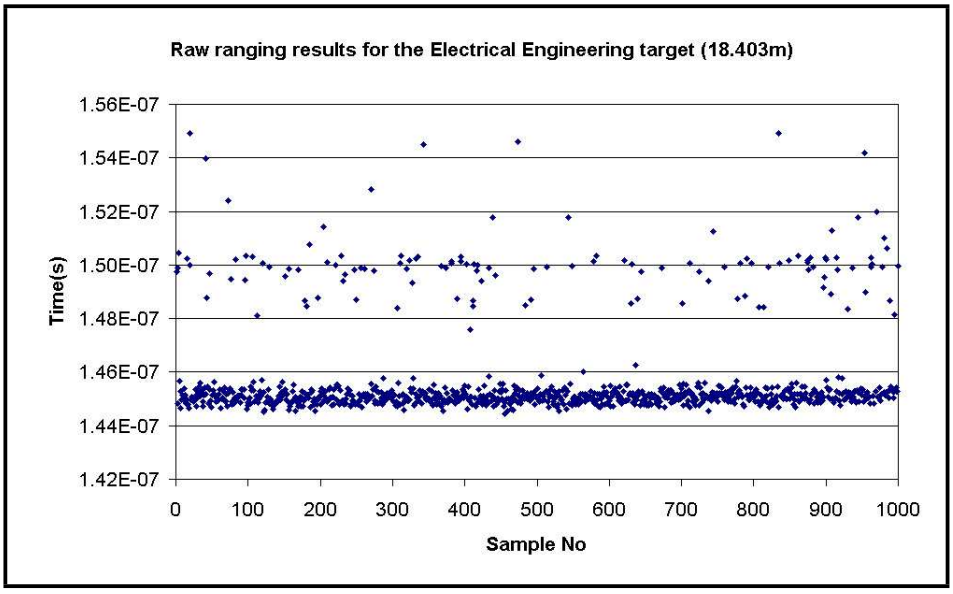

Figure 5.11: Graph of the unedited ranging time intervals for the Electrical Engineering target.

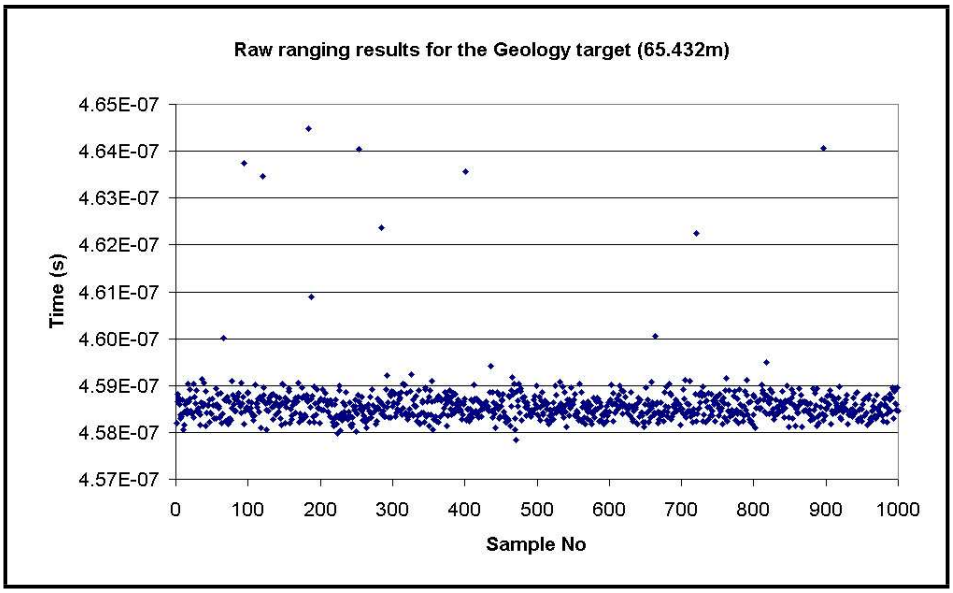

Figure 5.12: Graph of the unedited ranging time intervals for the Geology target.

2. The amount of signal permitted to impinge on the PMT caused the output signal from the amplifier to be clipped somewhat so that the trailing edge of the pulse was extremely erratic and non-regular with the leading edge. The blue trace in figure 5.14 shows the output from the amplifier after a large

Electrical Engineering target(18.403m)		*Geology target(65.432m)*	
Value	Time(ps)	Value	Time(ps)
Mean	145075.6483	Mean	458544.3239
Standard Error	7.794441594	Standard Error	7.222690497
Median	145063	Median	458534
Mode	145068	Mode	458594
Standard Deviation	229.9029974	Standard Deviation	227.0269828
Sample Variance	5.28554E-08	Sample Variance	5.15413E-08
Kurtosis	0.373428748	Kurtosis	-0.127662824
Skewness	0.396862805	Skewness	0.271727838
Range	1585	Range	1570
Minimum	144444	Minimum	457840
Maximum	146029	Maximum	459410
Sum	126215814	Sum	453041792
Count	870	Count	988
Largest(1)	146029	Largest(1)	459410
Smallest(1)	144444	Smallest(1)	457840
Confidence Level(95.0%)	15.29814008	Confidence Level(95.0%)	14.17360013
TIME DIFF(ps)	DIST OFF(m)	CAL DIST(m)	ERROR(m)
313468.6756	46.98777238	65.3908 ± 0.0684	0.0412

Figure 5.13: Results of descriptive statistic data analysis of the first ranging results after significant data filtering to remove outlying values. All figures are in (ps) except the rows indicated in orange. This produced a significant improvement in the the range error from 0.1282 m to 0.0412 m

optical signal is received by the PMT. The discriminator, which works on a zero crossing method would find such a non uniform pulse difficult to analyse to produce a suitable composite waveform (see figure 3.27, section 3.4.2, page 107) to register the zero crossing point.

3. The pulse compression method used with the SL212 laser is known to produce a good deal of output pulse energy variation. This pulse variation could not be tested at Curtin University as the appropriate equipment was not available. The SL212 laser does have an energy registration unit which can be switched to read 1 of 3 detectors mounted inside the laser.

   These detectors are labelled PD1, PD2 and PD3 in figure 3.9, section 3.2.5.2, page 71. These detectors read respectively the energy produced from the laser oscillator, the third pass through the amplifier and the second harmonic energy just before it exits the laser. The manufacturer of the laser (Ekspla Ltd) was consulted to establish if a useful scale could be applied to the numbers shown

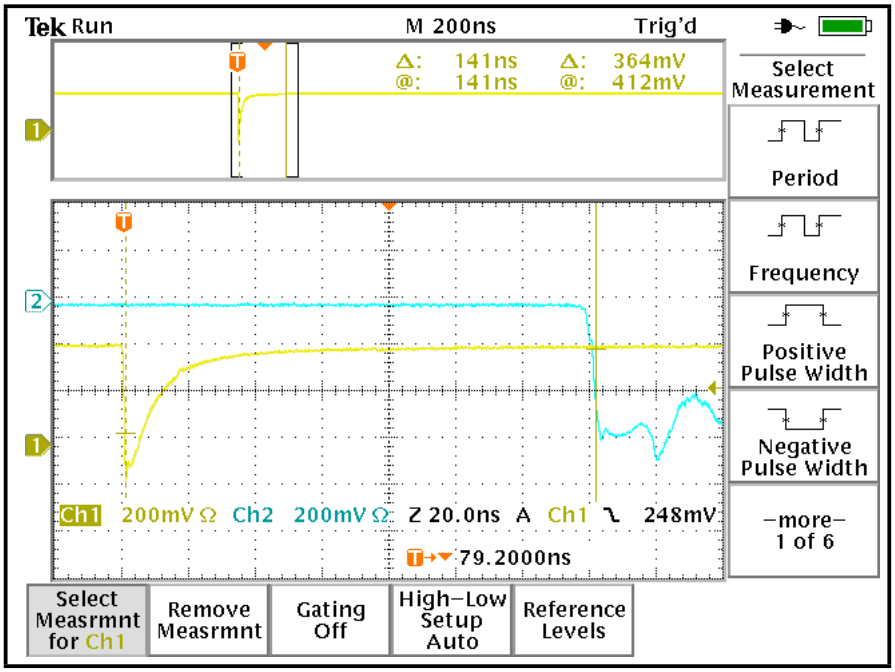

Figure 5.14: Screen capture from the Tektronix oscilloscope showing the result of a very large optical pulse on the PMT detector.

Figure 5.15: Comparative energy meter used with the SL212 laser. The selector switch on the right can be set for G - generator, A - amplifier or SH - second harmonic (final output).

on the meter (see figure 5.15). The information provided was that there is no actual calibrated scale and the meter is designed to provide a relative reading. Adjustments to the laser were made until the output shown on the meter was maximum. Once a relative maximum was obtained by adjustment a noticeable amount of jitter was observed on the meter under normal operation. The needle registered up to ± 10 (around the relative maximum value) occasionally but smaller variations were noticed constantly. For example, the oscillator photodetector would give a relative maximum value of 40 (see figure 5.15) on the meter scale. This would often drop to 30 and jump to 50. This jitter was present with all three detectors but seemed to be slightly worse in the detectors placed later in the optical path. As these are relative readings it is hard to gauge how much of an actual variation is present in terms of energy per pulse.

5.3.2 Post optical calibration ranging tests

In order to improve the ranging results to the fixed targets, the output optical system was extensively tested and re-aligned. The receive optical system was adjusted as well as was possible given the location of the telescope. Due to the location of the PSLR inside the facility it was not possible to place a suitable light source at an appropriate distance to establish a collimation range, or to view the night sky. It was not critical that the input optical system was correctly collimated over the distance that the ranging experiments were performed (high signal return meant that the focus of the main telescope need not be exact). The alignment was actually checked by firing at the two targets, removing the detector from the optical path, and checking that a return was visible and reasonably well centred at the position of the detector. This required some adjustment to ensure that the return beam could pass unperturbed through the optical path for both targets. While it was apparent that the precise relative beam path through the receiver system was not consistent when switching from one target position to another (depending on the target used

and the position on this target) all returns were able to pass through the entire input optical system freely. The telescope was later moved away from the firing range to collimate the telescope and view the sky, a process that showed that the collimation of the main telescope was poor during the ranging tests.

After the purchase of the Tektronix oscilloscope, it was apparent that there were problems with the pulses from the detector/amplifier electronics. The first problem noted was the size of the pulse from detector/amplifier electronics. The pulse appeared clipped at the top and had a very chaotic trailing edge (see figure 5.16). This indicated that the detection apparatus was saturated by the return signal.

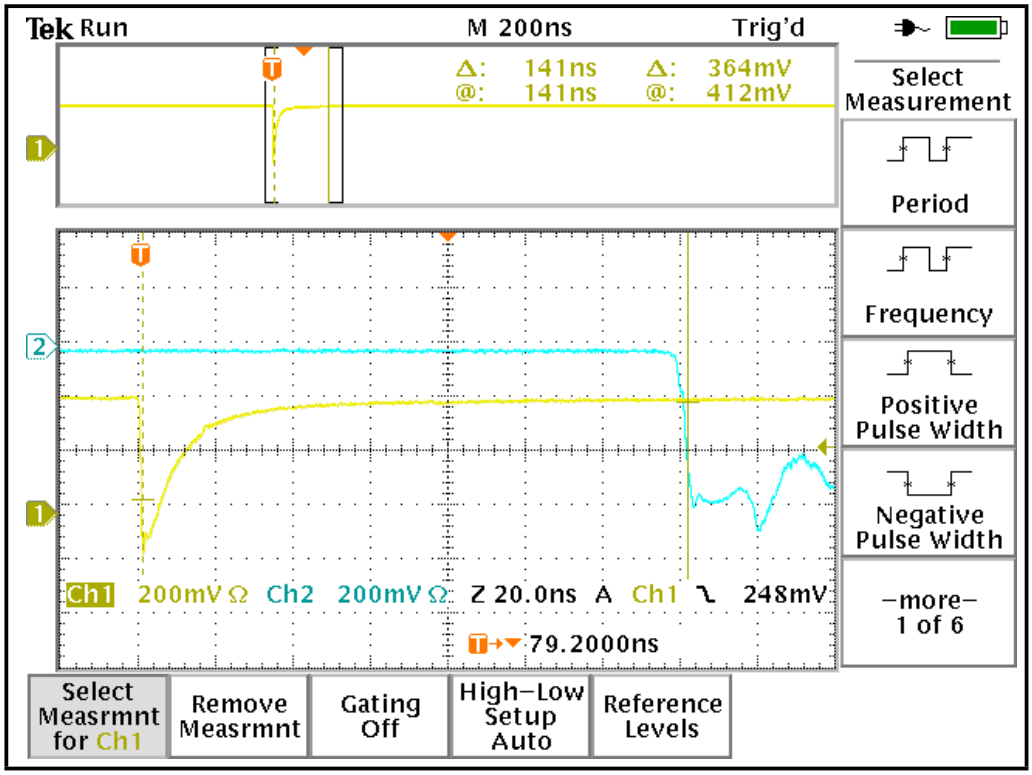

Figure 5.16: Screen capture from the TDS3052 (as shown in figure 5.14) with the original shape of the pulses from the PSLR start and stop detectors displayed. The blue trace is the pulse from the detector/amplifier arrangement which extends for quite some time past the position shown on the oscilloscope.

There were also considerable problems with poor earthing of the PMT power

supply and some of the signal cables. This caused ringing and degradation of the output pulse to the discriminator.

The oscilloscope provided instant feedback as to the shape and quality of the output pulses. This allowed the energy input into the detector to be restricted (by reducing the laser output energy and increasing the ND filtering) so that it did not cause saturation of the detector. It also ensured that noisy cables could be identified, repaired and/or replaced. The result was that a much more symmetrical pulse was generated by the detector/amplifier and fed into the discriminator. The result of the improvements in the detector hardware and the care taken to restrict the return pulse energy to the detector is shown in figure 5.17. The detector/amplifier pulse

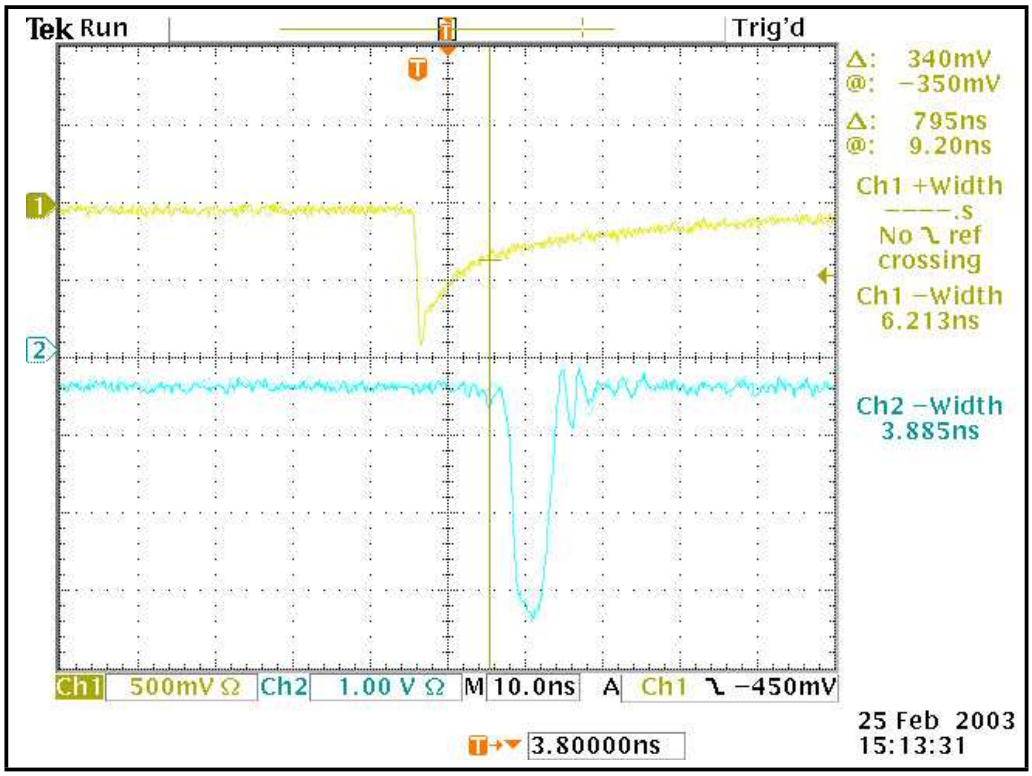

Figure 5.17: Screen capture from the TDS3052 showing pulses produced from the SL212 laser start detector (yellow trace) and from the R4124 detector using the dynode chain arrangement in figure 3.20, section 3.3.2.6, page 89 and the Ortec 9306 preamplifier (blue trace).

from figure 5.17 showed none of the evidence of clipping. The pulse was quite

symmetrical with only a slight hint of damped harmonic ringing on the back end which was most likely due to quenching in the amplifier. This pulse shape would be much easier for the discriminator to handle. Any timing error induced as signal time walk because of the erratic pulse shape (figure 5.16) should be eliminated with the uniform pulse shape in figure 5.17.

Many tests were also carried out on the setup of the discriminators and the SR620 timer. These devices all have level controls which will affect the switching times and consequent pulse output or timer activation. The SR620 could be adjusted to produce up to several nanoseconds of variability in the time interval readings by adjusting the start and stop channel levels. As both the start and stop detector pulses were sent to the same model of discriminator, the shape of the pulses input into the SR620 should be identical. The variability in time interval is due to later or earlier triggering of the input channels as a result of the pulse rise. It was reasonable to set the switching levels for both the start and stop channels on the SR620 to the same level. It was not essential to do this as long as they were not adjusted between firing from one target to the next. Ideally the level controls on the SR620 should be set to switch around the half voltage level of the pulses from the discriminators. The gate level controls remained constant during the post optical calibration ranging tests.

The discriminators, as well as having level adjustments have a slew compensation control. According to the Ortec product catalog, input amplitude can vary by up to 100:1 without significant shift in the timing output. The slew control on the discriminator is for fine tuning to minimise time slew due to excessive amplitude variation (ORTEC, 2001). The slew control can have a marked effect on the determined time interval by slewing a normally uniform gaussian data set. This effect is shown in figure 5.18.

Figure 5.18 shows how the slew control actually skewed the data so that the median is displaced from the center of the distribution. Ideally the distribution for laser ranging data should be as gaussian in form as possible. If it was found that the

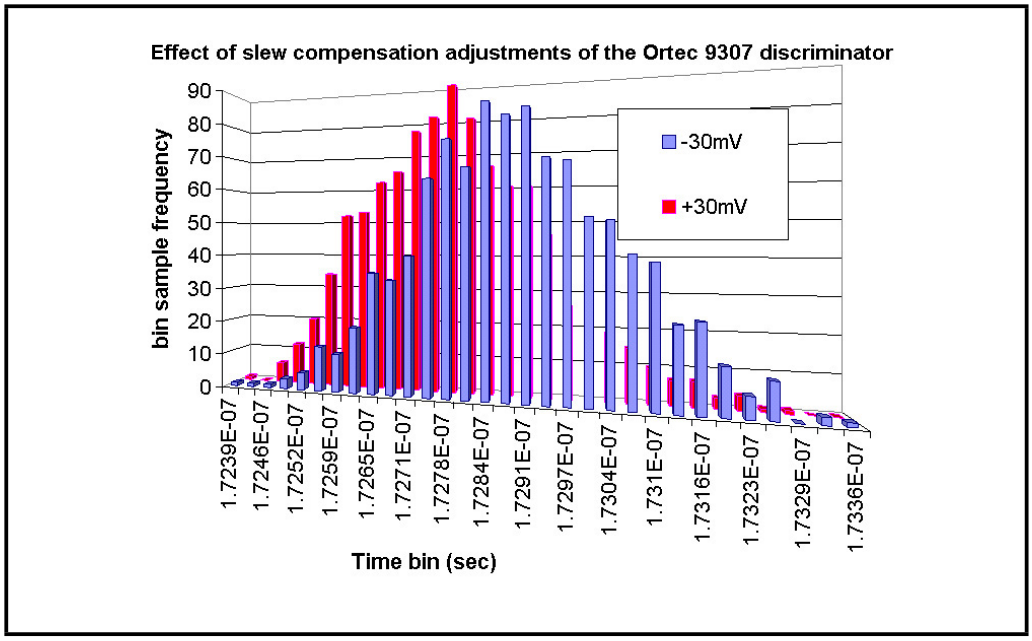

Figure 5.18: Histogram of binned range data for ranging results to the Electrical Engineering target. The voltage levels in the legend on the graph show the slew settings for both the start and stop discriminators for each data set.

data were not gaussian then the slew control could be used to compensate for this. Figure 5.19 shows the effect the slew control had on the average value for the timing data for the Electrical Engineering target. It can be seen that there was a good deal of variation over the entire range of slew adjustment. In the range -10mV to 10mV the variation of all of the plots is less than 100ps. It would seem prudent to set the discriminator slew adjustments in this region unless there was some expectation that a skewed data set would be produced (as a result of the return signal). The slew controls were set at -3mV for the start discriminator and 5mV for the stop discriminator as this seemed to produce the most even distribution of data.

Once the alignment was improved, the electronics were either repaired or replaced and the signal conditioning settings were resolved, the PSLR was ready to see if the initial ranging results could be improved upon.

One of the first tasks to improve the range determination was to calculate the correct speed of light for the atmospheric conditions at the time that the ranging

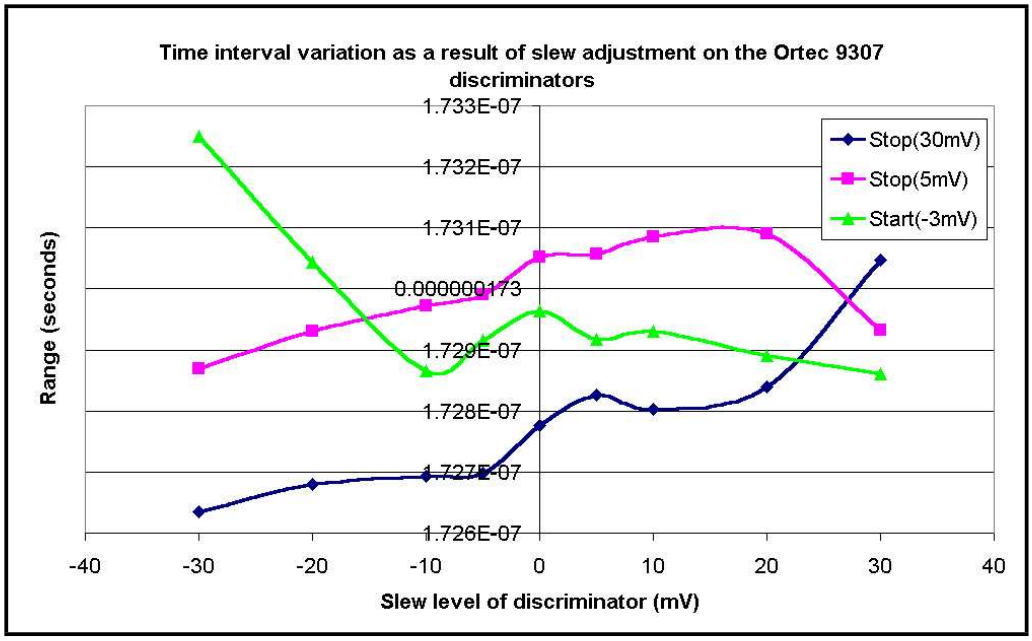

Figure 5.19: The plots in the above graph show the effect of slew adjustment on the mean of the range results for a series of shots where one discriminator adjustment was kept constant. The legend indicates which discriminator slew adjustment remained constant (and the level). The other discriminator slew was adjusted over the range indicated by the horizontal axis.

tests took place. The speed of light in a vacuum was used for the range determination in the previous tests. The actual speed of light is a result of the refractive index variability of atmospheric constituents and the wavelength of the ranging laser.

The speed of light in the atmosphere (or any medium) is related to the speed of light in a vacuum by its refractive index as,

$$v_{atm} = \frac{c}{n_{atm}}, \tag{5.4}$$

where v_{atm} is the velocity of light in the atmosphere, c is the speed of light in a vacuum, n_{atm} is the refractive index of the atmosphere.

The refractive index of dry air with a low CO_2 content at $P_s = 1013.25Kpa$ and $T_s = 288.15K$ can be found using,

$$n_s = 1 + 643.28 \times 10^{-7} + \frac{294981 \times 10^{-7}}{146 - \sigma^2} + \frac{2554^{-7}}{41 - \sigma^2}, \tag{5.5}$$

where n_s is the standard air refractive index at σ given σ is the wave number (or reciprocal of the laser vacuum wavelength in μm^{-1}). (Cox, 1976)

The refractive index can then be found by applying the correction,

$$n = 1 + (n_s - 1) \times (\frac{P_{loc}}{P_s}) \times (\frac{T_s}{T_{loc}}), \tag{5.6}$$

where P_{loc}, T_{loc} are the local atmospheric pressure and temperature, P_s, T_s are the standard values.

A correction should also be applied to the determined refractive index to compensate for the humidity of the atmosphere. When the ranging tests were conducted there was no humidity sensor available to record the local humidity so these corrections were not made.

In these later ranging tests the atmospheric pressure was recorded for every 100 laser returns from the targets or every 20 seconds. Each ranging test to a target consisted of 1000 shots, or a duration of less than 3.5 minutes. In all of the tests conducted, the amount of variation in pressure over the test period was generally less then 0.05 kpa. The temperature varied more but even this was less than 1 K. The value of n_s for the laser wavelength used by the PSLR laser (532 nm) at the standard conditions is 1.0000643196. When the corrections are applied to this value it alters n_s by 2.0 - 3.0 $\times 10^{-6}$ %.

More recent findings (Ciddor, 1996) have shown that there were up to several parts in 10^7 error in the refractive index from the research (published in 1966) that equations 5.5 and 5.6 are based upon. While this error would account for less than a tenth of a millimeter over the ranging distances used at Curtin University, it must

be taken into account at satellite ranging distances.

These small variations throughout the ranging tests have very little effect on the determination of the range. If the initial value for temperature and pressure at the start of the range tests are used rather than those obtained every 20 seconds, the difference was typically 2 - 3 tenths of a millimeter for the range determination. As this level of precision is not even remotely possible with the PSLR, it is valid to take the first recorded temperature and pressure readings if such a short duration ranging test is conducted. The following graphs and figures were determined using values for the speed of light calculated from the initial temperature and pressure readings for each ranging test.

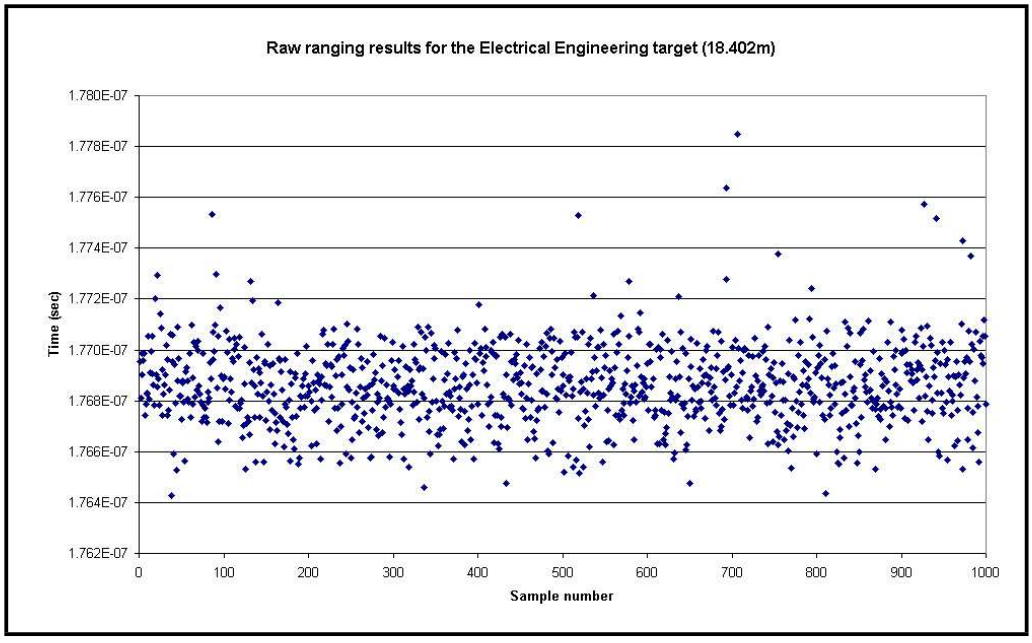

Figure 5.20: Plot of a thousand ranging shots to the Electrical Engineering target.

The set of ranging samples shown in figures 5.20 and 5.21 produced the least amount of range error between the two targets. All of the calculations used the data in an unedited state, exactly as displayed in figures 5.20 and 5.21. This accounts for the reasonably high standard deviations and total data range for each set of samples. The calculated range error is still better than the original ranging results (which were heavily edited) even in an unedited state. The table in figure 5.22 was

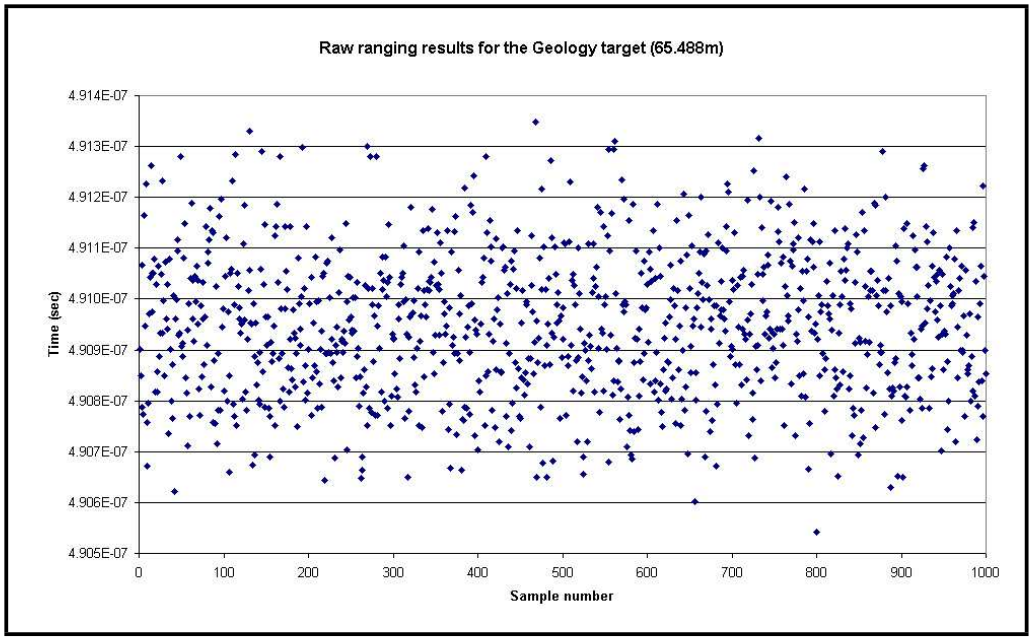

Figure 5.21: Plot of a thousand ranging shots to the Geology target.

produced primarily using the descriptive statistics feature in Microsoft Excel. The medium-dependant speeds of light were determined using equations 5.4, 5.5 and 5.6. The other values were calculated in the following way;

1. `Time Diff(sec)`- The mean time for the Electrical Engineering (EE) target is taken from the mean time for the Geology (Geo) target.

2. `Dist Off(m)`- This is a product of half `Time Diff(sec)` times the speed of light in the medium.

3. `Cal Dist(m)`- This is a sum of `Dist Off(m)` and the known distance to the EE target.

4. Cal Dist uncertainty - This is taken as the the difference in the range result if the corresponding standard deviation is removed from one mean and the standard deviation added to the other mean. The largest calculated uncertainty value is shown.

Electrical Engineering target (18.402m)		Geology target (65.488m)	
	Time(sec)		Time(sec)
Mean	1.76861E-07	Mean	4.90948E-07
Standard Error	4.96042E-12	Standard Error	4.39357E-12
Median	1.76858E-07	Median	4.90948E-07
Mode	1.76858E-07	Mode	4.90934E-07
Standard Deviation	1.56862E-10	Standard Deviation	1.38937E-10
Sample Variance	2.46057E-20	Sample Variance	1.93035E-20
Kurtosis	3.035093972	Kurtosis	-0.26757604
Skewness	0.646033059	Skewness	0.113166731
Range	1.421E-09	Range	8.08E-10
Minimum	1.76427E-07	Minimum	4.90541E-07
Maximum	1.77848E-07	Maximum	4.91349E-07
Sum	0.000176861	Sum	0.000490948
Count	1000	Count	1000
Largest(1)	1.77848E-07	Largest(1)	4.91349E-07
Smallest(1)	1.76427E-07	Smallest(1)	4.90541E-07
Confidence Level(95.0%)	9.73404E-12	Confidence Level(95.0%)	8.6217E-12
speed of light@1014.78Kpa, 298k, 532nm 299773785.842998 m/s		speed of light@1014.77Kpa, 298k, 532nm 299773786.026989 m/s	
TIME DIFF(sec)	**DIST OFF(m)**	**CAL DIST(m)**	**ERROR(m)**
3.14087E-07	47.078	65.479 ± 0.04	-0.0085

Figure 5.22: Descriptive statistics, calculated speed and distance results for the ranging times in figures 5.20 and 5.21. All figures are in seconds except for the rows marked in blue. The Geology target distance shown at the top of the right hand columns differs from the distance shown in earlier figures as the target was moved to improve the alignment between the target and the telescope.

5. `Error(m)`- The `Cal Dist(m)` is taken from the known distance to the Geo target.

The error result from figure 5.22 was very encouraging. A value of 8.5 mm range error with standard deviation figures of 156.8 ps (Electrical engineering target) and 138.9 ps (Geology target) is far superior to the original ranging result of 40.1 mm and standard deviations of 229.9 ps and 227.0 ps (for the respective targets) (after data editing) and shows the level of improvement obtainable with better instrument setup.

This error result was the best of a series of ranging tests. These tests involved moving the transmit direction of the laser pulse so that it reflected from the target

retroreflectors at different positions and consequently hit the main mirror in a different position to establish if there was any difference in range. If the main mirror was correctly aligned with the output telescope/periscope optics, then the return beam would always focus on the same spot on the PMT as the beam would always remain parallel to the return optical path of the instrument. Any misalignment would mean a focus on different parts of the return detector and some difference in the generated stop pulse.

Some of the range tests could not be analysed in raw form as they contained double ranges due to reflections from behind the actual target retroreflector. This was due to the laser beam direction being moved away from the centre of the retroreflector to the edge. Some of the beam actually hit the surface on which the retroreflector was mounted (see figure 5.23). Of the other examples that were valid none produced

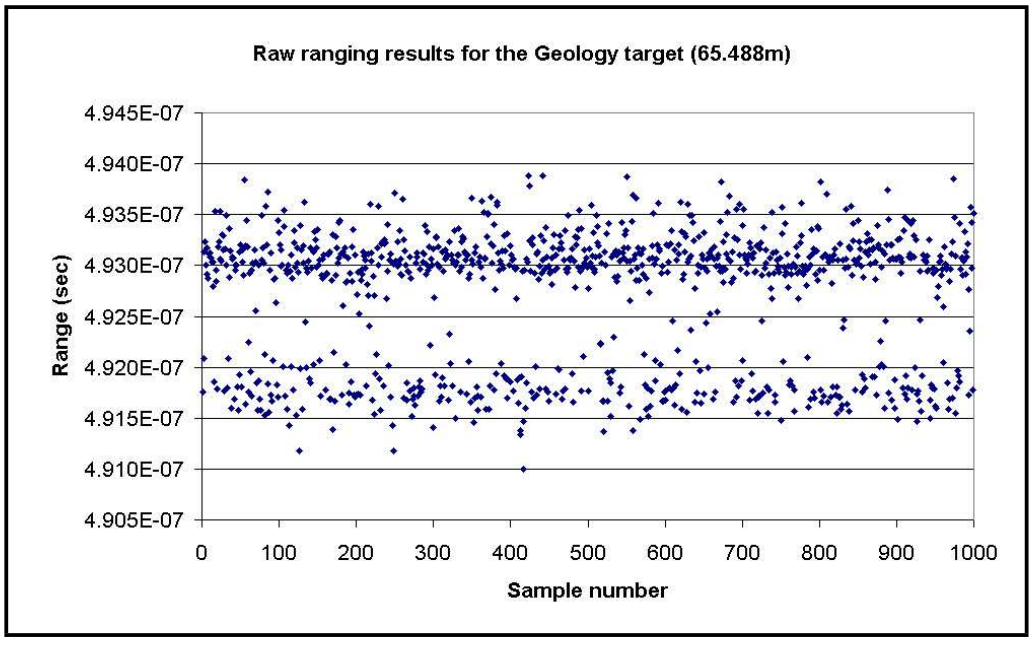

Figure 5.23: Plot of a thousand ranging shots to the Geology target showing the double range due to spurious reflections from behind the retroreflector target.

such good results as the 8.5 mm error result reported earlier. On average the error in the range was closer to 23mm.

Figure 5.24 shows the comparison of the system internal time delay (calculated by

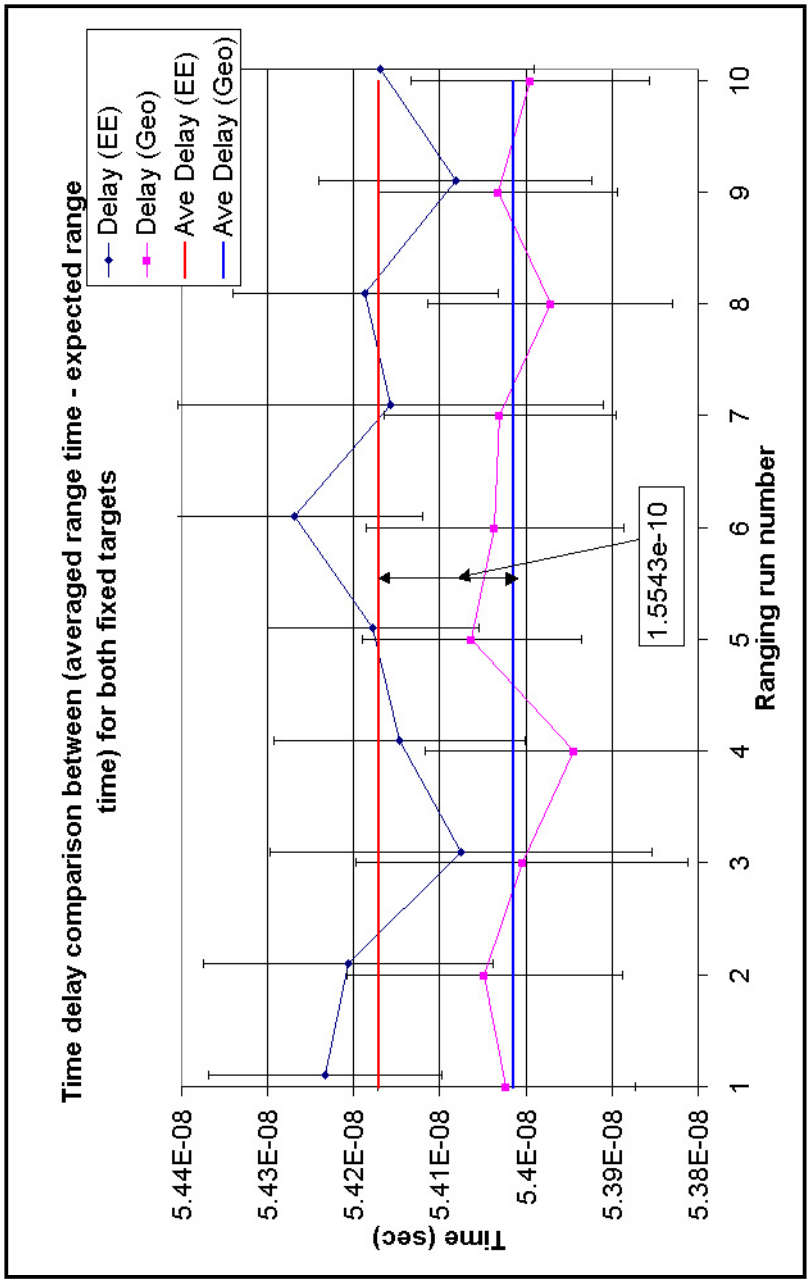

Figure 5.24: Comparison of the internal system delay of the PSLR instrument. This shows the internal system delay as calculated from a series of ranging cycles for each target. It also shows the average of the internal system delay for each target and the average error between targets. The error bars show the standard deviation of the data set used to determine each point.

rearranging equation 5.2 and using the known range to the target) when calculated from the measurements to both of the fixed targets. The expected time is calculated as ($2 \times (range) \times$ estimated speed of light in air). If this is taken from the actual ranging time then this should yield the system internal time delay. The system internal time delay should be independent of the actual range measurement taken and should be the same for any range measurement taken (neglecting changes due to temperature etc). As there is an apparent difference in the delay time when measured to both fixed targets, then there is some problem with the ranging equipment/setup or the ranges have been measured incorrectly in the first place. The known range was measured with a total station (survey theodolite and ranging instrument) setup so that it sat directly over the point on which the PSLR azimuth axis was centred. The height of the total station meant that the instrument detector head had to be tilted to measure the distance to the fixed retroreflector targets.

The Total Station measures distance using a diode source and detector which is mounted so that the direction of propagation of the detection light source is parallel with an imaginary line drawn between the remote target and the azimuth rotation axis of the instrument (see figure 5.25 (Leica Geosystems, 2003)).

When conducting ranging measurements with an SLR, the origin of the ground station coordinates are taken as the centre of rotation of the axes. All of the distance measurements are taken to this point. At SLR distances, the fact that there is some separation between the detector optical path and the receive optical path (as with a coaxial system) makes little difference as the return beam from the satellite target will always be wider than any separation of the optical paths, so it is possible to transmit the laser beam parallel with the receive optical axis. The PSLR, when pointing to near targets, where the final output of the laser beam is on an arm away from the centre of azimuth rotation of the PSLR, then there is a need to compensate for angle. This is shown graphically in figure 5.26. The PSLR uses a flip periscope arrangement when ranging to ground targets (see figure 4.2, page 173 and figure 4.10, page 182). This means that the nearer a ground target is to

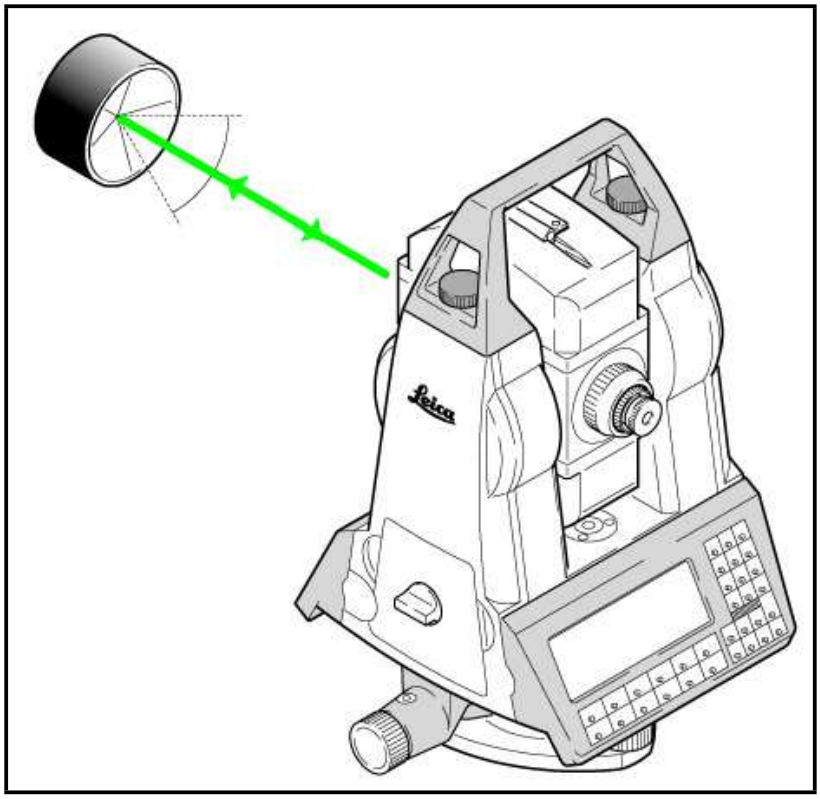

Figure 5.25: Illustration of a Total Station showing the orientation of the measurement optical signal with the target and the centre of rotation of the device. The optical signal travels from the total station to the target directly parallel with the imaginary line between the target and the centre of the Total Station rotation.

the PSLR, the greater the angle between the direction of the transmit laser and the imaginary line from the target to the centre of azimuth rotation. This can be seen in figure 5.26 where the angle associated with the Electrical Engineering (EE) target (α_E) is larger than the angle associated with the Geology (Geo) target (α_G). The result of this need for the PSLR to direct the laser beam so that it is not parallel with the afore mentioned imaginary line between the targets and azimuth centre is that the distances measured by the Total Station and the PSLR are not actually the same. It also indicates that the closer a target is to the PSLR, then the greater the difference in the distance measured by the Total Station and the PSLR. In retrospect and after attending the 13^{th} Laser ranging workshop in Washington

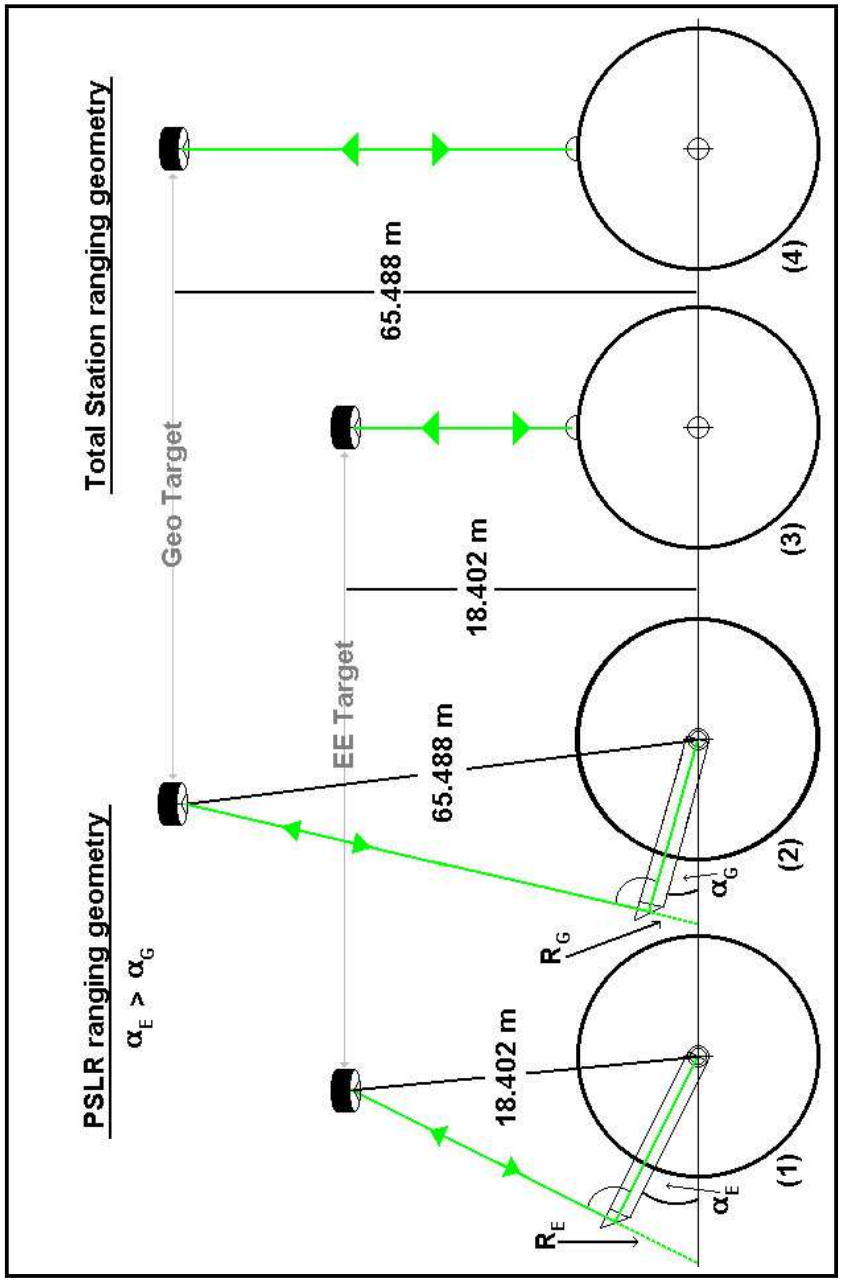

Figure 5.26: Comparison of the measurement geometry of the Total station and the PSLR. Examples (3) and (4) in the figure show the orientation of the Total Station detection optics in relation to the datum (cross hair in each circle) when ranging to the fixed targets used on campus. Examples (1) and (2) show the result of the laser transmit exit point of the PSLR not being in a straight line between the targets and the datum point. If $\alpha_E > \alpha_G$ then there will be a range error induced.

D.C (2003) a direct measurement to the intersection of axes would have been more useful and accurate as an indication of the ranges of the fixed targets, rather than the method employed. This process would have been quite simple with the PSLR as the position of the intersection of axes (the prism P1 in figures 4.2, 4.7 in section 4.2.1, page 177) is readily accessible. The graph in figure 5.24 shows that there is an average discrepancy in the internal system delay (between samples taken to the two targets) of 1.5543×10^{-10} seconds. The range measurements used to the two targets did not take into account the parallax error in the range due to the offset of the output optical system.

This parallax error certainly needs to be considered when conducting normal satellite laser ranging. If there is a range offset due to the orientation of a flip periscope it will need to be identified and taken into account when calibrating for the internal delay. The PSLR parallax can be identified by considering the orientation of the targets and the output periscope with respect to the intersection of the axes of rotation in 3 dimensions. Figure 5.27 shows the orientation of the of the targets with respect to the intersection of the axes of rotation of the total station used to measure the distances indicated in the figure. The elevation of the targets with respect to the horizontal plane through the intersection of axes shows that the targets are not in the same plane. If the PSLR intersection of axes was in the same horizontal plane as the intersection of axes of the total station then the elevations required for the PSLR to direct a pulse to the targets would be the same and as such the distances measured to the targets by the total station would be valid. Figure 5.30 shows that the PSLR and total station points of reference (intersection of axes) are not in the same horizontal plane so there will be a parallax induced range difference due to the elevation. Figure 5.28 shows the orientation of the flip periscope output centre (prism P4 in figure 4.2, page 173) and the point of reference ((prism P1 in figure 4.2, page 173) form an imaginary right triangle as indicated by the right side of figure 5.28. If the PSLR was tilted towards the horizontal in order to range to the targets shown in figure 5.27, this imaginary triangle would be oriented with the

PSLR point of reference as shown in figure 5.29. This shows that as the output of the transmit optical system is offset from the point of reference, it must be tilted toward the imaginary line between the target and the intersection of axes. This will then introduce a parallax range error due to the distance between the target and the intersection of axes. In effect the PSLR will measure the length D+B from figure 5.29 rather than the known distance E.

To determine the overall parallax range error, the error in azimuth and elevation are treated separately. To begin, the azimuth error is considered first (the following discussion of parallax refer to figures 5.27 - 5.30 where all uppercase letters indicate lengths and lowercase letters indicate angles).

The azimuth parallax error is evaluated by following the following steps:

1. Determine the length TPD from the total station measurement.

$$TPD = TS\cos(x) \tag{5.7}$$

2. Find the value of angle e.

$$e = 180^o - c \tag{5.8}$$

3. Determine the value of angle f.

$$f = \sin^{-1}[\frac{H\sin(e)}{X}] \tag{5.9}$$

4. The value of angle d is then self evident.

$$d = 180^o - e - f \tag{5.10}$$

5. Now the important length D can be evaluated.

$$D = \frac{X\sin(d)}{\sin(e)} \tag{5.11}$$

6. This then leads to the true parallax distance RPD in the azimuth plane.

$$RPD = B + D \tag{5.12}$$

The length of the flip periscope would need to be added to the true parallax distance (RPD+120 mm) during operation satellite laser ranging as the periscope is flipped out when ranging to satellites but used for calibration target ranging. The ranging to fixed targets at Curtin University was always conducted using the flip periscope so this length is ignored.

To find the overall parallax range, the path length different due to the elevation must now be taken into account. This involves the following steps:

1. Determine the length X

$$X = TS\sin(x) \tag{5.13}$$

2. Add this value to the difference in the reference points height above the datum.

$$Y = Z + X \tag{5.14}$$

3. The true parallax range error R can then be determined.

$$R = \sqrt{(RPD)^2 + (Y)^2} \tag{5.15}$$

These calculations produce the results shown in table 5.1 (Geology target) and table 5.2 (Engineering target).

What these results show is that even though the parallax was not taken into account when the results for the fixed target ranges were compared, the actual ranges were only 4 mm (Geology target) and 3mm (Engineering target) longer. The ranging data recorded by the PSLR (figure 5.24) indicates a range error between targets of 23 mm and as such shows that the parallax plays only a very small part.

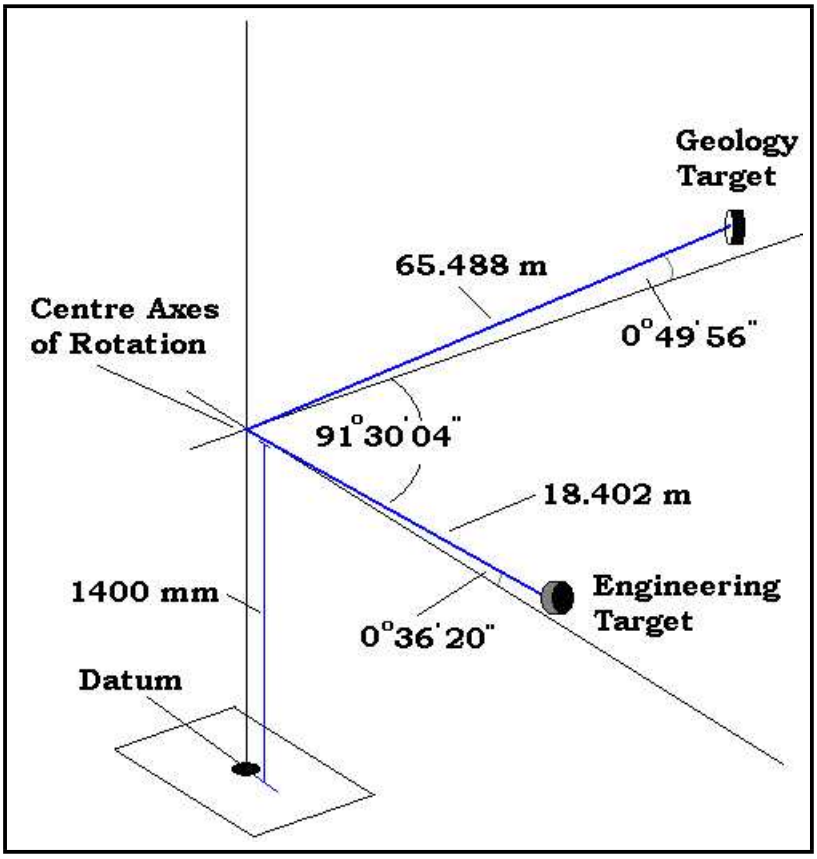

Figure 5.27: Illustration of the orientation of the retroreflector targets as determined by the Total Station. The total station intersection of axes was located 1400 mm above the datum.

A more likely scenario is a change of the alignment of the output optical axis due to the orientation of the PSLR mount. This could cause the output beam to exit the periscope without being orthogonal (see figure 5.31).

If Δe, which is only in the azimuth plane, was to vary between targets by 6 degrees (or 3 degrees in opposite directions from orthogonal for each target) it would produce a range error of 25.9 mm when propagated through equations 5.8 - 5.15. It is unlikely that there was this much variation as the alignment of the main telescope will not change it's orientation when the mount is moved. When the output optical system was aligned, it was adjusted until the return beam was centred on the return detector (the main telescope was assumed to then be orthogonal to the

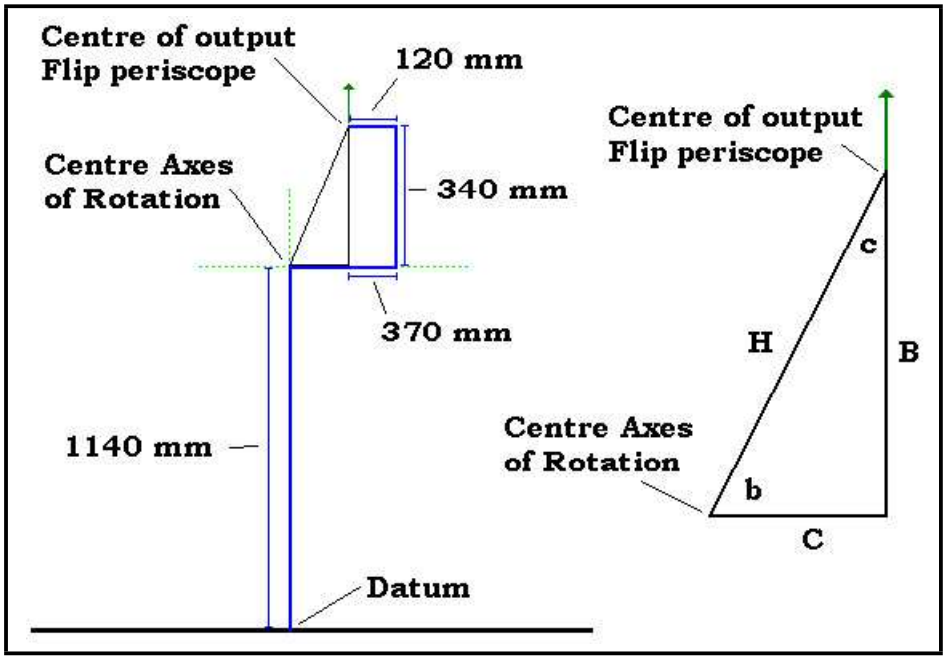

Figure 5.28: Illustration of the orientation of the centre of the flip periscope and the offset from the intersection of the PSLR axes. This forms a right angle triangle (in one plane) of the dimensions shown on the right of the figure. The values of c and b are; $c = 36^o19'43".39$ and $b = 53^o40'36".03$.

beam direction). This was done using the Geology target only. The only check on the alignment of the output beam for the Engineering target was to ensure it exited the output telescope through the centre of the aperture. The orthogonality of the beam was never tested. A large variation of Δe between the targets would mean the return beam would not reach the detector when ranging to the Engineering target as the return beam would be a long way off the optical axis of the main telescope. If there was a slight variation, the beam would make it to the detector but would fall on the outside of the detector. This will effect the accuracy of the timing system as well as inducing a parallax range error.

The return laser pulse from the Electrical Engineering target was somewhat larger in amplitude than the pulse from the Geology target. The pulse cross section returned from the Electrical Engineering target was observed on the surface of the main mirror as being only slightly larger than the beam output cross section from

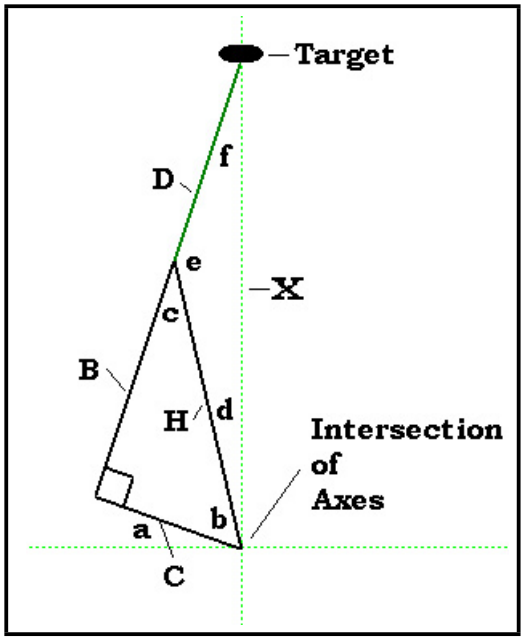

Figure 5.29: This figure shows the triangle formed between the intersection of axes and the centre of the output periscope(in one plane). If a straight line is drawn between the intersection of axes and a near target, then this triangle has to be rotated toward the straight line in order to point at the target. This parallax means that the length of D+B is measured rather than E. In the diagram lengths are represented by capital letters and angles are shown as lower case.

the flip periscope. The return pulse cross section from the farther target was 4 - 5 time larger than the beam output cross section. The main telescope and return optical system is designed to focus light impinging on the main mirror to a point: in this case, onto the front face of the PMT. The main mirror was not properly collimated when the ranging tests were conducted so it is unlikely that the entire beam was focused on the centre of the PMT. If the nearer target, with its much smaller return beam cross section was focused near the edge of the PMT tube this could account for the longer than expected time delay, the greater spread in average range values, and the higher values of standard deviation. The PMT tube has a quoted pulse transit time through the detector of 12 ns. This need only differ by 155 ps from one target to the next (due to detector edge effects) or only 1.3% of the

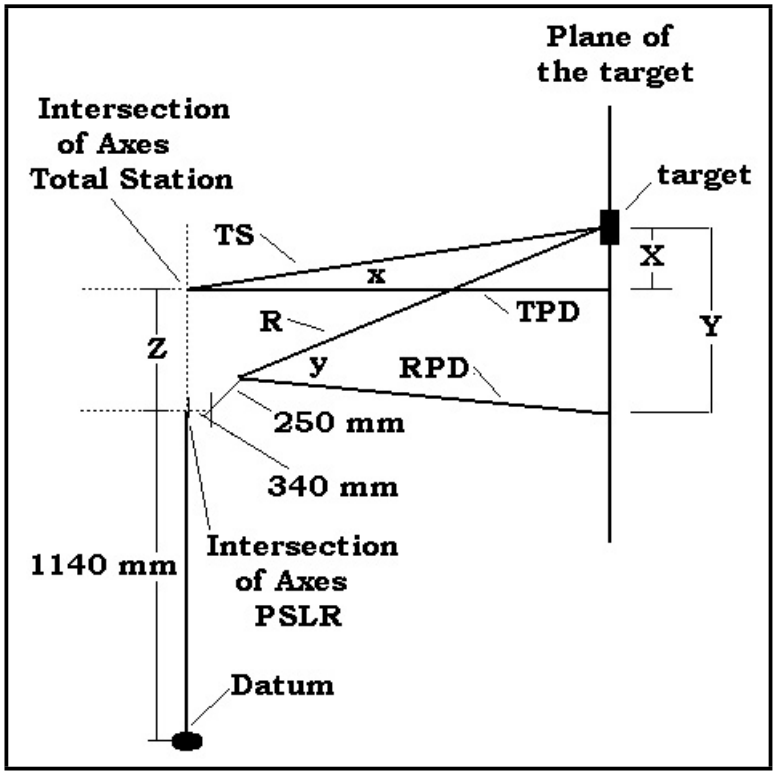

Figure 5.30: This figure illustrates the intersection of axes of both the PSLR and the total station (in relation to the datum in one plane) and the elevation of each instrument required to point at the target. Angles are represented by lower case and lengths are shown by Capital letters.

quoted transit time. PMT transit times can vary by at least this amount due to the input pulse characteristics (Hamamatsu Photonics, 1998).

As there was a definite time bias with the Electrical engineering target it must be due to the detection and timing apparatus or a range measurement error due to a misalignment of the output laser beam at various mount orientations or some combination of both effects. As the main telescope was poorly collimated and the near target required that the PSLR be rotated inward more (with respect to the imaginary line between target and centre) than would be required for the more distant target (see figure 5.26), the angle of incident on the main mirror would be more acute.

Angle	degree	Distances	metres
a	0^o12’48”.08	B	0.340
b	53^o40’36”.03	C	0.250
c	36^o19’43”.39	D	65.148
d	36^o06’35”.89	TPD	65.481
e	143^o40’16”.61	H	0.422
f	0^o13’07”.42	TS	65.488
x	0^o49’56”	RPD	65.481
		X	0.951
		Z	0.260
		Y	1.211
		R	65.492

Table 5.1: Values of the parallax calculations for the Geology target. These values relate to equations 5.7 - 5.15 and figures 5.27 - 5.30.

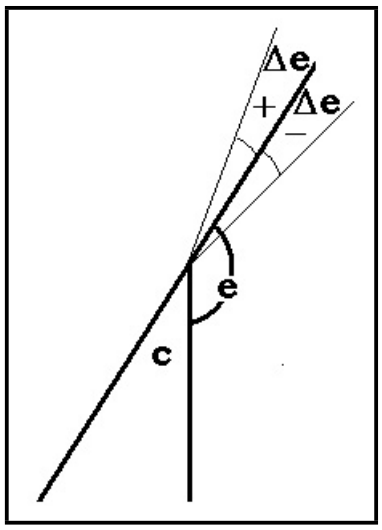

Figure 5.31: Illustration of the possible effect of a misalignment of the output optical axis due to the orientation of the mount. The angle e is from figure 5.29. Δe represents the amount of deviation from the orthogonal direction.

Angle	degree	Distances	metres
a	0^o46'23".02	B	0.340
b	53^o40'36".03	C	0.250
c	36^o19'43".39	D	18.060
d	35^o33'00".95	TPD	18.401
e	143^o40'16".61	H	0.422
f	0^o46'42".29	TS	18.402
x	0^o36'20"	RPD	18.401
		X	0.194
		Z	0.260
		Y	0.454
		R	18.405

Table 5.2: Values of the parallax calculations for the Engineering target. These values relate to equations 5.7 - 5.15 and figures 5.27 - 5.30.

As a result, the subsequent path travelled through the receive optical system would vary more than the returns from the more distant target and consequently would be more likely to enter the detector at the edges. This could be checked using a fixed target that was further away than the Geology target but the position of the PSLR test facility made this impossible as the target locations were chosen so there was no danger of exposing the Curtin University patrons to the laser beam. The ranging tests conducted to produce figure 5.24 had the PSLR moved slightly so that the the output laser beam hit each target in different positions and thus change the path of the return beam through the receive optical system. The internal system delays generated for each target showed a great deal of variability, over 200 ps in the case of the Electrical Engineering target (see figure 5.24) which is greater than the difference of the average internal system delays shown in figure 5.24. If the cause of this difference was largely a result of detector transit delay due to off centre focus on the detector, and several orientations were tested for each target, then the

	Quantity	Electrical Eng. Target	Geology Target
A	True range(TS)	18.402 ± 0.002 m	65.488 ± 0.002 m
B	PSLR measured range	26.525 ± 0.050 m	73.588 ± 0.045 m
C	Range error (B-A)	8.123 m	8.100 m
D	Max. measured range	26.539 ± 0.050 m	73.596 ± 0.045 m
E	Min. measured range	26.510 ± 0.050 m	73.578 ± 0.045 m
F	Range variation	0.029 ± 0.050 m	0.018 ± 0.045 m
G	Internal time delay	5.41703^{-8} s	5.40149×10^{-8} s
H	Average SD	1.68285^{-10} s	1.50675×10^{-10} s

Table 5.3: This table shows results of a series of ranging cycles to both targets. The uncertainty of the Total Station (TS) is given as specified by the manufacturer, the uncertainties shown for PSLR measurements are an average of the standard deviations (SD) of each target for each ranging cycle.

data for each target should overlap. The error bars from figure 5.24 on the internal delay traces should all overlap the internal delay trace generated by the other target. This would indicated that the difference between the average internal system delays shown in figure 5.24 was largely due to an actual range bias as a result of the the laser beam propagation orientation.

Over such a small range with a large number of samples, the range figures should approach the absolute accuracy of the timing apparatus (± 25 ps RMS for each target) or a distance of 7.5mm. The average determined difference between the ranges to each target was closer to 23 mm.

Given the variability in return times to the same range (for both targets) was over 100 ps, it would not be recommendable to use the PSLR as presently configured for laser ranging at this time. A variation of 100 ps would give an uncertainty of 15mm in the position of any fixed target used for system calibration. This uncertainty would be transferred to any satellite laser ranging calculations as the fixed target time and range are an integral part of the calibration procedure. Given that the

total range variation for the Electrical engineering target was 0.029 ± 0.050 m and 0.018 ± 0.045 m for the Geology target, and these targets are less than 100 m away, it seems unlikely that the PSLR would be capable of the precision required (when ranging to satellites) for an ILRS member station. Single shot precision to satellites for a majority of member stations is around 0.01 m. The best variation in a three hour ranging run (which included several averaged 1000 shot runs) over a number of months was 0.018 m, or almost twice what is perhaps an acceptable standard for single shot RMS accuracy given the performance of many stations world wide. This indicates that the PSLR is not currently capable of satisfactory ranging performance.

The particular concern is the alignment of the transmit optical components. It appears that even after a painstaking series of adjustments and tests were conducted (see chapter 4)that there was still beam propagation error induced by variations in the alignment due to the orientation of the mount. Without a well designed alignment scheme which utilises calibrated adjustments, there would be little chance of even experienced personnel achieving any success with the PSLR.

Chapter 6

Tracking considerations for SLR and the PSLR

6.1 Introduction

To successfully laser range to a satellite it is essential that a SLR system can direct a laser beam to the correct place in space at the correct time. This requires a number of factors to be in place. In this section the requirements of mount positioning will be discussed. The mount must be able to point the PSLR telescopes with a high degree of accuracy and maintain this accuracy over the entire range of movement.

6.2 Position reporting with the PSLR

The PSLR has two methods to record the orientation of the mount. Each axis of the Alt/Az mount is driven by a stepper motor and has an angular position encoder fixed to each axis of rotation. The stepper motors drive through a reduction gear box and clutch. The final drive is purely frictional with a steel wheel turning upon a steel track. The azimuth track and the elevation track are constructed exactly alike with the same thickness, depth and radius. The elevation track is a near semi-circle and the azimuth track a complete, unbroken ring.

6.2.1 Drive setups and considerations

The drivers, motors, angular encoders and gearbox assemblies for each axis are essentially identical. The final drive on each axis differs very slightly for a few distinct reasons. The first of these is the differing layout of the two axes.

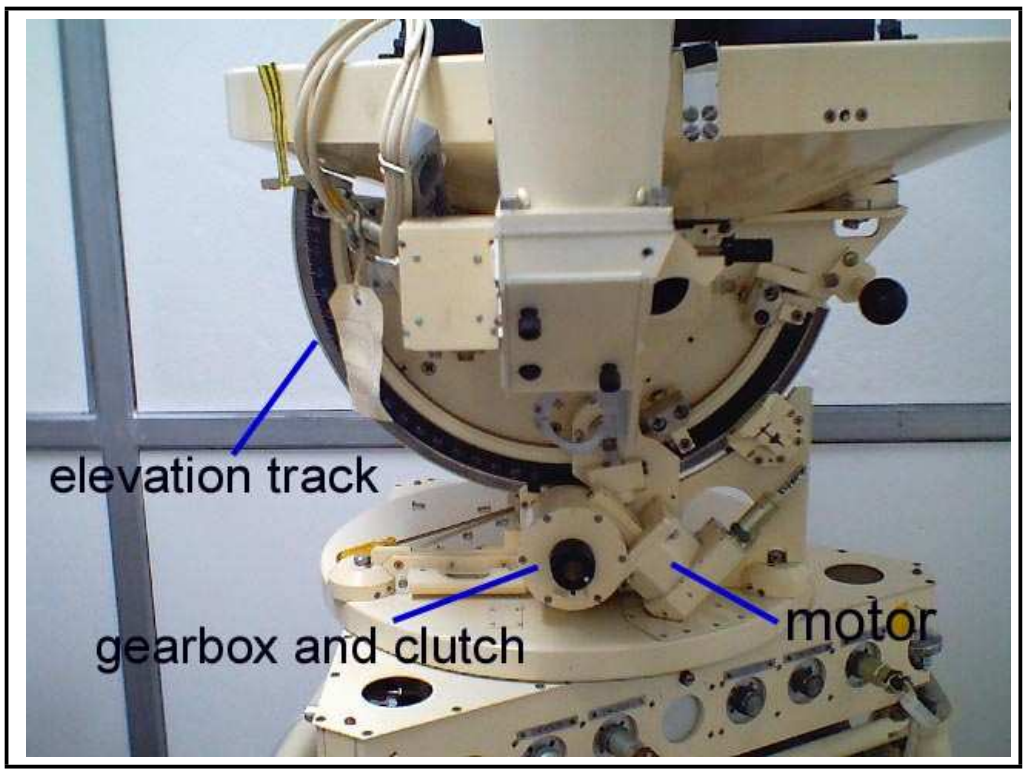

Figure 6.1: Photograph of the PSLR showing the location of the elevation motor assembly

Figure 6.1 shows the elevation track and figure 6.3 shows the friction wheel that is designed to run upon this track. The elevation friction wheel runs on the outside of the track whereas the azimuth friction wheel runs on the top of the track which is installed horizontally in the PSLR.

The azimuth drive wheel forms part of a three position pivot upon the azimuth track. The other two positions are at 120^0 separation with respect to the position of the drive wheel and each other. These idlers consist of four steel rollers with good bearings laid out in a rectangular configuration. These idlers are adjustable and apart from initial setup to align the mount, they are simply designed to support the

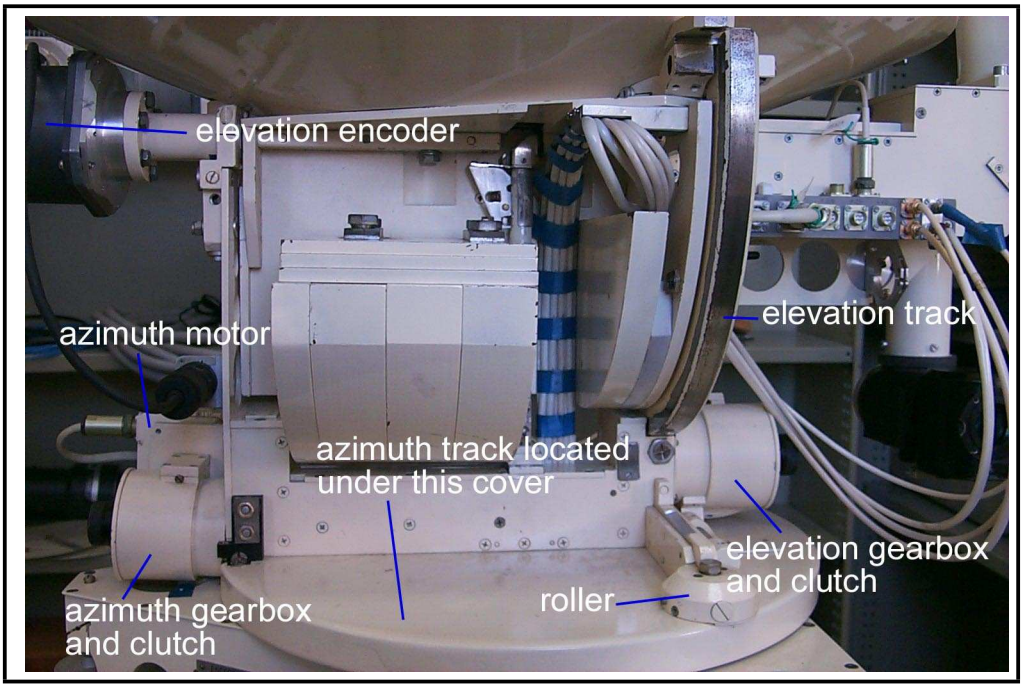

Figure 6.2: Photograph showing the arrangement of the mount motive assemblies and the elevation angular encoder

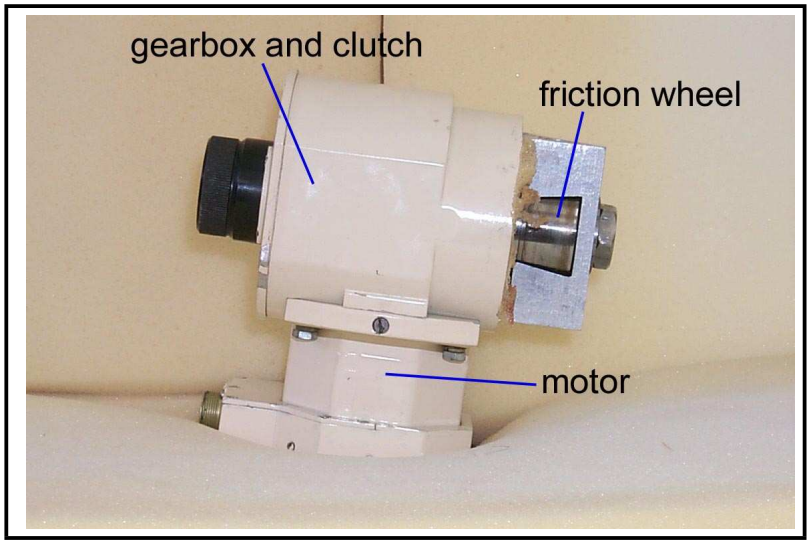

Figure 6.3: Photograph of the azimuth drive assembly removed from the mount

mount (see figure 6.4).

This means that the azimuth drive wheel does not make contact at the very edge of the drive ring.

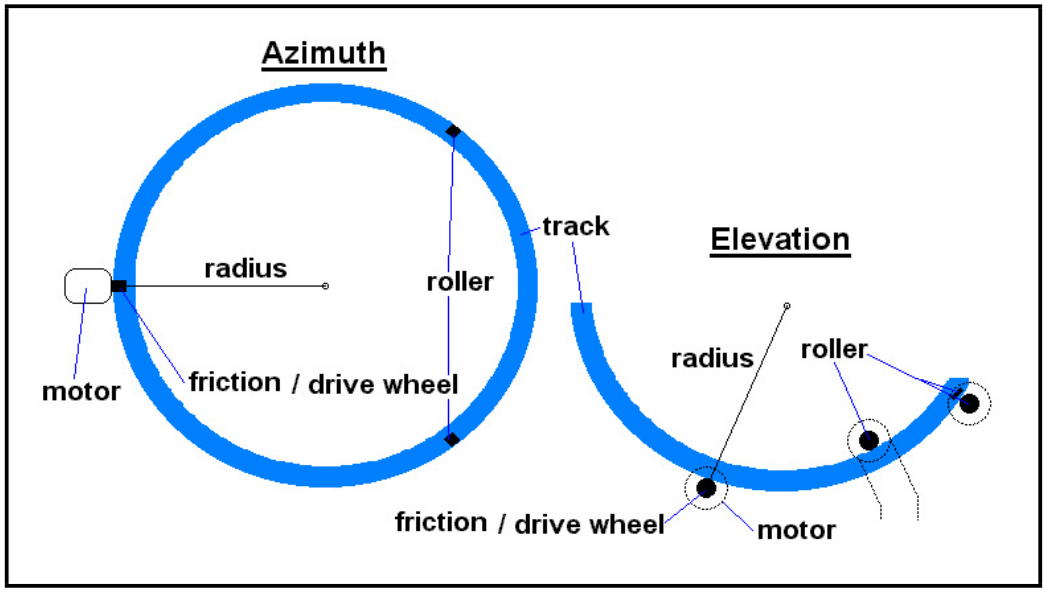

Figure 6.4: Illustration of the position of the drive wheels upon the tracks showing how each axis is pivoted

The elevation section of the mount is fixed at the non-drive end with the motive force for moving the mount applied at the semi-circular track. This track is secured by the elevation drive wheel, an idler wheel and a pinch roller which runs on the top of the elevation track to hold it in position against the drive wheel and the idler.

The elevation drive wheel runs on the very outside of the drive ring which means that the elevation drive radius is slightly bigger than the azimuth radius. Over a full revolution this small radial difference will be produce a noticeable difference with the elevation axis requiring more motor steps to accomplish the same amount of angular displacement.

The second consideration of mount drive performance is the distribution of load on each of the axes. The PSLR telescopes and associated equipment attached to the mount are not distributed evenly. Ideally the centre of mass should be located at the centre of rotation of both axes. This would allow the weight balance to remain constant regardless of the orientation of the mount. An illustration of this ideal situation is shown in figure 6.5.

The PSLR centre of mass is offset from both the azimuth and elevation centres

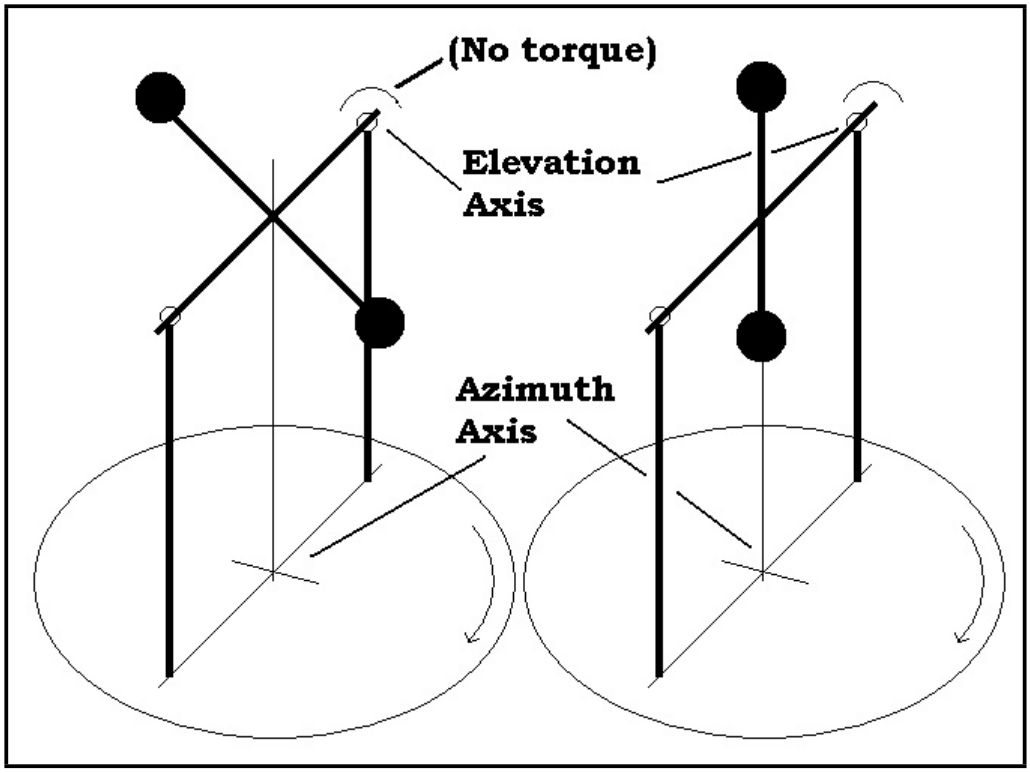

Figure 6.5: An ideal telescope would have the weight distributed about the axes of rotation. The weight in this illustration is represented by the dark circles. It shows that there is no torque on the elevation axis (when the telescope is stationary) regardless of the mount orientation.

of rotation. The unfortunate consequence of the mass distribution is constant but variable torque on the elevation axis. This causes the most trouble at an elevation of approximately 60^o. At this elevation the direction of the torque on the axis flips. As there is a small amount of slip in the PSLR drive gearboxes, this flip in the direction of torque causes the telescope to "jump" at the flip point. This makes it extremely hard to track anything at or around elevations of 60^o.

This is evident in figure 6.7 and 6.8. These graphs show the number of recorded encoder positions that each axis moves for one stepper motor revolution (2000 steps). The system was set to record the encoder position of each axis after each stepper motor had been sent 2000 step impulses (note: it does not mean that each of these steps was executed). The azimuth axis (figure 6.8) shows, apart from 7 of the 300

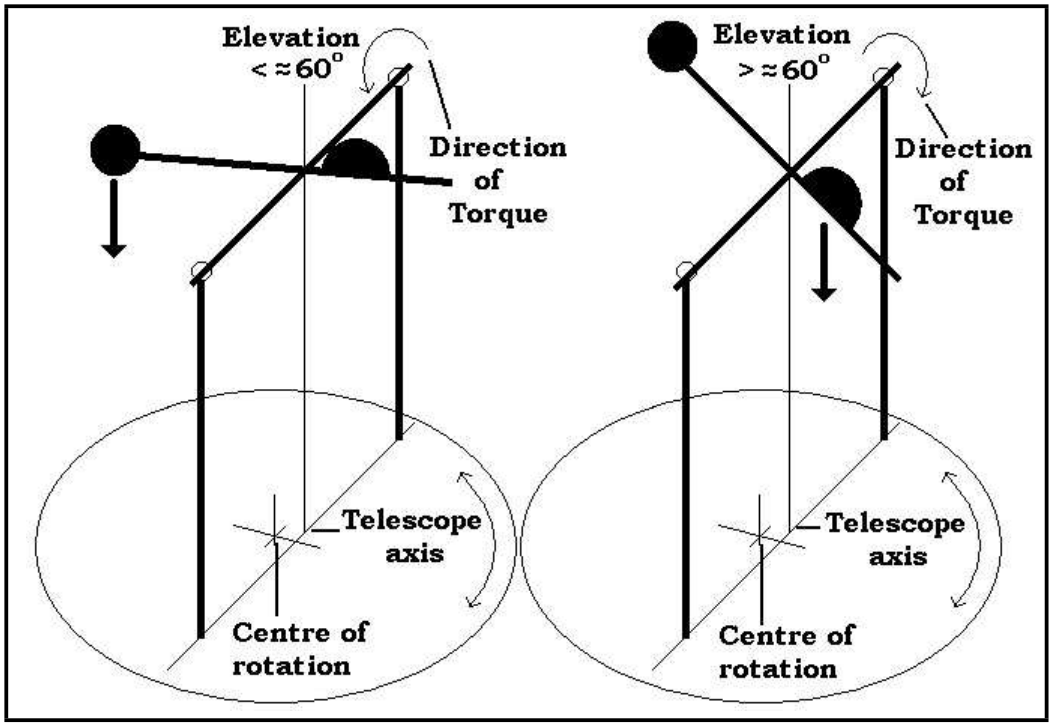

Figure 6.6: Illustration of the PSLR telescope mass distribution. The circle and semi-circle demonstrate the approximate mass distributions about the elevation axis. The axis of azimuth rotation and the telescope azimuth axis can clearly be seen to be offset. The direction of torque about the elevation axis is shown dependant on the elevation.

points, what one would expect to see if there was little or no slip on the axis. If one revolution of the stepper motor produced an angular displacement of 55.048 encoder steps (this was calculated from the data used to produce figures 6.7 and 6.8), then this equates to 0.86" greater than a reading of 55 encoder positions. The encoders will not produce a pulse unless they have passed a certain position. As the encoders used on the PSLR have a resolution of 18" this would indicate that there is just as much chance that the reading will be 54 as 55.

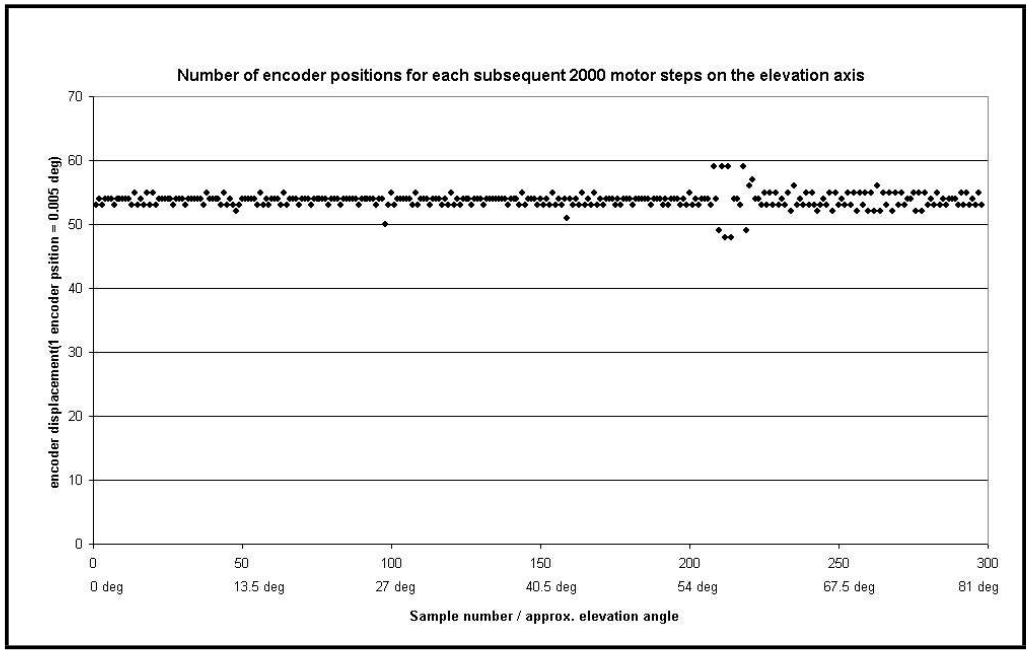

Figure 6.7: Comparison of the angular displacement of the elevation axis for each subsequent stepper motor revolution

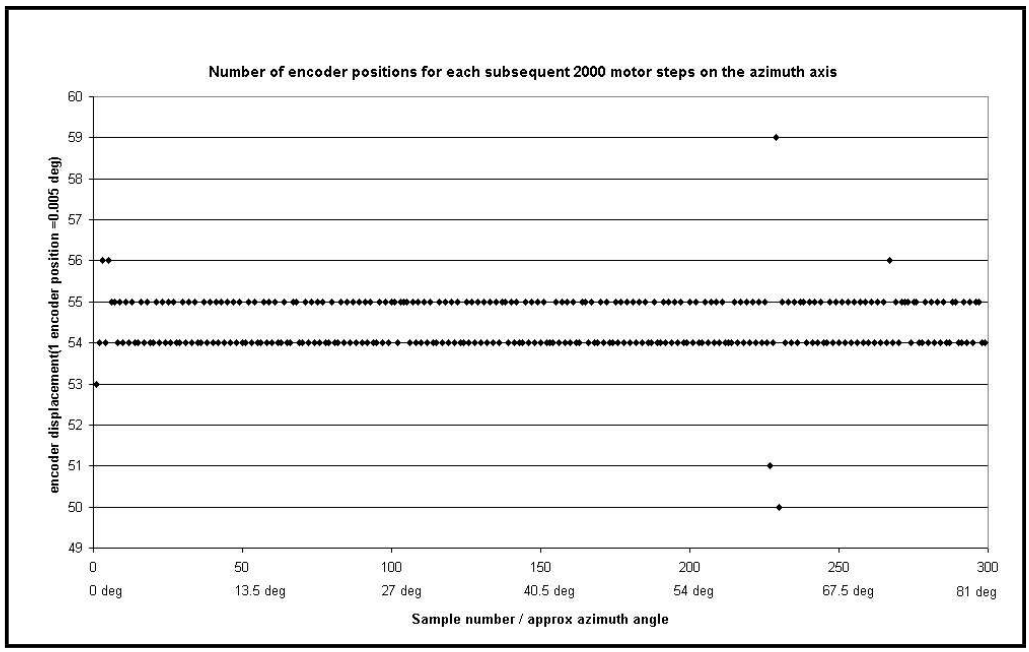

Figure 6.8: Comparison of the angular displacement of the azimuth axis for each subsequent stepper motor revolution

This difference, $\Delta\phi$ equates to $0.01^{"}$ for the calculated angular displacement for each motor step as shown by,

$$\begin{aligned}\Delta\phi &= 55 \div 2000 \times 0.005^{0} - 54 \div 2000 \times 0.005^{0} \\ &= 0.50^{"} - 0.49^{"} \\ &= 0.01^{"}\end{aligned} \tag{6.1}$$

where 0.005^{0} is the line spacing in the Heidenhain RON225 encoder.

The azimuth axis appears to be much better behaved than the elevation axis. The elevation axis data represented in figure 6.7 shows a great deal more variation, especially after the 54° mark. This test was conducted with the elevation axis being raised. When the telescope is raised to this point, there is a tipping force which is in the same direction as the motor drive direction. It would appear that the source of this instability in the elevation position encoding arises from the unbalanced loading of the mount. The counterweights cause a reversal of the tipping force during the elevation scan. The counterweights were added when the design was amended from coaxial to paraxial. The consequences for mount position encoding apparently were not anticipated nor addressed in this redesign.

The measurements discussed previously lead to a method of determining the amount of angular displacement per encoder step. Using the encoders as an absolute reference, the number of encoder counts per motor revolution (2000 steps) is plotted for each axis. A trend line is fitted to the data which shows a perfect fit in both cases. The equation for the trendline is included on each plot (figure 6.9 and figure 6.10). This shows that for the elevation axis there are 55.889 motor steps per encoder step and 55.048 motor steps per encoder count on the azimuth axis. These figures were collected for a very slow traverse on each axis (at a speed of 500 motor steps per second). This type of test was conducted a number of times for smaller traverses and at differing speeds with a different answer for the ratio of steps to encoder counts every time. To summarise the results, each reading gave a ratio over 55 and

under 56 motor steps per encoder count. The elevation axis always gave the larger value. This in turn gave an uncertainty in angular displacement per motor step of $0^0 00' 00.32''$ and $0^0 00' 00.33''$ for azimuth and elevation encoding respectively. This level of precision would be exceptional for static pointing. If the stepper motors only were used to record the mount position, this could give up to $0^0 12' 00.00"$ error over a 360^0 revolution which is totally unacceptable for SLR applications. If the stepper motors are used to mark position between encoder counts, a pointing accuracy of at best $0.33"$ is theoretically possible.

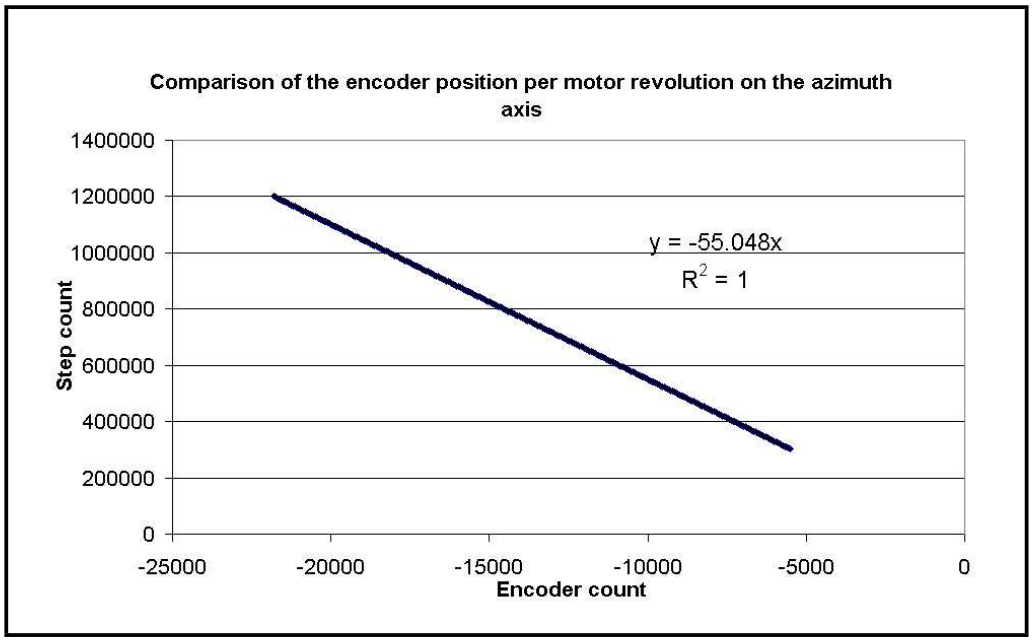

Figure 6.9: Plot of step count vs encoder count for the azimuth axis

6.3 Star tracking tests

With the PSLR control software under construction to accommodate new control cards, some method of assessing the ability of the PSLR to track targets needed to be found. Star pointing/tracking is used by SLR stations to test the alignment and pointing/tracking ability of their telescopes. Stars are ideal for this type of testing as the position relative to a terrestrial point can be calculated very precisely, the

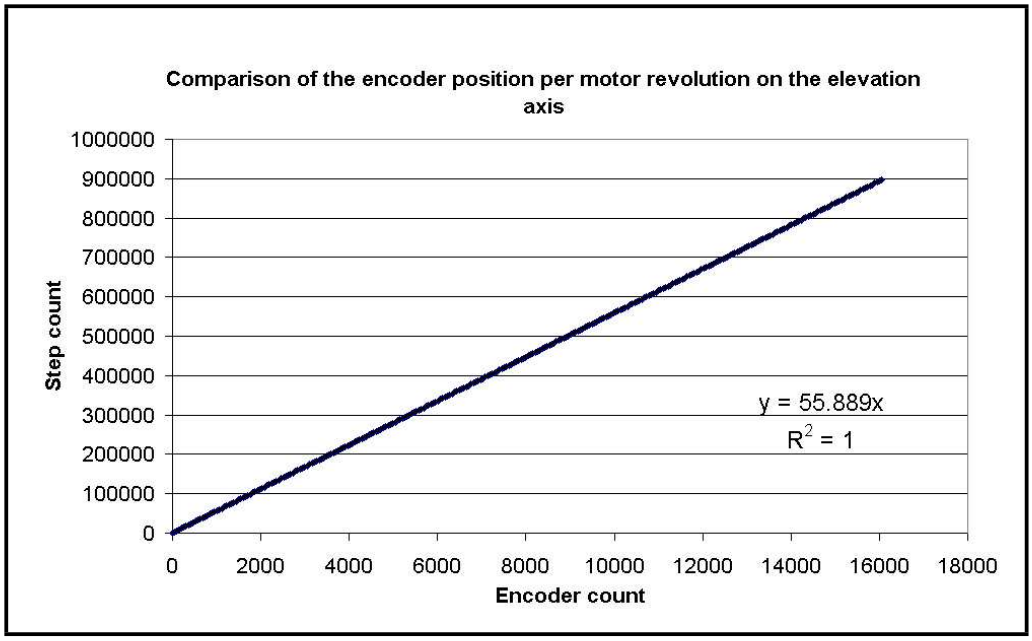

Figure 6.10: Plot of step count vs encoder count for the elevation axis

angular speed with respect to a terrestrial observer about the celestial poles is small ($\approx 15"$/sidereal second) (Trueblood and Genet, 1997), and there are stars located at every pointing orientation. If an SLR telescope system is unable to accurately track stars, it will certainly be unable to track a satellite.

With the properties of star motion relative to a terrestrial observer in mind, one approach to producing a simple tracking test for the PSLR was to write a program to track a star as it rotated about the celestial pole (CP). As stars move in the night sky, they describe a circular path about the celestial pole. In order to track a star path, the PSLR telescope only has to follow a circular path at the same rate as the rotation of the Earth. As this path can be well defined by calculation, it would give a good way to test the ability of the PSLR to track.

These positions may be defined by several reference frames. The two that relate most closely to terrestrially based telescopes are the equatorial and the altitude/azimuth (Alt/Az) reference frames.

The equatorial reference frame is based on the celestial sphere which is an imaginary sphere containing all of the stars on the inside of its surface. This sphere rotates

around the imaginary line drawn between the north and south celestial poles. The celestial sphere and poles are then figments of the rotation of the earth and the apparent movement of the stars about the earth. The location of the celestial poles in this reference frame is dependant on the latitude of the observer. The poles are located either due north (northern hemisphere) or due south (southern hemisphere) at an elevation (in Alt/AZ coordinates) equal to the latitude of observation. An Alt/Az telescope has its rotation axis aligned parallel to the imaginary line between the center of the earth and the position of observation. An equatorial telescope has its rotation axis aligned with the imaginary line between celestial poles. Once an equatorial telescope is pointed at a star only the rotation axis needs to be moved to keep the star in the field of view. The speed of movement needs to be opposite in direction to but at the same rate as the rotation of the earth. While the tracking of stars using an equatorial telescope is essentially this simple, there are complications as a result of the motion of the celestial poles caused by the precession of the earth about its own rotation axis, nutation caused by the nearby moon and solar system bodies, and atmospheric refraction. Apart from refraction, these changes occur very slowly. The period of precession of the Earth's axis is approximately 26,000 years and the nutation has several different periodic effects from 13.66 days to 18.6 years. Over the course of an evening's viewing the change in the equatorial reference frame is almost negligible. The changes due to refraction will change as quickly as the weather. With a good refraction model, observations over 20° elevation above the horizon will not be greatly affected.

As mentioned above, the PSLR telescope is aligned in an Alt/Az coordinate system so while stars viewed from a terrestrial position describe circles around the celestial poles, the motion of the PSLR telescope will not describe a circle when tracking stars as its rotational axis is offset from the rotational axis of the celestial sphere. As the task before the author was to test the ability of the PSLR telescope tracking system to follow extraterrestrial bodies and accurately report the telescope orientation, and not to create operational tracking software, a few simple methods

of generating star ephemerides were investigated. It was decided that the only truly sensible method of generating star ephemerides for simple testing purposes would be to generate coordinates in an equatorial coordinate system and then apply a coordinate transform to an Alt/Az coordinate system.

Due to time constraints, no operational star tracking software was produced. The tracking capabilities of the PSLR were tested using a far more tedious process.

This process involved tracking the stars manually by joystick control of the telescope and periodically recording the encoder positions. In order to establish a reference frame, the initial encoder positions were set as the current star position in the Alt/Az system. If, for example the initial position of Alpha Centauri was ($40^0 5' 3$" Alt, $145^0 6' 53$" Az) then the initial encoder position would be set to;

$$\begin{aligned} Alt &= round(\frac{18000}{90} \times (40.0842)) \\ &= 8017, \end{aligned} \tag{6.2}$$

and

$$\begin{aligned} Az &= round(\frac{72000}{360} \times (145.1147)) \\ &= 29023. \end{aligned} \tag{6.3}$$

All subsequent recorded positions of the encoders could then be converted back to coordinates in Alt/Az for comparison to the calculated expected position of the tracked star.

When stars were tracked manually and their positions recorded by the PSLR encoders, they were generally in good agreement with data calculated from SkyMap Pro 8 (see figure 6.11). SkyMap Pro 8 allows the user to enter an accurate observation position in latitude, longitude and height as well as entering humidity, temperature and atmospheric pressure. The figures produced by the program therefore not only account for observation position but correct for atmospheric refraction. The tracking tests revealed that the position reported by the PSLR eventually drifted

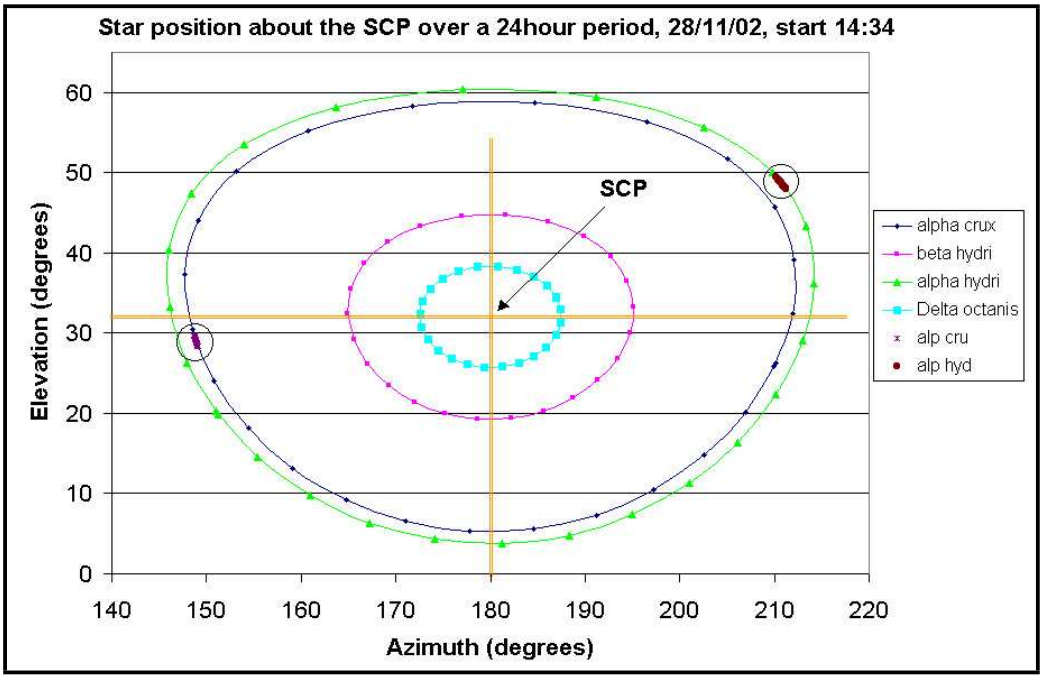

Figure 6.11: Plot of the star tracks generated by the Sky Pro 8 program. The two circled areas show actual positional data gathered by the PSLR while taking approximately 10 minute duration tracks of the stars

from the expected position. As the PSLR is able to return to a specified position with almost no error and the expected star positions were corrected for atmospheric refraction, the logical conclusion is that there were inconsistencies with the mount. These issues are discussed in detail in the next section.

6.3.1 Mount error model

The ability of a telescope to point to a specific direction in space is determined by a number of factors. The first step is to decide what is to be viewed. The second issue is to determine the reference frame of interest where and when the object is to be viewed. The telescope needs to be moved continually so that it will point in the desired direction. This requires that there be an accurate method of determining both the position and orientation of the telescope in the reference frame. The position of the telescope can be determined by GPS and survey techniques and can

be considered to be fixed. The orientation of the telescope is determined using a physical scale mounted to the axes of the telescope. This may be a setting circle but in the case of SLR is usually a positional encoder. Encoders measure either an absolute or relative position in response to some physical movement. In the case of an Alt/Az telescope they will measure the position of the axes of rotation. These positions are inferred from the reading of the encoder. Assuming that the encoders are firmly fixed to the axes of rotation and not slipping, then the movement of the encoders should directly correlate to the movement of the axes. This would be the case if;

- The encoders were perfectly aligned with the axes.
- The movements of the axes from one position to the next is always exact.
- The position reporting of the axes is exact.

This is of course not possible. Even when extreme care is taken with the manufacture of the encoder and the manufacture of the telescope, there will always be some fabrication error. As an example, the PSLR encoder uses a disk inscribed with a set of lines that are read as they pass a detector. This measures angular displacement. Any error in the position of these lines will result in angular uncertainties. The PSLR uses steel wheels on a steel track to move and support the axes. As these tracks and wheels will have fabrication inconsistencies, movement from one position to the next will not always produce the same amount of angular displacement, even if the encoders indicate that it did.

Even if the fabrication of the encoders and movement components were perfect, the alignment of the rotation axes with each other and with the selected reference frame would also need to be perfect. The elevation and azimuth axis on the telescope would need to be perfectly orthogonal with each other, and these axes would need to be perfectly aligned with zenith and the geometric horizon. This alignment would need to remain constant regardless of the orientation of the axes.

Assuming that the telescope was perfectly manufactured and perfectly aligned so that all of the axes remained aligned and the position reporting was also perfect, there is still the alignment of the optics to be considered. Most SLR telescopes contain many optical components which move in relation to one another. They have large masses located at some separation from the centres of rotation. In order for the telescope to perform its function of collecting and directing light to a specific point in the same orientation, the optical components must keep exactly the same orientation. If optical components are rotated about one another they will direct light depending on the orientation of the active surfaces or axes. As well as the SLR rotation problem causing alignment changes to optical components, there is a tendency for all materials to bend or sag when there is differential weight loading about a pivot. As a telescope that has a secondary mirror located at some separation from the primary mirror turns about the pivot point and approaches horizontal pointing, there will be more torque exerted around the pivot. This torque will reach a maximum at horizontal. As the torque increases, the amount of sag or strain also increases. This has the effect, with a telescope, of changing the alignment of the primary and secondary mirrors and changes the viewing direction of the telescope so that it will no longer be aligned with the pointing angle. Because this effect is related to the orientation of the telescope and the physical strength of materials, it is practically impossible to remove this effect by better fabrication.

The other important consideration is the atmosphere. Even with a perfectly manufactured telescope that moves and reports position perfectly and has no flexure, the pointing direction of the telescope still may not correspond to the direction of the object of interest. The atmosphere is composed of gases, water vapour, and many types of aerosols. This mixture is also turbulent and in a state of constant flux. The atmosphere is also much denser at the surface and decreases rapidly with height. As refractive index is principally related to a medium's density it follows that the refractive index has a gradient from the surface to the vacuum of space. According to Snell's law this will cause a path directional change. This path change is dependant

on the viewing angle from zenith with the least amount of path change at zenith and with maximum change at angles below 10^0. This change in apparent viewing position (from true position), at these low elevation angles, will be far greater than the angular resolution of the telescope direction reporting and may well be further from the expected direction than the field of view of the telescope. This will be the largest source of pointing error and must be taken into account. Given that atmospheric refraction can cause significant pointing errors, it must be taken into account.

Given all of these factors it might initially seem all but impossible to do high accuracy pointing and tracking of celestial objects from the surface of the Earth. The strong growth in adaptive optics in astronomy is testimony to the difficulty. With SLR the recorded pointing angle and true angle may not be the same, the only way to ensure that high precision pointing and tracking can occur is to measure the difference between pointing and seeing angle for every orientation of the telescope. In this way a correction to the pointing angle (for mount alignment errors, manufacturing errors, flexure and atmospheric refraction) can be made so that the desired object can be viewed by the telescope.

As it is both impractical and "near impossible" to perform this test for every single orientation, some compromise must be made. Using only a small number of positions spaced around the full range of telescope orientations, a model of the difference in pointing angle and seeing angle can be constructed. The model relies on the errors described above being consistent or describable with orientation. That is to say, that fabrication errors on axis tracks will always occur at the same pointing angle, the non-orthogonality of axes will not change, mechanical flexure will remain the same at the same angle, and the atmospheric refraction is able to be determined by modelling. Given consistent error behaviour, it is possible to construct a mount error model that will give, as its products, corrections to any pointing coordinates so that the actual seeing coordinates can be used.

The PSLR uses a mount error model which will correct, to some extent, the pointing errors caused by mount fabrication errors. According to the PSLR program users manual (Zarins, 1996), there are three error models available for use with the PSLR but model "0" is considered to be the best. This model (Zarins, 1996) is represented in equations 6.4 and 6.5 where dA and dE (although h was used instead of E in the referenced text, E is accepted term) represent corrections to the azimuth and elevation coordinates respectively.

$$\begin{aligned} dA = {} & a_0 + a_1\cos(E) + a_2\sin(E) + a_3\cos(2E) + a_4\sin(2E) \\ & + a_6\cos(A) + a_7\sin(A) + a_8\cos(2A) + a_9\sin(2A) \\ & + a_{10}\cos(10A) + a_{11}\sin(10A) + a_{12}\frac{\cos(A)}{\tan(E)} \\ & + a_{13}\frac{\sin(A)}{tan(E)} + \frac{a_{14}}{\cos(E)} \end{aligned} \tag{6.4}$$

$$\begin{aligned} dE = {} & b_0 + b_1\cos(E) + b_2\sin(E) + b_3\cos(2E) + b_4\sin(2E) \\ & + b_6\cos(A) + b_7\sin(A) + b_8\cos(2A) + b_9\sin(2A) \\ & + b_{10}\cos(10E) + b_{11}\sin(10E) + \frac{b_{12}}{\cos(E)} \end{aligned} \tag{6.5}$$

The terms a_0 and b_0 are constant and represent known offsets (if any) of the azimuth and elevation axes. These terms can be determined by star pointing but if this is done within the PSLR control program, the determination process is separate from the mount error model. The other constant terms $a_1 \ldots a_{14}$ and $b_1 \ldots b_{12}$ are produced from a least squares data reduction calculation performed by the program which fits the data from a number of star observations to equations 6.4, 6.5. Some of the terms represent some physical attributes of the mount which will affect the pointing direction of the telescope. An example of this are the terms $a_{10}\cos(10A) + a_{11}\sin(10A)$ and $b_{10}\cos(10h) + b_{11}\sin(10h)$ which attempt to compensate for eccentricities of the azimuth and elevation drive friction wheels respectively. Other terms in the error model are correlated in that a physical parameter is described by more than one term.

The mount error model used with the PSLR does not have any effect with elevations less than 11 degrees. This means that any offsets to ground targets have to be either modelled separately or directly specified. It will not make any significant difference to the tracking performance of the system as tracking under 20 degrees elevation is generally not attempted.

Tests on the tracking performance of the PSLR were performed to determine to what extent the absence of a mount error model would affect the tracking accuracy.

This required that a set of bright stars visible from the Curtin University Bentley campus could be found and tracked by the PSLR. Much of the computer code used in the initial tracking test was modified to enable this to be achieved. It also required the use of the TM1 GPS clock, the SR620 time interval counter, two CCD cameras (one mounted to the main telescope, the other to a spotter scope), and other ancillary equipment.

In order to begin the tests on a given night the telescope was referenced to a single star. The position of this star at a given time was calculated using the Sky Map Pro 8 program. The star was centered in the cross-hair (generated in the image by the CCD camera) of the main telescope and when the specified time was reached, a button on a joystick was activated and the position of the telescope's cross-hair was set to the star coordinates. The mount was then moved by the control program to find the reference marks (i.e. relative origin) within the encoders.

The PSLR angular encoders are relative position encoders. Absolute position encoders have schemes in place that will allow the orientation of the encoder to be determined almost as soon as a few pulses are processed. Relative position encoders merely provide direction and amount of displacement from one position to the next. To determine the absolute position careful count must be kept so that reading from the encoders can be referenced to a known position or origin. This process is performed when the PSLR is referenced to a star. In order that these encoders do not have to be referenced each time they are used, a reference mark is placed within the encoder. There is only one reference mark so if the encoder is

rotated a full 360^0 from any point it will always be found. As long as the encoder and the load do not move with respect to one another, once the position of the reference mark is determined, the load orientation can be accurately referenced.

When the reference marks are found by the PSLR tracking program these positions, relative to the reference star are recorded. Once the mount has been referenced in this manner, the telescope can be pointed to any required position. Generally, the sequence involved the telescope being pointed back to the star that was used to reference the mount. Because the star had moved since it was used to reference the mount, a new position for the star was retrieved from the Sky Map program. These coordinates were entered by the user and the telescope moved to the required position. This does not need to be absolutely perfect as the star only needs to end up in the field of view of the telescope as precise positioning is accomplished with manual joystick control of the mount. Once the telescope has finished this automatic move the joystick can be used to move the telescope from the current position to centre the star at the cross-hair. This is the point when the actual tracking begins. The object of the data gathering process is to record positional information and the time of position of a star so that it can be compared with calculated data at a later date. When the star is centered, a button on the joystick is activated. This button caused one of the digital outputs on the mount control card to change state and activate a relay as well as reading and storing the position of the mount encoders. The relay activates the SR620 timer. The timer was connected to an ancillary computer which was running another program designed to collect data. When the SR620 was activated it sent temperature and humidity readings to the ancillary computer. The program then read time from the GPS time machine and atmospheric pressure from the Druck barometer. Each star position was not only timed stamped but had a set of atmospheric data. As there was some time delay between the time reading and the pushing of the joystick button, the time reading had the delay time removed by the ancillary computer program (determined by testing). The star was tracked for approximately 10 minutes with positional readings taken at about 30 second

intervals. When the tracking for a particular star was finished, manual control was terminated and the user specified another star to be tracked. The mount automatically moved to the next star position. Manual control was reestablished after the automatic move as the program required that the new star position at the correct time was used to reference the mount. When the joystick button was activated, the mount automatically found the encoder reference positions with respect to the new star reference. The star tracking and data gathering process for the reference star was then repeated as per the method described above. For each new star tracked, this process was repeated. This gave numerous readings for the encoder reference positions and sets of tracked stars which were referenced to themselves. If the mount fabrication and setup was perfect then the positions of the encoder reference marks determined by each star should be the same.

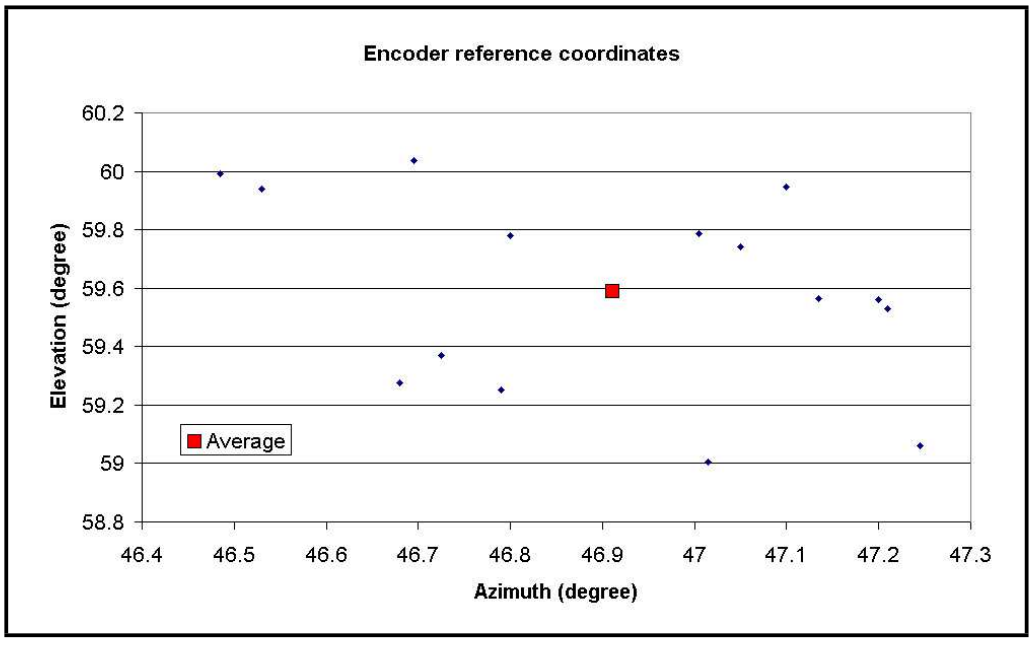

Figure 6.12: Encoder reference coordinates determined by referencing the mount to a single star. The average value of all the encoder reference position (not including the coordinate from Alpha Gruis) is clearly labelled.

Figures 6.12, 6.13, 6.14 show the position of the encoder reference marks after a different star located in a different position in the sky was used to reference the

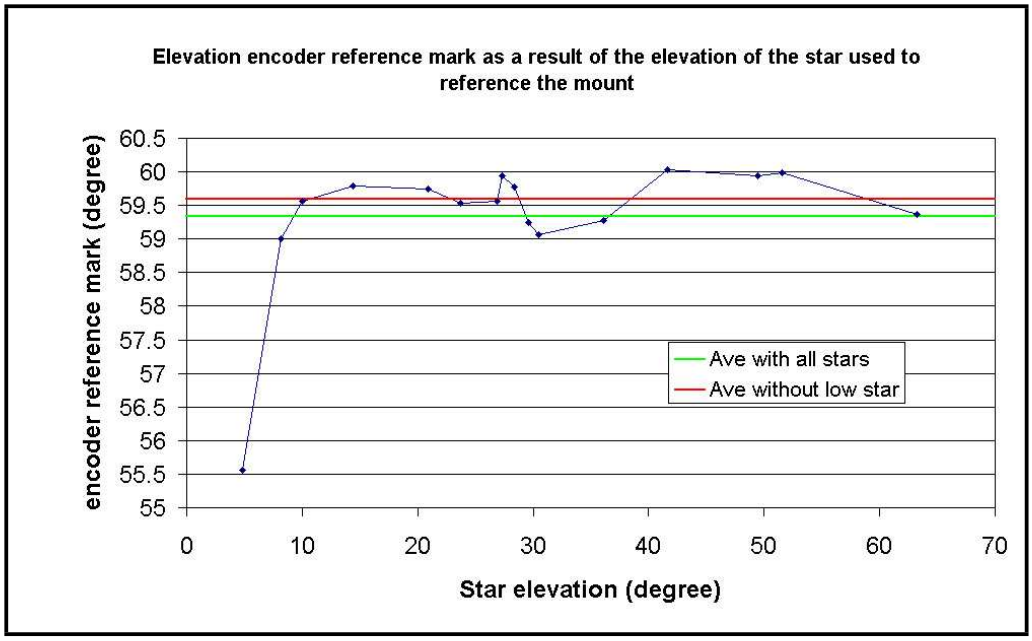

Figure 6.13: Illustration of the repeated determination of the elevation encoder reference position determined from referencing the mount using a single star. The encoder reference position is shown as a function of the initial elevation of the reference star.

mount. As the reference marks in the encoders will always be in the same physical position, it gives a very accurate way to compare differences in pointing and seeing angle for different orientations of the mount. The graph in figure 6.12 gives a coordinate in Alt/Az for the reference positions of the encoders for each star with the average of all of the positions clearly marked. This shows a large amount of variation but each point is less than a degree away from the average. Figures 6.13 and 6.14 show how the elevation or azimuth encoder reference marks varies with the elevation or azimuth of the star used to reference the mount. In each case, the elevation or azimuth figure used on the abscissa was taken as the first position recorded during the manual star tracking tests. The large variation in position seen in both graphs for one particular point was for a star at very low elevation. At such low angles, it is very difficult to even calculate the seeing position due to atmospheric refraction. The coordinates of this star entered as the mount reference position would have been some some distance away from the actual position and thus

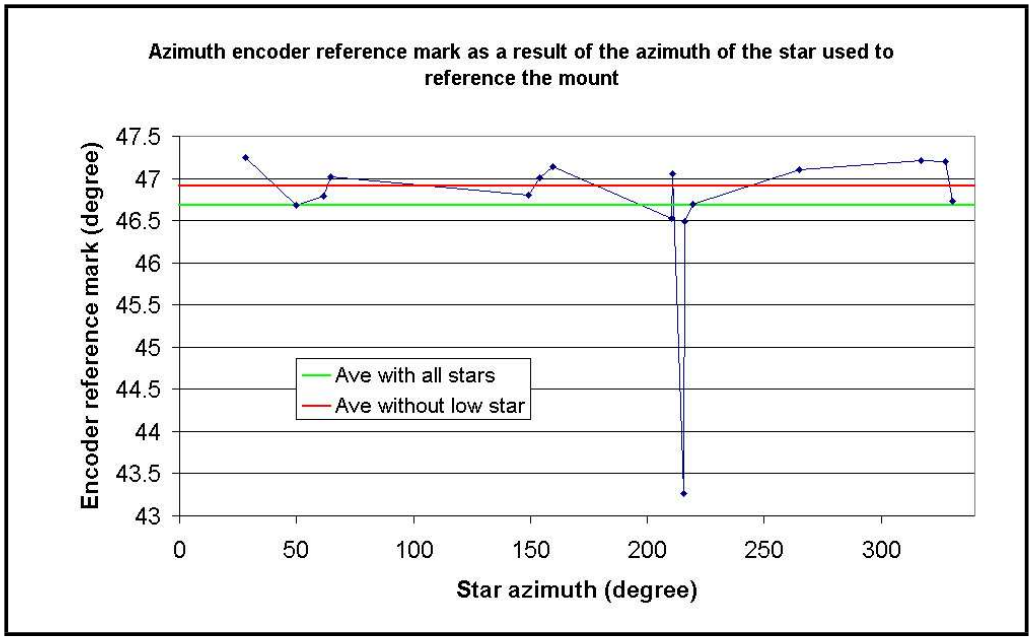

Figure 6.14: Illustration of the repeated determination of the azimuth encoder reference position determined from referencing the mount using a single star. The encoder reference position is shown as a function of the initial azimuth of the reference star.

the encoder reference position for this star is quite a long way from the others. Any star under ten degrees elevation above the horizon will be suspect due to excessive refraction error. Both of the low stars shown in figures 6.13, 6.14 should be ignored when calculating an average. Excluding the low star, figures 6.13 and 6.14 show that all of the reference positions are within 0.5° of the average. This indicates that the mount axes are poorly aligned to the Alt/Az reference frame. The sharp bump ($\approx$ transition of 1° in error) in the graph from figure 6.13 around the 30^0 mark shows a lot of variation over a small part of the sky. This would indicate that there may be a mechanical problem with the mount at this elevation. Variation is expected but this variation should be far less drastic over a small range of elevations. Time permitting, the mount could have been adjusted and these tests repeated to gauge the effect or action taken to remedy this irregularity.

The stars used for the tests were tracked for around 10 minutes with the position fixed every 30 seconds or so. Data were then generated using SkyMap Pro 8 so that

the short track could be compared to expected ephemeris data. If the mount setup is good the actual and calculated tracks should be nearly identical. The results of two such star tracks can be seen in figures 6.15 and 6.16.

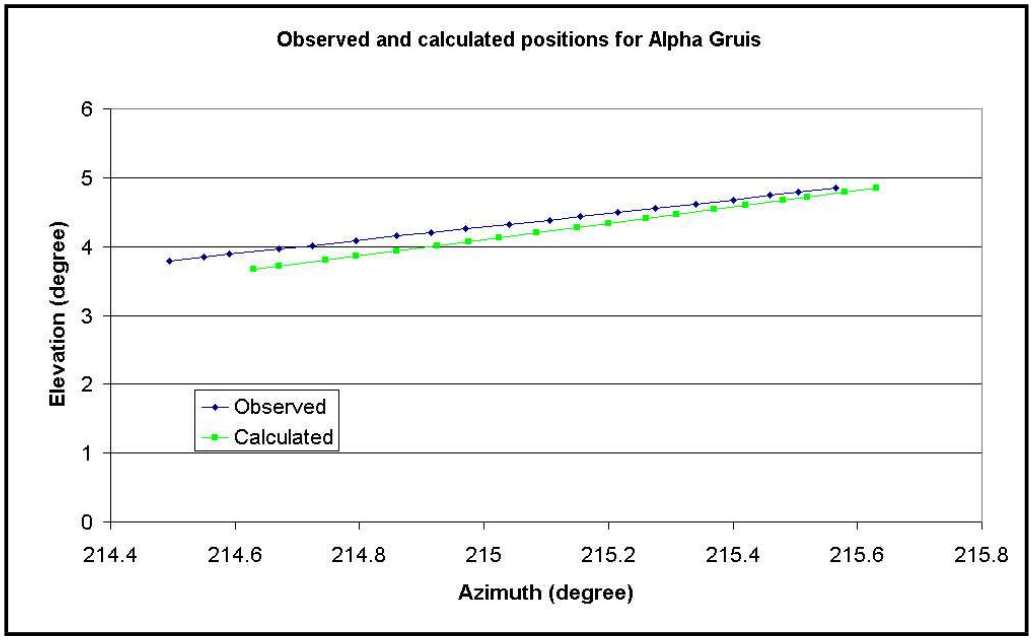

Figure 6.15: This shows the observed position of the star Alpha Gruis and the position calculated using Sky Map Pro 8, over time. The initial observation is shown on the top right hand side of the graph with consequent observation displayed to the left of the figure.

Figure 6.15 shows the graph of the actual observed coordinates of a low elevation star as well as the calculated coordinates for the star. It can be seen from this plot that not only are the comparative points separated significantly from each other but they diverge as the star is continued to be tracked. The mount was referenced to this star just before tracking was commenced. The mount was then sent to the encoder reference marks before returning to track the star. On its return, the mount had to be manually relocated to find the star a great deal further than for the higher stars. This would indicate that the calculation of star ephemerides at low angles is error prone. In this plot the first observations of the star are those to the far right of the plot. This plot shows that it is very difficult to calculate precise star positions at low sky elevations and thus these stars should not be used to identify mount parameters

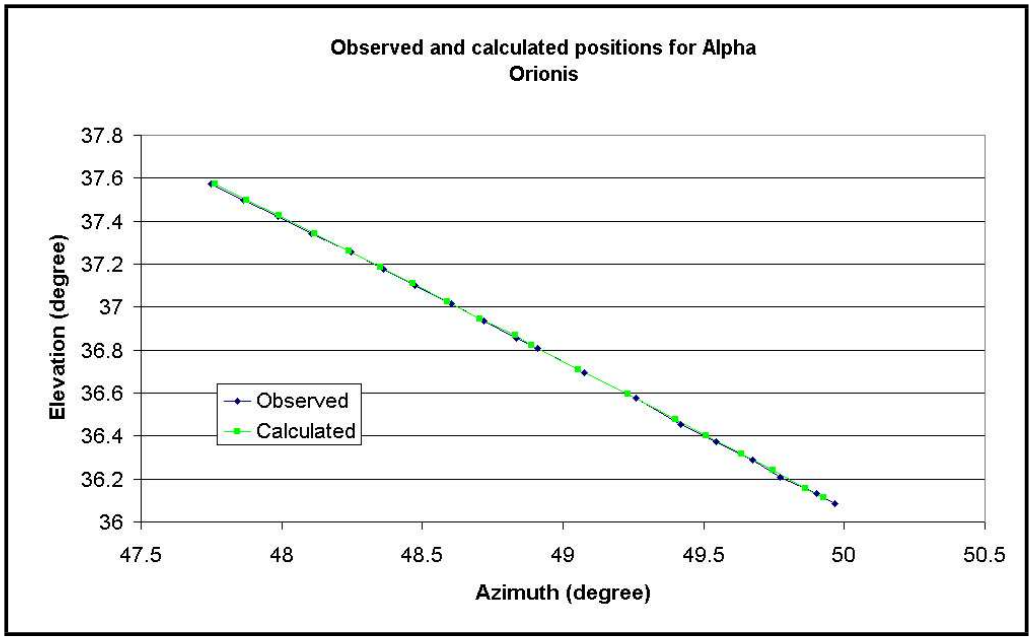

Figure 6.16: This shows the observed position of the star Alpha Orionis (Betelgeuse) and the position calculated using Sky Map Pro 8, over time. The initial observation is shown on the top left hand side of the graph with consequent observation displayed to the right of the figure.

because the positional information calculated is suspect.

Figure 6.16 shows a similar plot of the star Betelgeuse which had an elevation on the night of observation that was acceptable for star positional calculations. The initial points have good agreement between the observed and the calculated points. After these few minutes of observation, the two plots, although following approximately the same path, are drifting apart, especially in azimuth. This is principally due to the fact that the star is actually moving more in azimuth at the time of observations and as such is farther from the point at which the mount was referenced to the star. This drift would not be caused by refraction over such a small angular displacement and over such a small time period so it must be a result of the mount referencing. It shows that to be able to effectively track stars and other celestial objects, the PSLR requires implementation of an effective mount error model as well as significant improvement in the mount alignment.

6.4 Conclusion

Although the PSLR code gives indication on the form of the mount error model and how it is formed, the process of fitting observational data to the model is buried within the C++ code. As the PSLR project did not have a great deal of expertise in C++ it made the task of extracting the error model process far too time consuming to complete.

The tests, while not resulting in the preparation of an error model have shown some useful results:

- The position of the encoder reference marks with respect to a number of known star positions have shown that the mount is quite poorly aligned as the stars plotted in figure 6.12 shows a standard deviation in elevation to the mean of 0.253° and a standard deviation in azimuth of 0.337°. This would give a pointing error to LAGEOS satellites of over 35 km.

- It has shown that the PSLR telescope is capable of reasonable accuracy pointing and positioning when stars are first tracked after referencing the mount to the star (see figure 6.16). For the initial 10 points on this graph the error between the calculated data and the observed data vary between 0^o and 0.015^o. This relates to a variation of 3 encoder positions or a timing error of less than 4 seconds over a 5 minute period. This would give a maximum pointing error to LAGEOS of approximately 1.57 km. This would indicate that the motor drive, angular encoder systems and electronics would be capable of providing adequate tracking capability with a decent mount.

- The effect of atmospheric refraction on satellite tracking can be significant. Figures 6.13 and 6.14 show that ephemerides calculations at low angles can produce several degrees of pointing error.

At the completion of the tracking tests for the PSLR the major recommendations would be:

1. To completely realign the axes of rotation to enure that; a.) they remain orthogonal with respect to each other, and b.) the axes are aligned to the local Alt/Az reference frame.

2. Remove the counterweighting to improve the unwanted torque induced on the mount drive gear.

3. Conduct an extensive mount modelling program after changing the mount.

The PSLR system, at the completion of the tests at Curtin University was not able to track celestial objects automatically, and would require a great deal of work to accomplish this task.

Chapter 7

Summary, future recommendations and conclusions

7.1 Current or proposed improvements to SLR

There are a number of different innovations on the standard SLR technology/methods that are being developed. Most of these new approaches and equipment can be separated into categories based on their role in improving SLR.

7.1.1 Automation

The single biggest cost in running an SLR system is personnel. Some stations have streamlined their operations so only one person is required to run the instrument at any time. Many stations that had 24 hour operational coverage have reduced the number of working hours in an effort to reduce costs. The ultimate solution of this problem is to permanently remove the need for an operator.

The current plan of many stations is not only to remove the need for an on-site operator (as some systems can be operated remotely), but to remove human input completely in the day-to-day running of the laser ranging system. The SLR2000 refers to this approach as a pseudo-operator (PO). In essence, once the PO is pro-

vided with a tracking priority list, it will not only automatically track the satellites, but decide which satellites to track and when. If, for example a LEO satellite with a short orbital arc over the tracking station occurs during a long LAGEOS run, the PO must decide if it will break off the LAGEOS run, attempt to track the short LEO run and return to re-track LAGEOS. A human operator, from many years of experience, may know that the particular satellite with the short arc takes several minutes (on average) to acquire before it can be successfully tracked. In the case where it will only be visible to the station for a few minutes, the operator may decide that there is little point in attempting to track it. Some satellites are far easier to acquire than others and the actual acquisition of each satellite may require specific types of adjustments to the telescope position. The PO must either be programmed with this information, be able to learn for itself as to the quirks of the satellite-station relationship, or find a more logical and effective acquisition scheme.

Automation is easy, whereas machine based autonomy of operation is another matter and may take some years to be perfected. Examples of SLR systems that employ or wish to employ this type of approach are the SLR2000 and Mount Stromlo stations. Mount Stromlo station (before a terrible bush fire destroyed it) was able to operate autonomously for over 100 hours a week showing that long term operation of autonomous systems is more than possible.

7.1.2 Two colour laser ranging

Hardware used in modern SLR systems is now able to deliver detection and timing at such a precise level that system-based delay determinations can be reduced to sub-millimeter levels. The largest sources of error in laser ranging are all external to the laser ranging station. The largest source of error and the most difficult to remove is atmospheric error. The atmosphere is full of gaseous and particulate media which move, mix and change in a chaotic manner. In general these effects can be predicted from simple ground based measurements. Although these predictions are generally quite good (at higher telescope elevations) they are not perfect and are less

effective at low elevations. The only way to accurately correct for the atmosphere is to measure the delay along the path of the ranging laser. The only conceivable way to accomplish this is to remotely sense the path of the ranging laser.

The delay associated with the atmosphere, as well as being affected by the constituents of the atmosphere, is also wavelength dependant (for optical frequencies). The frequency-dependant atmospheric delay allows a direct measurement of the atmosphere by simultaneously measuring a range using two different wavelengths and comparing the difference in propagation time. The refractive index for a specific wavelength can be estimated using the equations 2.7, 2.8, 2.9, and the path length difference can be estimated from the refractive index calculation using equation 2.10 (see section 2.4.1.2, page 28).

This type of atmospheric delay calculation requires the use of streak cameras as the difference in propagation time of the two signals is in the order of picoseconds. Other methods have recently been proposed to evaluate the atmospheric delay parameters using conventional detectors and two colour transmission. One such method was proposed by (Riepl, 2001) where range estimates are calculated by separate normal point reduction of each ranging wavelength returns. The data are then treated in a manner similar to using equations 2.10. Given that it is nearly possible to reduce normal point data to millimeter or sub-millimeter levels, this type of approach is likely to become more and more feasible as technology and instrumentation improve. It will provide enough precision to separate the propagation times so that the atmospheric delay can be extracted from the data.

7.1.3 New target types

With NP accuracy for some new stations approaching the sub-millimeter level, error sources that were previously too small to influence measurement accuracy now need to be examined. A great deal of analysis has been undertaken to determine the effect of targets on the ranging error. Most target arrays are composed of many CCRs (Corner Cube Reflectors) which will contribute reflected photons to the return beam.

This multiple origin return beam can cause range error due to the distorted pulse shape that results. Experimentation and modelling have been carried out so that the target signatures for the specific satellite can be determined and compensated for in the range determination. These calculations depend on whether a multiple or single photon detector is used. The examination of target signatures has allowed NP reduced data to achieve range accuracy at 1mm and below. With sub-millimeter precision achievable due to improvements in other areas of SLR science/technology, it is not only target effect that need to be examined, but other, more subtle effects such as the velocity aberration of the return signal due to CCR impact on the returning wavefront. This velocity aberration is called the Fizeau effect. The Fizeau effect is a result of EM radiation passing through a moving (with respect to an observer and the EM radiation origin) medium. With SLR, this moving medium is the CCR glass. If it is assumed that the CCR is travelling orthogonally with respect to a transmitted beam, and that during time that the beam is being reflected from the CCR, the CCR travels some distance in the orthogonal direction, then the reflected beam will not only be reflected on a slightly different path but be smeared as the trailing edge of the laser pulse sees a different CCR orientation than the leading edge. The return wavefront from the CCR will not be orthogonal with the transmitted beam even though the return beam travel is orthogonal. The wavefront will have tilted with respect to the direction of propagation. The velocity aberration will affect the range determination up to a high fraction of a millimeter. As previous SLR systems could not achieve anywhere near this accuracy, and other error sources had a great deal more effect, the Fizeau effect was ignored. Now that SLR systems are approaching sub-millimeter accuracy, the Fizeau effect will limit further precision gains. One answer to this problem is to use a different target system that is less susceptible to the Fizeau effect than CCRs. One new target type that has been proposed is a spherical reflector based on the Luneberg Lens (Burmistrov et al., 2002).

The Luneberg lens has no specific optical axis but will focus any parallel beam

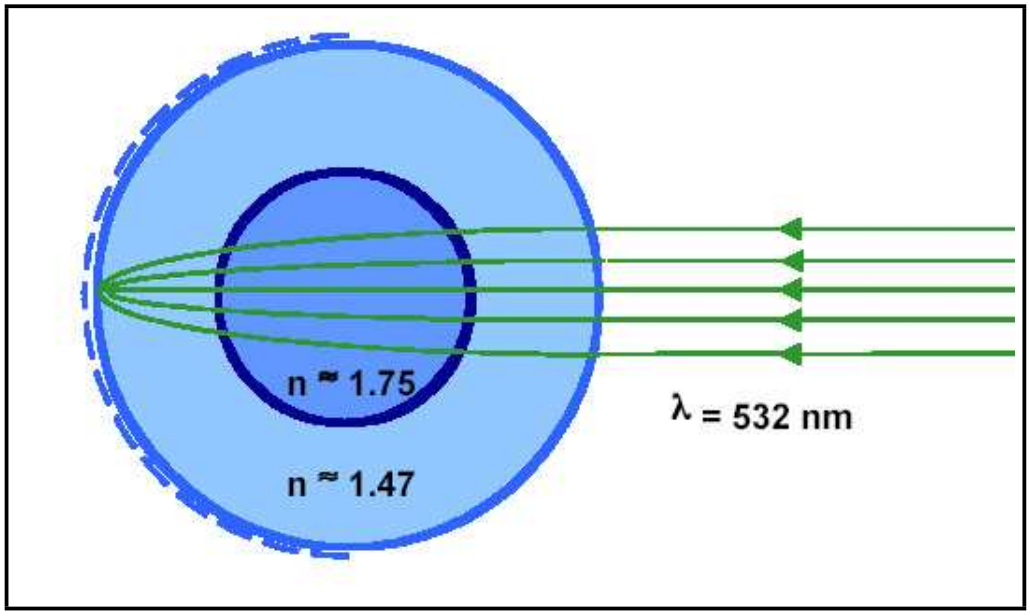

Figure 7.1: Illustration of the spherical Luneberg reflector on the METEOR-3M spacecraft.

of light on the rear of the lens. This focus condition is independent of direction. If the rear edge of such a lens is reflective then the focused parallel light will retrace its original path. As this effect is independent of orientation, the leading and trailing edges of a laser pulse will see exactly the same sort of reflective surface and as such will be reflected with virtually no velocity aberration. The target effect of this reflector is less than 0.1mm and this is attributed to path length variations in the reflector due to temperature variation (Burmistrov et al., 2002).

This type of reflector is proposed as a next generation geodetic satellite. This would comprise a passive spherical reflector with an external diameter of 214 mm and a mass of 14.5 kg.

7.1.4 High repetition rate, low energy lasers

With the major expense in SLR being skilled personnel to run the stations, and the current economic climate not favouring large yearly budgets, new SLR systems are being fully automated to reduce long term running costs. To help achieve these

ends the selection of the type of laser used with an automated system is highly important. Ideally any laser used in an automated facility would have the following characteristics;

1. low maintenance,
2. eye safe inside and certainly outside of the facility,
3. low voltage and low power consumption, and
4. able to produce the comparable signal level as higher powered systems.

These requirements can be met with a high repetition rate laser which will provide a comparable signal but, as each shot has low energy and consequent power, it does not exceed eye safe levels.

In order to reduce laser maintenance, the easiest method is to reduce the number of moving parts and limit the power required to run the laser. As solid state lasers are very inefficient and most of the wasted energy is in the form of heat, high powered lasers require a liquid cooling system. If a laser does not require liquid cooling, it greatly reduces the amount of moving parts.

Diode pumped lasers are ideal as diodes are much more efficient than flashlamps and do not require high voltage output power supplies. This will both reduce the size and weight of the system and decrease the laser down time as pumped diodes are less problematic than flashlamps so require less corrective and preventative maintenance.

In order to produce a signal level comparable with traditional pulsed systems, the laser must fire at a much higher repetition rate. The laser source to be used with NASA's SLR2000 system follows such an approach. The laser will have a repetition rate between 1 - 2 kHz and an energy per pulse around 220 μJ at a wavelength of 532 nm (Degnan, 2001). With losses through the optical path this will give an energy per pulse at the output aperture of 130 μJ which is under the eye safe level for a pulse train in the U.S.A. This type of pulse regime would result in a total energy output per second of 0.26 J. This would be equivalent to a normal Nd:YAG

laser ranging source operating at the normal 5 Hz rate with an energy per pulse of 52 mJ. The PSLR has laser source which is large compared to many SLR systems, having an output pulse energy of 130 mJ and an energy per second rating of 0.65 J (5Hz). At 10 Hz, the energy per second exceeds 1 J so the CW equivalent power is around 1 W. This type of laser is decidedly not eye safe and the minimum safe distance for this laser to preclude ocular hazard is several kilometers. Such systems require expensive radar equipment to avoid aircraft and can also have a declared aircraft exclusion zone such as exists for a forty kilometer radius around MOBLAS-5 in Yarragadee, Australia.

The difficulty with using such a high repetition rate (especially with a coaxial system) is detecting and timing from return pulses. Using a traditional interval counter this is not possible. The traditional sequence is to transmit, receive and time for one pulse before the next is transmitted. This allowed the use of electronic filters, hold-off pulses and gating levels to be employed to time only on the return pulse and to ignore any noise. With LAGEOS satellites, the highest repetition rate that will allow only a single pulse to be in transit at any time is approximately 14 Hz (at a maximum range of 70 ms). The allowable rate is far less for high satellites such as GPS and Glonass. With the high repetition rate, low energy laser not only are several thousand pulses in transit at the same time but the return levels are often not much higher than background noise. For this reason an event timer is used to record the return pulses referenced to a start epoch. While gating the detector on and off between expected return pulses reduces false triggering due to the background, it is not possible to completely compensate for the lower signal to noise ratio with high repetition rate lasers. The actual return can then be separated using statistical methods. If the system is performing well then the signal will be quite easy to identify, even with false triggering. Use of this approach is evident in figure 7.2 (Greene et al., 2002) which shows a track of a piece of space debris. The path of the debris is clearly visible through the noise.

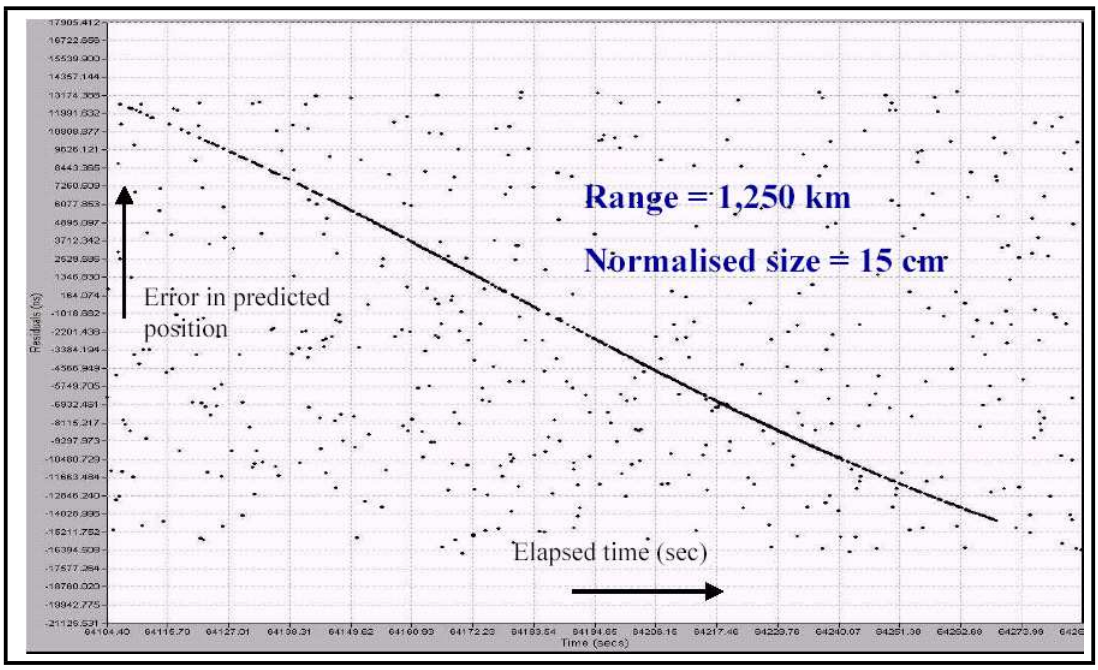

Figure 7.2: Example of removing the obvious signal from background noise when collecting every return with a high repetition rate laser.

This type of laser source is designed to be used in automated systems to reduce the need for aircraft detection and to remove the need for specialised personnel for preventative maintenance as there is no optical or electrical danger from the laser while inside the SLR2000 structure. The reduction of cost in SLR is essential as it is not a financial priority with Governmental agencies dispensing from the public purse for non-profit science. This is another step in automation of the SLR network in an effort to remain viable into the future.

7.2 How the PSLR would compare as a working system

The PSLR in its current incarnation is 8 - 10 years old. While it has some new components, it has not been substantially improved since 1994 - 1995. This is most apparent in the choice of detectors for the PSLR. The instrument still uses a standard

PMT as the main return detector. While its small size and cost are advantages, it is one of the largest contributing factors to the lack of performance.

The laser is physically small compared to most systems with the same or even less output energy. It requires a rack mounted power supply and heat exchange unit which are heavy. While these are not hard to move, a portable system would benefit from a smaller, lighter laser system as it would be easier to mount and improve the ability of the instrument to be modularised for ease of transport.

The interval timing and conditioning electronics are certainly adequate for the purpose for which they are used and exceed the the capability of both the start and stop detectors (ie rise time, transit times etc). The station timing was provided by a caesium frequency standard slaved to a GPS timer and a time code generator card slaved to the caesium. This system was theoretically able to provide station time to 100 ns RMS to UTC. This also exceeded the requirements of the rest of the system.

The positioning reporting scheme used angular encoders with a positional accuracy of $\pm$ 0.0025° with encoder positions every 0.005°. As the PSLR used stepper motors to position the mount, it is possible to divide each encoder position by the number of steps from one encoder position to the next. This then gives the capacity to register the position of the mount to approximately 0.33". This is far better than the actual capacity of the optical system to point at a celestial object. The Galil 1720 indexer card has a quoted long term velocity accuracy of 0.005% which would relate to approximately 0.56 steps per second when either axis is moved at a velocity of 1° per second or 11200 steps per second. This far exceeds the ability of the PSLR to position the mount, even to a static position.

The main foreseeable problem with the PSLR (if it was operational) would be with the opto-mechanical components. The main mirror is very large at 62 cm diameter, (roughly the same size as the MOBLAS systems) with the secondary mirror fitted about a metre above the primary. Both these mirrors, as well as the output telescope and most of the output optics, sit above the centre of rotation of the elevation axis. This requires that the elevation axis is heavily counter-weighted.

With the elevation axis pivoted as it is, it is not possible to keep the centre of mass of the elevation axis at the centre of rotation regardless of how the instrument is counterweighted (see section 6.2.1 and figures 6.5, 6.6, 268). This means that as the telescope is tilted, the drive wheel is subject to torque from the telescope. The direction of torque changes as the mount is moved past the balance point. If there is any loss in positive drive within the gearbox/motor system when the balance point is passed, the mount will fall or rise under the influence of its own mass. This would make tracking almost impossible at this point. The small size of the drive apparatus with respect to the telescope makes it susceptible to wind sheer. This has been observed while viewing stars and causes noticeable wobble of the object of interest in the field of view. As even slight changes in the pointing direction of the output telescope would cause the output laser beam to miss the satellite target, the PSLR would be unable to operate satisfactorily even in moderately windy conditions. Tests conducted at Curtin University have shown that the PSLR is capable of good positional accuracy in the tracking of stars. These tests also showed that the mount movement is very susceptible to inertial effects under high acceleration/deceleration conditions. There is noticeable hysteresis in mount movement at the instigation of even the gentlest acceleration and the mount will run on (especially in azimuth) if the mount is decelerated sharply from higher velocities. The mount will stop very accurately, under high deceleration if it is moving under approximately 50 steps per second ($\approx 16"$ per second). Without having tested the PSLR mount during satellite tracking tests it is not possible to say how it would perform but from experience with the tests carried out at Curtin University it is apparent that satellite tracking would be highly problematic.

Previous satellite laser ranging tests conducted at Yarragadee have shown that the PSLR is capable of ranging with an indicated sub-centimeter NP RMS error and a single shot RMS error of approximately 3 - 5 cm to LAGEOS satellites (see figures 1.1 and 1.2, section 1.2). Fixed target laser ranging at Curtin University showed that the system was able to produce sub-centimeter range results but in general

the figure was closer to 3 cm deviation from the true value for the optical range. These tests may well be biased due to the very large return signals, especially from the closest target used. It was expected that the instrument would produce better results using a longer range after the main telescope and return optical elements were aligned and correctly collimated. The ranging tests at Curtin University were conducted with the instrument in less than the best condition. It is expected that the accuracy of ranging could be improved from the level determined by the fixed target tests.

Many of the components used by the PSLR exceed the minimum requirements of the system and thus would enable other components to be upgraded to improve system performance. The weakest link in the PSLR system appears to be the mount. It does not seem to be sturdy enough to cope with movement of the mass of the telescope systems for such a precise application. The arrangement of the mount so that most of the mass is above the centre of elevation rotation means that there is differential torque on the drive system caused by the mass distribution. In order for the PSLR to meet the basic requirements of an SLR station, this must be the first issue addressed.

7.3 The requirements of portable satellite laser ranging systems

When building a portable SLR system the questions that need to be asked are:

- What are the requirements and expectations of the instrument?
- Does the instrument need to provide exactly the same sort of service as a large fixed system or are there specific uses for the system?

For a majority of SLR applications, stations need not track satellites further out than the LAGEOS satellites which orbit at approximately 6000km from the

terrestrial surface. Many of the obvious applications for a portable system would require ranging to satellites that orbit far closer to the Earth's surface (such as Topex/Poseiden at ≈1336km). If, for example, the major requirement of a portable system was to support altimetry satellites through precise orbital determinations over tide gauges, then the design of the system need not be all encompassing. If there is no need to range to GPS or Glonass (≈ 17,060km and 19,100km range respectively) then the upper limit of the output signal and telescope aperture size need only be sufficient to range to LAGEOS. In order for a station to receive endorsement from the ILRS, it must be able to at least track satellites at LAGEOS orbital distances.

With a truly portable system the main considerations (apart from performance as a SLR) are the mass, size and the ease of transferring from one site to the next. Mass and size can be reduced by using lasers and telescopes of only an adequate size to do the job required. If there is no need to have a 62cm primary mirror or a laser capable of producing an output pulse of 250 mJ then it is probably best not to use these in a portable system.

The only really comparable system to the PSLR is the French Transportable Laser Ranging System (FTLRS), shown in figure 7.3 (Centre de Recherche en Geodynamique et Astrometrie, 2003). It uses a single telescope of 13 cm diameter (close to the size of the PSLR transmit telescope) which has a mass of 9kg. The combined mass of the PSLR telescope systems is close to 40 kg (along with 20 kg for the counterweight). The laser used has an output energy per pulse less than half of the PSLR laser and is slightly lighter than the SL212 laser used with the PSLR. It uses a SPAD detector and as such can employ single photon measurements. The telescope is mounted on an electronic theodolite gimbal style mount (Pierron et al., 1998).

The FTLRS has been operating successfully for a number of years and maintains a good level of performance. Figure 7.4 shows that the FTLRS is achieving NP accuracies better than many fixed systems without using a large aperture telescope in the receive channel and with only modest laser output power.

Figure 7.3: Picture of the FTLRS in Ajaccio, Corsica.

The FTLRS is proof that systems can be made much smaller than fixed systems and still achieve good performance. Overconstruction, with consequent larger mass is a significant disadvantage for the stability of a portable system.

Portability of a system relies not only on the system being small and light weight (less than 500kg) but on the ease of pack up, transport, reinstallation and setup in a new location. In practice the PSLR must be largely dismantled for transport. Even if it was separated into a small number of modules, the main telescope must be completely dismantled as the main mirror needs to be transported in a separate case. Several other optical elements need to be removed before transport to reduce the risk of damage during transport. Regardless of the speed of dismantling and transporting of the PSLR, its usefulness as a portable system is severely diminished because of the time it takes to set the instrument up once it has been reassembled. The FTLRS seems far more usefully modularised.

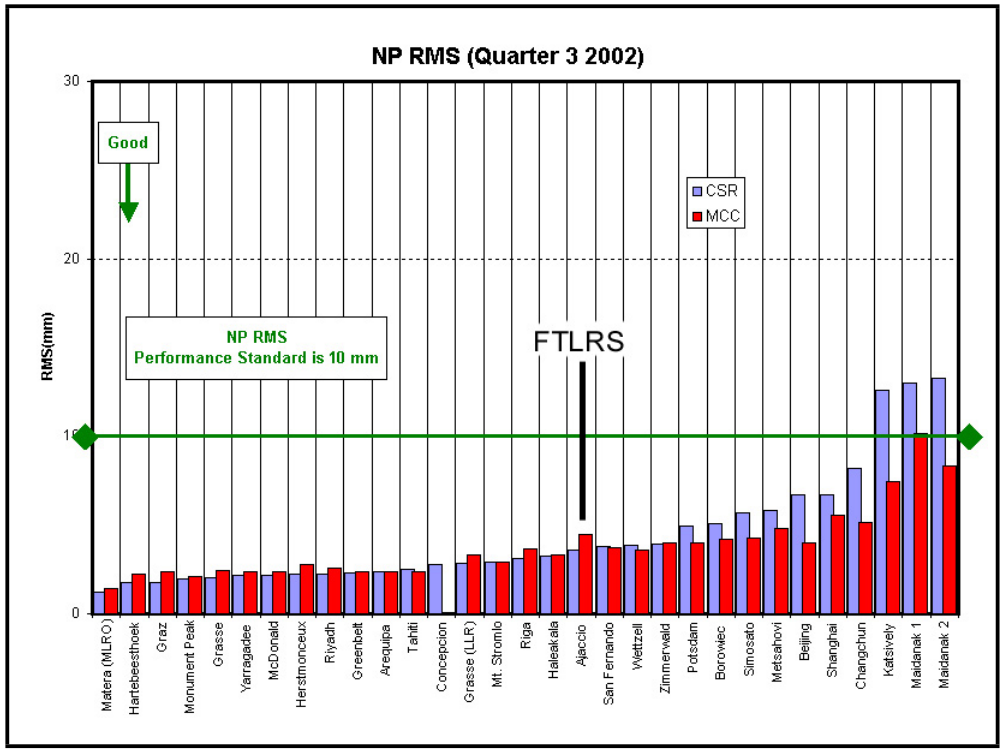

Figure 7.4: Third quarter 2002 SLR network performance comparison, NP accuracy, showing the performance of the FTLRS in Ajaccio, Corsica.

Ideally, relocating a portable system would require simply unplugging the power supplies, electronics and computers, dropping the unit in a box and shipping it to its new location. On arrival it would be removed from the box, placed over the new datum point, all of the equipment reconnected, and it will be ready for operation. It may require a few nights to lock into the geodetic reference frame through star pointing and laser tracking, and to perform mount modelling. For a truly portable system the turn around time for removing a fully operational system, transporting to another location and restoring full operation should take no longer than a standard working week (and preferably a couple of days). The PSLR, at present does not come remotely close to this requirement. Dismantling and reassembling the instrument can be accomplished easily in a couple of hours. Due to the dismantling of large parts of the optical and mechanical systems, on reconstruction, almost the entire system requires realignment. The instrument has multiple adjustments for the mechanical

and optical systems. These adjustments consist of screwdriver or wrench driven positioners, none of which have a scale to indicate the position of the adjustor. If an adjustment were to move during transport, there is no way to tell if it has moved. A majority of the adjustments do not have one degree of adjustment freedom. Moving one adjustment to achieve movement of prism M1 (see figure 4.2, section 4.2.1, page 173) in the horizontal plane, will affect the vertical plane as well. Achieving a specific adjustment can require numerous counter-adjustments, often at several adjustment points. This makes the entire process an application of feel rather than measurement. Achieving adequate alignment could take several weeks of tedious adjustment.

7.4 Redesign of the PSLR system

The PSLR's primary mirror and laser equal or exceed those used in many large fixed systems. However it uses a tripod mount not a great deal larger than the FTLRS (see figure 7.3). While the idea of recreating a large fixed system in a portable package is admirable, the actual execution is definitely problematic. Such a large telescope would be better suited to a gimbal mount where the centre of tilt rotation and the tilt centre of mass can be colocated. The problem with a gimbal system is there is a great deal of torque applied to the gearing system connected to the tilt axis as its circumference will be small. This requires a large motor and gearbox to overcome the torque. This is undesirable in a portable system so the PSLR tilt axis is designed to run on a track of large circumference. Driving the axis through this large track greatly reduces the torque required by a gearbox and motor. This track sits completely under the telescopes so the centre of rotation is nowhere near the centre of mass of the tilt axis. It also means that there is always some torque applied on the drive wheel by the mass of the mount. This torque changes with the elevation of the axis as the centre of mass of the mount is moved over the centre of rotation. This effect could be experienced by holding the bottom of a rod with a

heavy ball on the other end. As the ball is moved torque is exerted. The direction of torque depends on the position of the ball. There is only one point where there is no torque exerted on the bottom of the rod, and this is when it is directly over the centre of rotation. The PSLR exhibits the same behaviour.

This approach would have worked much better if the elevation track was larger and the telescopes sat so that the main mirror was at the centre of tilt. This would allow the secondary mirror to be counterbalanced by placing weight under the main mirror. Using the rod analogy, it would be like gripping the rod in the middle and placing another heavy ball at the unencumbered end. While this system would have a lot of inertia, it is possible to achieve balance.

The PSLR main telescope is also offset from the azimuth rotation axis. This is done so that the laser output optical path can be placed at the centre of the axes rotation. Both optical systems should be at the centres of rotation to improve the mass balance. The easiest way to achieve this goal is either to employ a single telescope and combine both optical systems (coaxial) or separate them completely so that each optical system has its own telescope and drive system. If, as is the case with the FTLRS, a small telescope is used, a coaxial system is ideal. Using a single telescope is cheaper, removes the problem of differential flexure and allows for a much more compact unit.

If a portable system is to emulate a fixed system by using a large aperture receive mirror, then a paraxial system with completely separate optical and drive systems would provide many advantages. To place a large mirror on a small mount, care needs to be taken to correctly balance the large mass. A telescope of the same dimensions as the PSLR, if it was pivoted properly could be counterbalanced by the detection electronics, pulse conditioning electronics and power supplies without taking up any more room than the current PSLR system. The PSLR currently uses over 50 kg of steel bolted to the elevation mount which can only partially counterbalance the mount. This is "dead-weight" which increases mount inertia and total system weight. The laser presently is located on a separate base so converting

this base to hold the laser and a small telescope, mount, and drive gear once again would not require any additional space.

The current PSLR indexer card (DMC 1700 or 1800) can be purchased off-the-shelf to control up to 8 axes. Controlling each axis (and mount) with this type of four-axis controller is essentially no harder to accomplish than controlling only two. With this control card it is possible to make one set of axes exactly mimic the movements of the other set of axes. Differential flexure (a potential problem with the PSLR) would be simple to rectify with a dual mount system by altering the control program as all axes can also be moved completely independently.

The current PSLR system could be altered to an independent paraxial system without any increase in weight and without significant expense. This would be the recommendation of the PSLR project if a large primary telescope was required with a portable system. The existing configuration of the PSLR has introduced far too many problems, problems that would be removed if a dual system was developed.

7.5 The state of the PSLR instrument

The PSLR hardware at the conclusion of this thesis is in operating order. The performance of the hardware varied from optimal (i.e. SR620 interval timer, TM-1 GPS time machine) to marginal (i.e. R4124 detector and preamplifier), to completely unacceptable (telescope mount). All of the PSLR sub-systems (laser, interval timing, station timing, etc) were shown to be functional and, to greater or lesser extent, have been operated much as they would if the PSLR had been engaged in satellite laser ranging. Tracking from the Curtin University campus is not permitted by the Civil Aviation and Safety Authority because of eye safety restrictions.

At the inception of the project at Curtin University in 1999 it was not known that the instrument delivered from Latvia was missing key components and also did not have a working version of the control software. These missing components were replaced with suitable alternatives, integrated and tested independent of the

PSLR control program to examine the operation and performance with regard to the functions these new components were required to undertake, functions previously handled by the missing components. Other control software independent tests were carried out on the existing hardware components to gauge the function and performance of the total system.

At the same time, project personnel were attempting to integrate the new components with the incomplete and non-functioning control software and repair or replace portions of the control software. Other personnel were attempting to update the control program to a 32 bit Microsoft Windows operating system instead of the 16 bit Windows 3.1 system in which the program was initially run.

While the function of most of the hardware was quite self explanatory, this was not the case with the control software. There was no programming manual, almost no in-code comments, a complete lack of proper programming structure or observance of protocols or standards. The facts were that the program, as much as the instrument, was a work in progress, and so the task of modifying the control software to incorporate the new control and tracking components proved to be next to impossible (given any reasonable timeframe). The only sensible option (given that this could probably be accomplished in less time than repairing the existing software) would be to rewrite the entire PSLR software suite in an operating system that is less likely to suffer from impending obsolescence (Windows 3.1 to Windows 2000) and is more compatible with a real-time environment. A choice, such as real-time Linux would be admirable since Windows was not really designed for this type of facility.

The lack of a working control program required that any testing attempted at Curtin University needed special purpose software to be written. Absence of documentation on the main control software meant it was inappropriate to write and integrate test software to both track, time, and range to enable assessment of the ability of the PSLR to operate as a satellite laser ranger. In hindsight, programming personnel would have been used more effectively in this capacity rather than

attempting to repair an antiquated, undocumented software suite.

The PSLR is, at the completion of the project, "a body without a brain". Even if fully operational, it is envisaged that the running of the instrument would be problematic. There is no point in returning the PSLR to operational capacity unless major changes are made to improve and update the system so that it is competitive with current portable systems.

As many of the applications of a portable system can be accomplished using GPS techniques there may be no real future for portable SLR except as pure research instruments or as part of a portable collocation calibrator for the wider SLR community.

7.6 Conclusion

This thesis has dealt with the instrumentation, processes, current status and future direction of SLR and portable SLR. It has described the steps involved in the attempts to make the PSLR operational from the point of view of the lay person because this was the position that the team at Curtin University found themselves in at the start of this project.

Much of the equipment discussed in this thesis is in common but declining use as new equipment has become available to the SLR community since the PSLR was built. The PSLR is an example of a second generation system:

1. 5 - 10 Hz high power, solid state laser
2. Photo-electric tube detector
3. Interval counter
4. Permanent operational staff.

The best of the second generation systems (MOBLAS-5 for example) are at the limit of achievable accuracy after many years of improvement in technique and

equipment. This limit is around 10mm RMS single shot and 1 - 3mm RMS for normal point reduced data. Improvement in accuracy will require new approaches to laser ranging and utilisation of the newest equipment. This has engendered rethinking to encompass new ranging methodologies.

The current economic climate has forced many groups involved in SLR to reduce personnel as people are by far the most expensive component in an SLR system. The requirement to automate systems is also driven by the possibility of improving the global coverage by placing systems in inhospitable and remote locations (such as Antarctica) where a provision for support personnel would make such a deployment unfeasible.

The improvements in equipment and new technology has allowed the development of new methods of SLR. Two colour laser ranging and high repetition range retrieval has opened new possibilities for study and improvement to the field. This sort of development is essential to ensure the future of SLR as GPS is approaching accuracy levels once thought impossible when using radiometric techniques. GPS is simple to use, requires no operators (in general), can be placed in remote locations as it is a passive detection method with no moving parts and in relation to SLR is exceedingly cheap. The future of SLR relies on being the most accurate method of satellite tracking available.

Portable SLR has a niche to fill but will find it difficult to establish itself as anything more than a research or calibration tool. Stations conducting experiments such as the time transfer by laser link, or tidal gauge evaluation of altimeter data with SLR calibration are probably the tasks most suited to portable SLR. If specific data is required from a specific location then portable SLR has a definite use.

One alternate use of a very stable portable system would be a world wide collocation experiment where all stations in the SLR community would be collocated against one instrument. This would provide a world wide baseline measurement and a definitive method of comparing all SLR systems to one another (although this is effectively done by analysis of SLR data).

The PSLR would not be the system most likely to be chosen for the task of world wide collocation. Although the hardware is operational, the control program will not interface with the new control components. Even with a suitable control program the chances of successful satellite laser ranging appear slim (at this time). The telescope and opto-mechanical systems are riddled with adjustments that are neither well understood nor have any definitive positioning effect. Any major movement of the PSLR would require a complete set of re-alignment tests as it is impossible to return adjustments to a previous position without some reference scale.

Even without the desired stability the PSLR system did prove that it had the potential to act as a ranging and tracking system. Stationary target ranging tests (conducted without correct optical collimation) showed that sub-centimeter ranging was possible. Tracking tests showed that the telescope and drive systems were capable of tracking slow moving objects such as stars at least in the short arcs attempted at Curtin University.

If the PSLR project were to continue, the instrument would benefit from redesign to reduce the system weight and improve the weight balance around the axes of rotation. A small telescope coaxial system or a dual telescope separated paraxial system are the suggested changes to achieve these goals. The coaxial system would reduce the mass and the effects associated with mass (inertia, wind loading, telescope sag) as well as increasing portability. Using a dual telescope system with separate drive facilities would allow the use of a large primary mirror and allow the main telescope to be properly balanced on its mount. A small transmit telescope on a separate mount would allow many of the inherent problems with a paraxial system to be corrected by software (alignment, differential sag).

While the PSLR project did not reach a successful conclusion during the course of the project it has been developed to the point where it is apparent that many changes are required. This thesis attempted to illustrate this point in the context of current SLR practices and future developments in the field.

Appendix A

List of Acronyms

1pps	1 pulse per second
APD	Avalanche PhotoDiode
BPSK	Binary Phase Shift Keying
BS	Brillouin Scattering
CCR	Corner Cube Reflector
CFD	Constant Fraction Discriminator
CP	Celestial Pole
C-SPAD	Compensated SPAD
CW	Constant Wave (laser)
DEC	Declination
DIP (switch)	Dual Inline Package
ECEF	Earth-Centred Earth-Fixed (coordinates)
EE	Electrical Engineering (Building) (Target)
EGC (card)	Encoder and Gating Control
EHP	Electron-Hole Pair
EM	Electromagnetic (radiation)
EMS	Electron Multiplier Stage
Eurolas	European laser tracking network
FFDP	Far Field Diffraction Pattern

FTLRS	French Transportable Laser Ranging Station
FWHM	Full Width Half Maximum
Geo	Geology (Building) (Target)
Glonass	GLObal'naya Navigatsionnay Sputnikovaya Sistema
GPS	Global Positioning System
GRACE	Gravity Recovery and Climate Experiment
ILRS	International Laser Ranging Service
IRV	Inter-Range Vector
ITS-90	International Temperature Scale of 1990
JPL	Jet Propulsion Laboratory (NASA)
KD*P	Potassium Dideuterium Phosphate (crystal)
LAGEOS	LASer GEOdynamics Satellite
LED	Light Emitting Diode
LEO	Low Earth Orbit (satellite)
LIDAR	LIght Direction and Ranging
MCP	Microchannel Plate (PMT)
MOBLAS	MOBile LASer ranger
MTLRS-1	Modular Transportable Laser Ranging System
NASA	National Aeronautic and Space Administration
ND	Neutral Density
Nd:YAG	Neodymium: Yttrium Aluminium Garnet (crystal)
Nd:YLF	Neodymium: Yttrium Lithium Fluoride (crystal)
NIM (pulse) (bin)	Nuclear Instrumentation Methods
PIN	P type, Intrinsic, N type (diode)
PMT	Photomultiplier Tube
PO	Pseudo-Operator
PRN	Pseudo Random Noise
PSLR	Portable Satellite Laser Ranger
PTD	Pico Timing Discriminator

RA	Right Ascention
SA	Selective Availability
SBS	Stimulated Brillouin Scattering
SCP	South Celestial Pole
SLR	Satellite Laser Ranging
SLRS	Satellite Laser Ranging Stations
SPAD	Single Photon Avalanche Diode
SV	Space Vehicle
TB	Time Bias
TB	Time Board
TC	Time Card
TEM	Transverse Electromagnetic Mode
TIC	Time Interval Counter
TTL	Transistor-Transistor Logic
USNO	United States Naval Observatory
UTC	Universal Coordinated Time
UV	Ultraviolet (light)
VLBI	Very Long Baseline Interferometry
WPLTN	Western Pacific Laser Tracking Network

References

Abshire, J. and Gardner, C. (1985). Atmospheric refractivity corrections in satellite laser ranging. *IEEE Transactions on Geoscience and Remote Sensing*, Vol GE-23(4):pp.414–425.

Allied Signals (1999). SLR global performance report card, 1998, fourth quarter. [URL]:-`http://www.dgfi.badw-muenchen.de/edc/ilrs/perf_98q4.html`.

Andover Corp. (2004a). Absortive neutral density filters. [URL]:-`http://www.andcorp.com/ Web_store/ Absorption_ND/ absortion_nd.html`.

Andover Corp. (2004b). General/ technical information. [URL]:-`http://www.andcorp.com/ Web_store/ General_info/ Technical.html`.

Arecchi, F. T. and Schulz-Dubois, E. O. (1972a). *Laser Handbook - Volume 1.* North-Holland Publishing Company, 1st edition.

Arecchi, F. T. and Schulz-Dubois, E. O. (1972b). *Laser Handbook - Volume 2.* North-Holland Publishing Company, 1st edition.

Breakiron, L. A. (1999). Cesium atomic clocks. [URL]:-`http://tycho.usno.navy.mil/cesium.html`.

Burmistrov, V., Parkhomenko, N., Roy, Y., Shargorodsky, V., V. Vasiliev, J. D., Habib, S., Glotov, V., and Sokolov, N. (2002). Spherical retroreflector with an

extremely small target error: International experiment in space. 13^{th} *International Workshop on Laser Ranging*.

Centre de Recherche en Geodynamique et Astrometrie (2003). Ftlrs in ajaccio, corsica. [URL]:-`http://grasse.obs-azur.fr/cerga/lassat/lasmobil.htm`.

Chaimowicz, J. C. (1992). *Optoelectronics an Introduction*. Butterworth-Heinemann Ltd, 2nd edition.

Ciddor, P. E. (1996). Refractive index of air: new equations for the visible and near infrared. *Applied Optics*, Vol 35(9):pp.1566 – 1573.

Cova, S., Lacaita, A., and Ripamonti, G. (1996). Performance optimization of detector electronics for millimeter laser ranging. 8^{th} *International Workshop on Laser Ranging*.

Cox, A. N. (1976). *Allen's Astrophysical Quantities*. AIP Press (Springer-Verlag), 4th edition.

Datum Inc. (1996). bc620at time and frequency processor, user's guide.

Degnan, J. J. (1985). Satellite laser ranging: Current status and future prospects. *IEEE Transactions on Geoscience and Remote Sensing*, Vol GE-23(4):pp.398–413.

Degnan, J. J. (1993). Millimeter accuracy satellite laser ranging: A rewiew. *Contributions of Space Geodesy to Geodynamics: Technology*, Vol 25:pp.133 – 162.

Degnan, J. J. (1996). Thirty years of satellite ranging. 9^{th} *International Workshop on Laser Ranging Instrumentation*.

Degnan, J. J. (2001). Slr2000 technical overview, status, and schedules. *NASA Headquarters Code Y Engineering Status Review*.

Farrell, J. and Barth, M. (1999). *The Global Positioning System and Inertial Navigation*. McGraw-Hill, 1st edition.

Fellay, A. (1998). Physics of brillouin scattering. [URL]:-`http://metwww.epfl.ch/Brillouin/physique-brillouinE.htm`.

GFZ (2000). Grace retroreflector array. [URL]:-`http://op.gfz-potsdam.de/grace/ index_GRACE.html`.

Gibbs, P. (2002). Comparisons of a single sr620 timer against a variety of timers from the eurolas network. 13^{th} *International Workshop on Laser Ranging*.

Greene, B., Gao, Y., Moore, C., Wang, Y., A. Boiko, Ian Ritchie, J. S., and Cotter, J. (2002). Laser tracking of space debris - workshop presentation. 13^{th} *International Workshop on Laser Ranging*.

Grunwaldt, L. and Fischer, H. (1994). Field experience with various detector types at slr-station 7836 potsdam. 9^{th} *International Workshop on Laser Ranging Instrumentation*.

Hamamatsu Photonics (1998). Photomultiplier tubes.

Hecht, E. and Zajac, A. (1974). *Optics*. Addison-Wesley Publishing company, 1st edition.

Hecht, J. (1994). *Understanding Lasers, an entry-level guide*. IEEE Press, 2nd edition.

Heidenhain, J. (1999). Angle encoders.

Hewlett Packard (1996). Gps and precision timing applications. *Application Note 1272*.

Hewlett Packard (1997). Hp5071a primary frequency standard, assembly-level service manual.

Holmes, A. (1999). Sbig technical memorandum using the sbig hartmann mask software. [URL]:-http://www.sbig.com/sbwhtmls/hartmann.htm.

HP (1997). Fundamentals of time interval measurements. Hewlett Packard Application Note 200-3.

ILRS (2003a). Historical summary of slr technology, programs, and accomplishments. [URL]:-http://ilrs.gsfc.nasa.gov/about_ ilrs/history/slr_history.html.

ILRS (2003b). Ilrs network. [URL]:-http://ilrs.gsfc.nasa.gov/station/network_map.

ILRS (2003). Slr data station, network and user flow path. [URL]:-http://ilrs.gsfc.nasa.gov/products_formats_procedures/data_flow.html.

ILRS (2003). Slr/llr mission support. [URL]:-http://ilrs.gsfc.nasa.gov/satellite_missions/slr_satellite_support.html.

ILRS (2003). Tof device manufacture specifications. [URL]:-http://ilrs.gsfc.nasa.gov/engineering_technology/timing/tof_devices/manufacture_spec/index.html.

International Laser Ranging Service (ILRS) (2003). Slr global performance report card. [URL]:-http://ilrs.gsfc.nasa.gov/stations/performance_statistics/perf_2002q4.html.

Jones, K. A. (1987). *Introduction to optical electronics*. Harper and Row.

Knoll, G. F. (1989). *Radiation detection and measurement*. John Wiley and Sons, 2nd edition.

Leica Geosystems (2003). Total station and reflector types.
[URL]:-http://www.leica-geosystems.com/ims/products
/images/5005z09-reflectortypes.gif.

Melles Griot (2004). Introduction to gaussian beam optics.
[URL]:-http://ltl.iams.sinica.edu.tw/ support/ opticsguide/ chap02
_gaussian_beam_optics.pdf.

Mendes, V. B. and Pavlis, E. C. (2002). Atmospheric refraction at optical wavelengths: Problems and solutions. 13^{th} *International Workshop on Laser Ranging*.

Michailovas, A. (1997). *SL212 laser Technical description and users manual*. EKSPLA Experimental Lasers.

NASA/JPL (2002). TOPEX/Poseiden.
[URL]:-http://topex-www.jpl.nasa.gov/ missions/topex.html.

National Institute of Standards and Technology (2003). Ceasium frequency standard.
[URL]:-http://www.boulder.NIST.gov/timefreq/general/enc-c.htm.

ORTEC (2001). *Modular Pulse-Processing Electronics, product guide*. PerkinElmer Instruments.

Pierron, F., Nicolas, J., Kasser, M., and Haase, J. (1998). Status and new capabilities of the french transportable laser ranging station. 11^{th} *International Workshop on Laser Ranging*.

Pressley, R. J. (1977). *CRC Handbook of lasers with selected data on optical technology*. CRC Press, 2nd edition.

Radarmet (2002). Propagation of electromagnet waves.
[URL]:-radarmet.atmos.colostate.edu/AT741/AT741docs/
2002/Chapter3-blackandwhitePDF.pdf.

Red Sword Corporation (1998). Historical timeline of radionavigation systems. [URL]:-http://www.redsword.com/GPS/apps/general/ timeline.htm#1989.

Riepl, S. (2001). Experimental verifcation of the marini-murray model by two colour slr. 12^{th} *International Workshop on Laser Ranging*.

Rosenberg, H. M. (1995). *The Solid State*. Oxford Science Publications, 3rd edition.

Serway, R. A. (1992). *Physics for Scientists and Engineers with Modern Physics*. Saunders College Publishing, 3rd edition.

Sinclair, A. T. (1997). Data screening and normal point formation. [URL]:-http://ilrs.gsfc.nasa.gov/np_algo.html.

Sperber, P., Motz, R., Schotz, P., Maberry, M., and Zane, R. (1994). Tests and developments at the mtlrs-1 receiving system. 9^{th} *International Workshop on Laser Ranging Instrumentation*.

SRS (1999). Making measurements with the sr620 time interval counter. Stanford Research Systems Application Note 2.

Standards Australia (1997). *Laser saftey Part 1: Equipment classification, requirements and user's guide*. Council of standards Australia, AS/NZS 2211.1:1997 edition.

Tal, J. (1999). Users manual Rev. 1.2e - DMC-1700/1800.

Trueblood, M. and Genet, R. M. (1997). *Telescope Control*. Willmann-Bell, Inc, 2nd edition.

Veltchev, I. T. (2001). *Stimulated Brillouin Scattering Pulse Compression and Harmonic Generation: Applications to Precision XUV Laser Spectroscopy*. PhD thesis, Atomic and Laser Physics Group, Free University, Amsterdam. [URL]:-http://www.nat.vu.nl/ iavor/.

Verveer, A. (2001). Private communication. Perth Observatory, Western Australia.

Wettzell (2003). Satellite link budget evaluation.
[URL]:-`http://www.wettzell.ifag.de/publ-cgi-bin/linkbudget.py`.

Zarins, A. (1996). Slr control interface for microsoft windows version 1.11 - users manual.